ISSN 1948-0210 (online)

World Journal of *Stem Cells*

World J Stem Cells 2023 September 26; 15(9): 876-959

Published by Baishideng Publishing Group Inc

WJSC

World Journal of Stem Cells

Contents

Monthly Volume 15 Number 9 September 26, 2023

ORIGINAL ARTICLE

Basic Study

Contents

ABOUT COVER

AIMS AND SCOPE

The primary aim of *World Journal of Stem Cells* (*WJSC*, *World J Stem Cells*) is to provide scholars and readers from various fields of stem cells with a platform to publish high-quality basic and clinical research articles and communicate their research findings online. *WJSC* publishes articles reporting research results obtained in the field of stem cell biology and regenerative medicine, related to the wide range of stem cells including embryonic stem cells, germline stem cells, tissue-specific stem cells, adult stem cells, mesenchymal stromal cells, induced pluripotent stem cells, embryonal carcinoma stem cells, hemangioblasts, lymphoid progenitor cells, *etc*.

INDEXING/ABSTRACTING

The *WJSC* is now abstracted and indexed in Science Citation Index Expanded (SCIE, also known as SciSearch®), Journal Citation Reports/Science Edition, PubMed, PubMed Central, Scopus, Biological Abstracts, BIOSIS Previews, Reference Citation Analysis, China National Knowledge Infrastructure, China Science and Technology Journal Database, and Superstar Journals Database. The 2023 Edition of Journal Citation Reports® cites the 2022 impact factor (IF) for *WJSC* as 4.1; IF without journal self cites: 3.9; 5-year IF: 4.5; Journal Citation Indicator: 0.53; Ranking: 15 among 29 journals in cell and tissue engineering; Quartile category: Q3; Ranking: 99 among 191 journals in cell biology; and Quartile category: Q3. The *WJSC*'s CiteScore for 2022 is 8.0 and Scopus CiteScore rank 2022: Histology is 9/57; Genetics is 68/325; Genetics (clinical) is 19/90; Molecular Biology is 119/380; Cell Biology is 95/274.

RESPONSIBLE EDITORS FOR THIS ISSUE

Production Editor: *Xiang-Di Zhang*; **Production Department Director:** *Xu Guo*; **Editorial Office Director:** *Jia-Ru Fan*.

NAME OF JOURNAL
World Journal of Stem Cells

ISSN
ISSN 1948-0210 (online)

LAUNCH DATE
December 31, 2009

FREQUENCY
Monthly

EDITORS-IN-CHIEF
Shengwen Calvin Li, Carlo Ventura

EDITORIAL BOARD MEMBERS
https://www.wjgnet.com/1948-0210/editorialboard.htm

PUBLICATION DATE
September 26, 2023

INSTRUCTIONS TO AUTHORS
https://www.wjgnet.com/bpg/gerinfo/204

GUIDELINES FOR ETHICS DOCUMENTS
https://www.wjgnet.com/bpg/GerInfo/287

GUIDELINES FOR NON-NATIVE SPEAKERS OF ENGLISH
https://www.wjgnet.com/bpg/gerinfo/240

PUBLICATION ETHICS
https://www.wjgnet.com/bpg/GerInfo/288

PUBLICATION MISCONDUCT
https://www.wjgnet.com/bpg/gerinfo/208

ARTICLE PROCESSING CHARGE
https://www.wjgnet.com/bpg/gerinfo/242

STEPS FOR SUBMITTING MANUSCRIPTS
https://www.wjgnet.com/bpg/GerInfo/239

ONLINE SUBMISSION
https://www.f6publishing.com

World Journal of Stem Cells

Submit a Manuscript: https://www.f6publishing.com

World J Stem Cells 2023 September 26; 15(9): 876-896

DOI: 10.4252/wjsc.v15.i9.876

ISSN 1948-0210 (online)

ORIGINAL ARTICLE

Basic Study

Interferon-γ priming enhances the therapeutic effects of menstrual blood-derived stromal cells in a mouse liver ischemia-reperfusion model

Qi Zhang, Si-Ning Zhou, Jia-Min Fu, Li-Jun Chen, Yang-Xin Fang, Zhen-Yu Xu, Hui-Kang Xu, Yin Yuan, Yu-Qi Huang, Ning Zhang, Yi-Fei Li, Charlie Xiang

Specialty type: Cell and tissue engineering

Provenance and peer review: Unsolicited article; Externally peer reviewed.

Peer-review model: Single blind

Peer-review report's scientific quality classification

Grade A (Excellent): A
Grade B (Very good): B, B
Grade C (Good): 0
Grade D (Fair): 0
Grade E (Poor): 0

P-Reviewer: Haque N, Bangladesh; Jeyaraman M, India; Shalaby MN, Egypt

Received: April 20, 2023
Peer-review started: April 20, 2023
First decision: June 7, 2023
Revised: June 21, 2023
Accepted: July 18, 2023
Article in press: July 18, 2023
Published online: September 26, 2023

Qi Zhang, Si-Ning Zhou, Jia-Min Fu, Li-Jun Chen, Yang-Xin Fang, Hui-Kang Xu, Yin Yuan, Yu-Qi Huang, Ning Zhang, Yi-Fei Li, State Key Laboratory for Diagnosis and Treatment of Infectious Diseases, National Clinical Research Center for Infectious Diseases, National Medical Center for Infectious Diseases, Collaborative Innovation Center for Diagnosis and Treatment of Infectious Diseases, The First Affiliated Hospital, Zhejiang University School of Medicine, Hangzhou 310003, Zhejiang Province, China

Qi Zhang, Si-Ning Zhou, Jia-Min Fu, Li-Jun Chen, Yang-Xin Fang, Hui-Kang Xu, Yin Yuan, Yu-Qi Huang, Ning Zhang, Yi-Fei Li, Research Units of Infectious Disease and Microecology, Chinese Academy of Medical Sciences, Hangzhou 310003, Zhejiang Province, China

Zhen-Yu Xu, Innovative Precision Medicine Group, Shulan Hospital, Hangzhou 311215, Zhejiang Province, China

Charlie Xiang, The First Affiliated Hospital, Zhejiang University School of Medicine, Hangzhou 310003, Zhejiang Province, China

Corresponding author: Charlie Xiang, PhD, Director, Professor, The First Affiliated Hospital, Zhejiang University School of Medicine, No. 79 Qingchun Road, Hangzhou 310003, Zhejiang Province, China. cxiang@zju.edu.cn

Abstract

BACKGROUND

Mesenchymal stem cells (MSCs) have been used in liver transplantation and have certain effects in alleviating liver ischemia-reperfusion injury (IRI) and regulating immune rejection. However, some studies have indicated that the effects of MSCs are not very significant. Therefore, approaches that enable MSCs to exert significant and stable therapeutic effects are worth further study.

AIM

To enhance the therapeutic potential of human menstrual blood-derived stromal cells (MenSCs) in the mouse liver ischemia-reperfusion (I/R) model *via* interferon-γ (IFN-γ) priming.

METHODS

Apoptosis was analyzed by flow cytometry to evaluate the safety of IFN-γ priming, and indoleamine 2,3-dioxygenase (IDO) levels were measured by quantitative real-time reverse transcription polymerase chain reaction, western blotting, and ELISA to evaluate the efficacy of IFN-γ priming. *In vivo*, the liver I/R model was established in male C57/BL mice, hematoxylin and eosin and TUNEL staining was performed and serum liver enzyme levels were measured to assess the degree of liver injury, and regulatory T cell (Treg) numbers in spleens were determined by flow cytometry to assess immune tolerance potential. Metabolomics analysis was conducted to elucidate the potential mechanism underlying the regulatory effects of primed MenSCs. *In vitro*, we established a hypoxia/reoxygenation (H/R) model and analyzed apoptosis by flow cytometry to investigate the mechanism through which primed MenSCs inhibit apoptosis. Transmission electron microscopy, western blotting, and immunofluorescence were used to analyze autophagy levels.

RESULTS

IFN-γ-primed MenSCs secreted higher levels of IDO, attenuated liver injury, and increased Treg numbers in the mouse spleens to greater degrees than untreated MenSCs. Metabolomics and autophagy analyses proved that primed MenSCs more strongly induced autophagy in the mouse livers. In the H/R model, autophagy inhibitors increased the level of H/R-induced apoptosis, indicating that autophagy exerted protective effects. In addition, primed MenSCs decreased the level of H/R-induced apoptosis *via* IDO and autophagy. Further rescue experiments proved that IDO enhanced the protective autophagy by inhibiting the mammalian target of rapamycin (mTOR) pathway and activating the AMPK pathway.

CONCLUSION

IFN-γ-primed MenSCs exerted better therapeutic effects in the liver I/R model by secreting higher IDO levels. MenSCs and IDO activated the AMPK-mTOR-autophagy axis to reduce IRI, and IDO increased Treg numbers in the spleen and enhanced the MenSC-mediated induction of immune tolerance. Our study suggests that IFN-γ-primed MenSCs may be a novel and superior MSC product for liver transplantation in the future.

Key Words: Mesenchymal stem cells; Cell therapy; Reperfusion injury; T-lymphocytes; Autophagy; Liver

Core Tip: In this study, we identified a suitable interferon-γ (IFN-γ) priming strategy for menstrual blood-derived stromal cells (MenSCs) in the liver ischemia-reperfusion (I/R) model and proved that primed MenSCs could significantly increase the number of regulatory cells in the spleen by secreting higher levels of indoleamine 2,3- dioxygenase (IDO) and thereby exhibited better immunoregulatory potential. Besides, through metabolomics and related molecular biology experiments, we found that IDO could reduce ischemia-reperfusion injury *via* the AMPK-mammalian target of rapamycin-autophagy axis. Our study suggests that IFN-γ-primed MenSCs may be a novel and superior mesenchymal stem cell product for liver transplantation in the future.

Citation: Zhang Q, Zhou SN, Fu JM, Chen LJ, Fang YX, Xu ZY, Xu HK, Yuan Y, Huang YQ, Zhang N, Li YF, Xiang C. Interferon-γ priming enhances the therapeutic effects of menstrual blood-derived stromal cells in a mouse liver ischemia-reperfusion model. *World J Stem Cells* 2023; 15(9): 876-896

URL: https://www.wjgnet.com/1948-0210/full/v15/i9/876.htm

DOI: https://dx.doi.org/10.4252/wjsc.v15.i9.876

INTRODUCTION

Liver transplantation is the only therapeutic option that is available to patients with terminal liver failure. Both liver ischemia-reperfusion injury (IRI), which occurs during surgery, and immune rejection, which occurs after surgery, affect the results of liver transplantation[1]. Therefore, there is an urgent need to develop effective strategies for treating IRI and immune rejection.

Mesenchymal stem cells (MSCs) have been used in liver transplantation and have shown certain therapeutic effects[2-4]. For example, MSCs alleviated hepatocellular apoptosis in a mouse liver ischemia-reperfusion (I/R) model *via* PINK1-dependent mitophagy[5]. In a clinical study, the percentage of regulatory T cells (Tregs) and the ratio of Tregs to T helper 17 (Th17) cells, which can be used as indicators of immune tolerance potential, were significantly increased in liver transplant recipients 4 wk after MSC infusion[6]. However, the results of another clinical study showed that the infusion of MSCs into liver transplant recipients before surgery was safe, but only mild changes in the peripheral blood immunoregulatory T cell numbers and natural killer cell numbers were observed in these patients[7]. In addition, the administration of immunosuppressive agents with MSCs showed no synergistic effect compared with the administration of immunosuppressive agents alone in a rat liver transplant study[8]. Therefore, approaches that enable MSCs to exert

more significant protective effects in reducing IRI and inducing immune tolerance in liver transplantation deserve further study.

Priming can induce an anti-inflammatory state in MSCs, causing them to secrete more bioactive molecules and improving their therapeutic effects[9,10]. Interferon (IFN)-γ-primed MSCs have been shown to have more stable and stronger abilities to regulate immune responses and prevent damage in many disease models[11-13]. Priming with IFN-γ increases the mRNA expression of Toll-like receptor 3 and the secretion of immunosuppressive molecules, such as indoleamine 2,3-dioxygenase (IDO), interleukin (IL)-10, hepatocyte growth factor, and kynurenine[14]. IDO, an enzyme involved in tryptophan metabolism, has been widely reported to regulate T-cell immunity, specifically by promoting the differentiation of Tregs, inhibiting Th17 cells, and promoting immune tolerance and immune escape[15,16]. Additionally, compared with control conditions, IFN-γ priming significantly induces IDO expression, enhances the immunoregulatory effect of MSCs on T cells, increases Treg differentiation, and promotes immune tolerance[17].

Menstrual blood-derived stromal cells (MenSCs) have been studied in several clinical and preclinical trials, and their safety and immunomodulatory properties have been fully demonstrated[18-20]. In addition, MenSCs can be collected in a manner that is painless, noninvasive, convenient, and inexpensive, thus, their use in cell-based therapy has high clinical and economic value. In this study, we hypothesized that IFN-γ-primed MenSCs could secrete higher levels of IDO to better induce immune tolerance in a mouse liver I/R model. However, whether priming with IFN-γ affects the viability of MenSCs themselves is unclear. Moreover, whether IFN-γ-primed MenSCs, which represent a new type of modified MSC product, can better mitigate liver injury in the liver I/R model has not been clarified. Therefore, it is worthwhile to further study appropriate priming strategies and whether primed MenSCs can exert better therapeutic effects in the liver I/R model.

MATERIALS AND METHODS

MenSCs

MenSCs were provided by the Innovative Precision Medicine Group (IPM, Hangzhou, China) and cultured as described in our previous study[2-4]. Briefly, the cells were cultured in α-minimum essential medium (Thermo Fisher Scientific, United States) supplemented with 10% foetal bovine serum (FBS) (Thermo Fisher Scientific, United States) and 1% penicillin-streptomycin solution (Thermo Fisher Scientific, United States) in an incubator at 37 °C with 5% CO_2. When the cells reached 80%-90% confluence, they were subcultured with 0.25% trypsin-EDTA (Thermo Fisher Scientific) and passaged 5-8 times before being used in experiments. MenSCs were identified based on their surface marker expression and differentiation potential.

Flow cytometry was performed to detect the surface markers of MenSCs. The cells were collected, washed twice with staining buffer (BD, Biosciences, San Jose, CA), and incubated with antibodies against CD29, CD34, CD45, CD73, CD90, CD105, CD117, and human leukocyte antigen-DR (HLA-DR) (PE, BD, Biosciences, San Jose, United States) at 4 °C for 30 min in the dark. Negative controls (NCs) were established with the corresponding isotype control antibodies. A flow cytometer (ACEA Biosciences, CA, United States) was used to analyze all the cells.

Osteogenic, adipogenic, and chondrogenic differentiation was induced to evaluate the multi-differentiation potential of the cells. Briefly, approximately 5 × 10^5 MenSCs were cultured in 6-well plates for 3-4 wk with osteogenic differentiation medium (Cyagen Biosciences, United States) or adipogenic differentiation medium (Cyagen Biosciences, United States) in an incubator at 37 °C with 5% CO_2 to promote osteogenic or adipogenic differentiation, respectively; the medium was changed every 1-3 d according to the instructions. After fixation with 4% formaldehyde, the cells were incubated with Alizarin Red or Oil Red O solution for 30 min to label calcium or neutral lipids, respectively. Chondrogenic differentiation was performed in a 15 mL centrifuge tube. Approximately 5 × 10^5 MenSCs were centrifuged and cultured with 1 mL of human MSC chondrogenic differentiation medium (Cyagen Biosciences, United States) in an incubator at 37 °C with 5% CO_2 for 3-4 wk; the medium was changed every 2-3 d according to the instructions. After fixation with 4% formaldehyde, the pelleted cells were embedded in paraffin, cut into 4 mm sections, and stained with Alcian blue solution to label cartilage.

Priming of MenSCs and IDO quantification

IFN-γ (Miltenyi Biotec Inc., Auburn, CA, United States) at a concentration of 100 or 200 ng/mL was used to prim MenSCs for 24, 48, or 72 h. After the cells were collected, RNA or protein was extracted to measure IDO expression by quantitative real-time reverse transcription polymerase chain reaction (qRT-PCR) or western blotting assays, respectively, as described below. Additionally, the supernatants were collected to evaluate the release of IDO using a Human IDO ELISA Kit (Sangon Biotech, Shanghai, China).

Establishment of the mouse liver I/R model and animal grouping

Six- to eight-week-old male C57BL/6J mice (Slac Laboratory Animal Corporation, Shanghai, China) were housed in a specific pathogen-free room (23 ± 2 °C, 12 h light/12 h dark cycle, and 50% humidity) at the Laboratory Animal Center of Zhejiang University with plenty of food and water for two weeks prior to experimentation. All the procedures used for the animal experiments, the number of animals, and the ethics of the animal housing environment were performed according to the 3Rs rule and approved by the Experimental Animal Center of Zhejiang University, and the ethical approval number is ZJU20210299.

Anesthesia: Before all the surgical procedures, 1% pentobarbital sodium (100 μL/10 g intraperitoneal injection) was used to anesthetize the mice (weight 20-23 g)[5]. Surgical procedure: All the mice received a ventral midline incision. Hepatic arteries, portal veins, and bile ducts were clipped with an atraumatic vascular clip to interrupt 70% of the blood supply to the liver. After 1 h of ischemia, the atraumatic vascular clamps were removed to terminate the ischemia; the wounds were sutured layer by layer, and erythromycin ointment was applied to prevent infection. The mice were resuscitated on a 37 °C blanket to maintain their body temperature. Group design: The sample size (total n = 27, and n = 3/group), grouping, and animal experiment schedule were decided based on a similar study published previously[2] and can be found in Figure 1. To establish the short-term I/R model, the mice were randomly divided into the sham group, IR group, IRM group, and IRM (IFN-γ) group (n = 3/group). The model mice in the IR, IRM, and IRM (IFN-γ) groups were administered 100 μL of phosphate buffered saline (PBS) or MenSCs (10^6/100 μL intravenous injection) or IFN-γ-primed MenSCs (10^6/100 μL intravenous injection) 1 h before the surgery. The mice in the sham group received only a ventral midline incision and were sutured after injection of PBS. After 6 h of reperfusion, the mice were euthanized in a classic, quick, and painless manner (150 mg/kg pentobarbital sodium, intraperitoneal injection), and tissue samples were collected for further investigation.

To establish the long-term I/R model, the mice were randomly divided into the sham group, IR group, IRM group, IRM (IFN-γ) group, and IRM (IFN-γ) + 1-methyl-D-tryptophan (1MT) group (n = 3/group). The treatment plan was similar to that used for the short-term model, with the exception that 1MT (2 mg/mL; MCE, New Orleans, LA, United States) was added to the drinking water of the mice in the IRM (IFN-γ) + 1MT group, and the mice in this group had continuous access to this supplemented water starting from the day of the surgery (day 0) until the seventh day (day 7). The mice in the other groups were given normal water without 1MT. All the long-term I/R model mice were euthanized (150 mg/kg pentobarbital sodium, intraperitoneal injection) on day 7 for tissue collection.

Assessment of liver injury

The serum alanine aminotransferase (ALT) and aspartate aminotransferase (AST) levels were measured using the ALT Kit and AST Kit (Nanjing Jiancheng Bioengineering Institute, Nanjing, China), respectively, to assess the liver injury. Liver injury was also assessed by hematoxylin and eosin staining. Sections were examined under a microscope, and Suzuki's injury criteria (Supplementary Table 1) were utilized to determine the histological damage score by a researcher who was blinded to the group of the immunohistochemistry sections.

qRT-PCR

To confirm the effects on the transcriptome, RNA was extracted from cells using the RNA Extraction Kit (TaKaRa, Beijing, China). Prime Script TMRT Master Mix and TB Green Premix Ex Taq Bulk (TaKaRa, Beijing, China) were used for qRT-PCR. First, Buffer RL was added to the cells to lyse them, and the lysis solution was transferred to a gDNA Eraser Spin Column to remove impurities and gDNA. Then, 70% ethanol was added to the filtrate, and the mixture was moved to an RNA spin column to capture the RNA. Then, the RNA spin column was cleaned with Buffer RWA and Buffer RWB. The RNA solution was obtained by eluting the RNA with RNase-free dH_2O. Then, we mixed an appropriate amount of RNA with 5 × A solution and RNase-free dH_2O to a final volume of 10 μL, and reverse transcription was performed to obtain cDNA. Then, the TB Green mix (12.5 μL), forward PCR primer (10 μM × 0.5 μL, Supplementary Table 2), reverse PCR primer (10 μM × 0.5 μL, Supplementary Table 2), DNA template (2 μL), and 9.5 μL ddH_2O were mixed in a final volume of 25 μL. The qRT-PCR conditions were as follows: 95 °C for 30 s ; 40 cycles of 95 °C for 5 s and 60 °C for 30 s for 2 step PCR; and 95 °C for 15 s, 60 °C for 30 s, and 95 °C for 15 s for dissociation. The melting curves were determined, and the cycle threshold (CT) values of the β-actin (ACTB) transcripts were used to normalize the CT values of the IDO transcripts. The qRT-PCR data were analyzed using the ΔΔCT method.

Western blotting

Liver tissues and cells were lysed with a moderate amount of lysis buffer, which was composed of radioimmunoprecipitation assay buffer (RIPA Lysis Buffer, 10 ×, Merck KGaA, Darmstadt, Germany), a protease and phosphatase inhibitor cocktail for mammalian cell and tissue extracts (Beyotime, Shang Hai, China) and ddH_2O, on ice for 30-60 min. Equal amounts of proteins were subjected to 12% or 8% SDS polyacrylamide gel electrophoresis and then transferred to polyvinylidene difluoride membranes (Millipore, Billerica, MA, United States). The membranes were incubated with 5% nonfat milk for 1 h and then with the primary antibodies overnight at 4 °C; the primary antibodies included antibodies against IDO (16630, Cell Signaling Technology, United States), LC3 (12741, Cell Signaling Technology, United States), AMPKα (total) (5831, Cell Signaling Technology, United States), p-AMPKα (50081, Cell Signaling Technology, United States), mammalian target of rapamycin (mTOR) (total) (2983, Cell Signaling Technology, United States), p-mTOR (5536, Cell Signaling Technology, United States), and β-actin (ACTB) (8227, Abcam, United States). The membranes were then washed three times with Tris-buffered saline with Tween 20 (TBST) and incubated with the secondary antibody [anti-rabbit immunoglobulin G (IgG), Sigma, United States or anti-mouse IgG, Sigma, United States] for 1 h at room temperature. The membranes were washed three times with TBST and visualized by enhanced chemiluminescence with a Fluor Chem Systems imager (Bio-Rad, CA, United States). The intensities of the bands were determined using ImageJ software.

Transmission electron microscopy

Liver samples were cut into 1-mm^3 pieces and fixed with 2.5% glutaraldehyde overnight at 4 °C. After fixation and dehydration, all the samples were stained with osmic acid and uranyl acetate. Then, we used an ultramicrotome to slice the samples and obtain ultrathin sections. All the samples were imaged with a transmission electron microscope (Talos

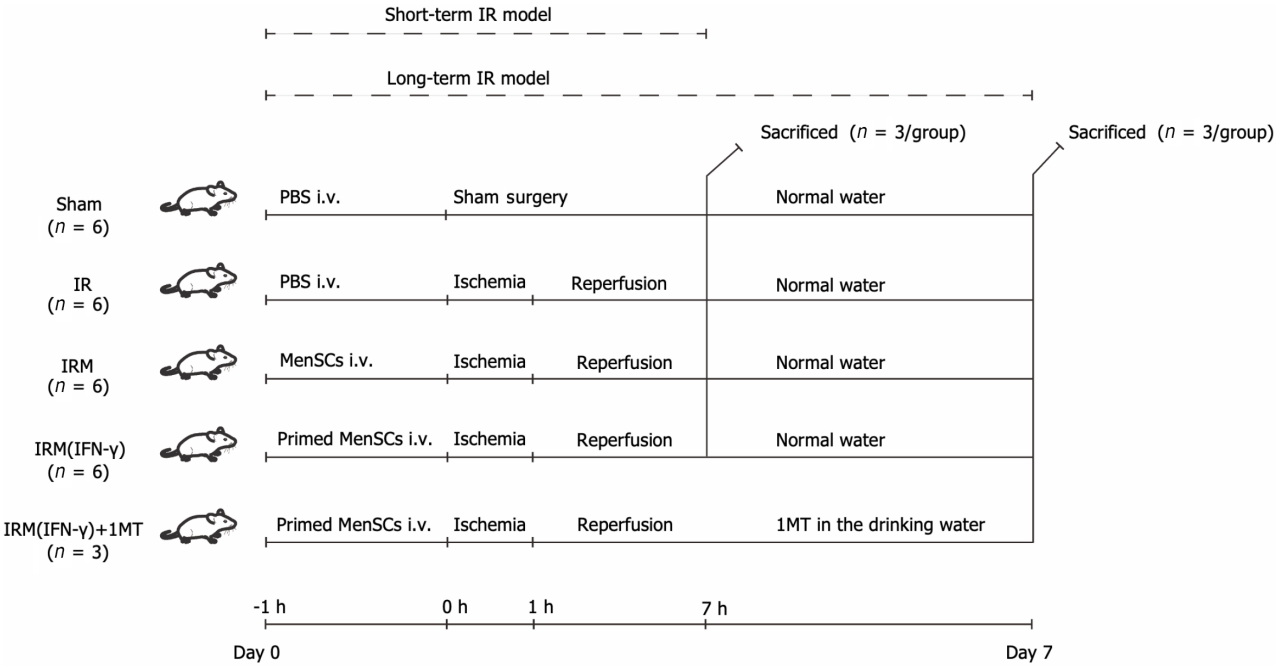

DOI: 10.4252/wjsc.v15.i9.876

Figure 1 Animal experiment grouping and timeline. Detailed descriptions are provided in the Materials and Methods. In brief, we established short-term and long-term liver ischemia-reperfusion mouse models to explore the therapeutic potential of menstrual blood-derived stromal cells (MenSCs) and primed MenSCs. MenSCs: Menstrual blood-derived stromal cells; IFN-γ: Interferon-γ; 1MT: 1-methyl-D-tryptophan; IR: Ischemia-reperfusion; IRM: Combination treated with ischemia-reperfusion and menstrual blood-derived stromal cells; IRM (IFN-γ): Combination treated with ischemia-reperfusion and interferon-γ-primed menstrual blood-derived stromal cells; PBS: Phosphate buffered saline; i.v.: Intravenous injection.

L120C, Thermo Fisher, Carlsbad, CA, United States) to confirm and monitor autophagy, and the number of autophagic vacuoles in each cell was quantified.

Establishment of the hypoxia/reoxygenation model in L02 cells and grouping

Under normoxic conditions, the L02 cells (FuHeng Biology, Shanghai, China) were cultured in 1640 complete medium (RPMI 1640 medium supplemented with 10% FBS and 1% penicillin-streptomycin) in a typical incubator at 37 °C with 5% CO_2. To simulate liver IRI, the L02 cells were subjected to hypoxia/reoxygenation (H/R). Briefly, after 6 h of culture in FBS-free 1640 medium in a 2.5 L sealed culture tank (MGC, Tokyo, Japan) under hypoxic conditions, the cells were transferred to atypical incubator for 4 h to allow reoxygenation. The hypoxic conditions in the sealed culture tank (94% N_2, 5% CO_2, and 1% O_2) were maintained by AnaeroPack-Anaero-5% (MGC, Tokyo, Japan).

Group design: The cells that were cultured under normal oxygen conditions were divided into the NC group, 3-methyladenine (3MA) group, 1MT group, MenSCs group, and MenSC (IFN-γ) group. The cells that were cultured under H/R conditions were divided into the HR group, HR + 3MA group, HR + 1MT group, HRM group, HRM (IFN-γ) group, HRM (IFN-γ) + 3MA group, and HRM (IFN-γ) + 1MT group.

The NC group consisted of cells cultured in 1640 complete medium without any other treatment. The cells in the 3MA group and 1MT group were cultured in 1640 complete medium with 10 mmol/L 3MA (an autophagy inhibitor, MCE, New Orleans, LA, United States) or 1 mmol/L 1MT (an IDO inhibitor, MCE, New Orleans, LA, United States). The cells in the MenSCs group and MenSC (IFN-γ) group were cocultured with MenSCs or MenSC (IFN-γ), respectively, in 1640 complete medium using a coculture chamber as described previously. The HR group, HR + 3MA group, HR + 1MT group, HRM group, and HRM (IFN-γ) group, were subjected to treatments that were similar to those used in the experiments conducted under normal oxygen conditions, but H/R treatment was added. In addition to the HRM (IFN-γ) treatment, the cells in the HRM (IFN-γ) + 3MA group and HRM (IFN-γ) + 1MT group received 3MA and 1MT in the medium, respectively.

Quantitative GFP-LC3 analysis

L02 cells in every group were transfected with pCMV-GFP-LC3 (Beyotime, Shang Hai, China) for 24 h before treatment. We used a confocal laser scanning microscope (Olympus Corporation, Japan) to detect fluorescence emission. Intense punctate GFP-LC3 aggregates in the nucleus and cytoplasm were considered to indicate autophagy, whereas diffuse distribution of GFP-LC3 was considered to indicate non-autophagic conditions. We counted the number of intense punctate GFP-LC3 aggregates in each cell to indicate the number of autophagosomes.

Treg analysis

The mononuclear cells in the spleen were harvested by gradient centrifugation using Ficoll 1.084 (Cytiva, Logan, UT, United States). FACS was performed with 3 fluorochrome-conjugated antibodies: Anti-CD4 monoclonal antibody (APC,

17-0041-83, eBioscience, CA, United States), anti-CD25 monoclonal antibody (PE, 12-0251-82, eBioscience, CA, United States), and anti-FOXP3monoclonal antibody (FITC, 11-5773-82, eBioscience, CA, United States). Nuclear permeabilization was performed with a FoxP3/transformation factor permeabilization buffer (00-5523-00, eBioscience, CA, United States) before the anti-FoxP3 antibody was added to the cells for incubation. Cell fluorescence was evaluated using a flow cytometer (ACEA Biosciences, CA, United States). The percentage of $CD4^+$ $CD25^+$ cells among all mononuclear cells and the percentage of $FoxP3^+$ cells among the $CD4^+CD25^+$ cells were recorded, and the product of these percentages was used to represent the percentage of Tregs among all mononuclear cells.

Statistical analysis

The metabolomics data were analyzed using the free online Majorbio choice platform (cloud.majorbio.com). Other data were analyzed using Prism version 5.0 (GraphPad, United States). The data are shown as the means ± SDs or means ± SEMs. One-way ANOVA was used for comparisons of three or more groups. A P value of <0.05 was considered to indicate a significant difference ($^aP < 0.05$, $^bP < 0.01$, $^cP < 0.001$, and $^dP < 0.0001$), and P values ≥ 0.05 were considered to indicate no significant difference (NS).

RESULTS

Characterization of MenSCs

Primary MenSCs were cultured and exhibited adherent growth after approximately 24 h, and obvious cell proliferation was observed as soon as the cells became round and fusiform. According to a phenotypic analysis, MenSCs expressed CD29, CD73, CD90, and CD105, but they did not express CD45, CD80, CD117, or HLA-DR (Figure 2A). Specific staining showed that MenSCs could undergo osteogenic, chondrogenic, and adipogenic lineage differentiation (Figures 2B-D). The MenSCs that were used in this study met the International Society for Cellular Therapy criteria for the definition of multipotent MSCs[21].

MenSC priming with IFN-γ

In this study, we hypothesized that IFN-γ-primed MenSCs could secrete higher levels of IDO to induce stronger immune tolerance in a liver I/R model. Therefore, to determine the appropriate priming strategy, we evaluated the safety and efficacy of priming by measuring the degree of cell apoptosis and the levels of IDO, respectively.

MenSCs were treated with 100 ng/mL IFN-γ (low concentration) or 200 ng/mL IFN-γ (high concentration) to determine the appropriate concentration for treatment. To accurately mimic the environment in which MenSCs perform their biological functions, we exposed MenSCs to H/R 72 h after priming[14,18]. Then, the cells were stained with Annexin V and propidium iodide (PI), and the proportions of apoptotic MenSCs in the different treatment groups were analyzed by flow cytometry. We found that H/R slightly increased stem cell apoptosis, but the difference was not significant (Figures 2E and F). Moreover, MenSCs that were primed with low and high IFN-γ concentrations were less resistant to H/R-induced apoptosis, and the overall proportions of apoptotic cells reached approximately 10% and 17%, respectively (Figures 2E and F). To maintain a relatively good state of MenSCs after intervention, we used the lower concentration of 100 ng/mL to prim MenSCs in the subsequent experiments.

As previously mentioned, IDO secreted by MSCs plays a key role in the regulation of T cells, and this metabolite can induce the differentiation of Tregs and thus promote immune tolerance[15,16]. Therefore, we used the IDO levels as an indicator to evaluate the efficacy of priming. The mRNA and protein levels of IDO in MenSCs were measured by qRT-PCR and western blotting, respectively, and the concentrations of IDO that were secreted by MenSCs were measured by ELISA. These results showed that the expression of IDO in MenSCs was upregulated 24 h after IFN-γ priming and reached a high level at 72 h. In addition, IDO continued to be expressed at a high level in MenSCs under H/R treatment conditions after the removal of IFN-γ (Figures 2G and H). Measurement of the IDO levels by ELISA showed that IDO was gradually secreted into the cell culture medium after priming, and when IFN-γ was removed after 72 h of priming, a considerable amount of IDO continued to be secreted by MenSCs under H/R treatment conditions (Figure 2I).

These results indicated that MenSCs could be maintained in a relatively good cell state when exposed to H/R after treatment with a low concentration of IFN-γ. Additionally, IFN-γ priming for 72 h promoted the expression and continuous secretion of IDO by MenSCs. Therefore, we chose 100 ng/mL IFN-γ for 72 h as the strategy for priming MenSCs to ensure that priming would be safe and effective.

IFN-γ-primed MenSCs attenuated liver IRI in the mouse short-term I/R model

The grouping and timeline of the animal experiments are shown in Figure 1. We administered MenSCs and IFN-γ-primed MenSCs (primed MenSCs) to short-term I/R model mice to explore their therapeutic potential. We found that the mice in the IR group showed significant hepatocyte injury after 6 h of reperfusion; this injury manifested as vacuole formation, increased inflammatory cell infiltration, disordered hepatic lobules, and tissue necrosis (Figure 3A), and these effects were accompanied by elevated serum levels of AST and ALT, which are indicators of liver function (Figures 3E and F), and relatively high Suzuki's injury scores (Figure 3B). However, the administration of MenSCs and primed MenSCs resulted in decreased ALT and AST levels, ameliorated IRI, and decreased Suzuki's injury scores (Figures 3A, B, E and F). Additionally, caspase-3 and TUNEL staining of liver tissue sections were performed to observe apoptosis. We reached the same conclusion, namely, that both MenSCs and IFN-primed MenSCs could attenuate I/R-induced hepatocyte apoptosis (Figures 3C and D). Moreover, these results also showed that primed MenSCs exerted a better therapeutic effect than

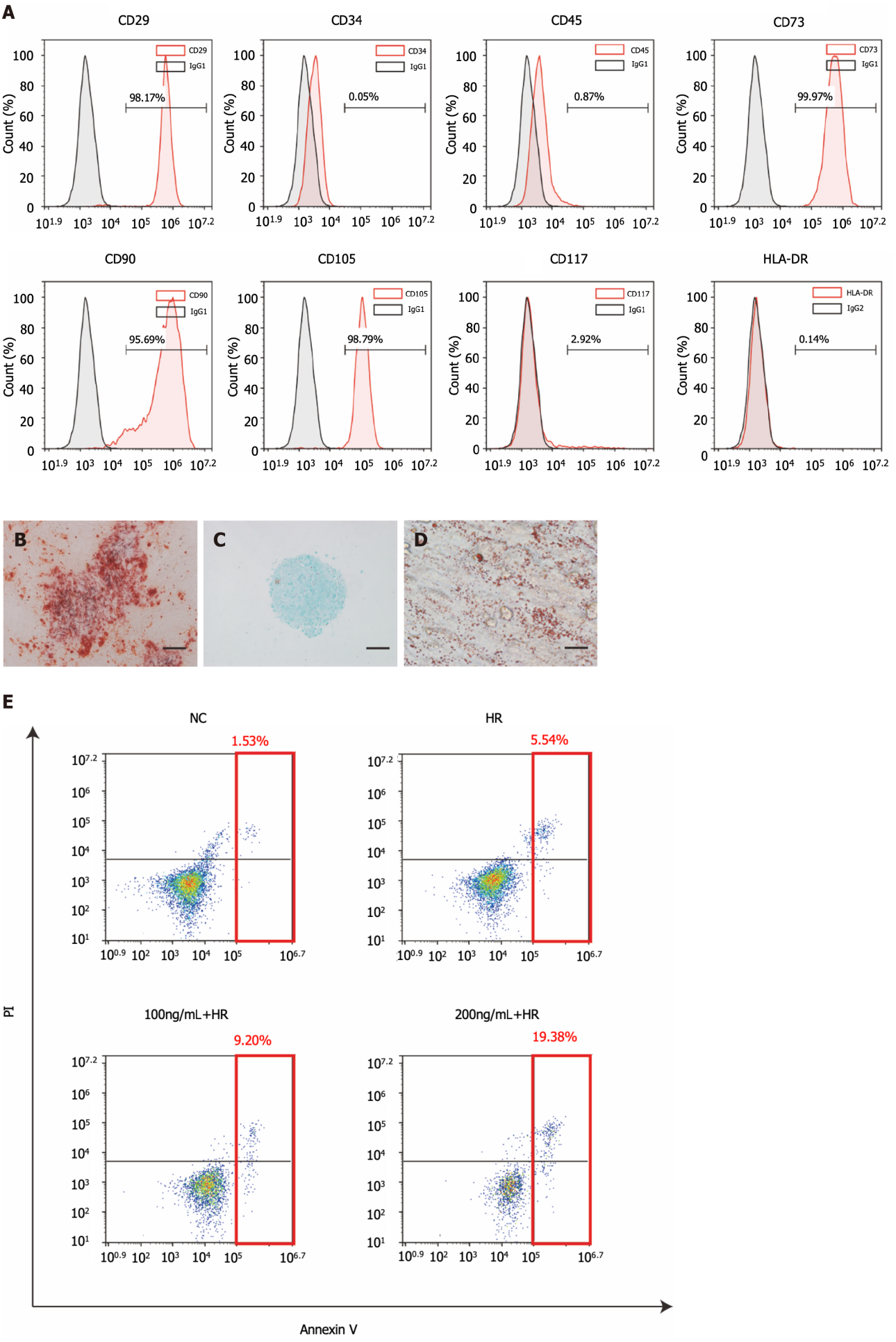
A
CD29
CD29
IgG1
98.17%
CD34
CD34
IgG1
0.05%
CD45
CD45
IgG1
0.87%
CD73
CD73
IgG1
99.97%
CD90
CD90
IgG1
95.69%
CD105
CD105
IgG1
98.79%
CD117
CD117
IgG1
2.92%
HLA-DR
HLA-DR
IgG2
0.14%
Count (%)
B
C
D
E
NC
1.53%
HR
5.54%
100ng/mL+HR
9.20%
200ng/mL+HR
19.38%
PI
Annexin V

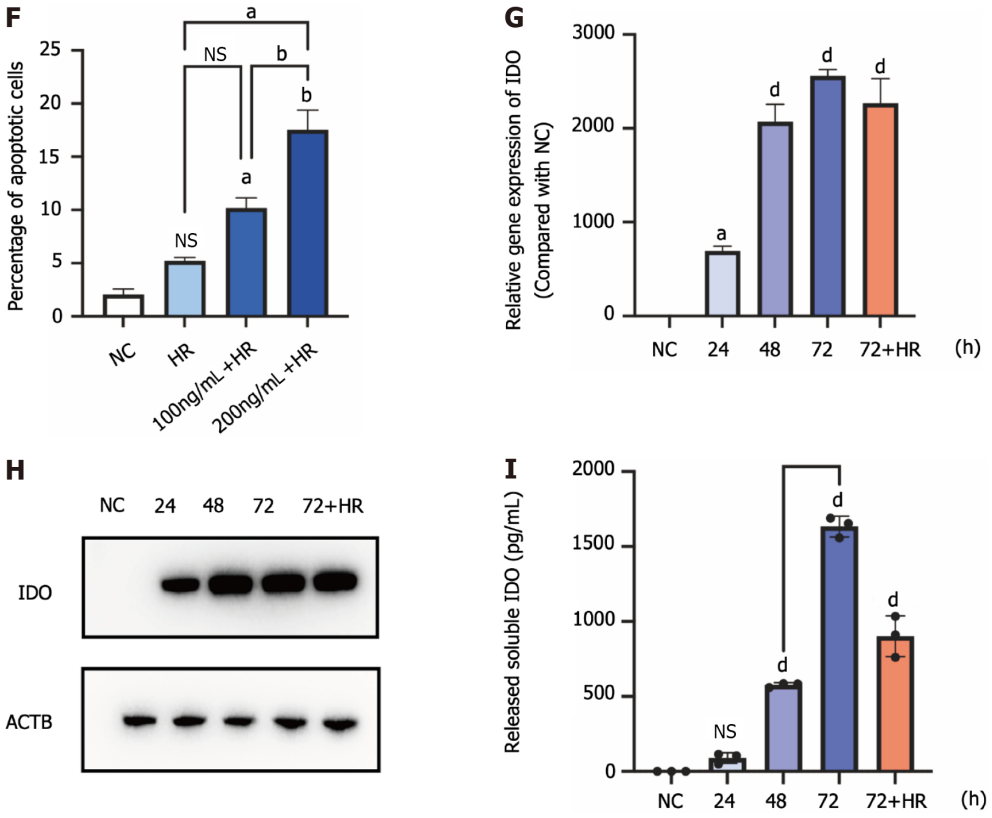

DOI: 10.4252/wjsc.v15.i9.876

Figure 2 Characterization of menstrual blood-derived stromal cells and menstrual blood-derived stromal cells primed with interferon-γ. A: The surface marker expression of menstrual blood-derived stromal cells (MenSCs) was assessed by flow cytometry analysis; B: The osteogenic differentiation potential of MenSCs. Scale bar 200 μm; C: The chondrogenic differentiation potential of MenSCs. Scale bar 200 μm; D: The adipogenic differentiation potential of MenSCs. Scale bar 200 μm; E: MenSC apoptosis was detected by flow cytometry. The red box indicates the sum of late and early apoptotic cells, which represent the overall level of apoptosis; F: The overall level of apoptosis was analyzed; G: After MenSC priming with 100 ng/mL interferon-γ for 24 h, 48 h, 72 h, and 72 h + hypoxia/reoxygenation, the mRNA levels of indoleamine 2,3-dioxygenase (IDO) in MenSCs were determined by quantitative real-time reverse transcription polymerase chain reaction analysis; H: The protein level of IDO in MenSCs was determined by western blotting; I: The level of IDO secreted by MenSCs into the cell culture supernatant was measured by ELISA. The data are shown as the means ± SEMs, $n = 3$. $^{a}P < 0.05$, $^{b}P < 0.01$, $^{c}P < 0.001$, $^{d}P < 0.0001$. NS represents not statistically significant. All *P* values were obtained by one-way ANOVA. HLA-DR: Human leukocyte antigen-DR; IgG: Immunoglobulin G; NC: Negative control; HR: Hypoxia/reoxygenation; PI: Propidium iodide; IDO: Indoleamine 2,3-dioxygenase.

untreated MenSCs (Figures 3A-F).

IFN-γ-primed MenSCs reduced hepatocellular damage and increased the Treg numbers in the mouse long-term I/R model

As IFN-γ-primed MenSCs could exert a better therapeutic effect in the short-term model, we used 7 d of reperfusion after I/R to establish a long-term model in order to further explore the long-term effects of primed MenSCs, particularly their potential to induce immune tolerance.

We found that after 7 d of ischemia, the liver tissues of the mice showed obvious edema, a large cavity, and necrosis, and these conditions resulted in high Suzuki's injury scores. However, MenSCs and particularly IFN-γ-primed MenSCs significantly inhibited these changes (Figures 4A and B). Additionally, we determined the Treg numbers in the spleen to assess the immune tolerance of the mice. To determine the number of Tregs, we analyzed the percentage of cells that were positive for CD4, CD25, and Foxp3. Tregs accounted for approximately 1% of the total lymphocyte population in the sham and IR groups, and primed MenSCs increased the percentage of Tregs in the lymphocyte population to a great extent (Figures 4C and D). However, although untreated MenSCs also increased the percentage of Tregs, no significant difference was found compared with the sham group (Figures 4C and D). To verify the correlation between the stronger immunomodulatory ability of primed MenSCs and IDO, we added 1MT to the drinking water of some mice and found that 1MT clearly reversed the increase in the percentage of Tregs in the spleen and inhibited the protective effect of primed MenSCs on the liver (Figures 4A-D).

These results indicated that after 7 d of reperfusion, IFN-γ-primed MenSCs exerted a stronger and more stable effect on reducing liver injury and increasing the percentage of Tregs in the spleen compared with untreated MenSCs. These stronger therapeutic effects were closely associated with IDO.

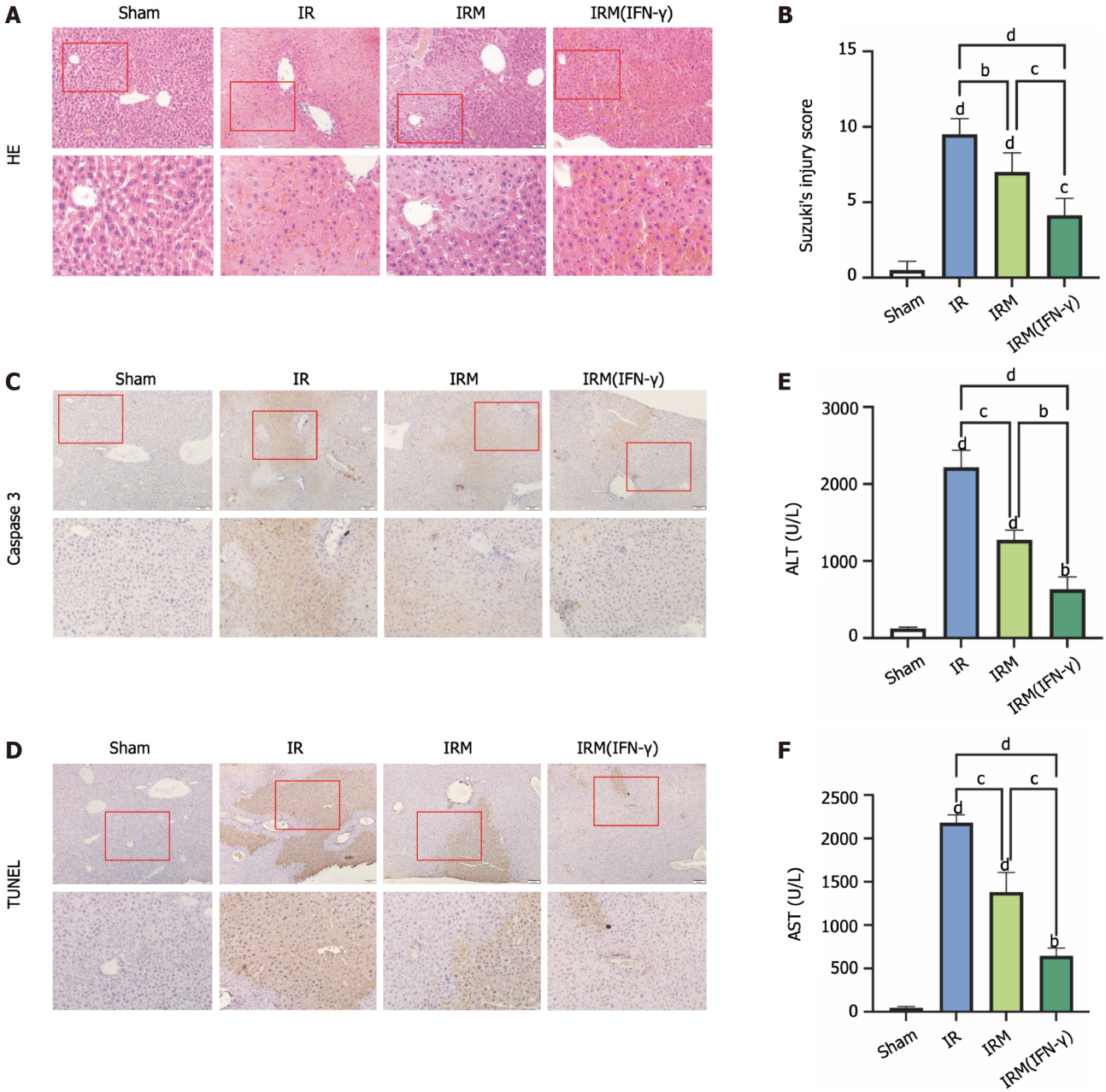

DOI: 10.4252/wjsc.v15.i9.876

Figure 3 Interferon-γ-primed menstrual blood-derived stromal cells attenuated liver ischemia-reperfusion injury in the mouse short-term ischemia-reperfusion model. A: Representative images of histological liver sections stained with hematoxylin and eosin (hematoxylin and eosin staining, magnification 200 ×, images in the second row are partial magnifications of regions indicated by the red box); B: The degree of liver injury in each group was determined according to Suzuki's injury score. The data are expressed as the means ± SEMs (n = 10/group); C: Representative images of liver sections from each group stained for caspase-3 to evaluate the apoptosis level (magnification 200 ×, images in the second row are partial magnifications of regions indicated by the red box); D: Representative liver sections from each group stained with TUNEL were obtained to evaluate the apoptosis level (magnification 200 ×, images in the second row are partial magnifications of regions indicated by the red box); E: The serum alanine aminotransferase levels were measured to indicate liver function levels, the data are expressed as the means ± SEMs (n = 3/group); F: The serum aspartate aminotransferase levels were measured to indicate liver function levels, and the data are expressed as the means ± SEMs (n = 3/group). $^{a}P < 0.05$, $^{b}P < 0.01$, $^{c}P < 0.001$, $^{d}P < 0.0001$. NS represents not statistically significant. All P values were obtained by one-way ANOVA. MenSCs: Menstrual blood-derived stromal cells; IFN-γ: Interferon-γ; IR: Ischemia-reperfusion; IRM: Combination treated with ischemia-reperfusion and menstrual blood-derived stromal cells; IRM (IFN-γ): Combination treated with ischemia-reperfusion and interferon-γ-primed menstrual blood-derived stromal cells; HE: Hematoxylin and eosin; TUNEL: Terminal deoxynucleotidyl transferase-mediated dUTP-biotin Nick End Labeling; ALT: Alanine aminotransferase; AST: Aspartate aminotransferase.

IFN-γ-primed MenSCs promoted autophagy in mouse livers

As described above, we verified that the more significant immunomodulatory effect of primed MenSCs was indeed related to IDO. Strikingly, the more significant effect of primed MenSCs in alleviating liver injury was also associated with IDO. To explore the specific mechanism through which primed MenSCs ameliorate IRI, metabolomics sequencing of mouse liver samples from the short-term model was performed.

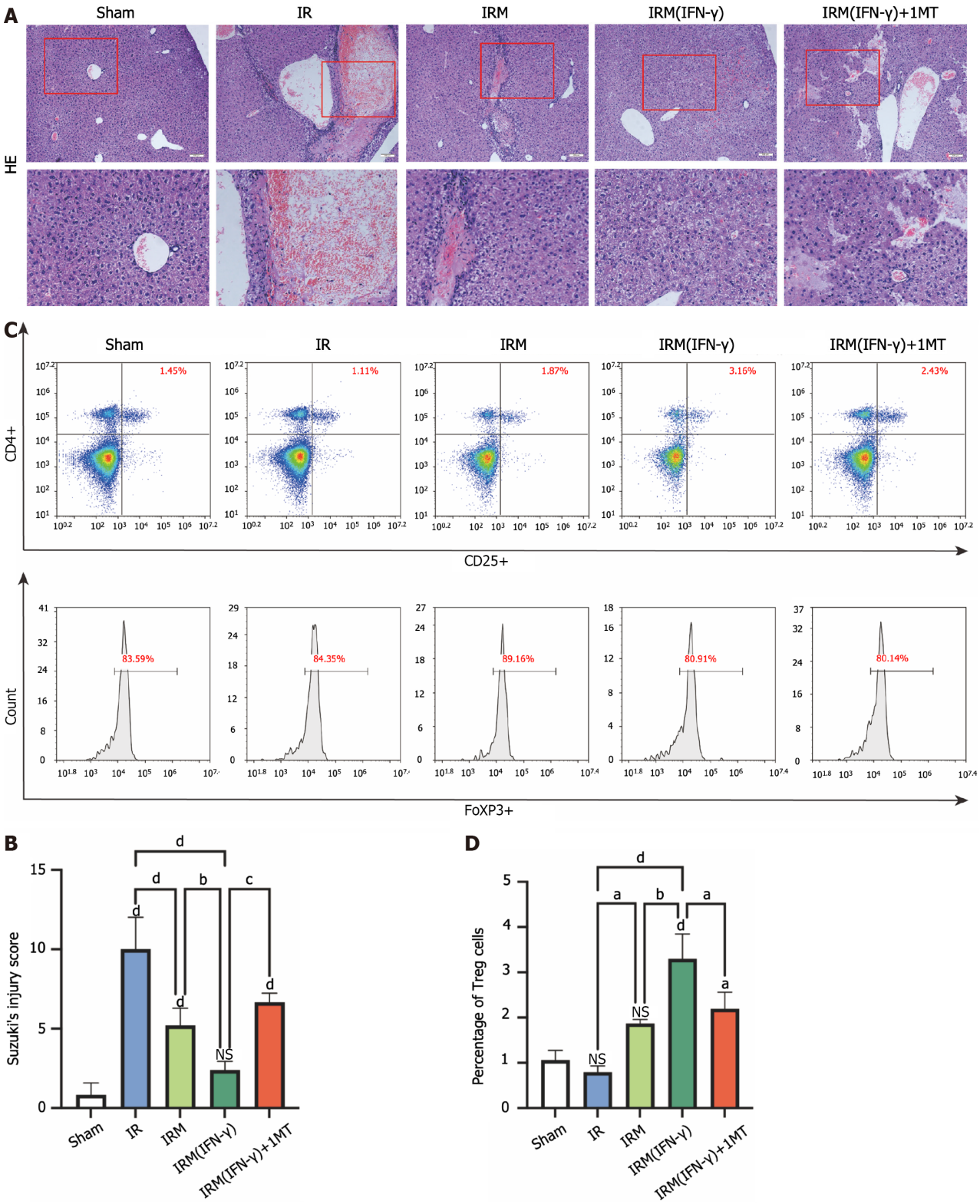

DOI: 10.4252/wjsc.v15.i9.876 **Copyright** ©The Author(s) 2023.

Figure 4 Interferon-γ-primed menstrual blood-derived stromal cells reduced hepatocellular damage and increased the Treg numbers in the mouse long-term ischemia-reperfusion model. A: Representative images of histological liver sections stained with hematoxylin and eosin were obtained (hematoxylin and eosin staining, magnification 200×, images in the second row are partial magnifications of regions indicated by the red box); B: The degree of liver injury in each group was determined according to Suzuki's injury score. The data are expressed as the means ± SEMs (n = 3-5/group); C: The numbers of CD4, CD25, and FoxP3 positive cells (regulatory T cells) in the spleen were determined by flow cytometry to estimate the ability of primed menstrual blood-derived stromal cells to induce immune tolerance; D: The percentages of Tregs are expressed as the means ± SEMs (n = 3/group). $^{a}P < 0.05$, $^{b}P < 0.01$, $^{c}P < 0.001$, $^{d}P < 0.0001$. NS represents not statistically significant. All P values were obtained by one-way ANOVA. MenSCs: Menstrual blood-derived stromal cells; IFN-γ: Interferon-γ; 1MT: 1-methyl-D-tryptophan; IR: Ischemia-reperfusion; IRM: Combination treated with ischemia-reperfusion and menstrual blood-derived stromal cells; IRM (IFN-γ): Combination treated with ischemia-reperfusion and interferon-γ-primed menstrual blood-derived stromal cells; HE: Hematoxylin and eosin; Treg: Regulatory T cell.

PCA and PLS-DA of samples from the two groups were performed to evaluate the degree of aggregation and dispersion of samples within a single group as well as between different groups, and the results indicated that the data could be used for subsequent analysis (Supplementary Figures 1A-D). A statistical heatmap of 45 metabolites that differed between the IR group and IRPM group [IRM (IFN-γ) group] was generated, and the results are also shown in the form of a volcano plot (Figures 5A and B). Kyoto Encyclopedia of Genes and Genomes (KEGG) annotation of the differential metabolites revealed that the differential metabolites are involved in a variety of biological processes, mainly including lipid metabolism, amino acid metabolism, signaling molecule transduction, and membrane transport (Figure 5C). To further elucidate the main biological functions of the differential metabolites, we performed KEGG pathway enrichment analysis of these differential metabolites, and the results showed that the differential metabolites were mainly enriched in autophagy (Figure 5D). Relative quantification of the level of the differential metabolite phosphatidyl ethanolamine (PE), which is related to autophagy, showed that treatment with IFN-γ-primed MenSCs increased the levels of PE in the livers (Figure 5E). The main role of PE in autophagy is mediating the formation of the autophagy membrane marker LC3II from LC3I. A higher PE level is related to a higher level of autophagy[22-25]. Therefore, we hypothesized that primed MenSCs may increase the level of autophagy in mouse liver tissues.

To further verify this hypothesis, we observed the autophagic bodies in mouse liver cells by transmission electron microscopy (TEM) and measured the expression of autophagy-related proteins in liver tissues by western blotting to evaluate the autophagy levels. MenSCs, and primed MenSCs increased the number of autophagosomes in liver tissues, and the increase was most obvious in the IRM (IFN-γ) group (Figures 6A and B). Consistent with the TEM results, LC3II expression was increased after I/R, suggesting that I/R could increase the level of autophagy in hepatocytes (Figures 6C and D). Moreover, the autophagic flux was amplified by MenSCs and particularly by primed MenSCs (Figures 6C and D). Additionally, we observed the changes in the AMPK pathway and the mTOR pathway, which are two classical pathways that are upstream of autophagy, and we found that I/R could promote AMPK phosphorylation and inhibit mTOR phosphorylation; in other words, I/R could activate the AMPK pathway and inhibit the mTOR pathway (Figures 6C and D). Moreover, most of these effects were enhanced by MenSCs and particularly primed MenSCs (Figures 6C and D).

In conclusion, we demonstrated that primed MenSCs amplified I/R-induced autophagy in the mouse livers through metabolome sequencing analysis and molecular biology experiments. However, the relationship between the enhanced autophagy and IDO and whether autophagy is related to the therapeutic effect of MenSCs in alleviating IRI still need to be further clarified.

IFN-γ-primed MenSCs decreased H/R-induced hepatocyte apoptosis via autophagy and IDO

To further investigate the relationship among the therapeutic effect of primed MenSCs, IDO, and enhanced autophagy, we established an *in vitro* H/R model in L02 cells with the corresponding treatment conditions.

First, we exposed L02 cells to H/R for different times to determine an approximately appropriate H/R time. Autophagy-related protein levels were measured by western blotting. The AMPK pathway activation that was caused by hypoxia gradually decreased with increases in the reoxygenation time, and primed MenSCs delayed this process (Supplementary Figure 2A). In addition, we observed that autophagy-related protein expression changed in a time-dependent manner in the mouse model (Supplementary Figure 2B). To allow significant comparisons, we selected 6 h of hypoxia and 4 h of reoxygenation as the H/R conditions.

Apoptotic cells were identified by PI/Annexin V staining, and flow cytometry was performed to analyze cells that were exposed to different treatments. Cells in the upper right corner represent late apoptotic cells, cells in the lower right corner represent early apoptotic cells, and the sum of these two populations represents the overall level of apoptosis. We treated LO2 cells with 3MA (an autophagy inhibitor), 1MT (an IDO inhibitor), MenSCs, and primed MenSCs under normoxic conditions. These treatments alone did not significantly affect apoptosis under normoxic conditions (Figures 7A and B). After H/R, significant L02 cell apoptosis was observed, and the total apoptotic cell proportion accounted for approximately 14.89% of the overall cell population. After treatment of the cells with 3MA to inhibit autophagy under H/R conditions, the total apoptotic cell proportion accounted for approximately 45.06% of the overall cell population (Figures 7A and B). This finding indicated that H/R induced L02 cell apoptosis, and inhibition of autophagy significantly increased H/R-induced apoptosis. In addition, we also observed that the proportion of apoptotic cells was significantly reduced after coculture with MenSCs and particularly with primed MenSCs under H/R conditions, and this result indicated that stem cells can protect L02 cells from H/R-induced apoptosis (Figures 7A and B). A comparison of the HRM (IFN-γ) and HRM (IFN-γ) + 3MA groups revealed that the protective effect of primed MenSCs was significantly reduced when autophagy was inhibited (Figures 7A and B). This finding indicated that primed MenSCs may protect L02 cells against H/R by enhancing autophagy. In addition, a comparison of the HRM (IFN-γ) and HRM (IFN-γ) + 1MT groups showed that inhibition of IDO by 1MT also inhibited the protective effect of primed MenSCs (Figures 7A and B). These results indicated that autophagy reduced H/R-induced apoptosis and that the more powerful protective effect of IFN-γ-primed MenSCs was closely associated with autophagy and IDO.

IDO secreted by primed MenSCs enhanced autophagy by inhibiting the mTOR pathway and activating the AMPK pathway

As mentioned above, primed MenSCs attenuated H/R-induced apoptosis *via* IDO and autophagy. To further investigate whether IDO is related to autophagy, we used 1MT to inhibit IDO and observed changes in autophagy. L02 cells were transfected with pCMV-GFP-LC3, exposed to the indicated treatments and then observed under a fluorescence microscope. We counted the number of intense punctate GFP-LC3 aggregates in each cell to assess autophagy. The results showed that H/R increased the level and aggregation of GFP-LC3 in cells, and this phenomenon was amplified by MenSCs and particularly by primed MenSCs (Figures 8A and B). In addition, the effect of primed MenSCs on GFP-LC3

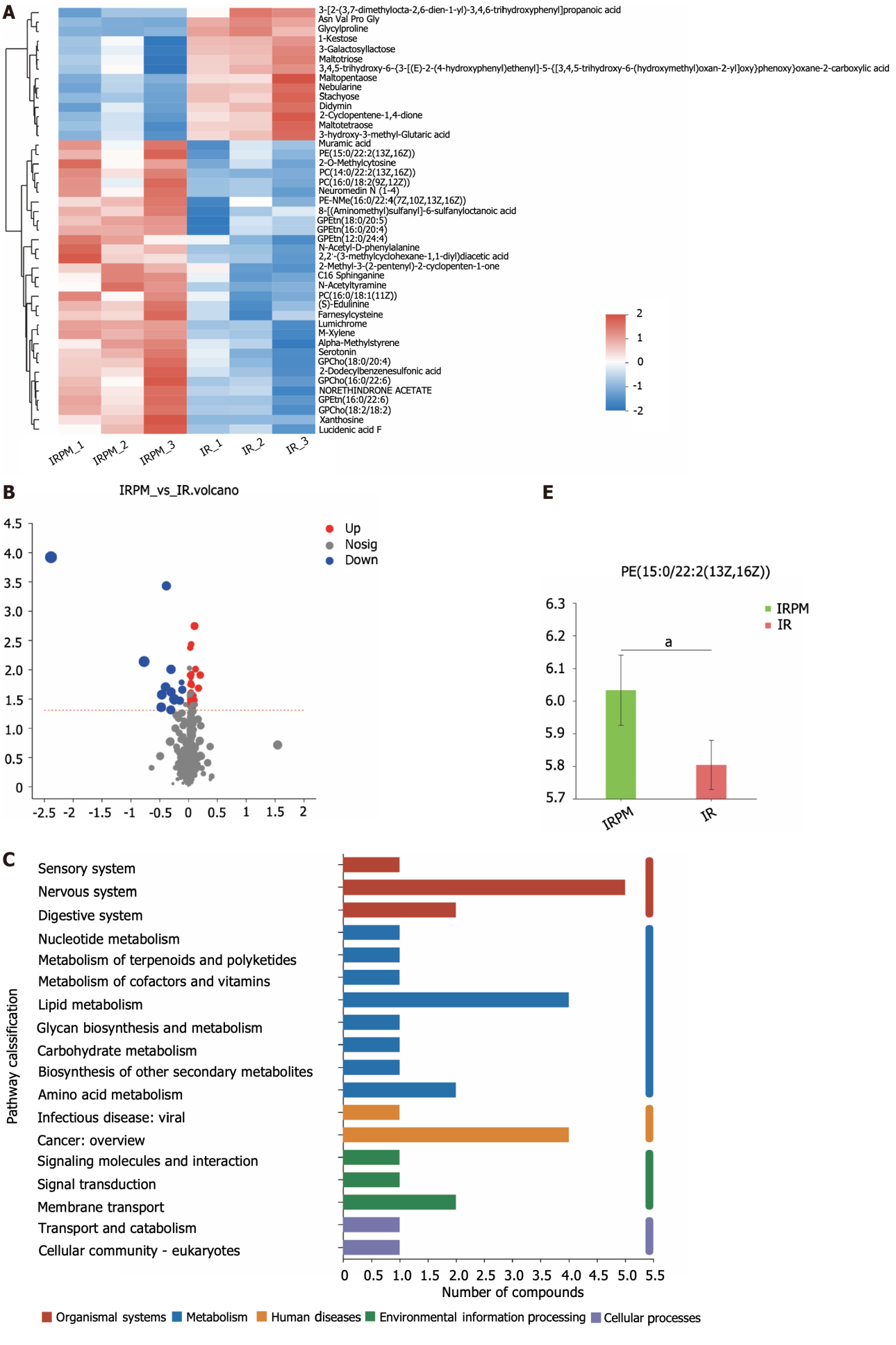
A
3-[2-(3,7-dimethylocta-2,6-dien-1-yl)-3,4,6-trihydroxyphenyl]propanoic acid
Asn Val Pro Gly
Glycylproline
1-Kestose
3-Galactosyllactose
Maltotriose
3,4,5-trihydroxy-6-{3-[(E)-2-(4-hydroxyphenyl)ethenyl]-5-{[3,4,5-trihydroxy-6-(hydroxymethyl)oxan-2-yl]oxy}phenoxy}oxane-2-carboxylic acid
Maltopentaose
Nebularine
Stachyose
Didymin
2-Cyclopentene-1,4-dione
Maltotetraose
3-hydroxy-3-methyl-Glutaric acid
Muramic acid
PE(15:0/22:2(13Z,16Z))
2-O-Methylcytosine
PC(14:0/22:2(13Z,16Z))
PC(16:0/18:2(9Z,12Z))
Neuromedin N (1-4)
PE-NMe(16:0/22:4(7Z,10Z,13Z,16Z))
8-[(Aminomethyl)sulfanyl]-6-sulfanyloctanoic acid
GPEtn(18:0/20:5)
GPEtn(16:0/20:4)
GPEtn(12:0/24:4)
N-Acetyl-D-phenylalanine
2,2'-(3-methylcyclohexane-1,1-diyl)diacetic acid
2-Methyl-3-(2-pentenyl)-2-cyclopenten-1-one
C16 Sphinganine
N-Acetyltyramine
PC(16:0/18:1(11Z))
(S)-Edulinine
Farnesylcysteine
Lumichrome
M-Xylene
Alpha-Methylstyrene
Serotonin
GPCho(18:0/20:4)
2-Dodecylbenzenesulfonic acid
GPCho(16:0/22:6)
NORETHINDRONE ACETATE
GPEtn(16:0/22:6)
GPCho(18:2/18:2)
Xanthosine
Lucidenic acid F
2
1
0
-1
-2
IRPM_1
IRPM_2
IRPM_3
IR_1
IR_2
IR_3
B
IRPM_vs_IR.volcano
Up
Nosig
Down
4.5
4.0
3.5
3.0
2.5
2.0
1.5
1.0
0.5
0
-2.5 -2 -1.5 -1 -0.5 0 0.5 1 1.5 2
E
PE(15:0/22:2(13Z,16Z))
IRPM
IR
6.3
6.2
6.1
6.0
5.9
5.8
5.7
a
IRPM
IR
C
Pathway calssification
Sensory system
Nervous system
Digestive system
Nucleotide metabolism
Metabolism of terpenoids and polyketides
Metabolism of cofactors and vitamins
Lipid metabolism
Glycan biosynthesis and metabolism
Carbohydrate metabolism
Biosynthesis of other secondary metabolites
Amino acid metabolism
Infectious disease: viral
Cancer: overview
Signaling molecules and interaction
Signal transduction
Membrane transport
Transport and catabolism
Cellular community - eukaryotes
0 0.5 1.0 1.5 2.0 2.5 3.0 3.5 4.0 4.5 5.0 5.5
Number of compounds
Organismal systems
Metabolism
Human diseases
Environmental information processing
Cellular processes

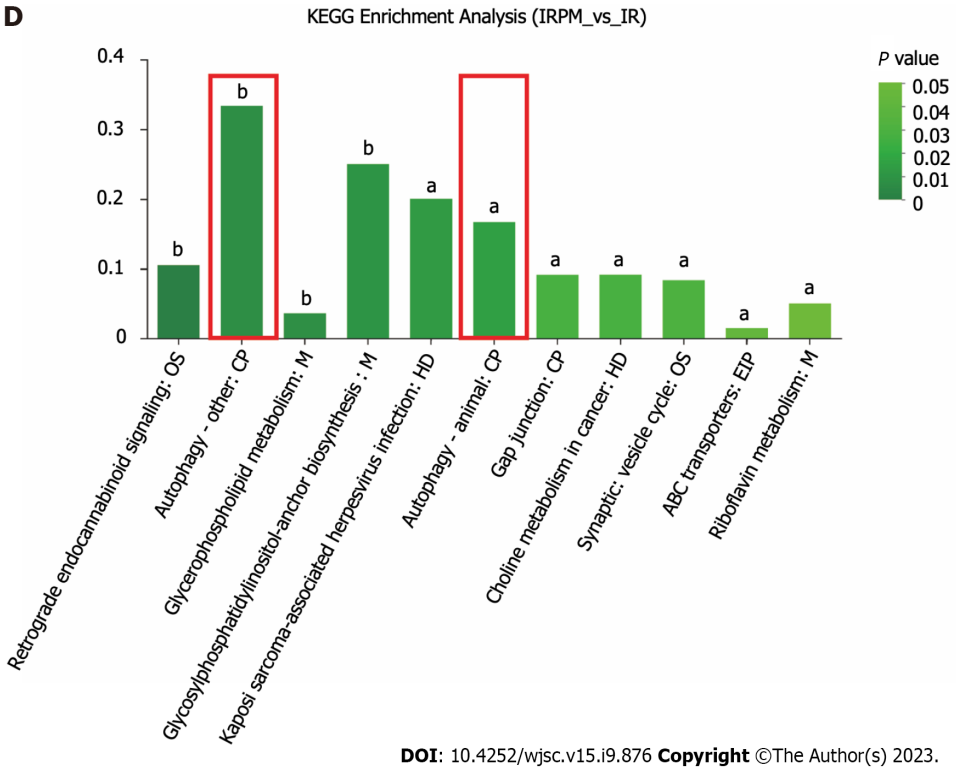

DOI: 10.4252/wjsc.v15.i9.876

Figure 5 Metabolomic data analysis. A: Heatmap of 45 differential metabolites between the ischemia-reperfusion (IR) group and IRM (interferon-γ) group; B: Volcano plot of 45 differential metabolites; C: The relevant pathways in which the differential metabolites are involved were analyzed by comparing the information in the Kyoto Encyclopedia of Genes and Genomes database; D: The main biological functions of differential metabolites were elucidated by pathway enrichment analysis; E: Relative quantitation of the differential metabolite phosphatidyl ethanolamine was performed to measure the effect of primed menstrual blood-derived stromal cells on the level of autophagy in liver tissues. MenSCs: Menstrual blood-derived stromal cells; IFN-γ: Interferon-γ; IR: Ischemia-reperfusion; IRM(IFN-γ) or IRPM: Combination treated with ischemia-reperfusion and interferon-γ-primed menstrual blood-derived stromal cells; PE: Phosphatidyl ethanolamine; OS: Organismal systems; M: Metabolism; HD: Human diseases; CP: Cellular processes; EIP: Environmental information processing; KEEG: Kyoto Encyclopedia of Genes and Genomes.

punctate aggregation was reversed by 1MT, which suggested that IDO was related to the promotion of autophagy (Figures 8A and B). Then, we measured the changes in autophagy-related protein expression by western blotting to further explore how IDO affects autophagy. The results showed that H/R could inhibit the mTOR pathway, activate the AMPK pathway, and increase autophagy, and these effects were enhanced by MenSCs and particularly by primed MenSCs (Figures 8C and D); furthermore, the enhanced effect of primed MenSCs on autophagy was reversed by the IDO inhibitor 1MT (Figures 8C and D). These results indicated that IDO secreted by primed MenSCs enhanced autophagy by inhibiting the mTOR pathway and activating the AMPK pathway.

DISCUSSION

In this study, we found that IDO secreted by IFN-γ-primed MenSCs enhanced the therapeutic effect of MenSCs in the mouse liver I/R model, and the related mechanisms are shown in Figure 9. However, some studies have indicated that the combination of IFN-γ and tumor necrosis factor-alpha (TNF-α) could more efficiently promote the secretion of IDO by MSCs[12]. Although our study showed that priming with 100 ng/mL IFN-γ for 72 h was sufficient to initiate IDO secretion by MenSCs, priming with multiple inflammatory factors to generate better and more functional MenSCs still has a very high experimental value. However, considering that the high concentration of IFN-γ decreased the tolerance of MenSCs to H/R-induced injury (Figures 2E and F), we hypothesized that the priming of MenSCs with multiple inflammatory cytokines may cause more severe damage. Consequently, the side effects of these inflammatory cytokines on MSCs need to be further investigated *in vitro* and *in vivo*.

In addition to priming MSCs with some inflammatory factors, such as transforming growth factor-β, IL-17, TNF-α, and IFN-γ, to promote the secretion of immune regulatory cytokines[26-28], MSCs could also be modified by gene editing to overexpress some immune regulatory factors and thus enhance their therapeutic effects. In one study, MSCs that overexpressed IDO were more effective in alleviating injury in dilated cardiomyopathy in mice and further enhanced the responses of Tregs and Th2 cells[29]. Therefore, subsequent studies may examine the differences in safety, efficacy, and cost between these two approaches to identify the more suitable method of MSC modification.

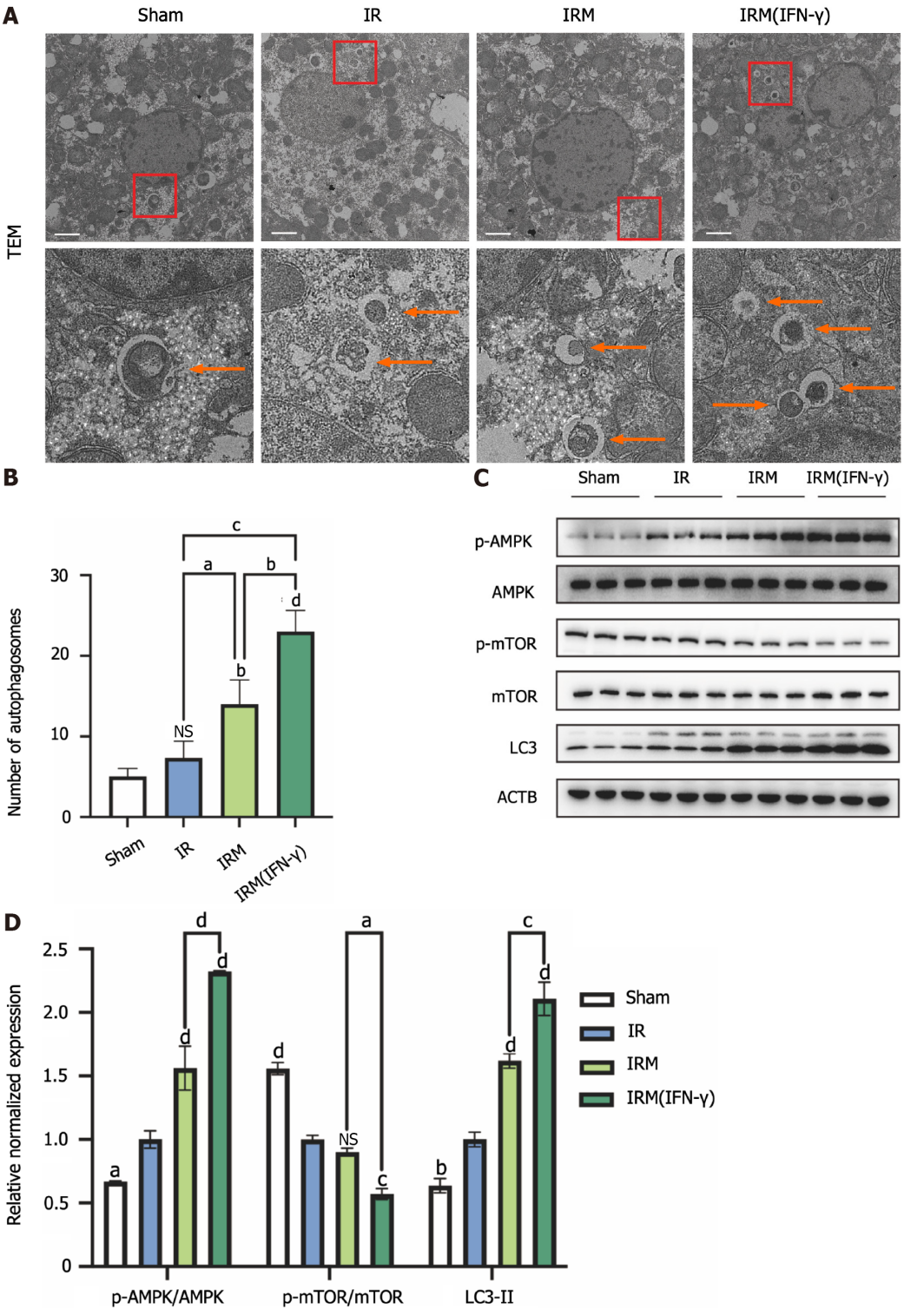

DOI: 10.4252/wjsc.v15.i9.876 **Copyright** ©The Author(s) 2023.

Figure 6 Interferon-γ-primed menstrual blood-derived stromal cells enhanced autophagy in mouse livers. A: Representative TEM images were used to determine the number of autophagic vacuoles in liver tissues from each experimental group. Scale bar 2 μm. The images in the second row are partial magnifications of the regions indicated by the red box; B: The number of autophagosomes was counted by TEM. The data are expressed as the means ± SEMs (n = 3/group); C: The expression of p-AMPK, AMPK, p-mammalian target of rapamycin (p-mTOR), mTOR, LC3, and ACTB in liver tissues was determined by western blotting; D: The relative normalized expression was quantified based on the intensities of the western blot bands (n = 3/group). The data are presented as the means ± SEMs. $^{a}P < 0.05$, $^{b}P < 0.01$, $^{c}P < 0.001$, $^{d}P < 0.0001$. NS represents not statistically significant. All P values were obtained by one-way ANOVA. MenSCs: Menstrual blood-derived stromal cells; IFN-γ: Interferon-γ; IR: Ischemia-reperfusion; IRM: Combination treated with ischemia-reperfusion and menstrual blood-derived stromal cells; IRM (IFN-γ): Combination treated with ischemia-reperfusion and interferon-γ-primed menstrual blood-derived stromal cells; TEM: Transmission electron microscopy; AMPK: The AMP-activated protein kinase signaling pathway; mTOR: Mammalian target of rapamycin; Tregs: Regulatory T cells.

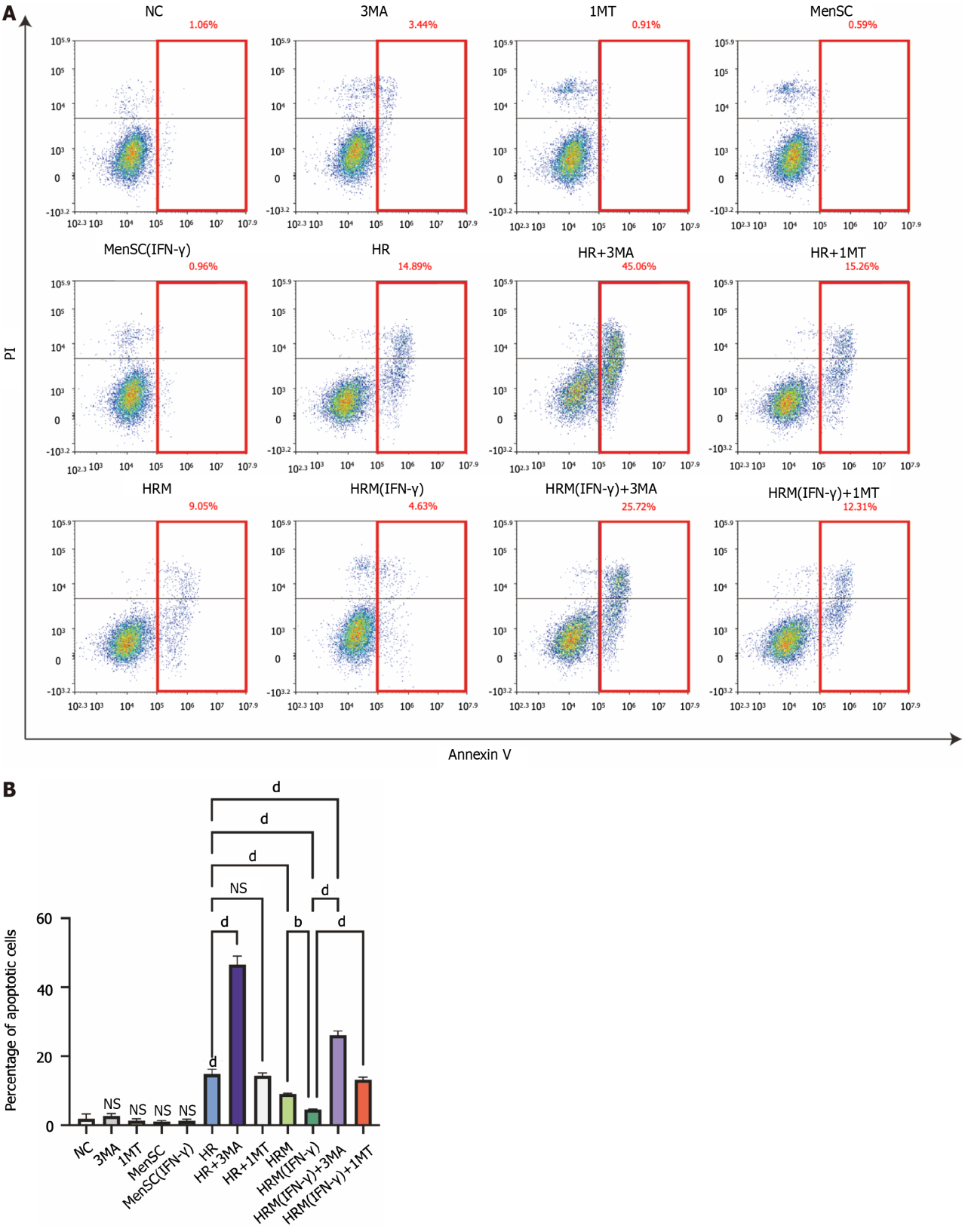

DOI: 10.4252/wjsc.v15.i9.876 **Copyright** ©The Author(s) 2023.

Figure 7 interferon-γ-primed menstrual blood-derived stromal cells decreased hypoxia/reoxygenation-induced cell apoptosis *via* autophagy and indoleamine 2,3-dioxygenase. A: Apoptosis of L02 cells after different treatments was analyzed; B: The sum of the percentage of early apoptotic cells and late apoptotic cells was analyzed. The total percentage of apoptotic cells (sum of the percentage of early apoptotic cells and late apoptotic cells) was analyzed. The data are shown as the mean ± SEM, $n = 3$; $^{b}P < 0.01$, $^{d}P < 0.0001$. NS represents not statistically significant. All P values were obtained by one-way ANOVA. PI: Propidium iodide; NC: Negative control; 3MA: 3-methyladenine; 1MT: 1-methyl-D-tryptophan; MenSCs: Menstrual blood-derived stromal cells; IFN-γ: Interferon-γ; HR: Hypoxia/reoxygenation; HRM: Combination treated with hypoxia/reoxygenation and menstrual blood-derived stromal cells; HRM (IFN-γ): Combination treated with hypoxia/reoxygenation and I interferon-γ-primed menstrual blood-derived stromal cells.

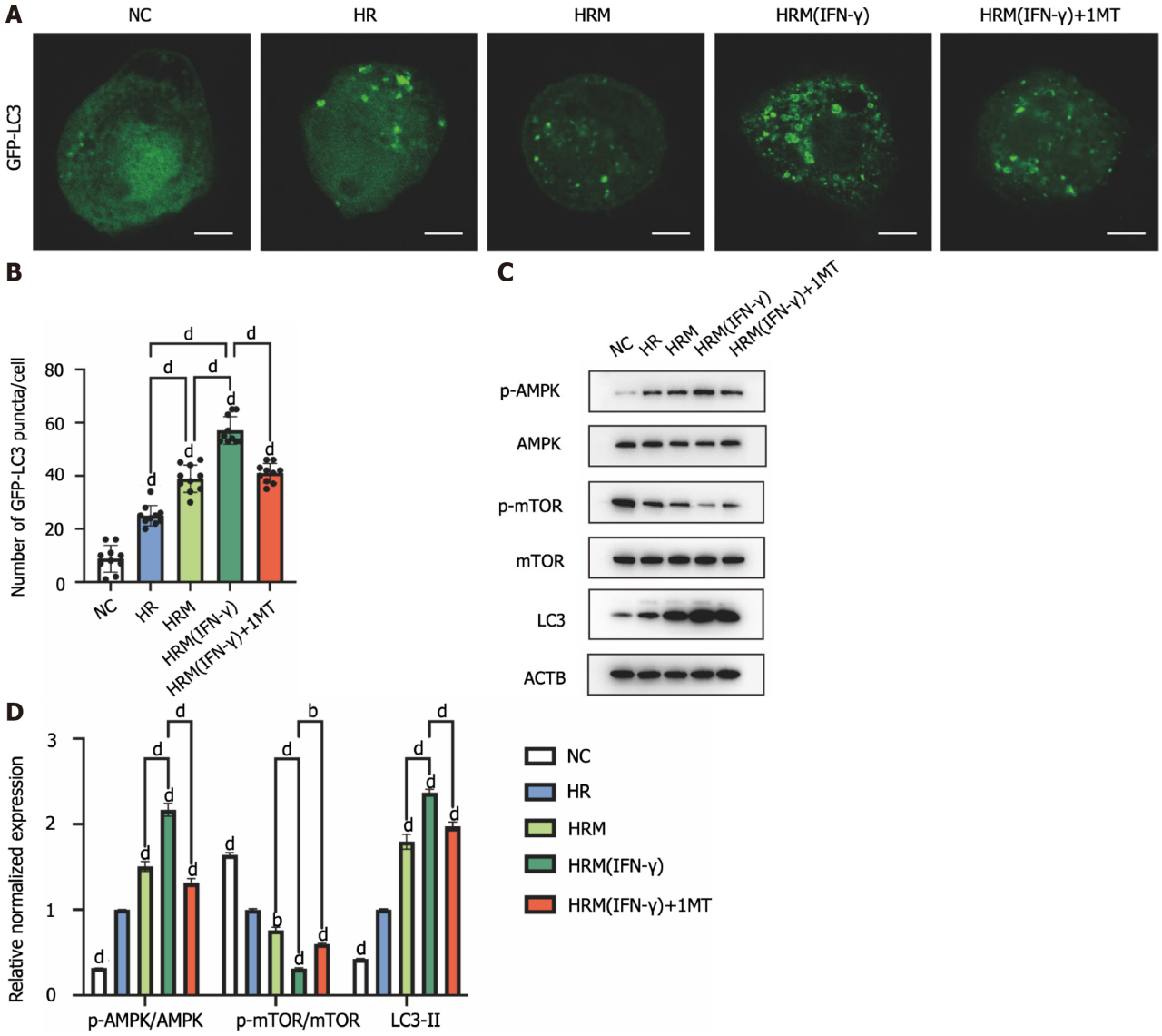

DOI: 10.4252/wjsc.v15.i9.876 **Copyright** ©The Author(s) 2023.

Figure 8 Indoleamine 2,3-dioxygenase secreted by interferon-γ-primed menstrual blood-derived stromal cells enhanced autophagy by inhibiting the mammalian target of rapamycin pathway and activating the AMPK pathway. A: Immunofluorescence images of GFP-LC3. Scale bar 2 μm; B: The number of intense punctate GFP-LC3 aggregates in each cell was counted to determine the level of autophagy in each group. The data are expressed as the means ± SEMs (n = 10/group); C: The expression of p-AMPK, AMPK, p-mammalian target of rapamycin (p-mTOR), mTOR, LC3, and ACTB in L02 cells was determined by western blotting; D: The relative normalized protein expression was quantified based on the intensities of the western blot bands (n = 3/group). The data are presented as the means ± SEMs. $^{a}P < 0.05$, $^{b}P < 0.01$, $^{c}P < 0.001$, $^{d}P < 0.0001$. NS represents not statistically significant. All P values were obtained by one-way ANOVA. NC: Negative control; 3MA: 3-methyladenine; 1MT: 1-methyl-D-tryptophan; MenSCs: Menstrual blood-derived stromal cells; IFN-γ: Interferon-γ; HR: Hypoxia/reoxygenation; HRM: Combination treated with hypoxia/reoxygenation and menstrual blood-derived stromal cells; HRM (IFN-γ): Combination treated with hypoxia/reoxygenation and I interferon-γ-primed menstrual blood-derived stromal cells; AMPK: AMP-activated protein kinase; mTOR: the Mammalian target of rapamycin signaling pathway.

To date, 79 clinical trials involving the use of MSCs to prevent or treat graft-*versus*-host disease (GVHD) have been conducted[30]. Most of the studies demonstrated the safety and efficacy of MSCs, but some studies showed that MSCs did not exert the desired protective effect; differences in the immunomodulatory effects of MSCs may be related to the origin and the dose of MSCs that were used. One study compared the therapeutic potential of MSCs from different origins in a mouse GVHD model and found that bone marrow-derived MSCs (BM-MSCs) induced a rapid proinflammatory response before exerting immunosuppressive effects and that BM-MSCs were less capable of inducing Treg differentiation than umbilical cord blood-derived MSCs (UC-MSCs)[31]. Therefore, differences in the origin of MSCs might be a reason why some MSCs did not exert the expected effects in some studies[7,8]. It has also been suggested that subsequent studies on MSCs may focus on the differences in the therapeutic potential of MSCs that are derived from different sources. Moreover, another study showed that a double dose of UC-MSCs exerted a better therapeutic effect than a single dose of UC-MSCs in a rat dilated cardiomyopathy model[29]. Consequently, in addition to improving MSCs, selecting the right MSC source and the right MSC dose is also crucial for research.

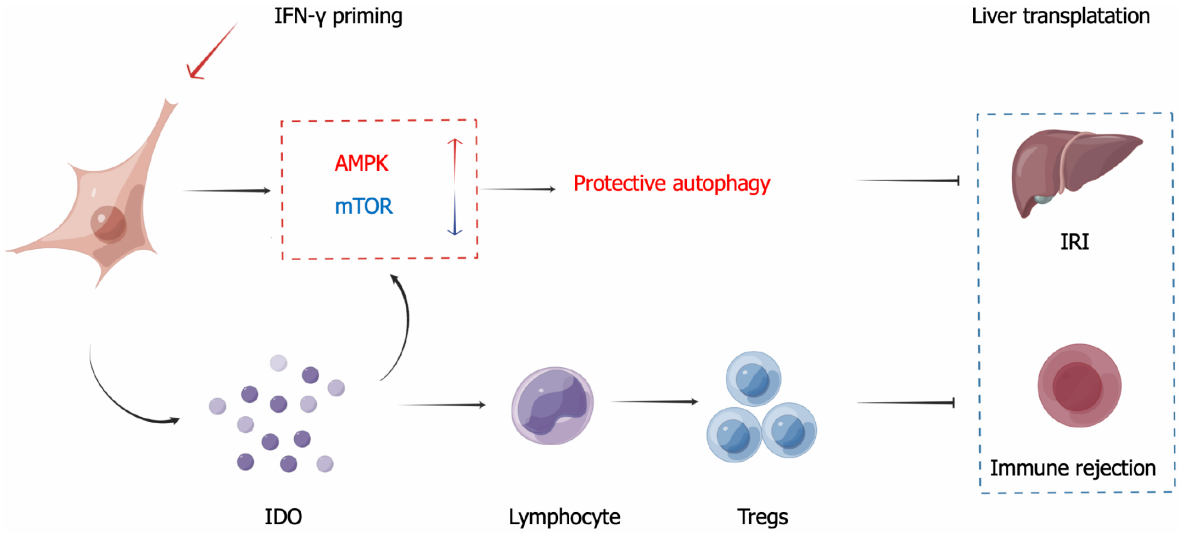

DOI: 10.4252/wjsc.v15.i9.876 **Copyright** ©The Author(s) 2023.

Figure 9 Schematic depiction of the mechanism. Ischemia-reperfusion injury (IRI) and immune rejection are two important factors that affect the prognosis of liver transplantation. After priming menstrual blood-derived stromal cells (MenSCs) with interferon-γ, the MenSCs secreted high levels of indoleamine 2,3-dioxygenase (IDO). On the one hand, MenSCs and IDO enhanced the AMPK-mammalian target of rapamycin-autophagy axis to reduce IRI; on the other hand, IDO promoted the differentiation of lymphocytes into Tregs to reduce immune rejection. IRI: Ischemia-reperfusion injury; MenSCs: Menstrual blood-derived stromal cells; IFN-γ: Interferon-γ; IDO: Indoleamine 2,3-dioxygenase; AMPK: AMP-activated protein kinase signaling pathway; mTOR: Mammalian target of rapamycin signaling pathway; Tregs: Regulatory T cells.

This study found that IDO secreted by IFN-γ-primed MenSCs was found to activate the AMPK pathway and inhibited the mTOR pathway, which resulted in inducing of protective autophagy in hepatocytes. However, the specific mechanism through which IDO activates the AMPK pathway or inhibits the mTOR pathway remains unclear. IDO is a metabolic enzyme that can promote tryptophan metabolism and produce kynurenine. Some studies have shown that IFN-γ priming and IDO overexpression can promote tryptophan depletion and kynurenine accumulation, and these phenomena induce autophagy in cervical cancer cells and promote phagocytosis by macrophages[32]. Studies have also shown that a protective autophagic response and amino acid metabolism, which are driven by IFN-γ-mediated induction of IDO enzyme activity, could inhibit antibody-mediated inflammatory kidney injury in a mouse model of nephrotoxic serum nephritis[33]. Another study showed that glucose metabolism is also related to the T cell inhibition caused by MSCs and IDO[34]. In this study, we found that primed MenSCs increased the relative expression of the autophagy-related metabolite PE in mouse livers, and corresponding experiments proved that primed MenSCs indeed promoted autophagy through IDO; however, we did not conduct targeted metabolomics analyses to quantify the absolute expression of PE. In addition, how IDO causes changes in the levels of PE are unclear. Therefore, further study is needed to determine how IDO triggers autophagy. Notably, tryptophan catabolism by IDO could alter inflammatory responses and favor T-cell tolerance in cancer[35,36]. Although there is no evidence showing that MSCs can promote tumor growth and our previous study showed that MSCs can inhibit the growth of hepatocellular carcinoma through epigenetic regulation[37], the use of primed MSCs in cancer patients may still be controversial.

In addition, because IDO secreted by MSCs could increase the Tregs to induce immune tolerance, as has been observed in several studies[14,17], we paid more attention to the potential of primed MenSCs to reduce liver IRI in this study, and only used the number of Tregs as an indicator to evaluate the MSC-induced - immune tolerance potential. Therefore, although primed MenSCs significantly increased the numbers of Tregs, it is still necessary to verify whether the increased Tregs could alleviate IRI[38] or better induce immune tolerance in the liver transplantation model. Besides, recent studies have shown that macrophage activation and neutrophil infiltration also play important roles in liver IRI[39,40], and the regulation of MSCs to different types of immune cells deserves further study.

Notably, untreated MenSCs could also activate the AMPK pathway, inhibit the mTOR pathway and enhance autophagy in the I/R or H/R models; however, untreated MenSCs secreted little IDO (Figures 2G-I). This finding indicates that the effect of MenSCs in enhancing autophagy is not entirely dependent on IDO and may be related to other mechanisms. How stem cells enhance autophagy in recipient cells is still worth further study.

CONCLUSION

IFN-γ-primed MenSCs could exert a better therapeutic effect in a liver I/R model than untreated MenSCs by secreting higher levels of IDO. On the one hand, MenSCs and IDO enhanced the AMPK-mTOR-autophagy axis to reduce IRI; on the other hand, IDO increased the Treg numbers in the spleen and enhanced the ability of MenSCs to induce immune tolerance. Our study suggests that IFN-γ-primed MenSCs may be a novel and improved MSC product for liver transplantation in the future.

ARTICLE HIGHLIGHTS

Research background

Ischemia-reperfusion injury (IRI) and immune rejection are two important factors that affect the prognosis of liver transplantation. Mesenchymal stem cells (MSCs) have been used in liver transplantation and showed certain beneficial effects.

Research motivation

Some studies have indicated that the effects of MSCs are not very significant. Therefore, there is an urgent to find a new way to make MSCs exert better therapeutic effect.

Research objectives

In this study, we attempted to enhance the therapeutic potential of human menstrual blood-derived stromal cells (MenSCs) in a mouse liver ischemia-reperfusion (I/R) model through interferon-γ (IFN-γ) priming strategies and explore the specific mechanisms.

Research methods

After determining the appropriate priming strategies, we applied MenSCs and primed MenSCs in the short-term and long-term mouse liver I/R models, and compared their therapeutic effects. In order to further explore the specific mechanism, we performed a metabolomic analysis of mouse liver samples.

Research results

IFN-γ-primed MenSCs secreted higher levels of indoleamine 2,3-dioxygenase (IDO), attenuated liver injury, and increased regulatory T cell (Treg) numbers in the mouse spleens to greater degrees than untreated MenSCs. Metabolomics and autophagy analyses proved that primed MenSCs more strongly induced protective autophagy in the mouse livers. Further experiments proved that IDO enhanced the protective autophagy by inhibiting the mammalian target of rapamycin (mTOR) pathway and activating the AMPK pathway.

Research conclusions

IFN-γ-primed MenSCs exerted better therapeutic effects in the liver I/R model through secreting higher IDO levels. IDO, on the one hand, increased Treg numbers in the spleen; on the other hand, activated the AMPK-mTOR-autophagy axis to reduce IRI.

Research perspectives

Our study suggests that IFN-γ-primed MenSCs may be a novel and superior MSC product for liver transplantation in the future, and the specific mechanism of how MSCs or IDO enhance autophagy in recipient cells is still worth further study.

ACKNOWLEDGEMENTS

We thank the *Reference Citation Analysis* (*RCA*, https://www.referencecitationanalysis.com/), which is an artificial intelligence technology-based open multidisciplinary citation analysis database, for its help in searching references. We thank Yu-Chen Zhang, Chen-Yu Yang, Xiao-Xia Wan, and Meng-Han Zhang in the Center of Cryo-Electron Microscopy, Zhejiang University for their technical assistance on TEM. We also thank Jia-Jia Wang, Jing-Yao Chen, Qiong Huang, and Jun-Li Xuan from the core facility platform of Zhejiang University, School of Medicine for their technical support on FACS, IHC, and Fluorescence imaging.

FOOTNOTES

Author contributions: Zhang Q, Zhou SN, Chen LJ, Xu ZY, and Xiang C designed the research study; Zhang Q, Zhou SN, Fu JM, Fang YX, Xu HK, Yuan Y, Huang YQ, Zhang N, and Li YF performed the research; Zhang Q, Zhou SN, and Chen LJ analyzed the data and wrote the manuscript; and all authors have read and approved the final manuscript.

Supported by National Key R&D Program of China, No. 2022YFA1105603 and 2022YFC2304405; Hangzhou Science and Technology Project, China, No. 20200224; National Natural Science Foundation of China, No. 81900563; Key Research & Development Plan of Zhejiang Province, China, No. 2019C03015 and 2020C04016.

Institutional review board statement: The study was reviewed and approved by the Research Ethics Committee of the First Affiliated Hospital of Zhejiang University Institutional Review Board.

Institutional animal care and use committee statement: All procedures involving animals were reviewed and approved by the Laboratory Animal Welfare and Ethics Committee of Zhejiang University (ZJU-IACUC), and the ethics code is ZJU20210299.

Conflict-of-interest statement: All the authors report no relevant conflicts of interest for this article.

Data sharing statement: All data mentioned in the article can be obtained by contacting the corresponding author.

ARRIVE guidelines statement: The authors have read the ARRIVE Guidelines, and the manuscript was prepared and revised according to the ARRIVE Guidelines.

Country/Territory of origin: China

ORCID number: Si-Ning Zhou 0000-0003-3680-2307; Li-Jun Chen 0000-0001-9374-6466; Hui-Kang Xu 0000-0001-8370-6444; Yi-Fei Li 0000-0003-3261-8182; Charlie Xiang 0000-0002-8194-2483.

S-Editor: Wang JJ
L-Editor: A
P-Editor: Zhang XD

REFERENCES

1 **Nakano R**, Tran LM, Geller DA, Macedo C, Metes DM, Thomson AW. Dendritic Cell-Mediated Regulation of Liver Ischemia-Reperfusion Injury and Liver Transplant Rejection. *Front Immunol* 2021; **12**: 705465 [PMID: 34262574 DOI: 10.3389/fimmu.2021.705465]

2 **Yang B**, Duan W, Wei L, Zhao Y, Han Z, Wang J, Wang M, Dai C, Zhang B, Chen D, Chen Z. Bone Marrow Mesenchymal Stem Cell-Derived Hepatocyte-Like Cell Exosomes Reduce Hepatic Ischemia/Reperfusion Injury by Enhancing Autophagy. *Stem Cells Dev* 2020; **29**: 372-379 [PMID: 31969065 DOI: 10.1089/scd.2019.0194]

3 **Yao J**, Zheng J, Cai J, Zeng K, Zhou C, Zhang J, Li S, Li H, Chen L, He L, Chen H, Fu H, Zhang Q, Chen G, Yang Y, Zhang Y. Extracellular vesicles derived from human umbilical cord mesenchymal stem cells alleviate rat hepatic ischemia-reperfusion injury by suppressing oxidative stress and neutrophil inflammatory response. *FASEB J* 2019; **33**: 1695-1710 [PMID: 30226809 DOI: 10.1096/fj.201800131RR]

4 **Grange C**, Bellucci L, Bussolati B, Ranghino A. Potential Applications of Extracellular Vesicles in Solid Organ Transplantation. *Cells* 2020; **9** [PMID: 32033489 DOI: 10.3390/cells9020369]

5 **Zheng J**, Chen L, Lu T, Zhang Y, Sui X, Li Y, Huang X, He L, Cai J, Zhou C, Liang J, Chen G, Yao J, Yang Y. MSCs ameliorate hepatocellular apoptosis mediated by PINK1-dependent mitophagy in liver ischemia/reperfusion injury through AMPKα activation. *Cell Death Dis* 2020; **11**: 256 [PMID: 32312955 DOI: 10.1038/s41419-020-2424-1]

6 **Shi M**, Liu Z, Wang Y, Xu R, Sun Y, Zhang M, Yu X, Wang H, Meng L, Su H, Jin L, Wang FS. A Pilot Study of Mesenchymal Stem Cell Therapy for Acute Liver Allograft Rejection. *Stem Cells Transl Med* 2017; **6**: 2053-2061 [PMID: 29178564 DOI: 10.1002/sctm.17-0134]

7 **Casiraghi F**, Perico N, Podestà MA, Todeschini M, Zambelli M, Colledan M, Camagni S, Fagiuoli S, Pinna AD, Cescon M, Bertuzzo V, Maroni L, Introna M, Capelli C, Golay JT, Buzzi M, Mister M, Ordonez PYR, Breno M, Mele C, Villa A, Remuzzi G; MSC-LIVER Study Group. Third-party bone marrow-derived mesenchymal stromal cell infusion before liver transplantation: A randomized controlled trial. *Am J Transplant* 2021; **21**: 2795-2809 [PMID: 33370477 DOI: 10.1111/ajt.16468]

8 **Vandermeulen M**, Erpicum P, Bletard N, Poma L, Jouret F, Detry O. Effect of the Combination of Everolimus and Mesenchymal Stromal Cells on Regulatory T Cells Levels and in a Liver Transplant Rejection Model in Rats. *Front Immunol* 2022; **13**: 877953 [PMID: 35757737 DOI: 10.3389/fimmu.2022.877953]

9 **Gonzalez-Pujana A**, Igartua M, Santos-Vizcaino E, Hernandez RM. Mesenchymal stromal cell based therapies for the treatment of immune disorders: recent milestones and future challenges. *Expert Opin Drug Deliv* 2020; **17**: 189-200 [PMID: 31918562 DOI: 10.1080/17425247.2020.1714587]

10 **Meenakshi Sundaram R**, Kadapakkam Nandabalan S, Rupert S, Srinivasan P, Sankar P, Patra B, Verma RS, Vennila R, Sathyanesan J, Rajagopal S. Differential immunomodulation of human mesenchymal stromal cells from various sources in an inflammation mimetic milieu. *Cytotherapy* 2022; **24**: 110-123 [PMID: 34740526 DOI: 10.1016/j.jcyt.2021.09.005]

11 **Lim JY**, Kim BS, Ryu DB, Kim TW, Park G, Min CK. The therapeutic efficacy of mesenchymal stromal cells on experimental colitis was improved by the IFN-γ and poly(I:C) priming through promoting the expression of indoleamine 2,3-dioxygenase. *Stem Cell Res Ther* 2021; **12**: 37 [PMID: 33413597 DOI: 10.1186/s13287-020-02087-7]

12 **Sun L**, Wang J, Wang Q, He Z, Sun T, Yao Y, Wang W, Shen P. Pretreatment of umbilical cord derived MSCs with IFN-γ and TNF-α enhances the tumor-suppressive effect on acute myeloid leukemia. *Biochem Pharmacol* 2022; **199**: 115007 [PMID: 35307345 DOI: 10.1016/j.bcp.2022.115007]

13 **Corbett JM**, Hawthorne I, Dunbar H, Coulter I, Chonghaile MN, Flynn CM, English K. Cyclosporine A and IFNγ licencing enhances human mesenchymal stromal cell potency in a humanised mouse model of acute graft versus host disease. *Stem Cell Res Ther* 2021; **12**: 238 [PMID: 33853687 DOI: 10.1186/s13287-021-02309-6]

14 **Deng J**, Li D, Huang X, Li W, Zhao F, Gu C, Shen L, Cao S, Ren Z, Zuo Z, Deng J, Yu S. Interferon-γ enhances the immunosuppressive ability of canine bone marrow-derived mesenchymal stem cells by activating the TLR3-dependent IDO/kynurenine pathway. *Mol Biol Rep* 2022; **49**: 8337-8347 [PMID: 35690960 DOI: 10.1007/s11033-022-07648-y]

15 **Favre D**, Mold J, Hunt PW, Kanwar B, Loke P, Seu L, Barbour JD, Lowe MM, Jayawardene A, Aweeka F, Huang Y, Douek DC, Brenchley JM, Martin JN, Hecht FM, Deeks SG, McCune JM. Tryptophan catabolism by indoleamine 2,3-dioxygenase 1 alters the balance of TH17 to regulatory T cells in HIV disease. *Sci Transl Med* 2010; **2**: 32ra36 [PMID: 20484731 DOI: 10.1126/scitranslmed.3000632]

16 **Matteoli G**, Mazzini E, Iliev ID, Mileti E, Fallarino F, Puccetti P, Chieppa M, Rescigno M. Gut CD103+ dendritic cells express indoleamine 2,3-dioxygenase which influences T regulatory/T effector cell balance and oral tolerance induction. *Gut* 2010; **59**: 595-604 [PMID: 20427394 DOI: 10.1136/gut.2009.185108]

17 **Mebarki M**, Iglicki N, Marigny C, Abadie C, Nicolet C, Churlaud G, Maheux C, Boucher H, Monsel A, Menasché P, Larghero J, Faivre L, Cras A. Development of a human umbilical cord-derived mesenchymal stromal cell-based advanced therapy medicinal product to treat immune and/or inflammatory diseases. *Stem Cell Res Ther* 2021; **12**: 571 [PMID: 34774107 DOI: 10.1186/s13287-021-02637-7]

18 **Chen X**, Wu Y, Wang Y, Chen L, Zheng W, Zhou S, Xu H, Li Y, Yuan L, Xiang C. Human menstrual blood-derived stem cells mitigate bleomycin-induced pulmonary fibrosis through anti-apoptosis and anti-inflammatory effects. *Stem Cell Res Ther* 2020; **11**: 477 [PMID: 33176882 DOI: 10.1186/s13287-020-01926-x]

19 **Xu X**, Jiang W, Chen L, Xu Z, Zhang Q, Zhu M, Ye P, Li H, Yu L, Zhou X, Zhou C, Chen X, Zheng X, Xu K, Cai H, Zheng S, Wu X, Li D, Luo Q, Wang Y, Qu J, Li Y, Zheng W, Jiang Y, Tang L, Xiang C, Li L. Evaluation of the safety and efficacy of using human menstrual blood-derived mesenchymal stromal cells in treating severe and critically ill COVID-19 patients: An exploratory clinical trial. *Clin Transl Med* 2021; **11**: e297 [PMID: 33634996 DOI: 10.1002/ctm2.297]

20 **Zhang S**, Chang Q, Li P, Tong X, Feng Y, Hao X, Zhang X, Yuan Z, Tan J. Concentrated small extracellular vesicles from menstrual blood-derived stromal cells improve intrauterine adhesion, a pre-clinical study in a rat model. *Nanoscale* 2021; **13**: 7334-7347 [PMID: 33889891 DOI: 10.1039/d0nr08942g]

21 **Dominici M**, Le Blanc K, Mueller I, Slaper-Cortenbach I, Marini F, Krause D, Deans R, Keating A, Prockop Dj, Horwitz E. Minimal criteria for defining multipotent mesenchymal stromal cells. The International Society for Cellular Therapy position statement. *Cytotherapy* 2006; **8**: 315-317 [PMID: 16923606 DOI: 10.1080/14653240600855905]

22 **Rockenfeller P**, Koska M, Pietrocola F, Minois N, Knittelfelder O, Sica V, Franz J, Carmona-Gutierrez D, Kroemer G, Madeo F. Phosphatidylethanolamine positively regulates autophagy and longevity. *Cell Death Differ* 2015; **22**: 499-508 [PMID: 25571976 DOI: 10.1038/cdd.2014.219]

23 **Li W**, Luo LX, Zhou QQ, Gong HB, Fu YY, Yan CY, Li E, Sun J, Luo Z, Ding ZJ, Zhang QY, Mu HL, Cao YF, Ouyang SH, Kurihara H, Li YF, Sun WY, Li M, He RR. Phospholipid peroxidation inhibits autophagy *via* stimulating the delipidation of oxidized LC3-PE. *Redox Biol* 2022; **55**: 102421 [PMID: 35964342 DOI: 10.1016/j.redox.2022.102421]

24 **Zhou J**, Li XY, Liu YJ, Feng J, Wu Y, Shen HM, Lu GD. Full-coverage regulations of autophagy by ROS: from induction to maturation. *Autophagy* 2022; **18**: 1240-1255 [PMID: 34662529 DOI: 10.1080/15548627.2021.1984656]

25 **Xu Y**, Wan W. Acetylation in the regulation of autophagy. *Autophagy* 2023; **19**: 379-387 [PMID: 35435793 DOI: 10.1080/15548627.2022.2062112]

26 **Lynch K**, Treacy O, Chen X, Murphy N, Lohan P, Islam MN, Donohoe E, Griffin MD, Watson L, McLoughlin S, O'Malley G, Ryan AE, Ritter T. TGF-β1-Licensed Murine MSCs Show Superior Therapeutic Efficacy in Modulating Corneal Allograft Immune Rejection In Vivo. *Mol Ther* 2020; **28**: 2023-2043 [PMID: 32531237 DOI: 10.1016/j.ymthe.2020.05.023]

27 **Bai M**, Zhang L, Fu B, Bai J, Zhang Y, Cai G, Bai X, Feng Z, Sun S, Chen X. IL-17A improves the efficacy of mesenchymal stem cells in ischemic-reperfusion renal injury by increasing Treg percentages by the COX-2/PGE2 pathway. *Kidney Int* 2018; **93**: 814-825 [PMID: 29132705 DOI: 10.1016/j.kint.2017.08.030]

28 **de Pedro MÁ**, Gómez-Serrano M, Marinaro F, López E, Pulido M, Preußer C, Pogge von Strandmann E, Sánchez-Margallo FM, Álvarez V, Casado JG. IFN-Gamma and TNF-Alpha as a Priming Strategy to Enhance the Immunomodulatory Capacity of Secretomes from Menstrual Blood-Derived Stromal Cells. *Int J Mol Sci* 2021; **22** [PMID: 34830067 DOI: 10.3390/ijms222212177]

29 **Gong C**, Chang L, Sun X, Qi Y, Huang R, Chen K, Wang B, Kang L, Wang L, Xu B. Infusion of two-dose mesenchymal stem cells is more effective than a single dose in a dilated cardiomyopathy rat model by upregulating indoleamine 2,3-dioxygenase expression. *Stem Cell Res Ther* 2022; **13**: 409 [PMID: 35962420 DOI: 10.1186/s13287-022-03101-w]

30 **Li Y**, Hao J, Hu Z, Yang YG, Zhou Q, Sun L, Wu J. Current status of clinical trials assessing mesenchymal stem cell therapy for graft versus host disease: a systematic review. *Stem Cell Res Ther* 2022; **13**: 93 [PMID: 35246235 DOI: 10.1186/s13287-022-02751-0]

31 **Grégoire C**, Ritacco C, Hannon M, Seidel L, Delens L, Belle L, Dubois S, Vériter S, Lechanteur C, Briquet A, Servais S, Ehx G, Beguin Y, Baron F. Comparison of Mesenchymal Stromal Cells From Different Origins for the Treatment of Graft-vs.-Host-Disease in a Humanized Mouse Model. *Front Immunol* 2019; **10**: 619 [PMID: 31001253 DOI: 10.3389/fimmu.2019.00619]

32 **Yang SL**, Tan HX, Niu TT, Liu YK, Gu CJ, Li DJ, Li MQ, Wang HY. The IFN-γ-IDO1-kynureine pathway-induced autophagy in cervical cancer cell promotes phagocytosis of macrophage. *Int J Biol Sci* 2021; **17**: 339-352 [PMID: 33390854 DOI: 10.7150/ijbs.51241]

33 **Chaudhary K**, Shinde R, Liu H, Gnana-Prakasam JP, Veeranan-Karmegam R, Huang L, Ravishankar B, Bradley J, Kvirkvelia N, McMenamin M, Xiao W, Kleven D, Mellor AL, Madaio MP, McGaha TL. Amino acid metabolism inhibits antibody-driven kidney injury by inducing autophagy. *J Immunol* 2015; **194**: 5713-5724 [PMID: 25980011 DOI: 10.4049/jimmunol.1500277]

34 **Böttcher M**, Hofmann AD, Bruns H, Haibach M, Loschinski R, Saul D, Mackensen A, Le Blanc K, Jitschin R, Mougiakakos D. Mesenchymal Stromal Cells Disrupt mTOR-Signaling and Aerobic Glycolysis During T-Cell Activation. *Stem Cells* 2016; **34**: 516-521 [PMID: 26485560 DOI: 10.1002/stem.2234]

35 **Metz R**, Rust S, Duhadaway JB, Mautino MR, Munn DH, Vahanian NN, Link CJ, Prendergast GC. IDO inhibits a tryptophan sufficiency signal that stimulates mTOR: A novel IDO effector pathway targeted by D-1-methyl-tryptophan. *Oncoimmunology* 2012; **1**: 1460-1468 [PMID: 23264892 DOI: 10.4161/onci.21716]

36 **Sharma MD**, Pacholczyk R, Shi H, Berrong ZJ, Zakharia Y, Greco A, Chang CS, Eathiraj S, Kennedy E, Cash T, Bollag RJ, Kolhe R, Sadek R, McGaha TL, Rodriguez P, Mandula J, Blazar BR, Johnson TS, Munn DH. Inhibition of the BTK-IDO-mTOR axis promotes differentiation of monocyte-lineage dendritic cells and enhances anti-tumor T cell immunity. *Immunity* 2021; **54**: 2354-2371.e8 [PMID: 34614413 DOI: 10.1016/j.immuni.2021.09.005]

37 **Wu Y**, Chen X, Zhao Y, Wang Y, Li Y, Xiang C. Genome-wide DNA methylation and hydroxymethylation analysis reveal human menstrual blood-derived stem cells inhibit hepatocellular carcinoma growth through oncogenic pathway suppression *via* regulating 5-hmC in enhancer elements. *Stem Cell Res Ther* 2019; **10**: 151 [PMID: 31151404 DOI: 10.1186/s13287-019-1243-8]

38 **Ren HZ**, Xia SZ, Qin XQ, Hu AY, Wang JL. FOXO1 Alleviates Liver Ischemia-reperfusion Injury by Regulating the Th17/Treg Ratio through the AKT/Stat3/FOXO1 Pathway. *J Clin Transl Hepatol* 2022; **10**: 1138-1147 [PMID: 36381102 DOI: 10.14218/JCTH.2021.00551]

39 **Hu Y**, Zhan F, Wang Y, Wang D, Lu H, Wu C, Xia Y, Meng L, Zhang F, Wang X, Zhou S. The Ninj1/Dusp1 Axis Contributes to Liver Ischemia Reperfusion Injury by Regulating Macrophage Activation and Neutrophil Infiltration. *Cell Mol Gastroenterol Hepatol* 2023; **15**: 1071-1084 [PMID: 36731792 DOI: 10.1016/j.jcmgh.2023.01.008]

40 **Lu T**, Li Q, Lin W, Zhao X, Li F, Ji J, Zhang Y, Xu N. Gut Microbiota-Derived Glutamine Attenuates Liver Ischemia/Reperfusion Injury *via* Macrophage Metabolic Reprogramming. *Cell Mol Gastroenterol Hepatol* 2023; **15**: 1255-1275 [PMID: 36706918 DOI: 10.1016/j.jcmgh.2023.01.004]

World Journal of Stem Cells

Submit a Manuscript: https://www.f6publishing.com

World J Stem Cells 2023 September 26; 15(9): 897-907

DOI: 10.4252/wjsc.v15.i9.897

ISSN 1948-0210 (online)

ORIGINAL ARTICLE

Basic Study

Mechanism of adipose-derived mesenchymal stem cell exosomes in the treatment of heart failure

Lei Wang, Jin-Jin Zhang, Sha-Sha Wang, Liang Li

Specialty type: Endocrinology and metabolism

Provenance and peer review: Unsolicited article; Externally peer reviewed.

Peer-review model: Single blind

Peer-review report's scientific quality classification

Grade A (Excellent): 0
Grade B (Very good): B
Grade C (Good): C
Grade D (Fair): 0
Grade E (Poor): 0

P-Reviewer: Emmert MY, Germany; Vallabhajosyula S, United States

Received: July 27, 2023
Peer-review started: July 27, 2023
First decision: August 3, 2023
Revised: August 16, 2023
Accepted: September 12, 2023
Article in press: September 12, 2023
Published online: September 26, 2023

Lei Wang, Jin-Jin Zhang, Sha-Sha Wang, Liang Li, Department of Geriatric Medicine, Fourth Medical Center of PLA General Hospital, Beijing 100048, China

Corresponding author: Liang Li, MM, Doctor, Department of Geriatric Medicine, Fourth Medical Center of PLA General Hospital, No. 51 Fucheng road, Haidian District, Beijing 100048, China. liliangcc@163.com

Abstract

BACKGROUND

Heart failure (HF) is a global health problem characterized by impaired heart function. Cardiac remodeling and cell death contribute to the development of HF. Although treatments such as digoxin and angiotensin receptor blocker drugs have been used, their effectiveness in reducing mortality is uncertain. Researchers are exploring the use of adipose-derived mesenchymal stem cell (ADMSC) exosomes (Exos) as a potential therapy for HF. These vesicles, secreted by cells, may aid in tissue repair and regulation of inflammation and immune responses. However, further investigation is needed to understand the specific role of these vesicles in HF treatment.

AIM

To investigate the mechanism of extracellular vesicles produced by ADMSC s in the treatment of HF.

METHODS

Exogenous surface markers of ADMSCs were found, and ADMSCs were cultured.

RESULTS

The identification of surface markers showed that the surface markers CD44 and CD29 of adipose-derived stem cells (ADSCs) were well expressed, while the surface markers CD45 and CD34 of ADSCs were negative, so the cultured cells were considered ADSCs. Western blotting detected the Exo surface marker protein, which expressed CD63 protein but did not express calnexin protein, indicating that ADSC-derived Exos were successfully extracted.

CONCLUSION

The secretion of MSCs from adipose tissue can increase ATP levels, block cardiomyocyte apoptosis, and enhance the heart function of animals susceptible to HF. The inhibition of Bax, caspase-3 and p53 protein expression may be related to

this process.

Key Words: Adipose-derived mesenchymal stem cell exosomes; Heart failure; Cardiomyocyte apoptosis

Core Tip: Our study highlights the potential of mesenchymal stem cell exosomes (Exos) from adipose tissue as a promising therapy for heart failure (HF). Administration of adipose-derived mesenchymal stem cell Exos improved cardiac function, evidenced by increased ATP content and enhanced parameters like ejection fraction, fractional shortening, and stroke volume. Furthermore, adipose-derived stem cells (ADSCs)-Exo reduced serum levels of b-type natriuretic peptide and atrial natriuretic peptide, associated with HF progression, and exhibited anti-apoptotic effects by regulating pro- and anti-apoptotic proteins in cardiac tissue. These findings suggest that ADSCs-Exo could prevent cardiomyocyte death and inhibit HF progression.

Citation: Wang L, Zhang JJ, Wang SS, Li L. Mechanism of adipose-derived mesenchymal stem cell exosomes in the treatment of heart failure. *World J Stem Cells* 2023; 15(9): 897-907
URL: https://www.wjgnet.com/1948-0210/full/v15/i9/897.htm
DOI: https://dx.doi.org/10.4252/wjsc.v15.i9.897

INTRODUCTION

Heart failure (HF), which is mainly caused by impaired ventricular diastolic or systolic function, is characterized by arterial ischemia or venous congestion. As the final stage of many diseases, HF is a significant public health issue that needs to be addressed globally[1,2]. Numerous studies have found that HF develops and is directly correlated with cardiac remodeling, while cardiomyocyte apoptosis is an important factor leading to myocardial remodeling[3,4]. Although the clinical treatment of HF has been effective in recent years, the prognosis for patients is generally dismal, and hospitalization and fatality rates are still high. We review recent progress in the diagnosis and treatment of chronic HF. Digoxin has been used clinically for more than 200 years and is an essential drug in the treatment of chronic HF. However, the results of the DIG study confirmed that digoxin did not reduce or increase mortality compared with that of the placebo but was superior to placebo in reducing hospitalization rates for HF. In recent years, with the accumulation of ELITEII, OPTIMAAL and VALIANT studies, especially the results of recent CHARM trials, the role of angiotensin receptor blocker drugs in the treatment of HF has been improved. In particular, there is clear evidence that candesartan and valsartan reduce mortality and disability. The recently published HEAAL study showed that losartan 150 mg daily (high-dose group) was more effective than losartan 50 mg daily (low-dose group) in the treatment of HF. Therefore, it is difficult to explore the pathogenesis of HF and find an effective treatment for HF. Mesenchymal stem cells (MSCs) comprise cells with a wide range of differentiation potential and include MSCs from adipose tissue, umbilical cord, bone marrow, and other sources[5]. Because adipose tissue is more abundant than other MSCs and benefits from simple access and consumption, it has been widely studied by an increasing number of scholars[6,7]. However, adipose-derived MSCs (ADMSCs) have relatively high requirements during storage and transportation, which causes the survival rate of these cells during transplantation to significantly decline. Therefore, the clinical use of adipose-derived stem cells (ADSCs) has certain limitations. Exosomes (Exos) are lipid bilayer vesicles secreted by cells with a diameter of 30-200 nm. In addition to being secreted into cells, these Exos can also be stored for a long time in any environment at 4 °C and easily transported. The discovery of Exos provides a new direction for the clinical use of ADSCs[8,9]. All cells secrete Exos in both normal and pathological states. Exos are mainly involved in intercellular communication and regulate a series of physiological processes in target cells. Exos from different cell types have different functions. Some studies have found that ADSC Exos have the functions of tissue repair and regeneration, inflammation inhibition and immune regulation. However, the effect of ADSC Exos on HF has not been confirmed. The goal of this research is to investigate how ADMSC Exos work to treat HF.

MATERIALS AND METHODS

Animal experiment

The license number for Jinan Pengyue Experimental Animal Breeding Co., LTD sale's of the rats used in this investigation was SCXK (Lu) 2019-0003. There were 30 rats with a body weight of 180-220 g Wistar and 20 C57 mice, all of which were male specific pathogen-free (SPF) grade. All the experimental animals were kept in the SPF animal room, drinking water freely and providing animal feed according to the standard. The room temperature was controlled at 20 °C to 26 °C, and the humidity was controlled at 50%-60%, ensuring that the indoor environment was controlled at 12 h/12 h alternating day and night.

Reagents and instruments

Mouse adipose stem cell complete medium (Suzhou Saiye Biotechnology Co., LTD.); antibodies against Bcl-2, Bax, and caspase-3 (Cell Signaling Technology, United States); hematoxylin staining and eosin staining (Beijing Yili Fine Chemicals Co., LTD.); ELISA kit (Wuhan Fien Biotechnology Co., LTD.); polyvinylidene fluoride (PVDF) transfer membrane (Millipore, United States); goat anti-rabbit IgG antibody that was HRP-labeled (Shanghai Biyuntian Biotechnology Co., LTD.); IE33 heart color exclusive Opo ultrasound instrument (Philips, Netherlands); RM2245 microtome and DW4-B biological microscope (Leica, Germany).

Extraction and culture of ADSCs

Ten C57 mice were sacrificed in a sterile environment, and the subcutaneous adipose tissue of the mice was taken and cut into pieces until the tissue was erosive and placed in a centrifuge tube. Then, 0.5% collagenase type I was added to the centrifuge tube, and the centrifuge tube was digested for 45 min in the dark. After that, an equal volume of α-MEM medium was added to the centrifuge tube to terminate digestion. The mixture in the centrifuge tube was filtered through a 200-mesh sterile steel sieve, and the filter was collected and centrifuged at 15000 r/min for 5 min. The supernatant was thrown away, and an equal volume of red blood cell lysate was added to the centrifuge tube to lyse the cells. After 5 min, the cells were centrifuged again, and then α-MEM complete medium was added to the centrifuge tube to obtain the cell suspension, which was completely spread in the culture dish. After 24 h, the cells began to grow adherent, and all the nonadherent cells were removed. Under a microscope, the cell morphology was observed, and the cell surface expression markers CD29, CD44, CD34 and CD45 were detected by a cell loss analyzer.

Extraction and identification of Exos derived from ADSCs

Fourth-generation ADSCs with a fusion degree of 80% were used, and serum-free MEM was used instead of complete medium. Cell supernatant was collected after 48 h of culture. The cells received the same amount of Exo extraction reagent and were cultured overnight at 4 °C. Then, the cells were placed into a centrifuge tube and centrifuged at 15000 r/min for 30 min to separate the Exos. The morphology of the Exos was identified by transmission electron microscopy, and the protein expression related to the Exos was determined by western blotting.

Grouping and model preparation

Thirty Wistar rats received 7 d of adapted feeding. Using a random number system, the rats were divided into groups that were not given any instructions. (Control group), HF rat model group (HF group), and HF rat model treated with ADSC-derived Exo intervention group (ADSCS-Exo group). Each group included ten rats. Except for the control group, the other rats were intraperitoneally injected with 0.8 mg/kg doxorubicin solution at a dose of 3 mg/kg in the first three weeks and 2 mg/kg in the second 3 wk. For six weeks, the control group of rats received weekly intraperitoneal injections of the same volume of NaCl solution. After the intervention, the cardiac function indices of the rats in each group were measured. The establishment of the rat model of HF was demonstrated by a left ejection fraction (LVEF) of 45%. Rats in the ADSC-Exo group were injected with 100 μL of ADSC-derived Exos suspension at a concentration of 0.2 mg/mL through the tail vein, and identical doses of phosphate buffered saline (PBS) solution were injected into the tail veins of the rats in the control and HF groups. Rats in each group were injected once every 2 d for two consecutive times.

Determination of cardiac function indices

After the drug intervention, the rats in each group were fasted for 12 h and allowed to drink water freely. The rats were fixed in the supine position after receiving an intraperitoneal injection of 20% urethane to induce anesthesia. By using color Doppler echocardiography, cardiac function markers, such as left ventricular ejection fraction, were found. Three consecutive cardiac cycles were used to test each group's LVEF, left ventricular fractional shortening (LVFS), and stroke volume (SV), with the average value being used.

Serum b-type natriuretic peptide and atrial natriuretic peptide levels were measured

The abdominal aortas of rats in each group were sampled for 5 mL of blood. After standing for 2 h at 3000 rpm and 4 °C, the blood samples were centrifuged for 10 min. According to the directions on the ELISA kit, serum b-type natriuretic peptide (BNP) was found. According to the directions on the ELISA kit, BNP and atrial natriuretic peptide (ANP) serum levels were discovered.

The pathological changes in myocardial histopathology were detected by hematoxylin and eosin staining

The rats in each group were killed by cutting the neck and chest to remove the blood stains on the surface of the heart disease. After placing the heart in ice, all tissues except the left ventricular myocardial tissue were removed. Dry filter paper was used to cut part of the left ventricular apex group. After dehydration, the heart was fixed in 4% paraformaldehyde solution, made transparent, and embedded in paraffin sections with a thickness of 4 μm. Hematoxylin and eosin (HE) staining, neutral resin and biopsy tissue were used to observe each group of sections under the microscope to find any abnormal myocardial changes.

Flow cytometry was used to detect cardiomyocyte apoptosis

By using a mechanical process, a single-cell suspension was created. Put AGAR in 200 stainless steel net, cut up the myocardial tissue in 2 net, rub while washed with PBS solution, after being fully knead, collected in AGAR suspension again through 300 mesh sieve, collected after cell suspension in centrifuge tube, in a speed of 2000 r centrifugal 5 min per

minute, suck out and discard the supernatant, collected after the cells. The cells were resuspended with PBS solution at 4 °C, then placed in the centrifuge tube again under the same conditions as above, washed and adjusted the cell density to 1 × 10^5/ mL. The cells were resuspended in 300 μL binding buffer, and after that, the cells were gently mixed with 5 L of Annexin V-FITC. The cells were cultured at room temperature for fifteen minutes, and then 5 μL PI and 200 μL binding buffer were added. To determine which group of cardiomyocytes had undergone apoptosis, the centrifuge tube was placed into a flow cytometer.

Comparison of ATP content in myocardial tissue of rats in each group

One hundred milligrams of rat myocardial tissue was taken, 500 μL of perchloric acid was added, and at room temperature for fifteen minutes, 200 μL of supernatant was taken, and 120 μL of 1 mol/L sodium hydroxide (NaOH) was added. Following a 5-min, 5000 r/min, 4 °C centrifugation, ATP content in rat myocardial tissue was detected by high performance liquid chromatography.

Western blotting was used to detect the protein expression of Bcl-2, Bax, caspase-3 and p53 in myocardial tissue

Fifty milligrams of myocardial tissue from each rat was lysed on ice until tissue homogenization was performed by centrifugation. The DAB technique was used to determine the protein content in the supernatant. The concentrations of the concentration and separation gel were 5% and 8%, respectively. The sample protein was added to the gel well, and the membrane was transferred after electrophoresis for 10 min. After 2 h of incubation, 5% blocking solution was added to the sample, after which it was activated and transported to the PVDF membrane, and the PVDF membrane was blocked for one hour. Overnight, the primary Bcl-2, Bax, caspase-3, and p53 antibodies were added. HRP-labeled secondary antibodies were added and incubated for another 2 h. The PVDF membrane was detected by ECL and imaged.

Statistical methods

SPSS 26.0 software was utilized for the statistical evaluation. The mean and standard deviation of the data were written as (mean ± SD). One-way analysis of variance was used to compare the groups. The LSD-*t* test was used for homogeneity of variance, and the nonhomogeneity of variance was corrected using the *t* test. At $P < 0.05$, statistics were deemed significant.

RESULTS

Morphological changes of ADSCs

ADSCs began to grow adherent after 24 h of primary culture, and the cell fusion rate was 80% at 5-7 d. The size of cells in the first generation was inconsistent, and the morphology was mostly spindle, round and polygon. At the fourth passage, the morphology of ADSCs gradually changed to a long spindle shape, which was similar to that of fibroblasts and arranged in a spiral shape, and the nuclei became significantly larger (Figure 1).

Identification of ADSC surface markers

The ADSC surface markers CD44 and CD29 were positively expressed, and the expression rates were 99.4% and 94.8%, respectively. The ADSC surface markers CD45 and CD34 were negative, with expression rates of 0.026% and 0.213%, respectively. Thus, the cultured cells were ADSCs (Figure 2).

Morphology and protein identification of ADSC-derived Exos

The Exos were spotted using transmission electron microscopy to have a round shape and an unbroken cell membrane (Figure 3A). Western blot detection of Exo surface marker protein showed that CD63 protein was expressed, but Calnexin protein was not expressed, indicating that ADSC-derived Exos were successfully extracted (Figure 3B).

Comparison of cardiac function in each group

Rats in the HF group had considerably lower LVEF, LVFS, and SV values than those in the control group ($P < 0.05$). The LVEF, LVFS, and SV of rats in the ADSCS-EXO group were significantly greater than those in the HF group ($P < 0.05$) (Table 1).

Comparison of BNP and ANP levels in the serum of rats in each group

BNP levels in serum were significantly higher in the HF group of rats and ANP compared to those in the control group ($P < 0.05$). Rats in the ADSCS-Exo group had significantly lower serum levels of BNP and ANP than the HF group ($P < 0.05$) (Table 2).

Comparison of myocardial histopathological changes in each group

The control group cardiomyocytes had a distinct, orderly, and closely packed structure. There was no degeneration or necrosis of the cells and no edema or congestion in the interstitium. The configuration of the cardiomyocytes in the HF group was noticeably different from that of the control group, with obvious swelling, cell degeneration or even necrosis, myocardial fiber breakage, and obvious interstitial edema. In contrast to the HF group, the myocardial tissue of the ADSCS-Exo group was greatly enhanced, with loose arrangement of cardiomyocytes, reduced swelling and necrotic cells (Figure 4).

Table 1 Comparison of left ejection fraction, left ventricular fractional shortening and stroke volume in each group (mean ± SD, %)

Group	*n*	LVEF	LVFS	SV
Control group	10	83.26 ± 3.41	50.01 ± 2.63	0.27 ± 0.03
HF group	10	40.16 ± 2.37[a]	28.65 ± 1.84[a]	0.13 ± 0.02[a]
ADSCs - exobiology group	10	70.85 ± 2.86[a,b]	40.27 ± 2.16[a,b]	0.22 ± 0.03[a,b]
F value		580.8	229.2	68.64
P value		< 0.0001	< 0.0001	< 0.0001

[a]*P* < 0.05, compared to control group.
[b]*P* < 0.05, compared with heart failure group.
ADSC: Adipose-derived stem cells; HF: Heart failure; LVEF: Left ejection fraction; LVFS: Left ventricular fractional shortening; SV: Stroke volume.

Table 2 Comparison b-type natriuretic peptide of and atrial natriuretic peptide contents in serum of rats in each group (mean ± SD, pg/mL)

Group	*n*	BNP	ANP
Control group	10	153.62 ± 10.42	123.46 ± 8.11
HF group	10	518.37 ± 15.91[a]	326.54 ± 11.42[a]
ADSCs - exobiology group	10	225.43 ± 13.65[a,b]	151.27 ± 9.34[a,b]
F value		2044	1283
P value		< 0.0001	< 0.0001

[a]*P* < 0.05, compared to control group.
[b]*P* < 0.05, compared with heart failure group.
ADSC: Adipose-derived stem cells; HF: Heart failure; BNP: B-type natriuretic peptide; ANP: Atrial natriuretic peptide.

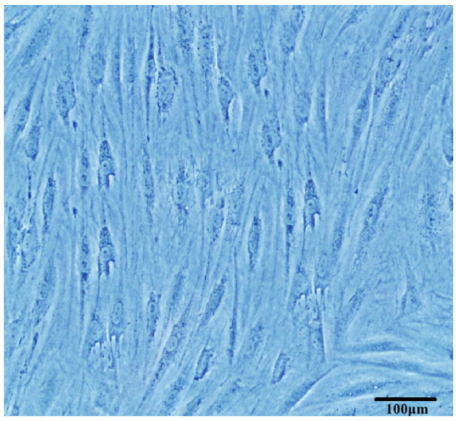

DOI: 10.4252/wjsc.v15.i9.897

Figure 1 Morphology of adipose-derived stem cells at passage 4 (× 100).

Comparison of cardiomyocyte apoptosis rate in each group

The rate of cardiomyocyte apoptosis in the HF group was much greater than that in the control group ($P < 0.05$). The cardiomyocyte apoptosis rate of the ADSC-Exo group was much lower than that of the HF group ($P < 0.05$) (Figure 5).

Comparison of ATP content in myocardial tissue of rats in each group

Rats in the HF group had considerably lower myocardial ATP content than those in the control group ($P < 0.05$). Rats in the ADSCS-Exo group had considerably more ATP in their cardiac tissue than the HF group ($P < 0.05$) (Figure 6).

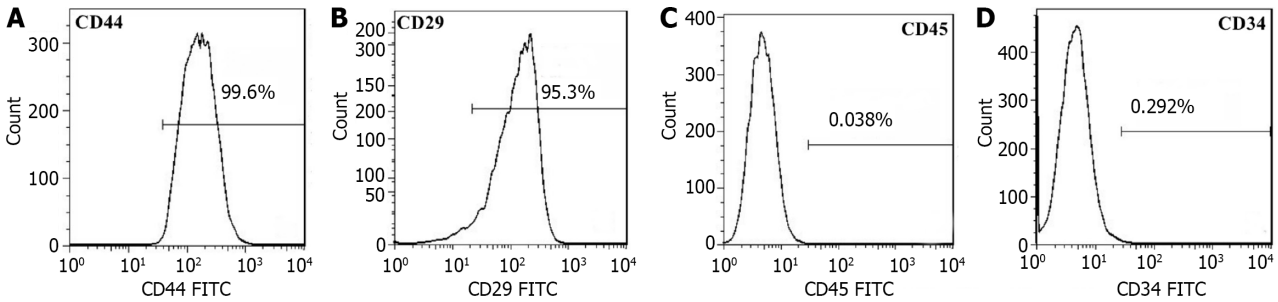

DOI: 10.4252/wjsc.v15.i9.897 **Copyright** ©The Author(s) 2023.

Figure 2 Detection of cell surface markers by flow cytometry. A: Positive expression of CD44; B: Positive expression of CD44; C: Negative expression of CD45; D: Negative expression of CD34.

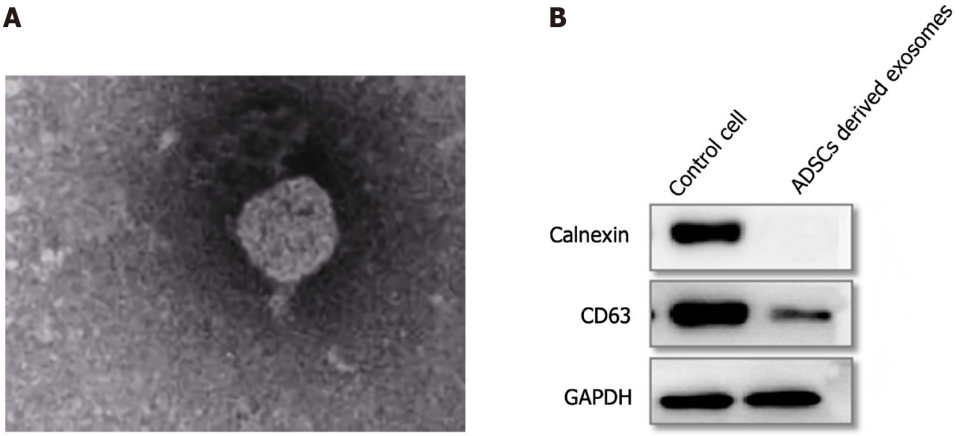

DOI: 10.4252/wjsc.v15.i9.897 **Copyright** ©The Author(s) 2023.

Figure 3 Morphology and protein identification of adipose-derived stem cell-derived exosomes. A: Adipose-derived stem cell (ADSC)-derived exosome morphology seen using transmission electron microscopy (× 15000); B: Surface detection of ADSC-derived exosomes by western blotting. ADSC: Adipose-derived stem cell.

Comparison of protein expression of Bcl-2, Bax, caspase-3 and p53 in myocardial tissue of rats in each group

Bcl-2 protein expression was considerably decreased relative to the control group in the HF group, and the HF group's Bax, caspase-3, and expression levels of the p53 protein were much greater than those of the control group. p53, caspase-3, and Bax protein levels were all substantially lower in the HF group than in the control group, while Bcl-2 protein expression was substantially greater in the ADSC-Exo group than in the HF group ($P < 0.05$) (Figure 7).

DISCUSSION

Current research suggests that HF is a chronic, naturally progressing condition[10]. HF is a disease with a pathogenesis induced by aberrant neuroendocrine system activation, which results in ventricular remodeling and cardiomyocyte death. When cardiomyocyte apoptosis occurs, the myocardium will not only maintain myocardial function due to a large amount of cell loss but also lead to myocardial failure and gradual deterioration when the number of cardiomyocytes is lost, thus forming a vicious cycle of pathological processes[11]. Therefore, by enhancing pump performance, prevention of cardiomyocyte apoptosis can successfully lower the incidence of myocardial remodeling and ease the onset and development of HF. Doxorubicin is a common anthracycline in clinical practice. Doxorubicin has been used to treat a variety of tumors, but its use is limited due to its dose-dependent and delayed cardiotoxicity[12]. Doxorubicin can often cause irreversible damage to the heart, including HF[13]. Doxorubicin was injected intraperitoneally to create a rat HF model for this investigation. LVEF < 45% was detected by cardiac color Doppler ultrasound, demonstrating the establishment of the rat model of cardiac failure. Current research on the molecular mechanism by which doxorubicin causes myocardial damage shows that doxorubicin can interact with DNA and inhibit protein synthesis-induced myocardial cell apoptosis, but there is currently no effective treatment for HF caused by adriamycin; thus, exploring new drugs for HF is a hotspot in current clinical studies[14].

ADSCs can grow rapidly in culture medium without excessive nutrient requirements, have strong proliferation and passage ability and are relatively stable in the genetic process, with multiple differentiation potential. Currently, it has been clinically found that ADSCs can purify ADSC-derived Exos in the supernatant of ADSC culture in either hypoxic or normoxic environments, and the diameter of the Exos is significantly larger than that of previously reported Exos[15].

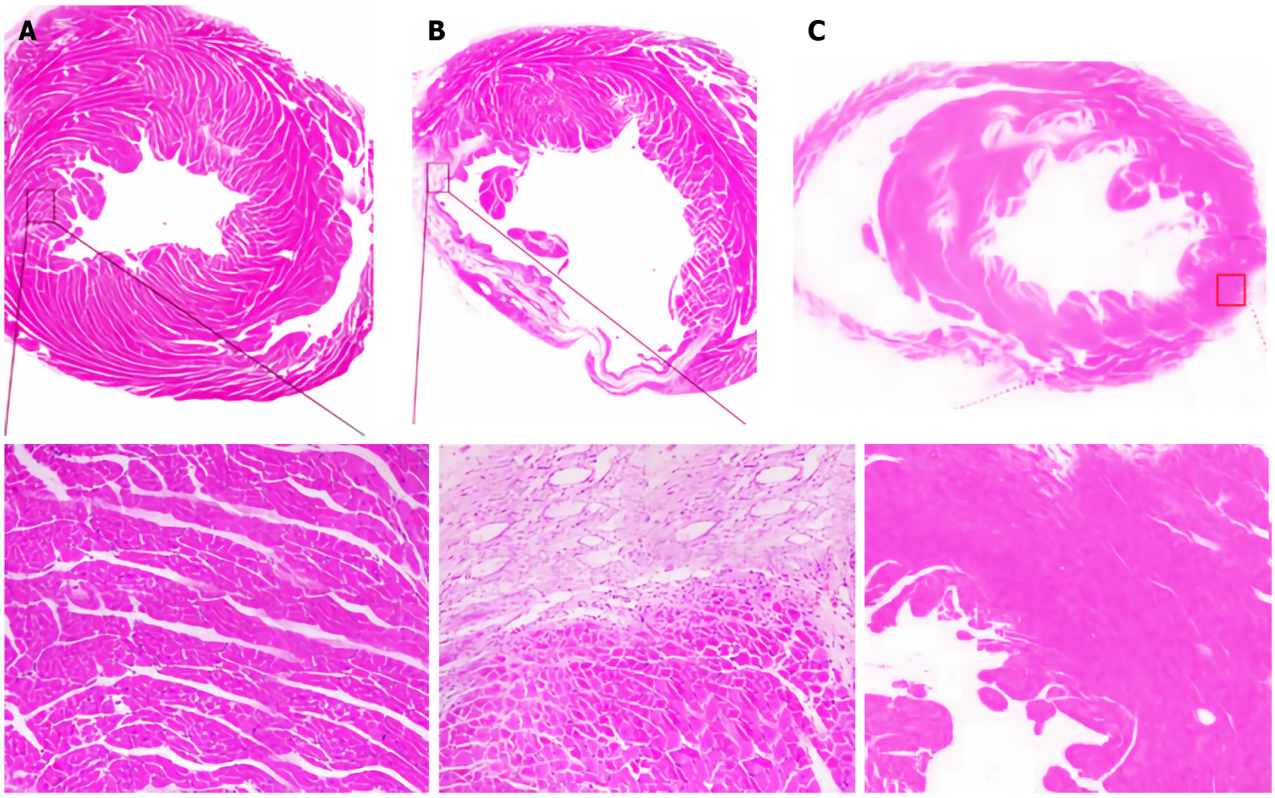

DOI: 10.4252/wjsc.v15.i9.897 **Copyright** ©The Author(s) 2023.

Figure 4 Hematoxylin and eosin staining of rat myocardial tissue. A: Myocardial tissue of rats in control group; B: Myocardial tissue of rats in heart failure group; C: Myocardial tissue of rats in adipose-derived stem cell-exosome group; Col: Control; HF: Heart failure; ADSCs-Exo: Adipose-derived stem cell-exosome.

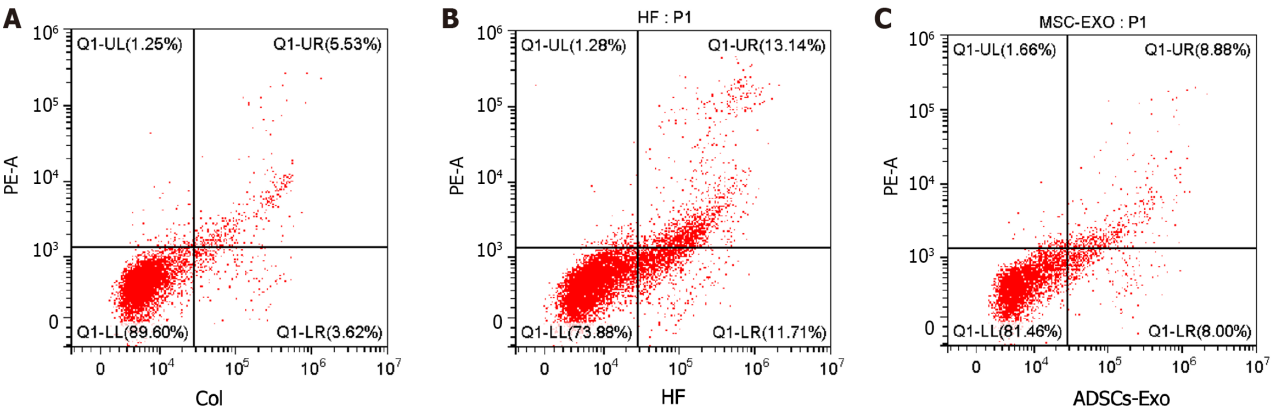

DOI: 10.4252/wjsc.v15.i9.897 **Copyright** ©The Author(s) 2023.

Figure 5 Comparison of cardiomyocyte apoptosis rate in each group. A: Cardiomyocyte apoptosis rate in control group; B: Cardiomyocyte apoptosis rate in heart failure group; C: Cardiomyocyte apoptosis rate in adipose-derived stem cell-exosome group. Col: Control; HF: Heart failure; ADSCs-Exo: Adipose-derived stem cell-exosome.

Numerous studies have found that Exos derived from ADSCs can promote vascular regeneration, wound healing, scar repair, and nerve regeneration and regulate immunity, the inflammatory response and tumor growth[16]. Some scholars have found that through the study of a myocardial ischemia model[17], ASC-derived Exos can inhibit cardiomyocyte apoptosis and alleviate myocardial structural remodeling. In this study, the surface markers of ADSC-Exos were identified, and Exos may be effectively extracted from adipose-derived mesenchymal cells and adipose tissue. After injecting ADSC-Exos into HF rats, it was found that the LVEF, LVFS and SV of rat heart function indices were significantly increased, suggesting that ADSC-Exos could alleviate cardiac function in rats with HF. Sun *et al*[18] discovered that Exos from MSCs generated from adipose tissue may treat old HF rats, and the mechanism may be due to miR-423-mediated control of 5p in the PI3K/Akt signaling pathway.

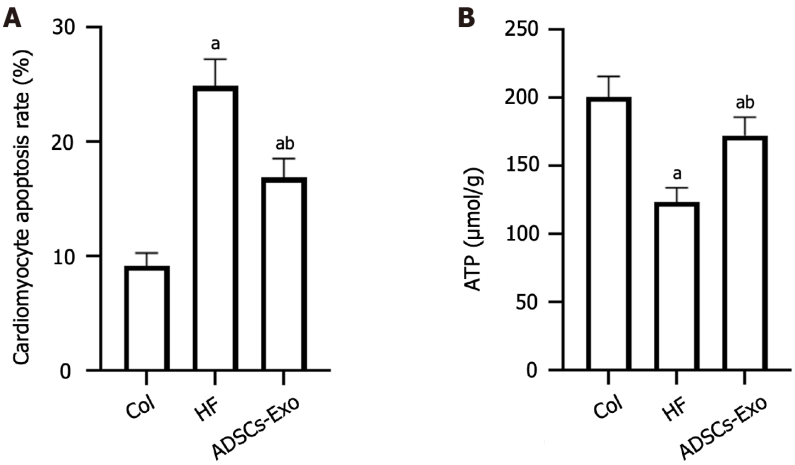

DOI: 10.4252/wjsc.v15.i9.897 **Copyright** ©The Author(s) 2023.

Figure 6 Comparison of ATP content in myocardial tissue of rats in each group. A: Apoptosis rate of cardiomyocytes in three groups of rats; B: ATP content in myocardial tissue of rats in three groups. [a]*P* < 0.05 compared with the control group; [b]*P* < 0.05 compared with the heart failure group. Col: Control; HF: Heart failure; ADSCs-Exo: Adipose-derived stem cell-exosome.

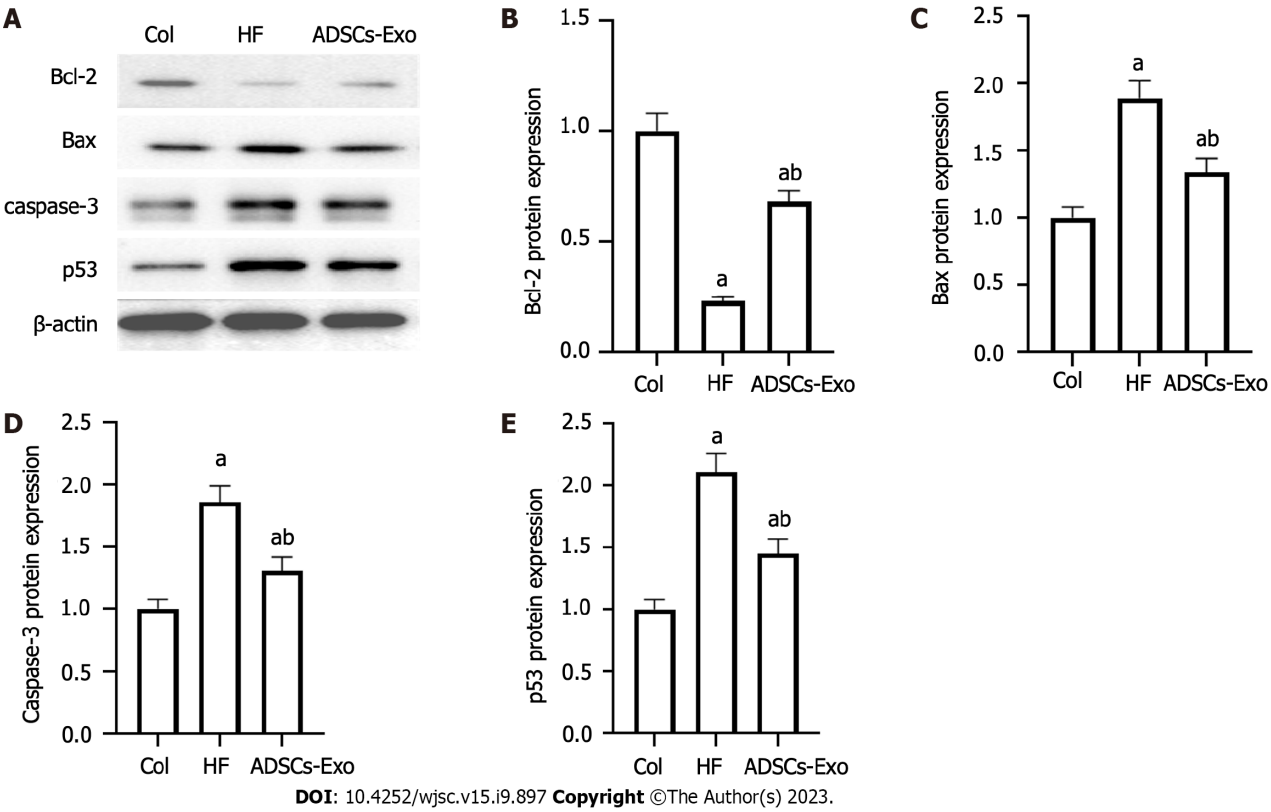

DOI: 10.4252/wjsc.v15.i9.897 **Copyright** ©The Author(s) 2023.

Figure 7 Comparison of the protein expression levels of Bcl-2, Bax, caspase-3, and p53 in the myocardial tissue of rats in each group. A: Myocardial tissue protein electrophoresis detection; B: Protein expression levels of Bcl-2; C: Protein expression levels of Bax; D: Protein expression levels of caspase-3; E: Protein expression levels of p53. [a]*P* < 0.05 compared with the control group; [b]*P* < 0.05 compared with the heart failure group. Col: Control; HF: Heart failure; ADSCs-Exo: Adipose-derived stem cell-exosome.

ANP is mainly synthesized by the atrium, where it is stored and secreted. ANP levels are frequently elevated in a number of illnesses, including HF, coronary heart disease, and chronic pulmonary obstruction, and elevated concentrations suggest poor prognosis. The findings of this investigation demonstrated that rats in the HF group had considerably higher serum levels of BNP and ANP, and serum BNP and ANP concentrations of rats after ADSCS-Exo intervention were significantly decreased, suggesting that by reducing the serum concentrations of BNP and ANP in HF-prone rats, ADSCS-Exo can enhance cardiac function. Chen and Li[19] showed that rats with HF have significantly higher serum levels of ANP and BNP, which can improve the cardiac function of patients by reducing the levels of ANP and BNP. The heart needs energy metabolism to sustain its typical physiological processes and energy needs because the most

direct source of energy for cellular functions is ATP. Some researchers have found that compared that of normal people, ATP in HF patients is significantly reduced by 30%-40%[20]. The findings of this investigation demonstrated that ADSC-Exos can enhance the amount of ATP in HF rat cardiac tissue, demonstrating that when HF occurs, ADSC-Exos can increase the amount of ATP in myocardial tissue and then maintain the energy required for normal myocardial activity by improving the dysfunction of mitochondrial energy metabolism. These results were consistent with the above studies.

The transition from compensatory to decompensatory HF is marked by cardiomyocyte apoptosis, which can be controlled by numerous genes associated with apoptosis, including the pro- and apoptotic protein Bcl-2. Bcl-2 protein family members that have received much research are Bcl-2 and Bax. The Bcl-2 to Bax ratio is highly associated with cell survival or death. By preserving mitochondrial integrity, cytochrome C cannot be released when Bcl-2 is present. By decreasing mitochondrial membrane potential, Bax can cause the release of cytochrome C and certain apoptotic precursors into the cytoplasm, and cytochrome C can form apoptotic bodies by activating APAF-1 and caspase-9. Cytochrome C can induce apoptosis by activating caspase-3 and caspase-7. P53 is a pro-apoptotic transcription factor that can mediate the induction of cardiomyocyte apoptosis and accelerate the progression of HF. When HF occurs, DNA is damaged in cardiomyocytes, and p53 protein is activated, which can accelerate the development of HF by inducing cardiomyocyte apoptosis by upregulating the competitive binding of Bax protein to Bcl-2 and lowering the Bcl-2 to Bax ratio by downregulating the expression of Bcl-2. The results of this study showed that ADSC-Exos could inhibit the expression of Bax, caspase-3 and p53 proteins in cardiac tissue and thereby improve cardiac function by inhibiting cardiomyocyte apoptosis. Sun *et al*[21] demonstrated that ADSC-Exo treatment can boost the production of the protein Bcl-2 while decreasing the presence of Bax and caspase-3 in cardiomyocytes and upregulate the ratio of Bcl-2/Bax to inhibit cardiomyocyte apoptosis, enhancing heart function in rats suffering from cardiomyocyte apoptosis.

CONCLUSION

In conclusion, our findings suggest that MSC Exos derived from adipose tissue have the potential to improve heart health in rats with HF. This finding is supported by the observed increase in ATP content and improvement in cardiac function parameters, such as LVEF, LVFS, and SV. In addition, the administration of ADSC-Exos was associated with a significant reduction in serum BNP and ANP levels, indicating a potential cardioprotective effect. Furthermore, ADSC-Exo treatment suppressed the expression of proteins involved in apoptosis, including Bax, caspase-3, and p53, while promoting the expression of the anti-apoptotic protein Bcl-2 in cardiac tissue.

These findings imply that ADSC-Exos may prevent cardiomyocyte death and inhibit the progression of HF. The ability of ADSC-Exos to modulate key factors involved in cell survival and apoptosis suggests their potential therapeutic application for treating HF. However, further research is needed to fully understand the underlying mechanisms and to optimize the dosage and administration protocol. Nevertheless, this study provides valuable insights into the potential use of ADSC-Exos as a novel therapeutic strategy for HF.

ARTICLE HIGHLIGHTS

Research background

This paper discusses the significant public health issue of heart failure (HF) and the limited efficacy of current treatment options. It explores the use of digoxin and angiotensin receptor blockers in HF treatment, with conflicting results regarding mortality reduction. The paper introduces mesenchymal stem cells (MSCs), specifically adipose-derived MSCs (ADMSCs), as a potential solution. However, storage and transportation requirements limit their clinical use. Exosomes (Exos), lipid bilayer vesicles secreted by cells, are proposed as an alternative. These Exos can be stored and transported easily and have shown potential in tissue repair, inflammation inhibition, and immune regulation. The aim of the research is to investigate the use of ADMSC Exos for treating HF.

Research motivation

The research motivation of the paper is to address the global public health issue of HF and the limitations of current treatment options. The authors aim to explore the potential of ADMSC Exos as a novel therapy for HF. By investigating the effects of these Exos on heart function, the researchers seek to provide insights into new diagnostic and treatment strategies for chronic HF.

Research objectives

The research objectives of the paper are to review the current state of diagnosis and treatment for chronic HF, explore the potential use of ADMSC Exos as a therapy, investigate the limitations of ADMSCs for clinical use, examine the functions of MSC Exos, and evaluate their effectiveness in treating HF. The ultimate goal is to contribute to the development of more effective diagnostic and treatment strategies for HF.

Research methods

The exogenous surface markers of adipose derived MSCs were found and adipose derived MSCs were cultured.

Research results

The identification of surface markers showed that the surface markers CD44 and CD29 of adipose-derived stem cells (ADSCs) were well expressed, while the surface markers CD45 and CD34 of ADSCs were negative, so the cultured cells were ADSCs. Western blotting detected the Exo surface marker protein, which expressed CD63 protein but did not express calnexin protein, indicating that ADSCs derived Exos were successfully extracted.

Research conclusions

The secretion of MSCs from adipose tissue can increase ATP level, block cardiomyocyte apoptosis, and enhance the heart function of animals susceptible to HF. The inhibition of Bax, caspase-3 and p53 protein expression may be related to this process.

Research perspectives

Current research suggests that HF is a chronic condition caused by neuroendocrine system activation, leading to ventricular remodeling and cardiomyocyte death. Preventing cardiomyocyte apoptosis is crucial in managing HF. Doxorubicin, a chemotherapy drug, can cause heart damage. ADSC Exos have shown potential in promoting heart regeneration and immune regulation. They can inhibit cardiomyocyte apoptosis, alleviate structural remodeling, and improve cardiac function. ADSC Exos may achieve these effects through the PI3K/Akt signaling pathway. Elevated levels of atrial natriuretic peptide (ANP) are associated with HF, and ADSC Exos can reduce ANP and b-type natriuretic peptide concentrations, improving cardiac function. ADSC Exos can also increase ATP content in cardiac tissue to maintain normal myocardial activity. They inhibit the expression of apoptotic proteins while promoting anti-apoptotic protein expression, thus improving cardiac function. Overall, ADSC Exos have therapeutic potential for HF, but further research is needed.

FOOTNOTES

Author contributions: Wang L, Zhang JJ, and Wang SS contributed equally to this work and are co-first authors. Wang L, Zhang JJ, and Wang SS proposed the overall research goal and designed the research plan and model design, conducted statistical processing and analysis of the data, and are responsible for writing the first draft of the paper; Wang L, Zhang JJ, Wang SS, and Li L conducted feasibility analysis, review and supervision of the experiment; and are responsible for the review, revision and quality control of the paper; and all authors determined the final draft of the paper.

Institutional animal care and use committee statement: This study was approved by the Experimental Animal Ethics Committee of Fourth Medical Center of PLA General Hospital.

Conflict-of-interest statement: All the authors report no relevant conflicts of interest for this article.

Data sharing statement: The datasets generated and analyzed during the current study are available from the corresponding author on reasonable request.

ARRIVE guidelines statement: The authors have read the ARRIVE guidelines, and the manuscript was prepared and revised according to the ARRIVE guidelines.

Country/Territory of origin: China

ORCID number: Liang Li 0000-0001-9652-9782.

S-Editor: Wang JJ
L-Editor: A
P-Editor: Zhang XD

REFERENCES

1 **Lopaschuk GD**, Karwi QG, Tian R, Wende AR, Abel ED. Cardiac Energy Metabolism in Heart Failure. *Circ Res* 2021; **128**: 1487-1513 [PMID: 33983836 DOI: 10.1161/CIRCRESAHA.121.318241]

2 **Anker SD**, Butler J, Filippatos G, Ferreira JP, Bocchi E, Böhm M, Brunner-La Rocca HP, Choi DJ, Chopra V, Chuquiure-Valenzuela E, Giannetti N, Gomez-Mesa JE, Janssens S, Januzzi JL, Gonzalez-Juanatey JR, Merkely B, Nicholls SJ, Perrone SV, Piña IL, Ponikowski P, Senni M, Sim D, Spinar J, Squire I, Taddei S, Tsutsui H, Verma S, Vinereanu D, Zhang J, Carson P, Lam CSP, Marx N, Zeller C, Sattar N, Jamal W, Schnaidt S, Schnee JM, Brueckmann M, Pocock SJ, Zannad F, Packer M; EMPEROR-Preserved Trial Investigators. Empagliflozin

in Heart Failure with a Preserved Ejection Fraction. *N Engl J Med* 2021; **385**: 1451-1461 [PMID: 34449189 DOI: 10.1056/NEJMoa2107038]

3 **Bauersachs J**. Heart failure drug treatment: the fantastic four. *Eur Heart J* 2021; **42**: 681-683 [PMID: 33447845 DOI: 10.1093/eurheartj/ehaa1012]

4 **Andrzejewska A**, Dabrowska S, Lukomska B, Janowski M. Mesenchymal Stem Cells for Neurological Disorders. *Adv Sci (Weinh)* 2021; **8**: 2002944 [PMID: 33854883 DOI: 10.1002/advs.202002944]

5 **Xie X**, Zhang W, Wang H, Li L, Feng Z, Wang Z, Pan X. Dynamic adaptive residual network for liver CT image segmentation. *Comput Electr Eng* 2021; **91**: 107024 [DOI: 10.1016/j.compeleceng.2021.107024]

6 **Gentile P**, Garcovich S. Systematic Review: Adipose-Derived Mesenchymal Stem Cells, Platelet-Rich Plasma and Biomaterials as New Regenerative Strategies in Chronic Skin Wounds and Soft Tissue Defects. *Int J Mol Sci* 2021; **22** [PMID: 33546464 DOI: 10.3390/ijms22041538]

7 **Wang X**, Zhu Y, Wu C, Liu W, He Y, Yang Q. Adipose-Derived Mesenchymal Stem Cells-Derived Exosomes Carry MicroRNA-671 to Alleviate Myocardial Infarction Through Inactivating the TGFBR2/Smad2 Axis. *Inflammation* 2021; **44**: 1815-1830 [PMID: 33881681 DOI: 10.1007/s10753-021-01460-9]

8 **Xie X**, Pan X, Shao F, Zhang W, An J. Mci-net: Multi-scale context integrated network for liver ct image segmentation. *Comput Electr Eng* 2022; **101**: 108085 [DOI: 10.1016/j.compeleceng.2022.108085]

9 **Liu H**, Zhang M, Shi M, Zhang T, Lu W, Yang S, Cui Q, Li Z. Adipose-derived mesenchymal stromal cell-derived exosomes promote tendon healing by activating both SMAD1/5/9 and SMAD2/3. *Stem Cell Res Ther* 2021; **12**: 338 [PMID: 34112236 DOI: 10.1186/s13287-021-02410-w]

10 **Ramu B**, Masotti M, Tedford RJ, Cogswell RJ. Heart Transplantation in Adriamycin-Associated Cardiomyopathy in the Contemporary Era of Advanced Heart Failure Therapies. *JACC CardioOncol* 2021; **3**: 294-301 [PMID: 34396337 DOI: 10.1016/j.jaccao.2021.02.010]

11 **Xie X**, Pan X, Zhang W, An J. A context hierarchical integrated network for medical image segmentation. *Comput Electr Eng* 2022; **101**: 108029 [DOI: 10.1016/j.compeleceng.2022.108029]

12 **Wang C**, Liang J, Yang W, Wang S, Yu J, Jia P, Du Y, Wang M, Li Y, Zheng X. Ultra-Performance Liquid Chromatography-Q-Exactive Orbitrap-Mass Spectrometry Analysis for Metabolic Communication between Heart and Kidney in Adriamycin-Induced Nephropathy Rats. *Kidney Blood Press Res* 2022; **47**: 31-42 [PMID: 34662875 DOI: 10.1159/000519015]

13 **Zhang J**, Zhang S, Yang Y, Liu L. Transplantation of umbilical cord blood-derived mesenchymal stem cells as therapy for adriamycin induced-cardiomyopathy. *Bioengineered* 2022; **13**: 9564-9574 [PMID: 35387551 DOI: 10.1080/21655979.2022.2061145]

14 **Fang Y**, Zhang Y, Zhou J, Cao K. Adipose-derived mesenchymal stem cell exosomes: a novel pathway for tissues repair. *Cell Tissue Bank* 2019; **20**: 153-161 [PMID: 30852701 DOI: 10.1007/s10561-019-09761-y]

15 **Shen T**, Zheng QQ, Shen J, Li QS, Song XH, Luo HB, Hong CY, Yao K. Effects of Adipose-derived Mesenchymal Stem Cell Exosomes on Corneal Stromal Fibroblast Viability and Extracellular Matrix Synthesis. *Chin Med J (Engl)* 2018; **131**: 704-712 [PMID: 29521294 DOI: 10.4103/0366-6999.226889]

16 **González-Cubero E**, González-Fernández ML, Gutiérrez-Velasco L, Navarro-Ramírez E, Villar-Suárez V. Isolation and characterization of exosomes from adipose tissue-derived mesenchymal stem cells. *J Anat* 2021; **238**: 1203-1217 [PMID: 33372709 DOI: 10.1111/joa.13365]

17 **Chai HT**, Sheu JJ, Chiang JY, Shao PL, Wu SC, Chen YL, Li YC, Sung PH, Lee FY, Yip HK. Early administration of cold water and adipose derived mesenchymal stem cell derived exosome effectively protects the heart from ischemia-reperfusion injury. *Am J Transl Res* 2019; **11**: 5375-5389 [PMID: 31632517]

18 **Sun LH**, Lv ZY, Xing SF, Zhang YL, Zhang Y. [Role of mIR-423-5p in treatment of aged HF rats with adipose mesenchymal stem cells-derived exosomes and its mechanism]. *Chinese J Geriatric Heart Brain Vessel Diseases* 2020; 1308-1311 [DOI: 10.3969/j.issn.1009-0126.2020.12.020]

19 **Chen HM**, Li SS. [Effects of fasudil on cardiac function and BNP hs-CRP ET-1 and ANP in patients with heart failure]. *Hebei Med* 2020; 576-580

20 **Blanco-Rivero J**, Couto GK, Paula SM, Fontes MT, Rossoni LV. Enhanced sympathetic neurotransduction in the superior mesenteric artery in a rat model of heart failure: role of noradrenaline and ATP. *Am J Physiol Heart Circ Physiol* 2021; **320**: H563-H574 [PMID: 33164582 DOI: 10.1152/ajpheart.00444.2020]

21 **Sun BX**, Li XJ, Cai QL, Jia YJ. [Effect of New Shengmai Decoction on apoptosis and protein expression of Bax,Bcl-2, and Caspase-3 of cardiomyocyte induced by adriamycin]. *Chin Tradit Herb Drugs* 2020; **51**: 433-438 [DOI: 10.7501/j.issn.0253-2670.2020.02.021]

World Journal of Stem Cells

Submit a Manuscript: https://www.f6publishing.com

World J Stem Cells 2023 September 26; 15(9): 908-930

DOI: 10.4252/wjsc.v15.i9.908

ISSN 1948-0210 (online)

ORIGINAL ARTICLE

Basic Study

Multiomics reveal human umbilical cord mesenchymal stem cells improving acute lung injury *via* the lung-gut axis

Lu Lv, En-Hai Cui, Bin Wang, Li-Qin Li, Feng Hua, Hua-Dong Lu, Na Chen, Wen-Yan Chen

Specialty type: Cell and tissue engineering

Provenance and peer review: Unsolicited article; Externally peer reviewed.

Peer-review model: Single blind

Peer-review report's scientific quality classification

Grade A (Excellent): A
Grade B (Very good): B
Grade C (Good): C, C
Grade D (Fair): 0
Grade E (Poor): 0

P-Reviewer: Shamseldeen AM, Egypt; Sheykhhasan M, Iran; Sultana N, Bangladesh; Li SC, United States

Received: May 12, 2023
Peer-review started: May 12, 2023
First decision: June 29, 2023
Revised: July 23, 2023
Accepted: September 6, 2023
Article in press: September 6, 2023
Published online: September 26, 2023

Lu Lv, En-Hai Cui, Bin Wang, Feng Hua, Hua-Dong Lu, Na Chen, Wen-Yan Chen, Department of Respiratory and Critical Care Medicine, Huzhou Central Hospital, Affiliated Huzhou Hospital, Zhejiang University School of Medicine, Huzhou 313000, Zhejiang Province, China

Li-Qin Li, Traditional Chinese Medicine Key Laboratory Cultivation Base of Zhejiang Province for the Development and Clinical Transformation of Immunomodulatory Drugs, Huzhou 313000, Zhejiang Province, China

Corresponding author: En-Hai Cui, BM BCh, Doctor, Department of Respiratory and Critical Care Medicine, Huzhou Central Hospital, Affiliated Huzhou Hospital, Zhejiang University School of Medicine, No. 1558 Third Ring North Road, Huzhou 313000, Zhejiang Province, China. kjkceh@126.com

Abstract

BACKGROUND

Acute lung injury (ALI) and its final severe stage, acute respiratory distress syndrome, are associated with high morbidity and mortality rates in patients due to the lack of effective specific treatments. Gut microbiota homeostasis, including that in ALI, is important for human health. Evidence suggests that the gut microbiota improves lung injury through the lung-gut axis. Human umbilical cord mesenchymal cells (HUC-MSCs) have attractive prospects for ALI treatment. This study hypothesized that HUC-MSCs improve ALI *via* the lung-gut microflora.

AIM

To explore the effects of HUC-MSCs on lipopolysaccharide (LPS)-induced ALI in mice and the involvement of the lung-gut axis in this process.

METHODS

C57BL/6 mice were randomly divided into four groups (18 rats per group): Sham, sham + HUC-MSCs, LPS, and LPS + HUC-MSCs. ALI was induced in mice by intraperitoneal injections of LPS (10 mg/kg). After 6 h, mice were intervened with 0.5 mL phosphate buffered saline (PBS) containing 1 × 10^6 HUC-MSCs by intraperitoneal injections. For the negative control, 100 mL 0.9% NaCl and 0.5 mL PBS were used. Bronchoalveolar lavage fluid (BALF) was obtained from anesthetized mice, and their blood, lungs, ileum, and feces were obtained by an aseptic technique following CO_2 euthanasia. Wright's staining, enzyme-linked immunosorbent assay, hematoxylin-eosin staining, Evans blue dye leakage assay,

immunohistochemistry, fluorescence *in situ* hybridization, western blot, 16S rDNA sequencing, and non-targeted metabolomics were used to observe the effect of HUC-MSCs on ALI mice, and the involvement of the lung-gut axis in this process was explored. One-way analysis of variance with post-hoc Tukey's test, independent-sample Student's *t*-test, Wilcoxon rank-sum test, and Pearson correlation analysis were used for statistical analyses.

RESULTS

HUC-MSCs were observed to improve pulmonary edema and lung and ileal injury, and decrease mononuclear cell and neutrophil counts, protein concentrations in BALF and inflammatory cytokine levels in the serum, lung, and ileum of ALI mice. Especially, HUC-MSCs decreased Evans blue concentration and Toll-like receptor 4, myeloid differentiation factor 88, p-nuclear factor kappa-B (NF-κB)/NF-κB, and p-inhibitor α of NF-κB (p-IκBα)/IκBα expression levels in the lung, and raised the pulmonary vascular endothelial-cadherin, zonula occludens-1 (ZO-1), and occludin levels and ileal ZO-1, claudin-1, and occludin expression levels. HUC-MSCs improved gut and BALF microbial homeostases. The number of pathogenic bacteria decreased in the BALF of ALI mice treated with HUC-MSCs. Concurrently, the abundances of *Oscillospira* and *Coprococcus* in the feces of HUS-MSC-treated ALI mice were significantly increased. In addition, *Lactobacillus*, *Bacteroides*, and *unidentified_Rikenellaceae* genera appeared in both feces and BALF. Moreover, this study performed metabolomic analysis on the lung tissue and identified five upregulated metabolites and 11 downregulated metabolites in the LPS + MSC group compared to the LPS group, which were related to the purine metabolism and the taste transduction signaling pathways. Therefore, an intrinsic link between lung metabolite levels and BALF flora homeostasis was established.

CONCLUSION

This study suggests that HUM-MSCs attenuate ALI by redefining the gut and lung microbiota.

Key Words: Acute lung injury; Human umbilical cord mesenchymal cells; Lipopolysaccharide; Microflora; Untargeted metabolomics; Toll-like receptor 4/nuclear factor kappa-B signaling pathway

Core Tip: The results of this study suggest that human umbilical cord mesenchymal cells (HUC-MSCs) inhibit the inflammatory cytokine expression levels in serum and the lung of mice with acute lung injury (ALI), which may be achieved by redefining the gut and lung microbiota. This study not only provides a scientific basis for the pathophysiological mechanisms and clinical application of HUC-MSCs, but it also provides new ideas for the development of therapeutic strategies for ALI.

Citation: Lv L, Cui EH, Wang B, Li LQ, Hua F, Lu HD, Chen N, Chen WY. Multiomics reveal human umbilical cord mesenchymal stem cells improving acute lung injury *via* the lung-gut axis. *World J Stem Cells* 2023; 15(9): 908-930
URL: https://www.wjgnet.com/1948-0210/full/v15/i9/908.htm
DOI: https://dx.doi.org/10.4252/wjsc.v15.i9.908

INTRODUCTION

Acute lung injury (ALI), whose final severe stage is defined as acute respiratory distress syndrome (ARDS), is caused by various pathogenic factors, including acute pneumonia, sepsis, severe trauma, and acute pancreatitis[1]. It is primarily characterized by pulmonary edema and acute inflammation[2], and has high morbidity and mortality rates in patients due to the lack of effective patient-specific treatments[3]. Therefore, ALI has received much attention from the academic community, and significant developments have been made in understanding its pathophysiological mechanisms; however, clinically available treatments for ALI are still limited[4]. Lipopolysaccharide (LPS), a common pathogenic factor associated with ALI, is the main constituent of the Gram-negative bacterial cell wall[5]. A previous study found that LPS induced lung tissue damage and increased the expression of inflammatory factors in the bronchoalveolar lavage fluid (BALF)[6]. Animal models of LPS-induced lung injury are commonly used to study ALI[7]. Interestingly, LPS-induced ALI mice have a gut microbiota imbalance, and improvement in gut microbiota homeostasis can ameliorate lung inflammation of ALI mice and inhibit Toll-like receptor 4 (TLR4)/nuclear factor kappa-B (NF-κB) signaling in the lungs [8], suggesting the possible involvement of the intestinal microbiota in ALI.

A prospective observational cohort study focused on the relationship between lung microbiota and ALI and found that BALF microbiota can predict clinical outcomes in critically ill patients, especially the enrichment of gut-associated bacteria in BALF[9]. There is increasing evidence that the effects of host-microorganism interactions extend well beyond the local environment and influence the responses of peripheral tissues[7]. Homeostasis of the gut microbiota is important for human health, including its modulatory effects on ALI[10]. A study, based on 16S rRNA amplicon and metagenomic sequencing, found that the composition of the gut microbiota has a significant impact on wasting and death

in mice with ALI, suggesting the importance of the lung-gut microbiota crosstalk in lung injury[11]. Moreover, the depletion of gut microbes using an antibiotic cocktail improves lung injury and decreases interleukin (IL)-6 levels in the BALF of ALI mice[12]. A clinical cohort study found that the gut microbiome composition in patients with coronavirus disease 2019 (COVID-19), a respiratory illness, was significantly altered compared with that in non-COVID-19 individuals, irrespective of whether patients had received medication, and that the gut microbiome composition was correlated with disease severity[13]. Additionally, intestinal diseases alter the composition of the pulmonary microbiota and their metabolites[14]. Therefore, changes in the abundance and composition of the gut microbiota may be key to improving ALI *via* the lung-gut microflora. Recently, the impact of gut microbiota homeostasis on lung diseases has come into focus.

Mesenchymal stem cells (MSCs) are multipotent cells that can differentiate into various specialized cell types, including osteoblasts, chondrocytes, and adipocytes[15]. They originate from the mesoderm and are widely derived from adult stem cells with multi-differentiation potential, and can be isolated from a variety of tissues, such as the bone marrow, umbilical cord, amniotic membrane, adipose tissue, and skeletal muscle[16]. In addition, they have been shown to have beneficial effects in ALI[17]. Human umbilical cord mesenchymal cells (HUC-MSCs) have gained popularity in stem cell research and applications because of their specific advantages, including easy availability, abundance, lack of tumorigenicity, and ethical compliance[18]. Ahn *et al*[19] found that HUC-MSCs improved chronic lung disease and bronchopulmonary dysplasia in premature infants, without any transplantation-related adverse outcomes. Additionally, HUC-MSCs improved lung injury and inhibited the pro-inflammatory cytokine levels in the lungs of LPS-induced ALI mice[20]. HUC-MSC treatment ameliorated lung inflammation and fibrosis in bleomycin-induced pulmonary fibrosis mice[21]. Furthermore, researchers have reported that intraperitoneal infusions of HUC-MSCs improve colitis by reshaping the diversification of the gut microbiota[22]. Additionally, the gut microbiota of pulmonary hypertension mice was reversed by MSC treatment[23]. Studies on the HUC-MSC treatment of inflammation-related diseases are developing rapidly; however, their mechanisms of action are poorly understood. Therefore, by analyzing the lung-gut microbiota and lung metabolomics, this study aimed to explore the mechanisms underlying the amelioration of ALI by HUC-MSCs to provide a scientific basis for the clinical application of HUC-MSCs and a direction for the development of therapeutic strategies for ALI/ARDS.

MATERIALS AND METHODS

Animals and cells

A total of 72 6-8-wk-old male C57BL/6 mice were purchased from Beijing Vital River Laboratory Animal Technology Co., Ltd. (Beijing, China) and housed in a standard specific pathogen-free environment. The mice were isolated and allowed to adapt for one week. All procedures involving animals were approved and supervised by the Animal Experimentation Ethics Committee of Zhejiang Eyong Pharmaceutical Research and Development Center. Mycoplasma free HUC-MSCs (HUM-iCell-e009) were purchased from iCell Bioscience Inc. (Shanghai, China) and cultured in a specialized medium (PriMed-iCELL-012; iCell Bioscience, China) containing supplements at 37 °C in a 5% CO_2 incubator. The purity of HUC-MSCs was assessed by flow cytometry and was typically greater than 90%. Cell identification was performed by iCell Bioscience Inc.

Animal model of ALI

The random number method was used to divide mice into four groups, namely, sham, sham + MSCs, LPS, and LPS + MSCs groups, with 18 mice in each group. The 36 randomly selected mice were intraperitoneally injected with 100 mL of LPS (10 mg/kg) to induce ALI[7], and sham mice were administered 100 mL of 0.9% NaCl as controls. After 6 h, half of the ALI mice and half of the sham mice were given 0.5 mL of phosphate buffered saline (PBS) containing HUC-MSCs (1×10^6 cells/mL) by intraperitoneal injections[24], and the other half of the ALI mice and sham mice were given 0.5 mL of 0.9% NaCl. The mice were reared under standard laboratory conditions. The experiments were carried out by expert technicians who were blinded to the animal grouping.

Sample preparation

Three days after HUC-MSC intervention in ALI mice, BALF was obtained after the mice were anesthetized with isoflurane as reported by Wu *et al*[24]. Briefly, the trachea was flushed five times with PBS *via* a 20-gauge catheter, and all liquids were collected. Subsequently, all mice were euthanized with CO_2, and the blood, lungs, ileum, and feces were obtained using aseptic techniques. The lungs (one lung was evenly divided into four) from three mice in each group were taken, weighed, and then baked in an oven at 80 °C for 48 h to determine the dry weight to calculate the ratio of wet lung weight to dry lung weight (W/D weight ratio) as reported by Li *et al*[25]. In addition, a part of the remaining lung and ileum were made into paraffin blocks separately, and the other were stored at 80 °C for further analysis. The BALF was divided into two parts for inflammation cytokine detection and 16S rDNA sequencing, respectively.

Detection of immune cells and inflammatory cytokines

The protein concentration in the BALF was measured using the BCA assay (Beyotime, China). Additionally, the cells in BALF were precipitated and resuspended, and mononuclear cells and neutrophils were counted after Wright's staining. The levels of tumor necrosis factor (TNF)-α (ml002095-1, Enzyme-linked, China), IL-1β (ml063132-1, Enzyme-linked, China), and IL-6 (ml002293-1, Enzyme-linked, China) in the serum, lungs, and ileum were measured by enzyme-linked

Table 1 Information of antibodies used in this study

Antibody	Dilution ratio	Manufacturer	Country	Cat. No.
VE-cadherin antibody	1:2000	Affinity	United States	AF6265
ZO-1 antibody	1:5000	Proteintech	United States	21773-1-AP
Occludin antibody	1:1000	Affinity	United States	DF7504
TLR4 antibody	1:2000	Affinity	United States	AF7017
Myd88 antibody	1:1000	Affinity	United States	AF5195
p-NF-κB p65 antibody	1:2000	Affinity	United States	AF2006
NF-κB p65 antibody	1:2000	Affinity	United States	AF5006
p-IκBα antibody	1:2000	Affinity	United States	AF2002
IκB antibody	1:2000	Affinity	United States	AF5002
Claudin-1 antibody	1:3000	Affinity	United States	AF0127
Anti-rabbit IgG, HRP-linked antibody	1:6000	Cell signaling technology	United States	7074
Anti-mouse IgG, HRP-linked antibody	1:6000	Cell signaling technology	United States	7076
β-actin antibody	1:10000	Affinity	United States	AF7018

VE: Vascular endothelia; ZO-1: Zonula occludens-1; TLR4: Toll-like receptor; Myd88: Myeloid differentiation factor 88; NF-κB: Nuclear factor kappa-B; IκB α: Inhibitor α of nuclear factor kappa-B; HRP: Horse radish peroxidase.

immuno sorbent assay (ELISA) according to the manufacturer's instructions.

Histopathological observation

Hematoxylin-eosin (H&E) staining was performed to observe the histopathology of the lungs and ileum. Briefly, the lungs and ileum were fixed in 10% formalin. The tissues were then placed in paraffin and sectioned, and sections were stained with H&E. The injury of lungs and ileum were scored in a blinded fashion as previously reported[26,27].

Measurement of alveolar-capillary permeability

Three mice were randomly selected from each group for the Evans blue dye leakage assay to explore the function of the lung tissue endothelial barrier as previously reported[28]. This assay was performed using 25 mg/kg of 0.5% blue dye (Sigma, United States) injected into mice *via* the tail vein 2 h before isoflurane anesthesia. After the heart of the anesthetized mice was exposed, the left ventricle was intubated and flushed with 4% normal saline. Subsequently, the mice were euthanized using CO_2. Lungs were homogenized in 2 mL PBS and treated with formamide (Sigma, United States) at 60 °C for 24 h. Finally, the concentration of Evans blue dye in the lung tissue was determined at 620 nm using a microplate reader (CMaxPlus, Molecular Devices, United States).

Immunohistochemistry

Immunohistochemistry (IHC) was performed as described by Peng *et al*[29]. Paraffin sections of lung tissue were deparaffinized, permeabilized, and blocked. The sections were then incubated at 4 °C overnight with anti-TLR4 antibody (1:100 dilution; Affinity, United States). After washing with PBS, the slides were incubated with goat anti-rabbit IgG HRP (Abcam, United States) at 37 °C for 30 min. The slides were washed again, mounted with DAPI (Vector Laboratories, Burlingame, CA), and examined using an E100 fluorescence microscope (Nikon, Japan).

Fluorescence in situ hybridization

Fluorescence *in situ* hybridization (FISH) was performed on slides of ileum and lung tissues as previously described[30], using a pan-bacteria FITC-labeled probe (EUB338) and an RNA FISH kit (Genepharma, China). After DAPI staining, the slides were visualized under an inverted fluorescence microscope (Ts2-FL; Nikon, Japan). Images were acquired using Micro-Manager and analyzed using ImageJ/FIJI software (National Institutes of Health, United States, version 1.53c).

Western blot analysis

The antibodies used for western blot (WB) are shown in Table 1. The lung and ileum tissues were homogenized in a lysis solution for the extraction of proteins. After centrifugation and supernatant collection, the samples were uniformly concentrated and denatured. Briefly, sodium dodecyl sulfate-gel electrophoresis and membrane transfer were performed for 20 μg protein per group as reported by Li *et al*[3]. The membranes were incubated with primary antibodies overnight and then with secondary antibodies for 1 h. Finally, the membranes were subjected to chemiluminescence reactions and protein levels were measured by enhanced chemiluminescence. ImageJ/FIJI software was used for semiquantitative analysis.

16S rDNA sequencing

High-throughput 16S rDNA sequencing was performed to analyze the gut and pulmonary microflora by BioDeep Co., Ltd (Suzhou, China). A sequencing library was prepared using the TruSeq Nano DNA LT Library Prep Kit of Illumina. A NovaSeq6000 system (PE250, Illumina, United States) was used for sequencing as reported by Yi *et al*[31]. Then the QIIME2 DADA2 and OmicStudio platforms[32] were used to analyze the data.

Metabolomics for lung tissue

The non-targeted metabolomics approach was performed by PANOMIX Biomedical Tech Co., Ltd. (Suzhou, China). The samples were treated with 75% methanol-chloroform (9:1) and 25% water for sonication and centrifugation to extract the metabolites. The samples (2 μL) were analyzed by liquid chromatography-mass spectrum (MS) detection with the Vanquish UHPLC System (Thermo, United States). Additionally, an Orbitrap Exploris mass spectrometer (Thermo, United States) was used for mass spectrometry analysis. After data acquisition, the Proteowizard package (v3.0.8789) and the R xcms package were used to preprocess the data. Metabolites were identified on the public databases such as the Human Metabolome Database[33], MassBank (https://massbank.eu/MassBank/), Lipid Maps (https://Lipidmaps.org/), mzCloud (https://www.mzcloud.org/), Kyoto Encyclopedia of Genes and Genomes (KEGG)[34], and self-building repository, and Orthogonal Projections to Latent Structures Discriminant Analysis (OPLS-DA) analysis was performed to screen the differential metabolites.

Statistical analysis

Statistical analyses were performed using SPSS (version 16.0; IBM, Armonk, NY, United States). Data from multiple *in vivo* experiments were analyzed using one-way analysis of variance (ANOVA) with a post-hoc Tukey test. The independent-samples Student's *t*-test was used for comparison between the two groups. The Wilcoxon rank-sum test was conducted to explore the microflora with a significant difference in abundance. Pearson's correlation analysis was used to explore the intrinsic associations. Additionally, the Variable Importance for the Projection (VIP) of OPLS-DA was used to screen for metabolites with biomarker potential (VIP > 1). Two-way Orthogonal Partial Least Squares (O2PLS) analysis was used to explore the links between BALF microbiota and lung metabolism. The threshold for significance was $P < 0.05$ for all tests.

RESULTS

HUC-MSC treatment alleviates lung injury and inflammation in ALI mice

This study used LPS to induce ALI in mice and then collected their lungs and BALF to explore the ameliorating effect of HUC-MSCs on ALI by H&E staining and ELISA. ALI mice had a higher lung W/D weight ratio and more mononuclear cells and neutrophils than sham mice ($P < 0.01$), whereas HUC-MSC treatment on ALI mice decreased the lung W/D weight ratio ($P < 0.05$), mononuclear cell and neutrophil counts, and protein concentration ($P < 0.01$) (Figures 1A and B). Additionally, compared to sham mice, the lung of ALI mice had markedly thickened alveolar septa with significant inflammatory cell infiltration; however, HUC-MSC treatment alleviated the degree of alveolar septal thickening and inflammatory cell infiltration in ALI mice (Figure 1C). Likewise, the score of lung injury in the LPS group was higher than those in the sham ($P < 0.01$) and LPS + MSC groups ($P < 0.05$) (Figure 1D). Moreover, ALI mice had significantly increased levels of TNF-α, IL-1β, and IL-6 in their serum and lung tissues ($P < 0.01$) (Figures 1E and F). In particular, the above-mentioned inflammatory factor levels were decreased in the ALI mice treated with HUC-MSCs ($P < 0.01$) (Figures 1E and F).

HUC-MSC treatment improves endothelial barrier function and integrity in the lungs of ALI mice

In addition, this study observed the endothelial barrier function and integrity of the lungs using Evans blue, WB, and IHC assays. As shown in Figure 2A, ALI mice had a higher concentration of Evans blue dye in the lungs than the sham mice, and HUC-MSC treatment reduced Evans blue concentration in the lungs of ALI mice ($P < 0.01$). In particular, the levels of endothelial barrier-associated proteins, such as vascular endothelial (VE)-cadherin, zonula occludens-1 (ZO-1), and occludin, were markedly decreased in ALI mice ($P < 0.05$ or $P < 0.01$); however, HUC-MSC treatment reversed the expression levels of these proteins ($P < 0.01$) (Figures 2B-D). In addition, this study explored the signal intensity of the TLR4/myeloid differentiation factor 88 (Myd88)/NF-κB signaling pathway. The TLR4, Myd88, p-NF-κB/NF-κB, and p-inhibitor α of NF-κB (p-IκBα)/IκBα expression levels in the lung were all increased in ALI mice compared to the sham mice ($P < 0.01$); however, in ALI mice treated with HUC-MSCs, the expression levels of these proteins were decreased ($P < 0.05$ or $P < 0.01$) (Figures 2E-I). Similarly, TLR4 detected by IHC had a strong positive expression in the lungs of ALI mice, whereas HUC-MSC treatment attenuated the positive expression of TLR4 ($P < 0.05$ or $P < 0.01$) (Figures 2J and K).

HUC-MSC treatment improves injury, endothelial barrier integrity, and bacterial translocation in the ileum of ALI mice

Studies have reported not only lung function injury but also intestinal dysfunction in ALI[17]. Therefore, the ileum was examined using H&E staining, ELISA, WB, and FISH. The ileal tissue of ALI mice had shorter and ruptured villi with significant inflammatory cell infiltration compared to sham mice, whereas these ileal injuries in ALI mice treated with HUC-MSCs were improved ($P < 0.05$ or $P < 0.01$) (Figure 3A). In addition, LPS treatment on mice markedly increased the ileal TNF-α, IL-1β, and IL-6 levels ($P < 0.01$), whereas HUC-MSC treatment inhibited them ($P < 0.01$) (Figure 3B). The suppressed expression of endothelial barrier-associated proteins, including claudin, ZO-1, and occludin by LPS was

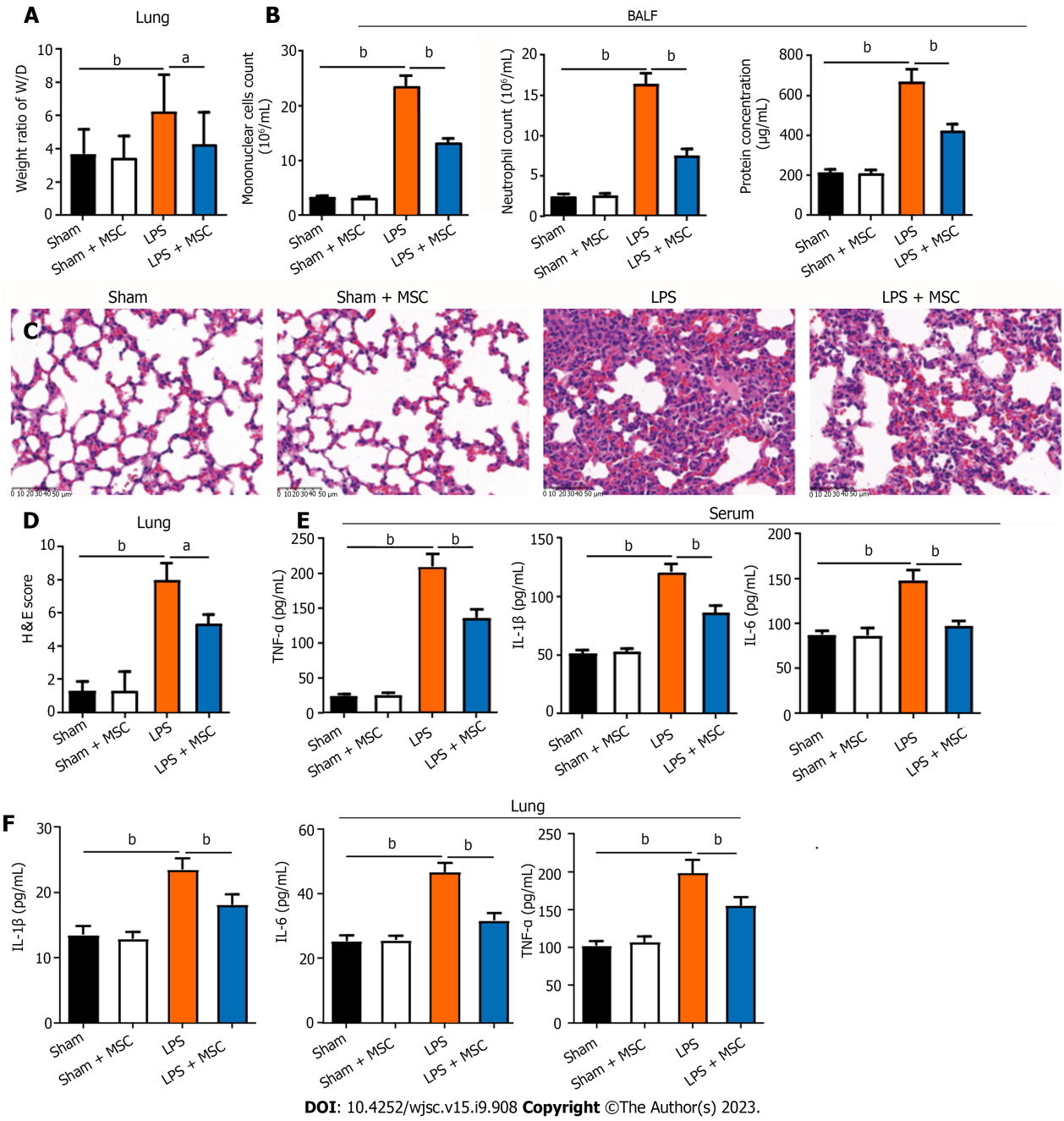

DOI: 10.4252/wjsc.v15.i9.908

Figure 1 Human umbilical cord mesenchymal stem cells attenuate lipopolysaccharide-induced lung injury and inflammation in acute lung injury mice. A: In acute lung injury (ALI) mice, the wet-to-dry (W/D) weight ratio of the lung was higher than that of human umbilical cord mesenchymal stem cell (HUC-MSC)-treated ALI mice (n = 3); B: ALI mice had more mononuclear cells and neutrophils, and higher protein concentration in bronchoalveolar lavage fluid (BALF) than sham mice, while HUC-MSC treatment decreased these parameters (n = 12); C: Representative images of hematoxylin-eosin (H&E)-stained lung tissues (× 400, scale = 50 μm); D: Lung histopathological damage in mice (H&E staining; n = 3); E: Serum tumor necrosis factor (TNF)-α, interleukin (IL)-1β, IL-6, and lipopolysaccharide levels were higher in ALI mice and HUC-MSC treatment decreased their levels (n = 12); F: TNF-α, IL-1β, and IL-6 levels in the lungs of ALI mice were hugely increased than those in sham mice, while HUC-MSC treatment in ALI mice decreased them (n = 12). $^{a}P < 0.05$, $^{b}P < 0.01$. LPS: Lipopolysaccharide; MSC: Mesenchymal stem cell; BALF: Bronchoalveolar lavage fluid; H&E: Hematoxylin-eosin; IL: Interleukin; TNF: Tumor necrosis factor.

enhanced by HUC-MSC treatment in ALI mice ($P < 0.05$) (Figures 3C and D). Furthermore, the EUB338 counts of the ileum epithelium and lungs in ALI mice were measured to observe the lung translocation of gut bacteria, and it was found that they were increased in ALI mice, whereas HUC-MSC treatment reduced them ($P < 0.01$) (Figures 3E-H).

HUC-MSC treatment attenuates ALI via regulating lung-gut microbiota homeostasis

16S rDNA sequencing was used to explore the effect of the lung and gut microbiota on the HUC-MSC-mediated amelioration of ALI. BALF and fecal samples were collected for 16S rDNA sequencing. After homogenizing the sequencing depth of each group, 48 BALF and fecal samples from the four groups were identified at the genus level, with an average of 48.25 units in each group. Figures 4A and B shows the top 20 flora with the highest average abundance at the genus level. The Shannon and Simpson indices of alpha diversity reflect richness and community evenness,

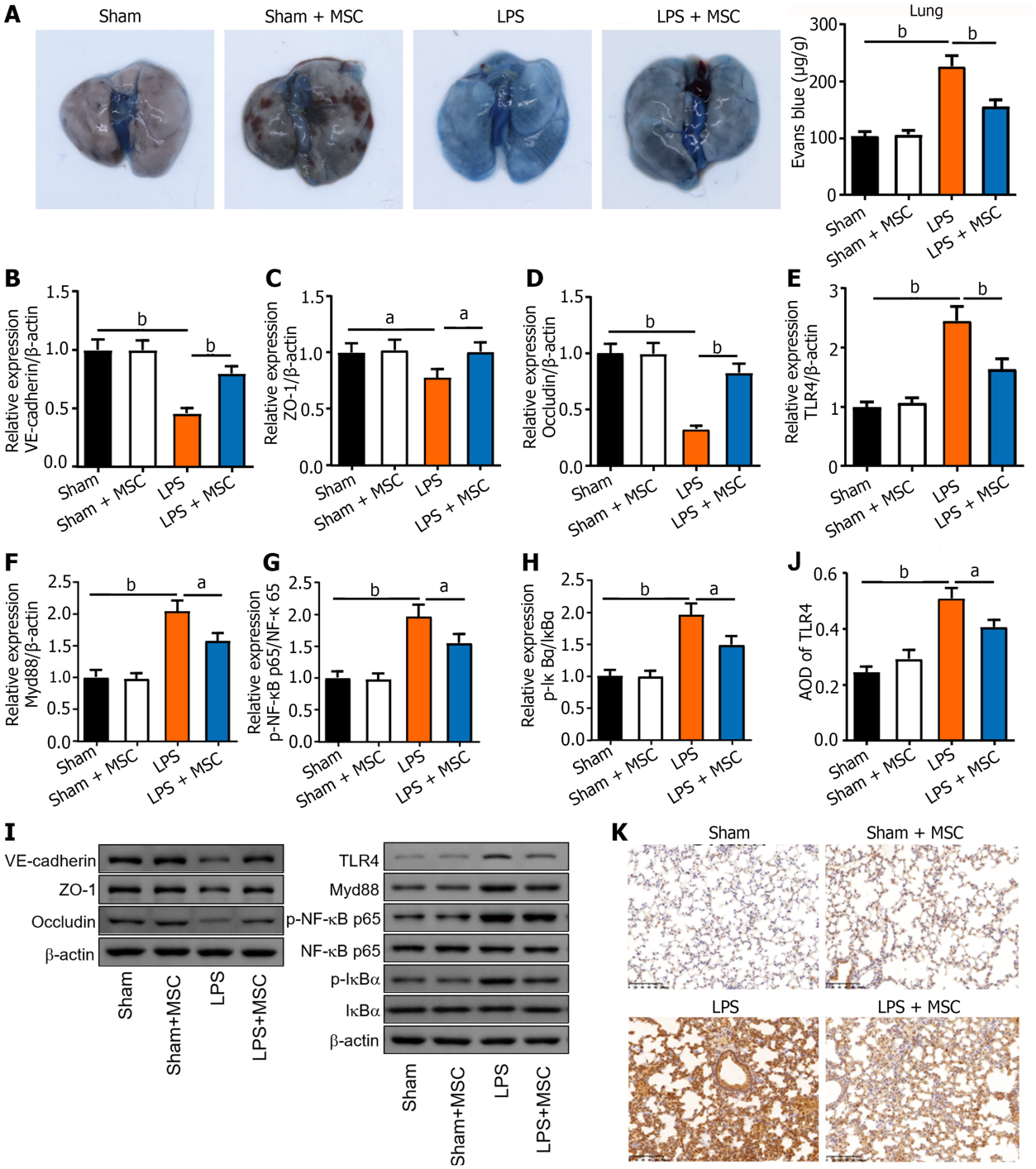

DOI: 10.4252/wjsc.v15.i9.908

Figure 2 Human umbilical cord mesenchymal stem cells improve endothelial barrier function *in vivo* and regulate related protein expression. A: The Evans blue assay was carried out to assess lung endothelial barrier function in acute lung injury (ALI) mice (n = 3). The ALI mice [lipopolysaccharide (LPS) group] had the largest amount of Evans blue contents; human umbilical cord mesenchymal stem cell (HUC-MSC) treatment in ALI mice (LPS + MSC group) decreased the contents in the lung; B-H: LPS treatment in mice inhibited the expression of vascular endothelial-cadherin (B), zonula occludens-1 (C), and occludin (D) and raised the expression of Toll-like receptor 4 (TLR4) (E), myeloid differentiation factor 88 (F), p-nuclear factor kappa-B (NF-κB)/NF-κB (G), and p-inhibitor α of NF-κB (IκBα)/IκBα (H) (n = 3), while HUC-MSC treatment antagonized the effects of LPS; I: Representative western blot bands of the above proteins; J and K: Statistical results of immunohistochemistry and its representative images. It was showed that TLR4 was highly expressed in the lung tissue of ALI mice and HUC-MSC treatment could decrease its expression (n = 3). $^{a}P < 0.05$, $^{b}P < 0.01$. LPS: Lipopolysaccharide; MSC: Mesenchymal stem cell; LPS: Lipopolysaccharide; VE: Vascular endothelial; ZO-1: Zonula occludens-1; TLR4: Toll-like receptor 4; Myd88: Myeloid differentiation factor 88; NF-κB: Nuclear factor kappa-B; IκBα: Inhibitor α of nuclear factor kappa-B.

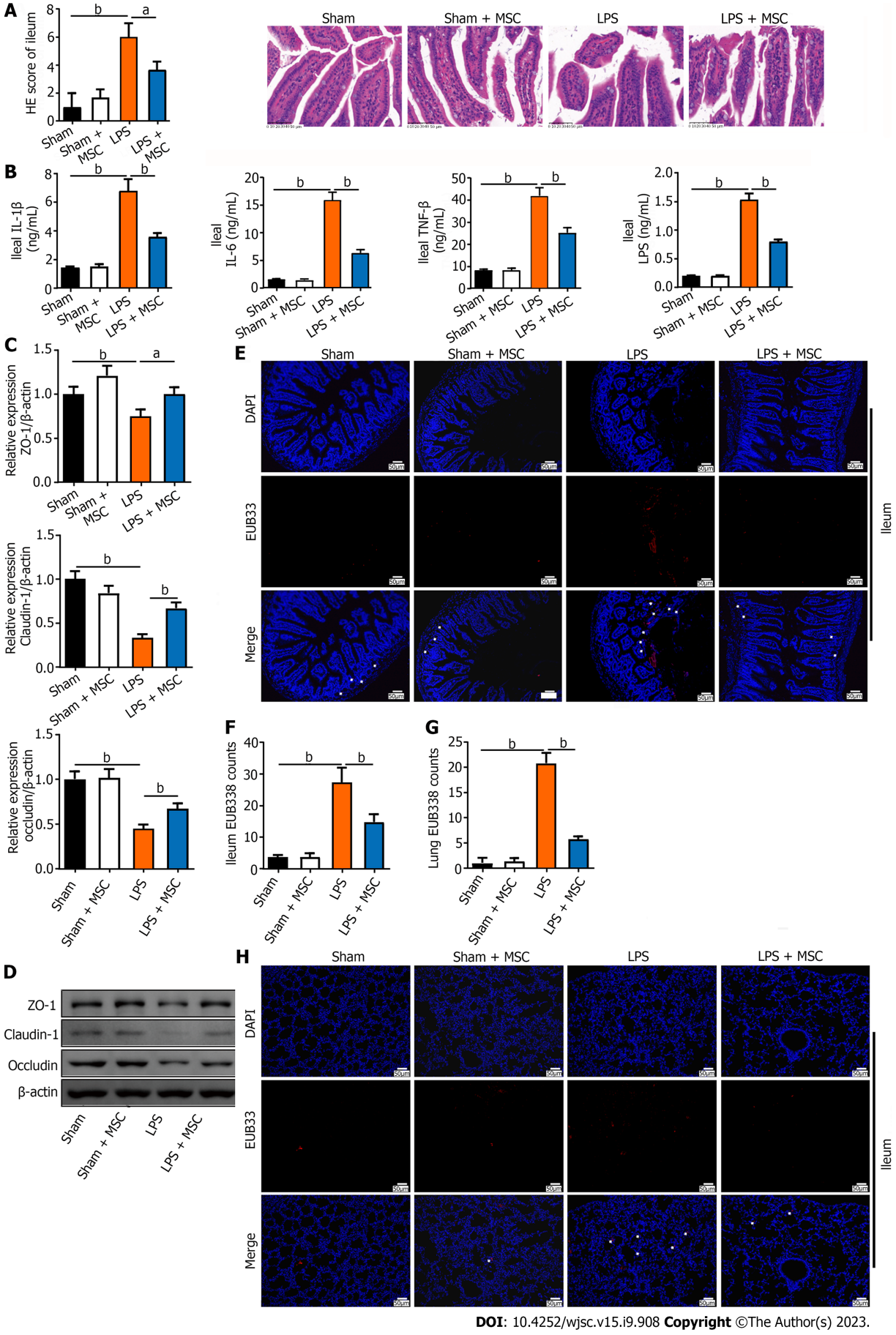

DOI: 10.4252/wjsc.v15.i9.908 **Copyright** ©The Author(s) 2023.

Figure 3 Human umbilical cord mesenchymal stem cells improve histopathology, inflammation, and endothelial barrier integrity of the

ileum in acute lung injury mice. A: Ileum tissue injury in acute lung injury (ALI) mice was observed after hematoxylin-eosin staining. ALI mice had severe ileum tissue injury while human umbilical cord mesenchymal stem cell (HUC-MSC) treatment improved such injury (n = 3); B: Tumor necrosis factor (TNF)-α, interleukin (IL)-1β, IL-6, and lipopolysaccharide (LPS) levels in the ileum were measured by ELISA (n = 12), and ALI mice had higher levels of TNF-α, IL-1β, IL-6, and LPS compared to sham mice, while HUC-MSC treatment decreased the levels of these factors; C: Zonula occludens-1 (ZO-1), claudin-1, and occludin levels were measured to observe the integrity of the ileum barrier (n = 3); D: Representative western blot bands of ZO-1, claudin-1, and occludin; E-H: Bacterial translocation was determined by fluorescence *in situ* hybridization, and the EUB338 counts in the ileum epithelium and lung per field were quantified (n = 3). $^{a}P < 0.05$, $^{b}P < 0.01$. MSC: Mesenchymal stem cell; LPS: Lipopolysaccharide; ZO-1: Zonula occludens-1; HE: Hematoxylin-eosin; IL: Interleukin; TNF: Tumor necrosis factor.

respectively. According to the Kruskal-Wallis rank-sum test, the Shannon index showed no significant differences among the groups (P = 0.056) (Figure 4C). Additionally, the Bray-Curtis distance of beta diversity reflects microbial diversity between groups and was analyzed by principal coordinates analysis, which revealed that the projection distance of the LPS + MSC group on the coordinate axis was closer to that of the negative control group than that of the LPS group (Figure 4C). Similarly, the Simpson index showed no significant differences among the groups (P = 0.058), and the projection distance of the gut microflora was closer to that of the negative control group than to that of the LPS group (Figure 4D).

Subsequently, the Wilcoxon rank-sum test was performed to explore the microflora with a significant difference in abundance (marked microflorae) (Figures 4E and F). In particular, there were 21 microflorae with upregulated abundance and 12 microflorae with downregulated abundance in the BALF of mice in the LPS + MSC group compared to the LPS group ($P < 0.05$) (Figure 4E), and 17 microflorae with upregulated abundance and 3 microflorae with downregulated abundance in feces ($P < 0.05$) (Figure 4F). The 33 marked microflorae with the largest upregulation or downregulation of operational taxonomic units in the BALF of ALI mice with/without HUC-MSC treatment are shown in Figure 5A, and 20 marked microflorae in feces are shown in Figure 5B. *Rhizobiales* had the largest log2 fold change (FC) in the BALF of mice in the LPS + MSC group compared to the LPS group [log2(FC) = 9.3264, P = 0.0284], and *Elizabethkingia* had the lowest log2FC in the BALF of mice in the LPS + MSC group compared to that of the LPS group [log2(FC) = -5.1799, P = 0.028] (Figure 5A). In fecal samples, the log2FC of *unclassified_Bacteroidales* was the highest in the marked microflorae of the LPS + MSC group compared to that of the LPS group [log2(FC) = 4.7549, P = 0.027], and that of the unidentified_F16 was the lowest [log2(FC) = -4.6328, P = 0.012] (Figure 5B).

Furthermore, the Pearson's correlation analysis was used to analyze the correlation between marked microflorae of the gut and lungs, and most of the bacteria in the BALF and feces had a strong or extremely strong correlation (Figure 6). The *Desulfovibrio* genus in feces was positively correlated with *Stenotrophomonas* in BALF ($P < 0.05$) (Supplementary Table 1).

HUC-MSC treatment regulates metabolic profile of lung tissue in ALI mice

The base peak chromatograms in the positive and negative modes of the four groups showed similar trends, suggesting good repeatability and reliable results (Figure 7A). Additionally, Partial Least Squares-Discriminant Analysis (PLS-DA) was used to distinguish metabolite differences between groups in the positive/negative mode. In particular, all blue Q2 positions in the permutation test chart were lower than the original points on the far right, suggesting that the PLS-DA models were valid (Figures 7B and C). In the positive mode, MS analysis identified a total of 1206 common biomarkers between the sham and LPS + MSC groups, 362 between the LPS and sham + MSC groups, 347 between the LPS and sham groups, 343 between the LPS + MSC and LPS groups, and 181 between the sham + MSC and sham groups (Figure 7D). In the negative mode, this study identified 905 common biomarkers between the sham and LPS + MSC groups, 476 between the LPS and sham + MSC groups, 225 between the LPS and sham groups, 112 between the LPS + MSC and LPS groups, and 139 between the sham + MSC and sham groups (Figure 7E).

Subsequently, precise screening of the metabolic profiles by MS/MS was performed to eliminate false positives. This study identified four upregulated metabolites (3-succinoylpyridine, nicotinamide ribotide, aldosterone, and phenylacetic acid) and one downregulated metabolite (lithocholic acid) in the sham + MSC group compared to the sham group. In addition, KEGG enrichment analysis suggested that these differential metabolites might participate in nicotinate and nicotinamide metabolism, aldosterone-regulated sodium reabsorption, and aldosterone synthesis and secretion pathways (Figures 8A-C). Additionally, 12 markedly upregulated metabolites (hydroxyindole, xanthine, and N-acetyl-L-aspartic acid, *etc.*) and 20 markedly downregulated metabolites (prostaglandin E2, argininosuccinic acid, and guanine, *etc.*) were identified in the LPS group compared to the sham group, and these metabolites were predicted to be potentially involved in alanine, aspartate, and glutamate metabolism, oxidative phosphorylation, the cAMP signaling pathway, and so on (Figures 8A, D and E). In particular, five upregulated metabolites (anabasine, IMP, lidocaine, salicylic acid, and propionylcarnitine) and 11 downregulated metabolites (N-acetylleucine, guanosine, guanine, *etc.*) were identified in the LPS + MSC group compared to the LPS group (Figures 8A and F). They were related to purine metabolism and the taste signaling transduction pathways ($P < 0.001$) (Figure 8G).

Significant correlations between microbes in BALF and metabolites in lung tissue

To explore the role of HUC-MSCs in regulating the microflora of the lung-gut axis to improve ALI, we performed an O2PLS correlation analysis on the expression of microflora in BALF and the expression of metabolites in the lungs to determine the microflora involved in the improvement of ALI by HUC-MSCs and their impact on metabolism. In Figure 9A, the top 25 bacteria and top 25 metabolites are shown with large absolute joint loading values, suggesting that they have a large weight in the improvement of ALI following HUC-MSC treatment. Subsequently, these flora and metabolites were analyzed using correlation analysis (Supplementary Table 1). Significantly related bacteria and metabolites were screened based on $P < 0.05$. The number of metabolites that significantly correlated with BALF microbes

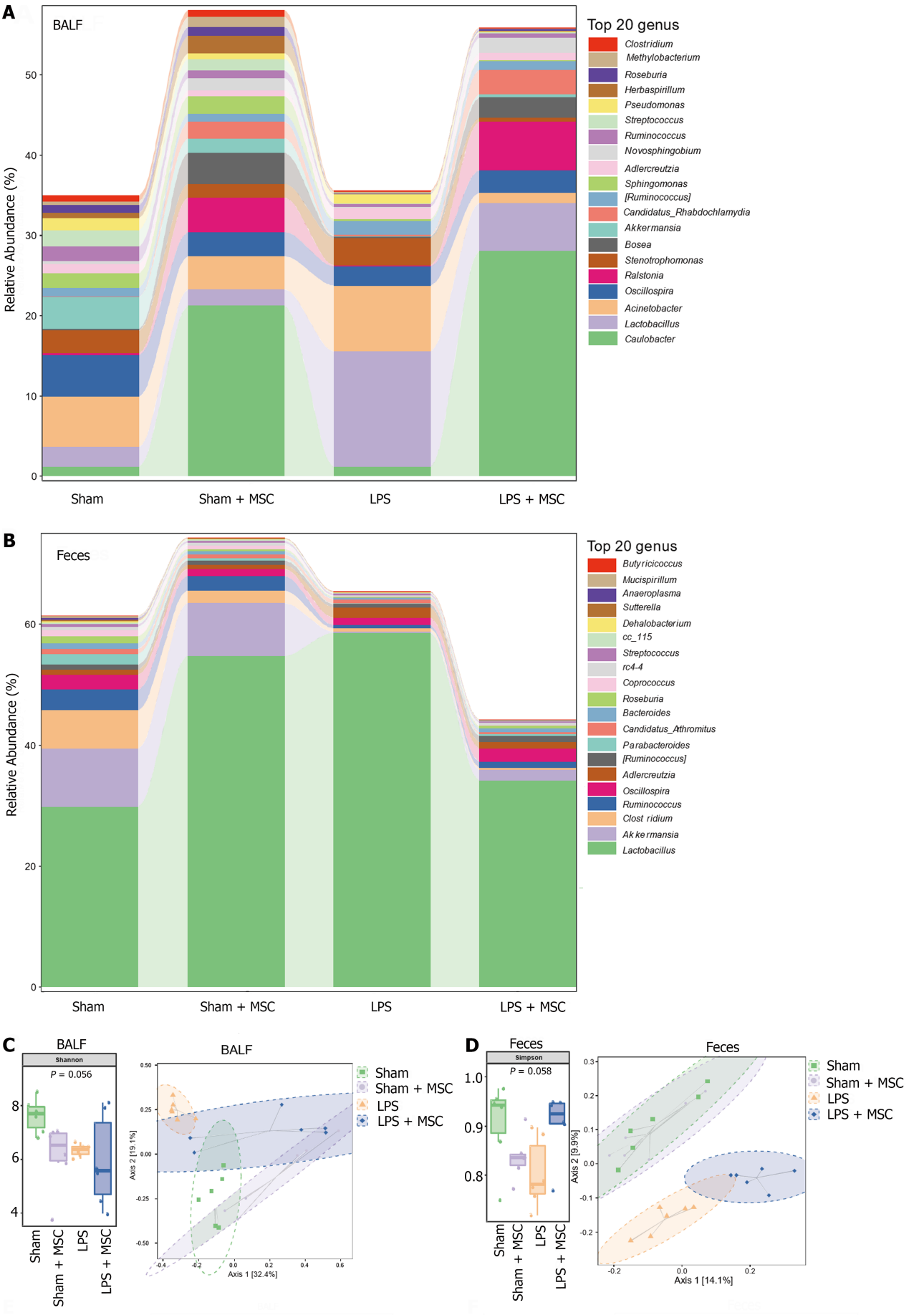
A
BALF
Relative Abundance (%)
0
10
20
30
40
50
Sham
Sham + MSC
LPS
LPS + MSC
Top 20 genus
Clostridium
Methylobacterium
Roseburia
Herbaspirillum
Pseudomonas
Streptococcus
Ruminococcus
Novosphingobium
Adlercreutzia
Sphingomonas
[Ruminococcus]
Candidatus_Rhabdochlamydia
Akkermansia
Bosea
Stenotrophomonas
Ralstonia
Oscillospira
Acinetobacter
Lactobacillus
Caulobacter
B
Feces
Relative Abundance (%)
0
20
40
60
Sham
Sham + MSC
LPS
LPS + MSC
Top 20 genus
Butyricicoccus
Mucispirillum
Anaeroplasma
Sutterella
Dehalobacterium
cc_115
Streptococcus
rc4-4
Coprococcus
Roseburia
Bacteroides
Candidatus_Athromitus
Parabacteroides
[Ruminococcus]
Adlercreutzia
Oscillospira
Ruminococcus
Clost ridium
Ak ke rmansia
Lactobacillus
C
BALF
Shannon
P = 0.056
4
6
8
Sham
Sham + MSC
LPS
LPS + MSC
BALF
Axis 2 [19.1%]
Axis 1 [32.4%]
Sham
Sham + MSC
LPS
LPS + MSC
D
Feces
Simpson
P = 0.058
0.8
0.9
1.0
Sham
Sham + MSC
LPS
LPS + MSC
Feces
Axis 2 [9.9%]
Axis 1 [14.1%]
Sham
Sham + MSC
LPS
LPS + MSC

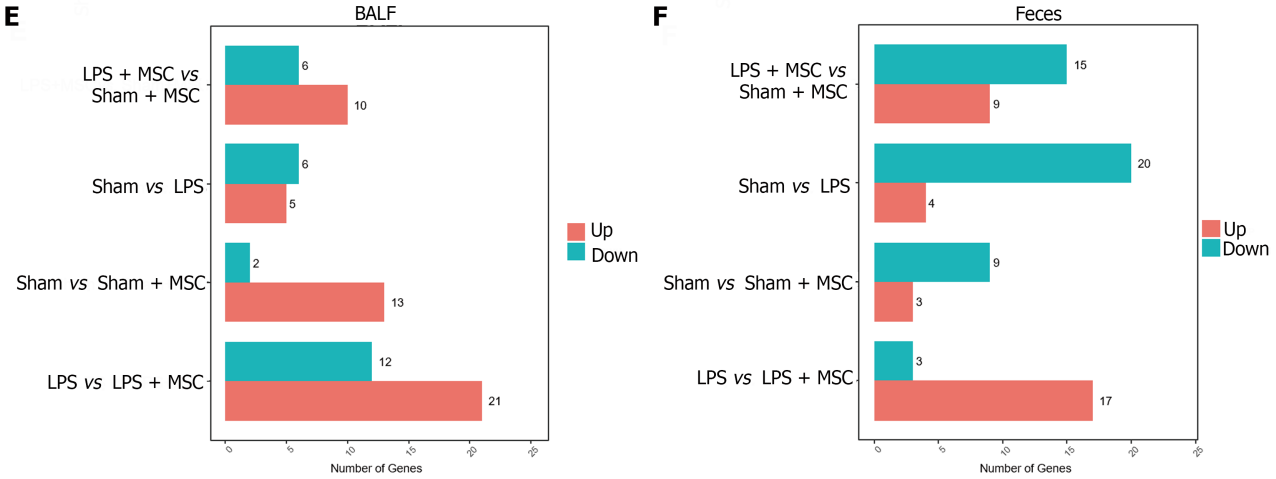

DOI: 10.4252/wjsc.v15.i9.908 **Copyright** ©The Author(s) 2023.

Figure 4 Microflora homeostasis in bronchoalveolar lavage fluid and feces of acute lung injury mice (*n* = 6). A and B: Relative abundance of top 20 genera of microflora in bronchoalveolar lavage fluid (BALF) and feces; C and D: The within-sample richness and evenness (alpha diversity) were statistically analyzed by Shannon index, Simpson index, and the bray-Curtis based principal coordinates analysis of similarity coefficients in the BALF and feces of different groups (beta diversity); E and F: The Wilcoxon rank sum test was used to explore microflorae with a significant difference in abundance on OmicShare Tools. The number of differential microflorae in lipopolysaccharide (LPS) + mesenchymal stem cells (MSCs) group *vs* sham + MSC group, sham group *vs* LPS group, sham group *vs* sham + MSC group, and LPS group *vs* LPS + MSCs group is presented. The length of the red bar indicates the number of up-regulated microflorae and the length of the blue-green bar indicates the number of down-regulated microflorae. LPS: Lipopolysaccharide; MSC: Mesenchymal stem cell; BALF: Bronchoalveolar lavage fluid.

is shown in Figure 9B. Additionally, metabolites with a large role in the improvement of ALI by HUC-MSC treatment were subjected to KEGG enrichment analysis and were found to be mainly involved in the signaling pathways of drug metabolism-other enzymes, tyrosine metabolism, autophagy-animal, and endocytosis (Figure 9C).

DISCUSSION

MSCs have emerged as a promising therapeutic strategy for inflammatory diseases, owing to their low immunogenicity, ability to stabilize immunity, and ability to ameliorate inflammatory responses[35]. Moreover, HUC-MSCs not only ameliorate acute and chronic pneumonia, but also enteritis[36,37]. This study found that HUC-MSCs improved pulmonary edema, alleviated pathological damage to the lungs and ileum, and inhibited the levels of inflammatory cells in the BALF and inflammatory factors in the serum, BALF, lungs, and ileum. Furthermore, HUC-MSC treatment of ALI mice improved endothelial barrier integrity in the lungs and ileum. Endothelial permeability is regulated by intercellular junctions including adherens junctions and tight junctions, which are composed of cell junction proteins including occludin, claudin 1, VE-cadherin, *etc*[38]. Claudin-1 in the ileum and VE-cadherin, ZO-1, and occludin in the lung and ileum play key roles in maintaining vascular integrity. This decrease indicated endothelial barrier disruption in the lungs and ileum. In this study, HUC-MSC treatment of ALI mice advanced lung VE-cadherin, ZO-1, and occludin expression signal intensity and upregulated claudin-1, ZO-1, and occludin expression levels in the ileum. Collectively, treatment of ALI mice with HUC-MSCs ameliorates lung and ileal barrier integrity.

Inflammatory factors and cells promote ALI injury. A study reported that TNF-α could promote M1 macrophage activation which has pro-inflammatory effects in sepsis-related ALI[39]. Neutrophil overactivation promotes the development of inflammation and injury in ALI[40]. Microvascular endothelial barrier dysfunction, the main pathophysiological feature of ARDS/ALI, induces capillary leakage and edema, which further intensifies inflammatory injury, thus causing high morbidity and mortality[41]. Botros and colleagues reported that stabilizing the endothelial barrier during inflammation alleviated inflammatory responses, edema, and lung injury in mice with ALI[42]. Interestingly, the inhibition of the TLR4 signaling pathways is related to the integrity of the pulmonary endothelial barrier. One study found that TLR4 knockdown decreased the sensitivity to particulate matter-induced pulmonary edema in ALI mice and increased the signal expression intensity of VE-cadherin[43]. Furthermore, MSC treatment in paraquat-induced ALI rats downregulated the TLR4 and NF-κB protein levels in the lungs[44]. Besides, LPS facilitates TLR4 activation to recruit MyD88 and thereby activates NF-κB to promote the production of pro-inflammatory factors such as TNF-α and IL-6[45]. Similarly, this study reported the inhibitory effect of HUC-MSCs on TLR4, Myd88, and NF-κB in the lungs of LPS-induced ALI mice, which suggests that HUC-MSCs may mitigate microvascular endothelial barrier dysfunction and inflammation in ALI *via* the TLR4/Myd88/NF-κB signaling pathway.

There is a correlation between microbiota levels and lung diseases[46]. By analyzing the 16S rDNA of microflora in BALF, we observed a decrease in some pathogenic bacteria. For example, the *Stenotrophomonas* genus was decreased in the BALF of mice in the LPS + MSC group. One study has reported that *Stenotrophomonas* maltophilia is commonly found

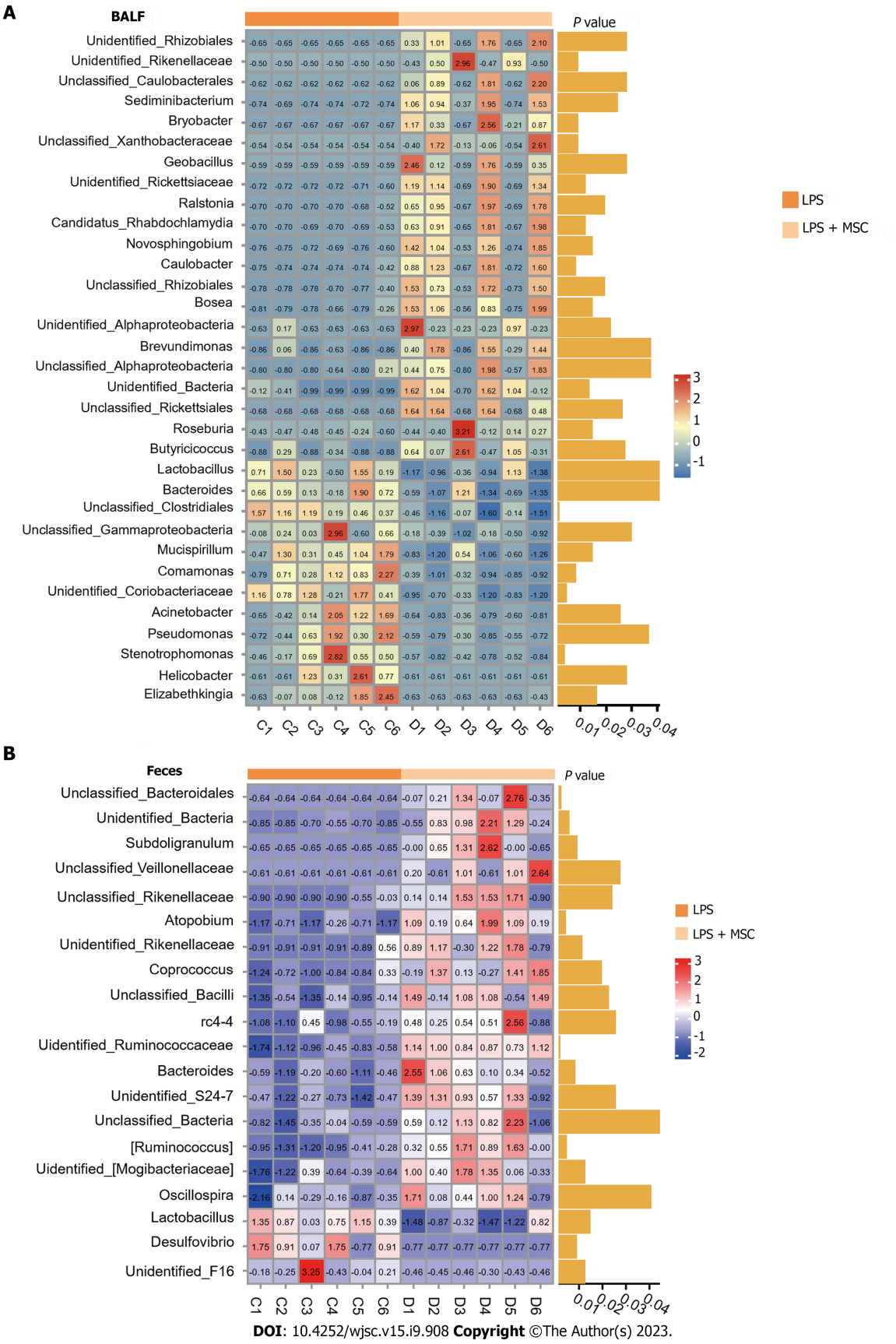

DOI: 10.4252/wjsc.v15.i9.908 **Copyright** ©The Author(s) 2023.

Figure 5 Differences in genus abundance of different microflorae in bronchoalveolar lavage fluid and feces of acute lung injury mice treated with human umbilical cord mesenchymal stem cells (*n* = 6). A and B: Heatmaps showing the differences in the genus abundance of different microflorae in bronchoalveolar lavage fluid and feces. Red represents the genus that is more highly abundant; blue/purple represents the genus that is less abundant; white/yellow indicates no difference in expression between groups. Abundance is homogenized by Z-score. The value displayed in the middle of the grid is log2 (fold change). LPS: Lipopolysaccharide; MSC: Mesenchymal stem cell; BALF: Bronchoalveolar lavage fluid.

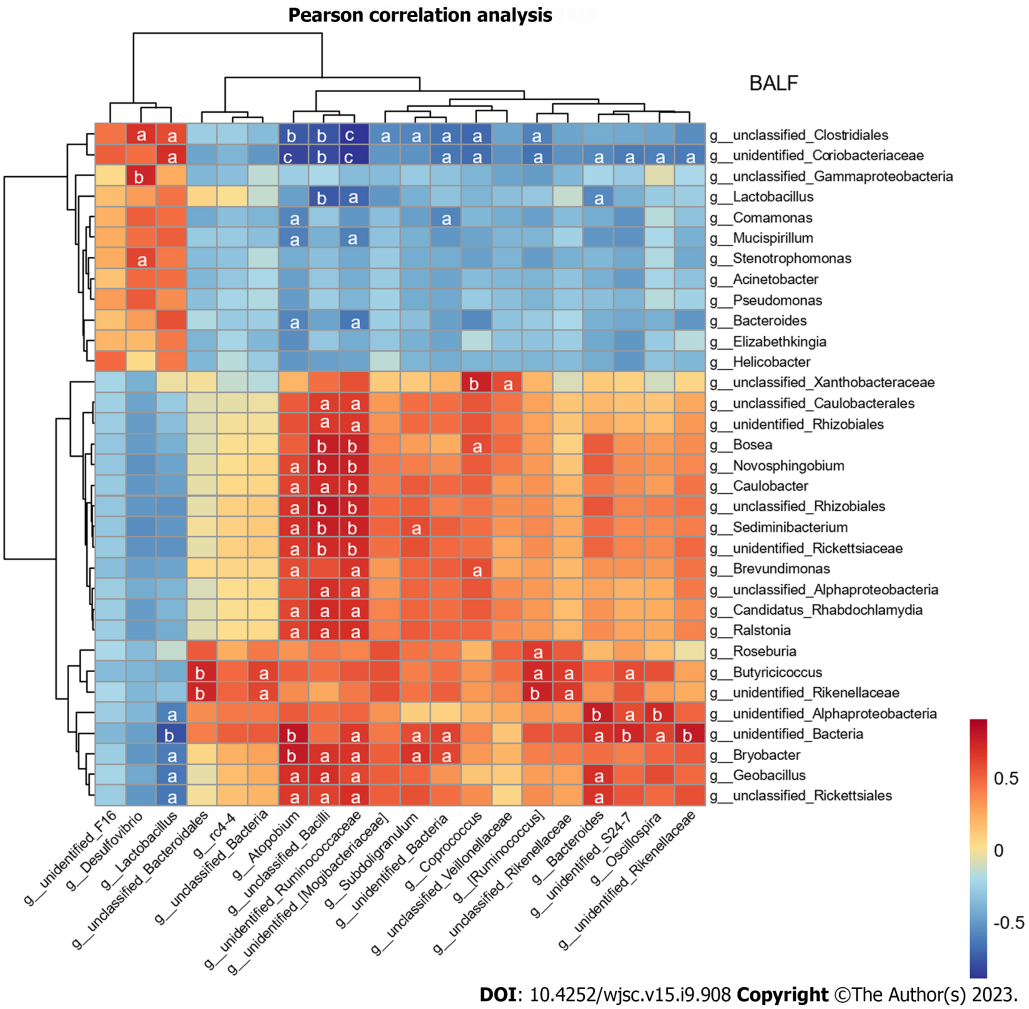

DOI: 10.4252/wjsc.v15.i9.908

Figure 6 Correlation analysis between gut and lung microflorae. Person correlation analysis was used to analyze the correlation between marked microflorae of the gut and lung with OmicsStudio Tools. Red indicates positive correlation and blue indicates negative correlation. $^{a}P < 0.05$, $^{b}P < 0.01$, and $^{c}P < 0.001$ *vs* lipopolysaccharide group. BALF: Bronchoalveolar lavage fluid.

in respiratory tract infections[47]. Additionally, the *Comamonas* genus is an important opportunistic pathogen in human [48]. The genus *Elizabethkingia* has recently emerged as the cause of life-threatening infections in humans, most commonly causing meningitis[49]. *Acinetobacter Baumannii* infections have also been linked to ventilator-associated pneumonia[50]. These findings suggest that HUC-MSCs ameliorate ALI by inhibiting the abundance of pathogenic bacteria. Additionally, by analyzing the microflora in the feces, *Oscillospira* and *Coprococcus* genus abundance in the LPS + MSC group was increased. *Oscillospira*, a common genus of gut bacteria, positively correlates with gut microbiota diversity[51]. Moreover, butyrate, a product of the *Coprococcus* genus, is thought to be able to participate in anti-inflammatory processes[52]. Thus, *Oscillospira* and *Coprococcus* may be involved in the restorative effects of HUC-MSC treatment on gut microflora homeostasis. Additionally, some bacteria have contradictory roles in various diseases. The *Mucispirillum* genus is associated with Crohn's disease-like colitis in immunodeficient mice and is linked to health promotion in immunocompetent hosts[53]. In this study, the improvements in ALI may have been correlated with the abundance of microflora.

Correlation analysis of the gut and lung microflora noticed that the *Desulfovibrio* genus was positively correlated with *Stenotrophomonas*. The *Desulfovibrio* genus is a candidate microbe that induces weight loss of mice with ALI and is directly related to survival[11]. This study not only noted bacteria that strongly correlated with the downregulation of pathogenic bacterial abundance in BALF but also those that were present in both the gut and lungs. *Lactobacillus, Bacteroides,* and *unidentified_Rikenellaceae* genera appeared in the feces and BALF. Moreover, the *Bacteroides* in feces were significantly related to *Lactobacillus* in the BALF. Significant changes in their abundance may be associated with the mechanism of the lung-gut axis. Although the *Lactobacillus* genus is a beneficial flora most of the time in colitis[54], *Lactobacillus rhamnosus* GG treatment in patients with severe pneumonia does not improve the clinical outcomes[55], suggesting that changes in the abundance of *Lactobacillus* may be a consequence of the improvement of ALI by HUM-MSCs and could be used as biomarkers. *Lactobacillus, Bacteroides,* and *unidentified_Rikenellaceae* genera are potential biomarkers for evaluating the treatment efficacy of HUC-MSCs.

Moreover, lung tissue metabolomics was performed in this study, and the composition of metabolites was different in sham mice and ALI mice; HUM-MSC treatment in ALI mice changed the lung metabolite composition. The results of the metabolomic analysis suggest that HUM-MSC treatment alters the bile secretion pathway. Bile and its nuclear receptor farnesoid X are involved in inflammatory liver and bowel diseases[56]. In addition, this study verified the correlation

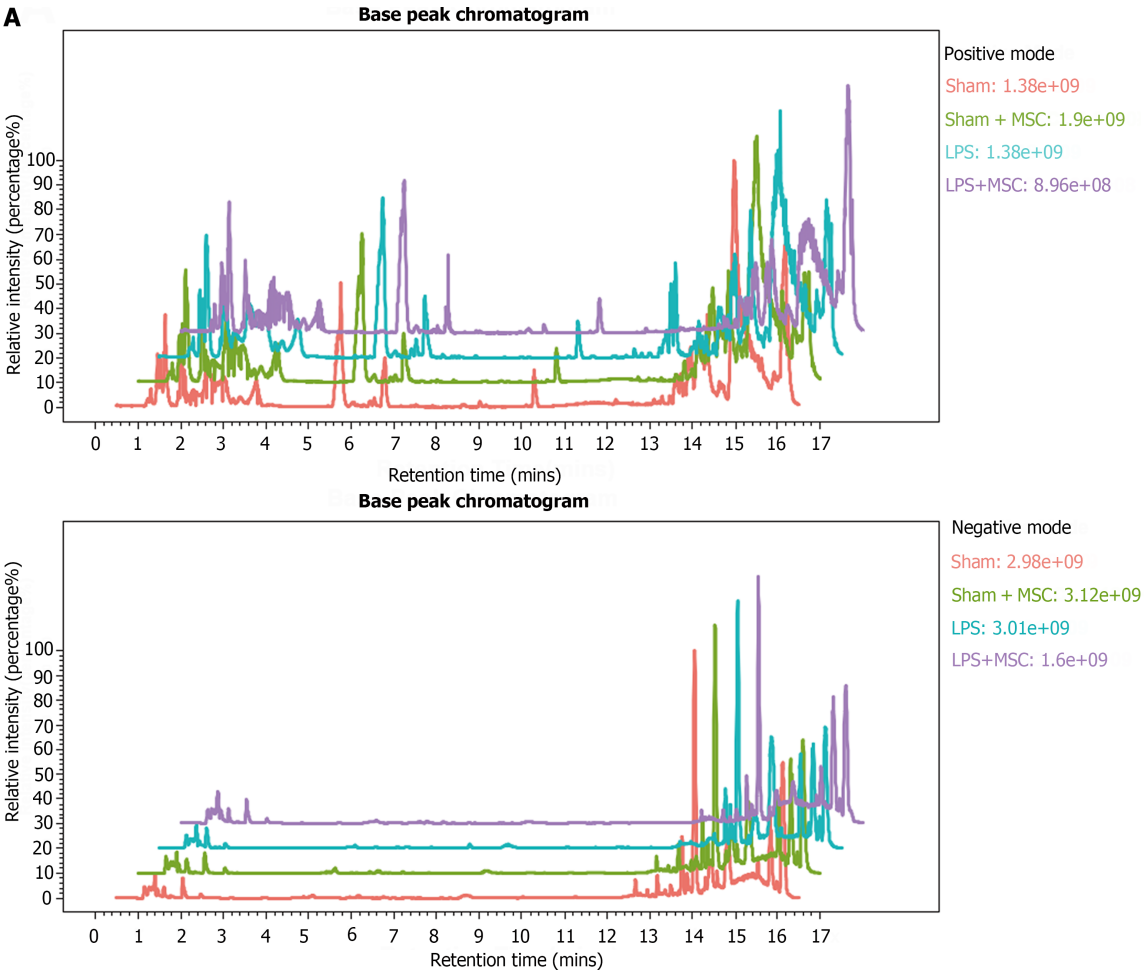
A
Base peak chromatogram
Relative intensity (percentage%)
Retention time (mins)
Positive mode
Sham: 1.38e+09
Sham + MSC: 1.9e+09
LPS: 1.38e+09
LPS+MSC: 8.96e+08
Base peak chromatogram
Relative intensity (percentage%)
Retention time (mins)
Negative mode
Sham: 2.98e+09
Sham + MSC: 3.12e+09
LPS: 3.01e+09
LPS+MSC: 1.6e+09

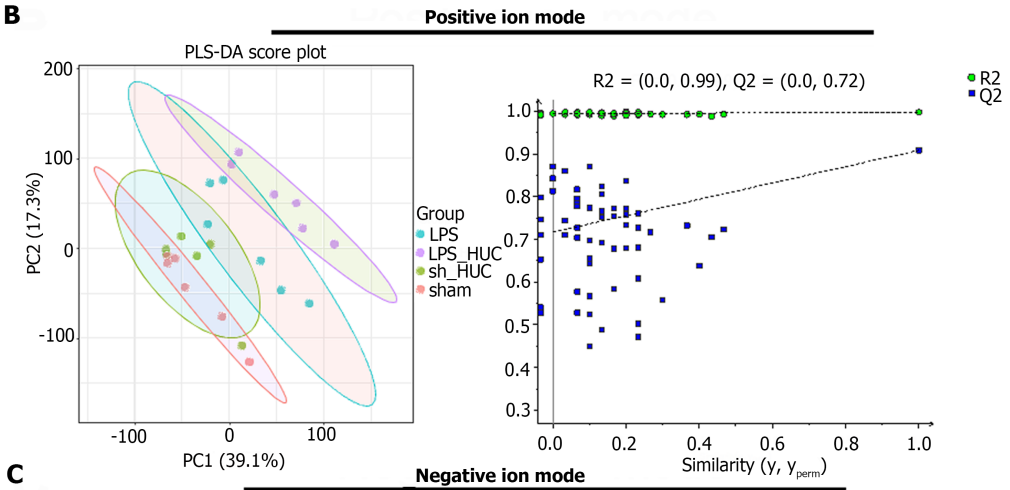
B
Positive ion mode
PLS-DA score plot
PC2 (17.3%)
PC1 (39.1%)
Group
LPS
LPS_HUC
sh_HUC
sham
R2 = (0.0, 0.99), Q2 = (0.0, 0.72)
R2
Q2
Similarity (y, y_perm)

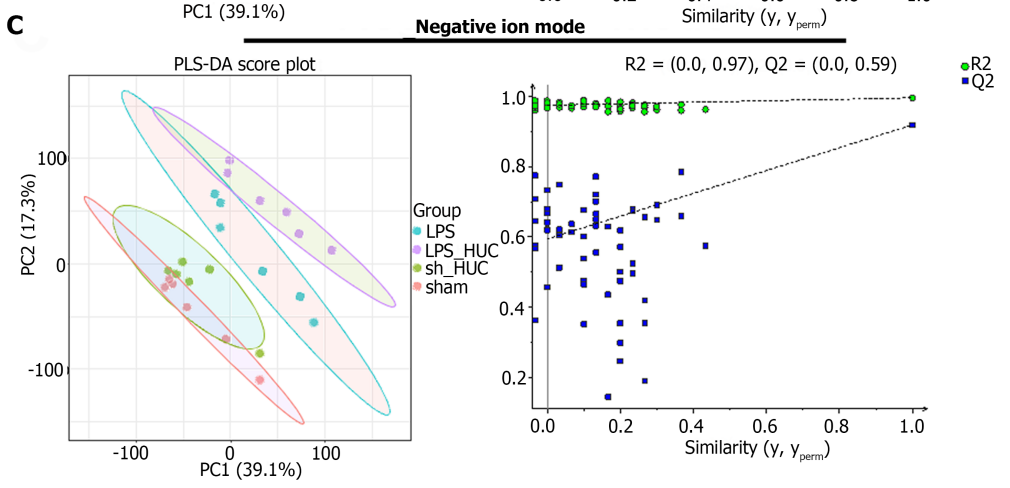
C
Negative ion mode
PLS-DA score plot
PC2 (17.3%)
PC1 (39.1%)
Group
LPS
LPS_HUC
sh_HUC
sham
R2 = (0.0, 0.97), Q2 = (0.0, 0.59)
R2
Q2
Similarity (y, y_perm)

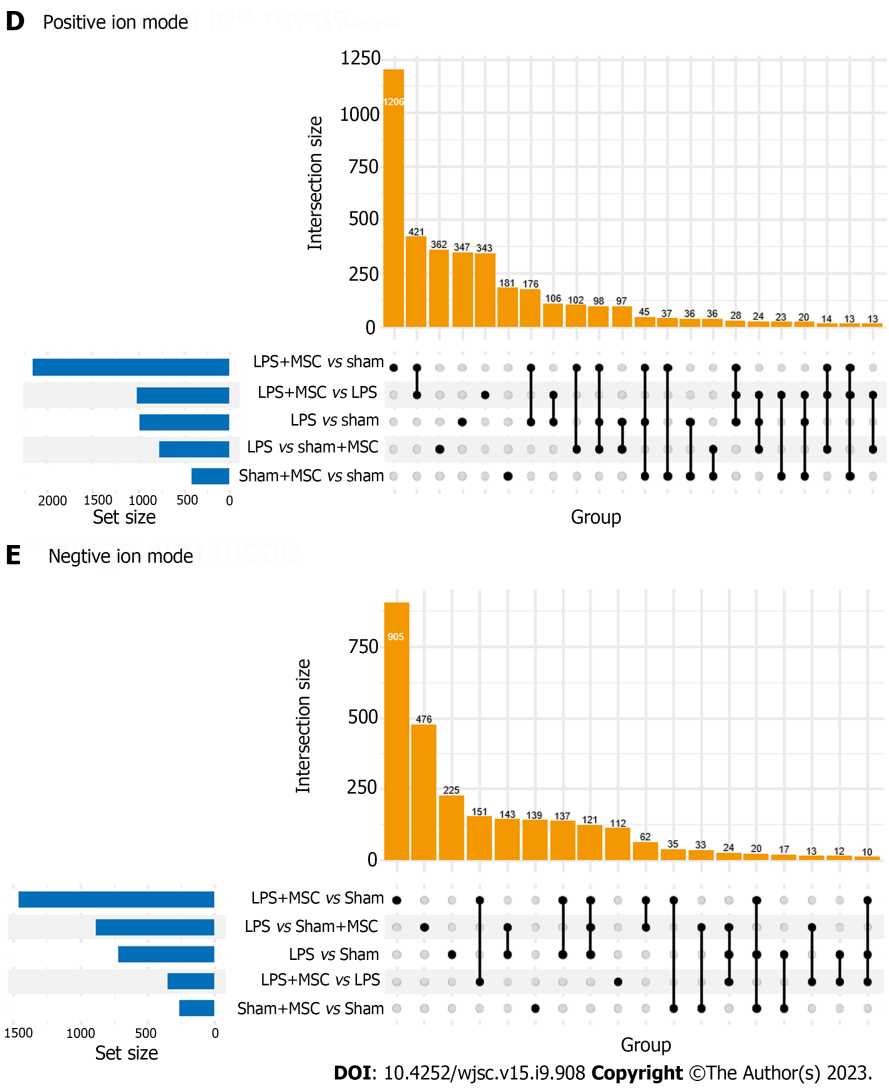

DOI: 10.4252/wjsc.v15.i9.908

Figure 7 Metabolomics for the lung (*n* = 6). A: Base peak chromatogram in positive/negative mode; B and C: The Partial Least Squares-Discriminant Analysis was used to distinguish metabolite differences between groups in positive/negative mode; D and E: Upset Venn diagrams were used to count the number of common and unique differential metabolites in different groups. The bar chart at the bottom left represents the total number of differential metabolites between two groups. The bar chart above shows common metabolites. The results are based on mass spectrum analysis data. LPS: Lipopolysaccharide; MSC: Mesenchymal stem cell.

between the BALF microflora and lung tissue metabolites using the O2PLS method. *Haemophilus* has a pivotal role in improving ALI mice by HUC-MSCs. One study reported that non-typeable *Haemophilus influenzae* induces neutrophilic inflammation in severe asthma[57]. Moreover, Yue *et al*[58] found that autophagy can combat the inflammation caused by *Haemophilus parasuis*, acting as a cellular defense mechanism. Similarly, KEGG enrichment results of the high-impact metabolites predicted by O2PLS suggested that autophagy-related pathways may play a critical role in HUC-MSC treatment in ALI mice. The exploration of lung metabolites contributes to the biological mechanism and biomarker discovery of HUM-MSCs treatment in ALI.

Naturally, this study only examined the correlation between microarray and metabolomics in the lung and gut and cannot have conclusive evidence to confirm that the lung-gut axis microbiota is a crucial factor behind the ability of HUC-MSCs to improve ALI. Animal and clinical studies are necessary to validate the role of gut and lung microorganisms in the improvement of ALI by HUC-MSCs. As depicted in Figure 10, this research showcases the crucial involvement of the lung-intestinal axis in safeguarding the lungs and intestines of ALI rats treated with HUC-MSCs, highlighting the interconnectedness of the lung-intestinal microbiota and metabolites.

CONCLUSION

This study showed that HUM-MSC treatment of ALI improved the edema, tissue injury, and endothelial barrier function of the lung; upregulated the VE-cadherin, ZO-1, and occludin levels in the lung; and inhibited the inflammatory cytokine expression levels in the serum and lung. Moreover, HUM-MSC treatment of ALI attenuated the expression of the TLR4/Myd88/NF-κB signaling pathway in the lung tissue. In addition, HUM-MSC treatment of ALI mice improved ileal histopathological damage, reduced the levels of inflammatory factors, promoted ZO-1, claudin-1, and occludin protein

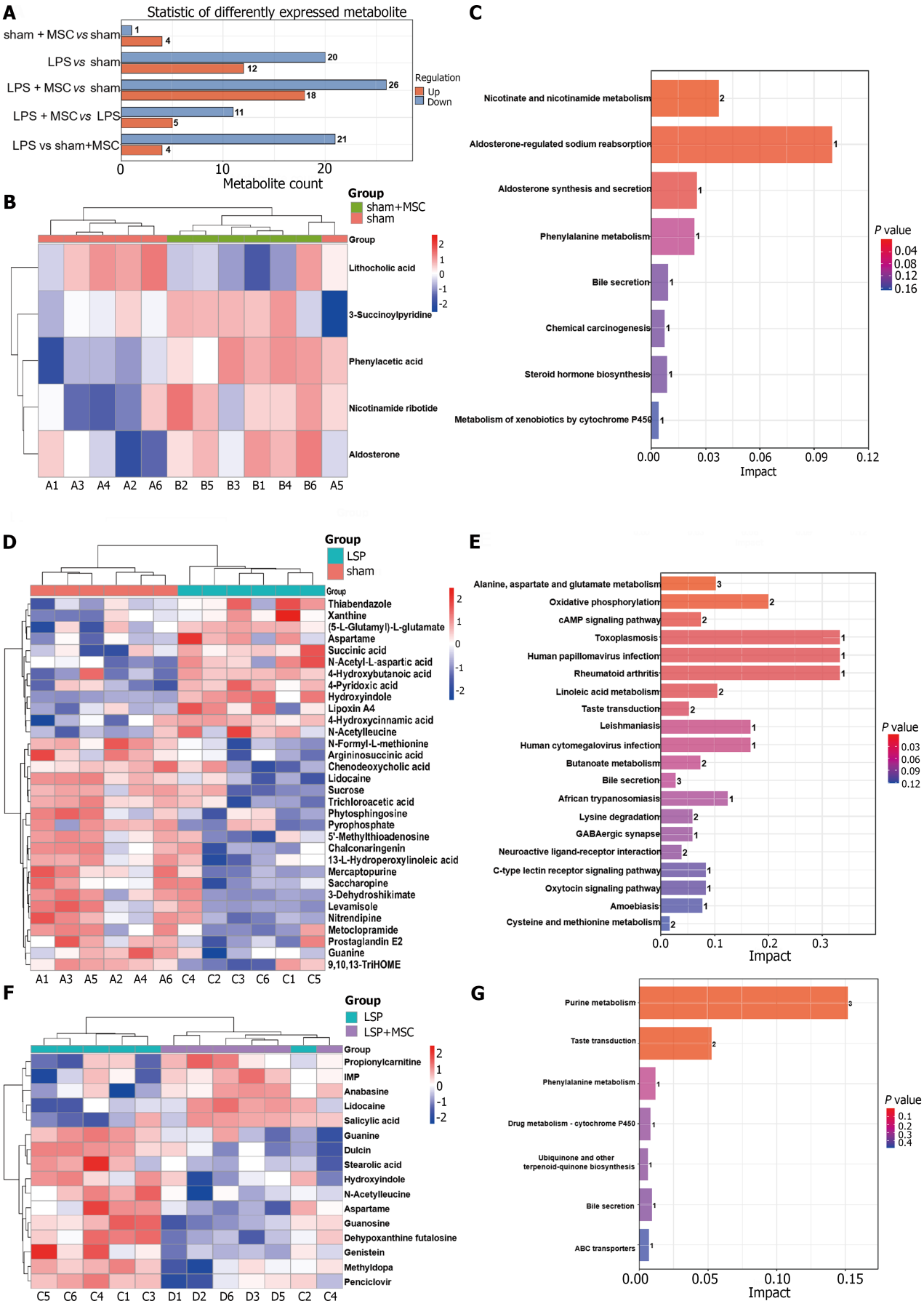

DOI: 10.4252/wjsc.v15.i9.908

Figure 8 Screening of differently expressed metabolites in acute lung injury mice treated with human umbilical cord mesenchymal stem

cells (*n* = 6). A: Statistic of differently expressed metabolites under liquid chromatography-tandem mass spectrometry mode; B: Heatmaps of sham + mesenchymal stem cells (MSCs) group *vs* sham group; C: Kyoto Encyclopedia of Genes and Genomes (KEGG) pathways enriched by differently expressed metabolites of sham + MSC group *vs* sham group; D: The lipopolysaccharide (LPS) group *vs* sham group were used to analyze and display differently expressed metabolites; E: KEGG pathway enriched by differently expressed metabolites of LPS group *vs* sham group; F: Heatmaps of LPS group *vs* LPS + MSC group; G: KEGG pathways enriched by differently expressed metabolites of sham + MSC group *vs* sham group. LPS: Lipopolysaccharide; MSC: Mesenchymal stem cell.

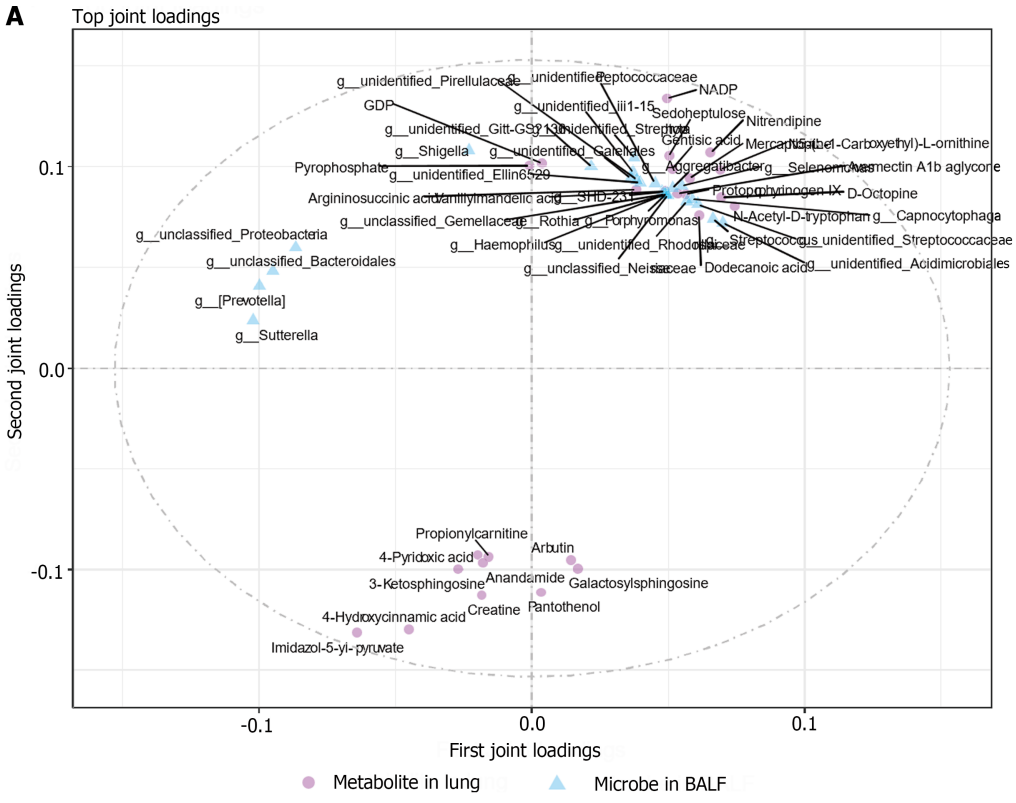

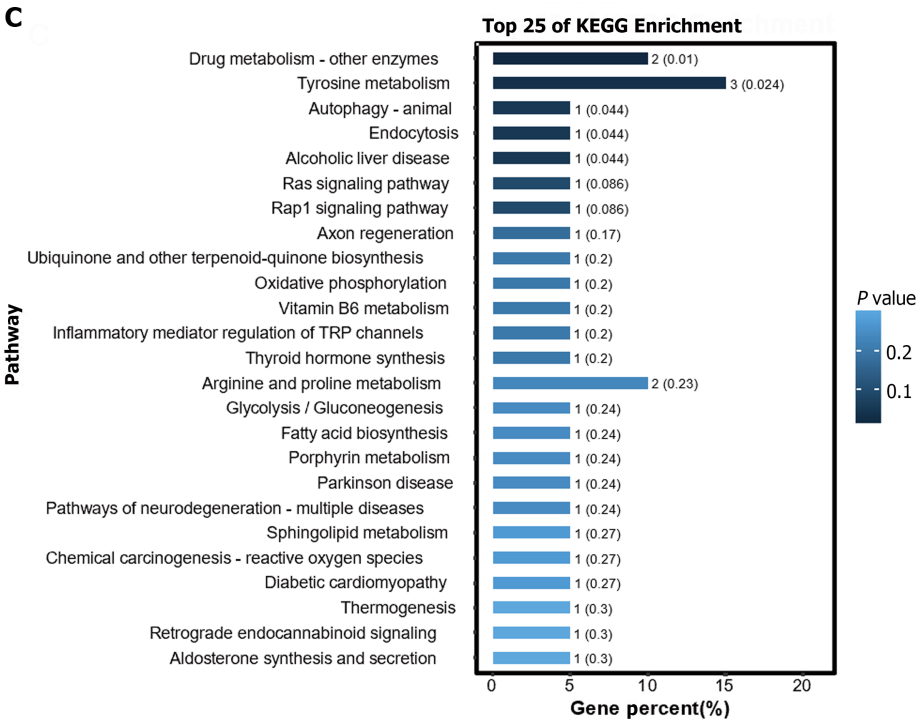

DOI: 10.4252/wjsc.v15.i9.908 **Copyright** ©The Author(s) 2023.

Figure 9 Extent of correlation between lung metabolites and bronchoalveolar lavage fluid microflorae. A: Top 25 lung metabolites and top 25 bronchoalveolar lavage fluid (BALF) microflorae were analyzed by the two-way Orthogonal Partial Least Squares analysis. A larger absolute value in a coordinate indicates a greater degree of association. Circles represent metabolites in lung tissues and squares represent microflora in BALF; B: The number of lung metabolites which were related with BALF microflorae; C: Kyoto Encyclopedia of Genes and Genomes enrichment analysis of top 25 BALF microflorae with strong association. KEGG: Kyoto Encyclopedia of Genes and Genomes; BALF: Bronchoalveolar lavage fluid.

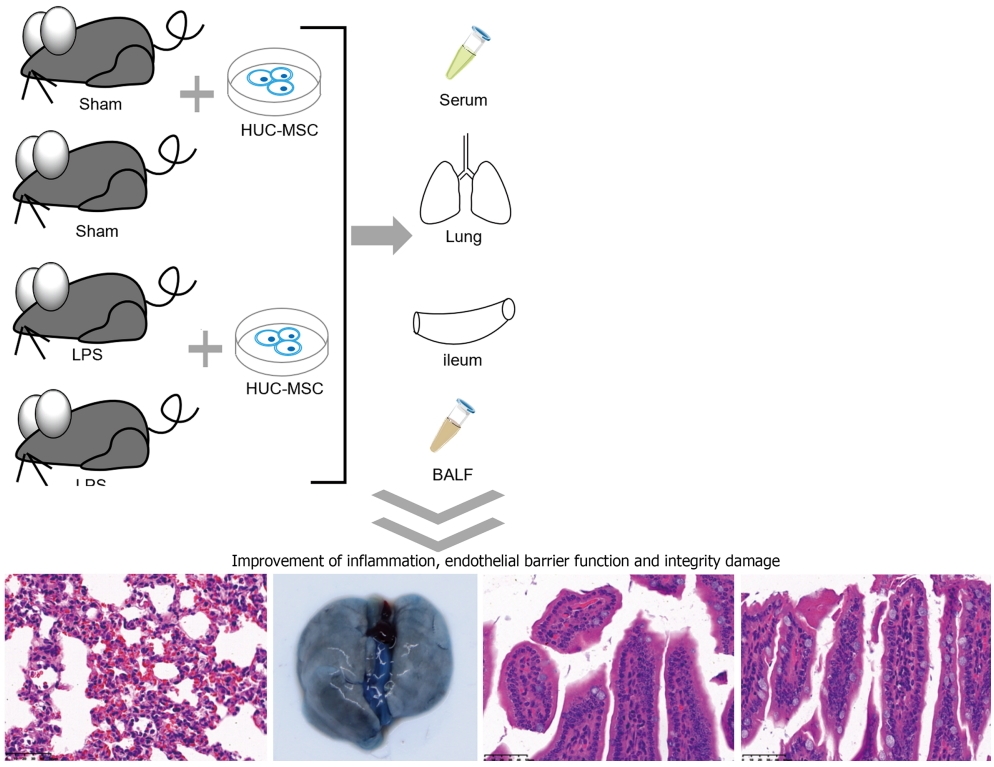

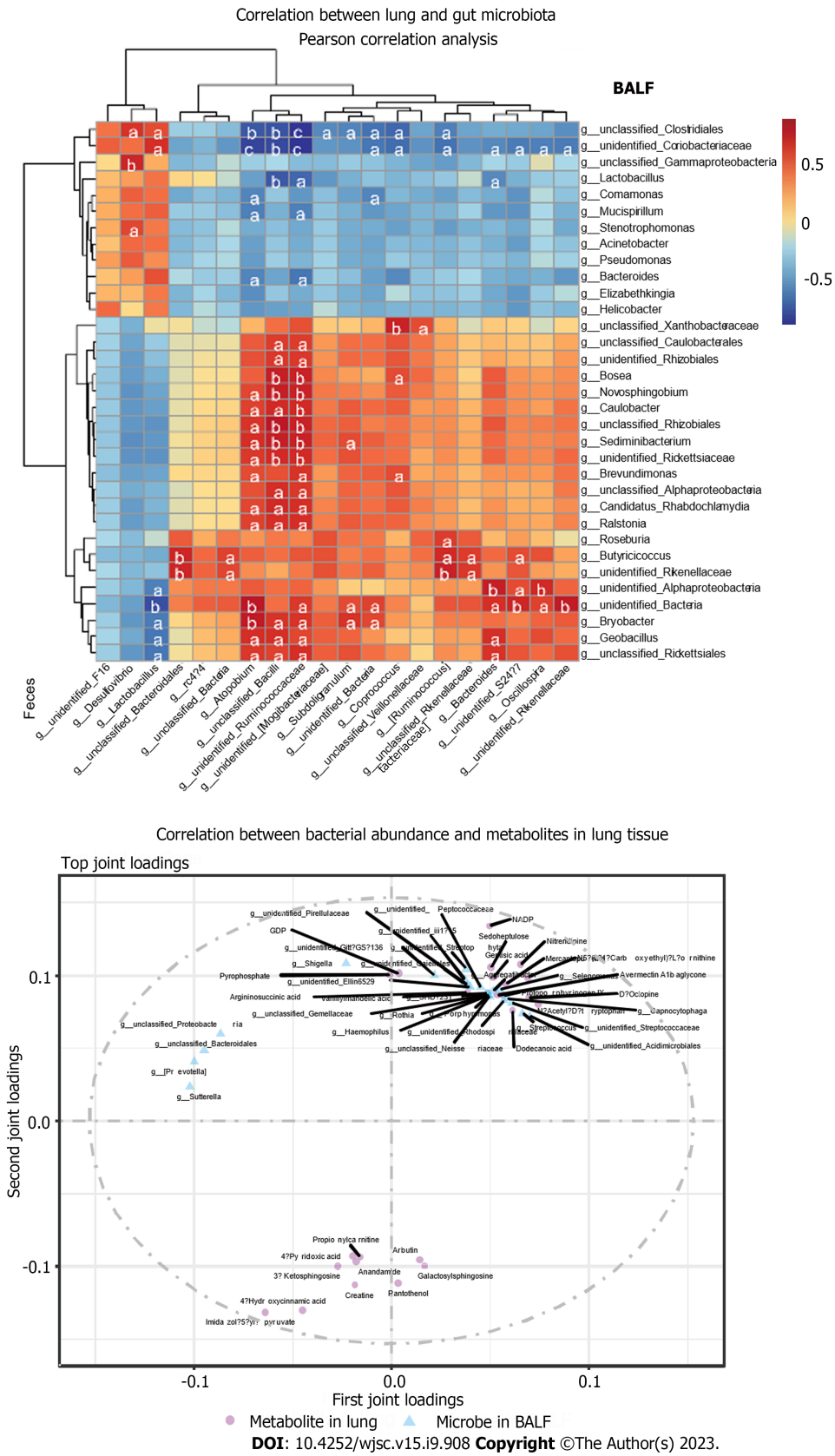

Figure 10 Graphical abstract. LPS: Lipopolysaccharide; MSC: Mesenchymal stem cell; BALF: Bronchoalveolar lavage fluid.

expression, and decreased EUB338 counts in the lung and ileum. In particular, this study found that the gut and lung microflora and metabolites were significantly different between ALI mice untreated and treated with HUM-MSCs. There was a correlation between the abundances of the gut and lung microflora. *Lactobacillus*, *Bacteroides*, and *unidentifiedden-tified_Rikenellaceae* genera are potential biomarkers for evaluating the treatment efficacy of HUC-MSCs. Additionally, this study contributes to the biological mechanism and biomarker discovery of HUM-MSC treatment of ALI by the combined

analysis of lung tissue metabolomics and microbiota, providing a scientific basis for the biological mechanism and clinical application of HUC-MSCs and new ideas for the development of therapeutic strategies for ALI.

ARTICLE HIGHLIGHTS

Research background

Acute lung injury (ALI) has high morbidity and mortality rates and needs effective treatment. Research has found that the gut microbiota improves lung injury through the lung-gut axis. Human umbilical cord mesenchymal cells (HUC-MSCs) can improve ALI.

Research motivation

Although HUC-MSCs can improve ALI, their biological mechanism of action is not yet clear.

Research objectives

To explore changes in the microbiota in the lung-gut axis and the relationship with HUC-MSC treatment.

Research methods

C57BL/6 mice were used to establish an ALI animal model by intraperitoneal injections of lipopolysaccharide. Wright's staining, ELISA, hematoxylin-eosin staining, Evans blue dye leakage assay, immunohistochemistry, fluorescence *in situ* hybridization, and western blot were used to observe the improvement of ALI mice by HUC-MSCs. High-throughput 16S rDNA sequencing was used to observe the microbiota homeostases in the lung-gut axis. The non-targeted metabolomics was used to explore changes in lung tissue metabolites.

Research results

HUC-MSCs ameliorated histopathological damage in the lung and ileum of ALI mice. HUC-MSC treatment improved inflammation, endothelial barrier integrity, and bacterial translocation in the lungs and ileum of ALI mice. HUC-MSCs regulated lung-gut microbiota homeostasis. HUC-MSC treatment regulated the metabolic profile in the lung and ileum of ALI mice.

Research conclusions

This study shows the improvement of changes in the lung and ileum of ALI mice by HUC-MSCs, and suggests a correlation between HUM-MSC-improved ALI and gut and lung microbiota homeostases.

Research perspectives

This study explores the biological mechanism of HUC-MSCs in improving ALI from the perspective of the correlation between the microbiota in the lung-gut axis and lung tissue metabolites, providing a research basis for HUC-MSC treatment.

FOOTNOTES

Author contributions: Cui EH, Lv L, and Wang B conceived and designed the research; Lv L, Li LQ, and Lu HD acquired the data; Cui EH, Li LQ, and Hua F analyzed and interpreted the data; Lv L, Lu HD, Chen WY, and Chen N performed statistical analysis; Cui EH and Wang B obtained the funding; Lv L and Cui EH drafted the manuscript; Cui EH, Wang B, and Hua F revised the manuscript for important intellectual content; and all authors approved the final version of the article.

Supported by the Key Research and Development Project of Science and Technology Department of Zhejiang Province, No. 2019C03041.

Institutional review board statement: The study was reviewed and approved by the Animal Experimentation Ethics Committee of Zhejiang Eyong Pharmaceutical Research and Development Center (License No. SYXK(Zhe)2021-0033).

Institutional animal care and use committee statement: All animal experiments conformed to the internationally accepted principles for the care and use of laboratory animals (Approval No. ZJEY-20220721-02).

Conflict-of-interest statement: All the authors report no relevant conflicts of interest for this article.

Data sharing statement: No additional data are available.

ARRIVE guidelines statement: The authors have read the ARRIVE guidelines, and the manuscript was prepared and revised according to the ARRIVE guidelines.

Country/Territory of origin: China

ORCID number: En-Hai Cui 0000-0002-8808-8793.

S-Editor: Wang JJ
L-Editor: Wang TQ
P-Editor: Cai YX

REFERENCES

1 **Xia L**, Zhang C, Lv N, Liang Z, Ma T, Cheng H, Xia Y, Shi L. AdMSC-derived exosomes alleviate acute lung injury *via* transferring mitochondrial component to improve homeostasis of alveolar macrophages. *Theranostics* 2022; **12**: 2928-2947 [PMID: 35401830 DOI: 10.7150/thno.69533]
2 **Palikova YA**, Palikov VA, Novikova NI, Slashcheva GA, Rasskazova EA, Tukhovskaya EA, Danilkovich AV, Dyachenko IA, Belogurov AA Jr, Kudriaeva AA, Bugrimov DY, Krasnorutskaya ON, Murashev AN. Derinat(®) has an immunomodulatory and anti-inflammatory effect on the model of acute lung injury in male SD rats. *Front Pharmacol* 2022; **13**: 1111340 [PMID: 36642990 DOI: 10.3389/fphar.2022.1111340]
3 **Li J**, Deng SH, Li J, Li L, Zhang F, Zou Y, Wu DM, Xu Y. Obacunone alleviates ferroptosis during lipopolysaccharide-induced acute lung injury by upregulating Nrf2-dependent antioxidant responses. *Cell Mol Biol Lett* 2022; **27**: 29 [PMID: 35305560 DOI: 10.1186/s11658-022-00318-8]
4 **Fan E**, Brodie D, Slutsky AS. Acute Respiratory Distress Syndrome: Advances in Diagnosis and Treatment. *JAMA* 2018; **319**: 698-710 [PMID: 29466596 DOI: 10.1001/jama.2017.21907]
5 **Hou L**, Zhang J, Liu Y, Fang H, Liao L, Wang Z, Yuan J, Wang X, Sun J, Tang B, Chen H, Ye P, Ding Z, Lu H, Wang Y. MitoQ alleviates LPS-mediated acute lung injury through regulating Nrf2/Drp1 pathway. *Free Radic Biol Med* 2021; **165**: 219-228 [PMID: 33539948 DOI: 10.1016/j.freeradbiomed.2021.01.045]
6 **Ju M**, Liu B, He H, Gu Z, Liu Y, Su Y, Zhu D, Cang J, Luo Z. MicroRNA-27a alleviates LPS-induced acute lung injury in mice *via* inhibiting inflammation and apoptosis through modulating TLR4/MyD88/NF-κB pathway. *Cell Cycle* 2018; **17**: 2001-2018 [PMID: 30231673 DOI: 10.1080/15384101.2018.1509635]
7 **Yang C**, Song C, Liu Y, Qu J, Li H, Xiao W, Kong L, Ge H, Sun Y, Lv W. Re-Du-Ning injection ameliorates LPS-induced lung injury through inhibiting neutrophil extracellular traps formation. *Phytomedicine* 2021; **90**: 153635 [PMID: 34229173 DOI: 10.1016/j.phymed.2021.153635]
8 **Tang J**, Xu L, Zeng Y, Gong F. Effect of gut microbiota on LPS-induced acute lung injury by regulating the TLR4/NF-kB signaling pathway. *Int Immunopharmacol* 2021; **91**: 107272 [PMID: 33360370 DOI: 10.1016/j.intimp.2020.107272]
9 **Dickson RP**, Schultz MJ, van der Poll T, Schouten LR, Falkowski NR, Luth JE, Sjoding MW, Brown CA, Chanderraj R, Huffnagle GB, Bos LDJ; Biomarker Analysis in Septic ICU Patients (BASIC) Consortium. Lung Microbiota Predict Clinical Outcomes in Critically Ill Patients. *Am J Respir Crit Care Med* 2020; **201**: 555-563 [PMID: 31973575 DOI: 10.1164/rccm.201907-1487OC]
10 **Jin C**, Chen J, Gu J, Zhang W. Gut-lymph-lung pathway mediates sepsis-induced acute lung injury. *Chin Med J (Engl)* 2020; **133**: 2212-2218 [PMID: 32858588 DOI: 10.1097/CM9.0000000000000928]
11 **Yoon YM**, Hrusch CL, Fei N, Barrón GM, Mills KAM, Hollinger MK, Velez TE, Leone VA, Chang EB, Sperling AI. Gut microbiota modulates bleomycin-induced acute lung injury response in mice. *Respir Res* 2022; **23**: 337 [PMID: 36496380 DOI: 10.1186/s12931-022-02264-7]
12 **Hashimoto Y**, Eguchi A, Wei Y, Shinno-Hashimoto H, Fujita Y, Ishima T, Chang L, Mori C, Suzuki T, Hashimoto K. Antibiotic-induced microbiome depletion improves LPS-induced acute lung injury *via* gut-lung axis. *Life Sci* 2022; **307**: 120885 [PMID: 35981631 DOI: 10.1016/j.lfs.2022.120885]
13 **Yeoh YK**, Zuo T, Lui GC, Zhang F, Liu Q, Li AY, Chung AC, Cheung CP, Tso EY, Fung KS, Chan V, Ling L, Joynt G, Hui DS, Chow KM, Ng SSS, Li TC, Ng RW, Yip TC, Wong GL, Chan FK, Wong CK, Chan PK, Ng SC. Gut microbiota composition reflects disease severity and dysfunctional immune responses in patients with COVID-19. *Gut* 2021; **70**: 698-706 [PMID: 33431578 DOI: 10.1136/gutjnl-2020-323020]
14 **Tang Q**, Liu R, Chu G, Wang Y, Cui H, Zhang T, Bi K, Gao P, Song Z, Li Q. A Comprehensive Analysis of Microflora and Metabolites in the Development of Ulcerative Colitis into Colorectal Cancer Based on the Lung-Gut Correlation Theory. *Molecules* 2022; **27** [PMID: 36144573 DOI: 10.3390/molecules27185838]
15 **Samsonraj RM**, Raghunath M, Nurcombe V, Hui JH, van Wijnen AJ, Cool SM. Concise Review: Multifaceted Characterization of Human Mesenchymal Stem Cells for Use in Regenerative Medicine. *Stem Cells Transl Med* 2017; **6**: 2173-2185 [PMID: 29076267 DOI: 10.1002/sctm.17-0129]
16 **Ding DC**, Shyu WC, Lin SZ. Mesenchymal stem cells. *Cell Transplant* 2011; **20**: 5-14 [PMID: 21396235 DOI: 10.3727/096368910X]
17 **Xu Y**, Zhu J, Feng B, Lin F, Zhou J, Liu J, Shi X, Lu X, Pan Q, Yu J, Zhang Y, Li L, Cao H. Immunosuppressive effect of mesenchymal stem cells on lung and gut CD8(+) T cells in lipopolysaccharide-induced acute lung injury in mice. *Cell Prolif* 2021; **54**: e13028 [PMID: 33738881 DOI: 10.1111/cpr.13028]
18 **Kakabadze Z**, Kipshidze N, Paresishvili T, Vadachkoria Z, Chakhunashvili D. Human Placental Mesenchymal Stem Cells for the Treatment of ARDS in Rat. *Stem Cells Int* 2022; **2022**: 8418509 [PMID: 35756754 DOI: 10.1155/2022/8418509]
19 **Ahn SY**, Chang YS, Kim JH, Sung SI, Park WS. Two-Year Follow-Up Outcomes of Premature Infants Enrolled in the Phase I Trial of Mesenchymal Stem Cells Transplantation for Bronchopulmonary Dysplasia. *J Pediatr* 2017; **185**: 49-54.e2 [PMID: 28341525 DOI: 10.1016/j.jpeds.2017.02.061]
20 **Tu C**, Wang Z, Xiang E, Zhang Q, Zhang Y, Wu P, Li C, Wu D. Human Umbilical Cord Mesenchymal Stem Cells Promote Macrophage PD-L1 Expression and Attenuate Acute Lung Injury in Mice. *Curr Stem Cell Res Ther* 2022; **17**: 564-575 [PMID: 35086457 DOI: 10.2174/1574888X17666220127110332]

21 **Choi SM**, Mo Y, Bang JY, Ko YG, Ahn YH, Kim HY, Koh J, Yim JJ, Kang HR. Classical monocyte-derived macrophages as therapeutic targets of umbilical cord mesenchymal stem cells: comparison of intratracheal and intravenous administration in a mouse model of pulmonary fibrosis. *Respir Res* 2023; **24**: 68 [PMID: 36870972 DOI: 10.1186/s12931-023-02357-x]

22 **Liu A**, Wang X, Liang X, Wang W, Li C, Qian J, Zhang X. Human umbilical cord mesenchymal stem cells regulate immunoglobulin a secretion and remodel the diversification of intestinal microbiota to improve colitis. *Front Cell Infect Microbiol* 2022; **12**: 960208 [PMID: 36118029 DOI: 10.3389/fcimb.2022.960208]

23 **Luo L**, Chen Q, Yang L, Zhang Z, Xu J, Gou D. MSCs Therapy Reverse the Gut Microbiota in Hypoxia-Induced Pulmonary Hypertension Mice. *Front Physiol* 2021; **12**: 712139 [PMID: 34531759 DOI: 10.3389/fphys.2021.712139]

24 **Wu KH**, Li JP, Chao WR, Lee YJ, Yang SF, Cheng CC, Chao YH. Immunomodulation *via* MyD88-NFκB Signaling Pathway from Human Umbilical Cord-Derived Mesenchymal Stem Cells in Acute Lung Injury. *Int J Mol Sci* 2022; **23** [PMID: 35628107 DOI: 10.3390/ijms23105295]

25 **Li Y**, Xu J, Shi W, Chen C, Shao Y, Zhu L, Lu W, Han X. Mesenchymal stromal cell treatment prevents H9N2 avian influenza virus-induced acute lung injury in mice. *Stem Cell Res Ther* 2016; **7**: 159 [PMID: 27793190 DOI: 10.1186/s13287-016-0395-z]

26 **Hao X**, Wei H. LncRNA H19 alleviates sepsis-induced acute lung injury by regulating the miR-107/TGFBR3 axis. *BMC Pulm Med* 2022; **22**: 371 [PMID: 36180862 DOI: 10.1186/s12890-022-02091-y]

27 **Yang J**, Watkins D, Chen CL, Bhushan B, Zhou Y, Besner GE. Heparin-binding epidermal growth factor-like growth factor and mesenchymal stem cells act synergistically to prevent experimental necrotizing enterocolitis. *J Am Coll Surg* 2012; **215**: 534-545 [PMID: 22819639 DOI: 10.1016/j.jamcollsurg.2012.05.037]

28 **Jin S**, Ding X, Yang C, Li W, Deng M, Liao H, Lv X, Pitt BR, Billiar TR, Zhang LM, Li Q. Mechanical Ventilation Exacerbates Poly (I:C) Induced Acute Lung Injury: Central Role for Caspase-11 and Gut-Lung Axis. *Front Immunol* 2021; **12**: 693874 [PMID: 34349759 DOI: 10.3389/fimmu.2021.693874]

29 **Peng J**, Li J, Huang J, Xu P, Huang H, Liu Y, Yu L, Yang Y, Zhou B, Jiang H, Chen K, Dang Y, Zhang Y, Luo C, Li G. p300/CBP inhibitor A-485 alleviates acute liver injury by regulating macrophage activation and polarization. *Theranostics* 2019; **9**: 8344-8361 [PMID: 31754401 DOI: 10.7150/thno.30707]

30 **Liu X**, Song Y, Li R. The use of combined PCR, fluorescence in situ hybridisation and immunohistochemical staining to diagnose mucormycosis from formalin-fixed paraffin-embedded tissues. *Mycoses* 2021; **64**: 1460-1470 [PMID: 34674327 DOI: 10.1111/myc.13382]

31 **Yi Q**, Liu J, Zhang Y, Qiao H, Chen F, Zhang S, Guan W. Anethole Attenuates Enterotoxigenic Escherichia coli-Induced Intestinal Barrier Disruption and Intestinal Inflammation *via* Modification of TLR Signaling and Intestinal Microbiota. *Front Microbiol* 2021; **12**: 647242 [PMID: 33841372 DOI: 10.3389/fmicb.2021.647242]

32 **Lyu F**, Han F, Ge C, Mao W, Chen L, Hu H, Chen G, Lang Q, Fang C. Omicstudio: A composable bioinformatics cloud platform with real-time feedback that can generate high-quality graphs for publication. *iMeta* 2023; **2** [DOI: 10.1002/imt2.85]

33 **Wishart DS**, Guo A, Oler E, Wang F, Anjum A, Peters H, Dizon R, Sayeeda Z, Tian S, Lee BL, Berjanskii M, Mah R, Yamamoto M, Jovel J, Torres-Calzada C, Hiebert-Giesbrecht M, Lui VW, Varshavi D, Allen D, Arndt D, Khetarpal N, Sivakumaran A, Harford K, Sanford S, Yee K, Cao X, Budinski Z, Liigand J, Zhang L, Zheng J, Mandal R, Karu N, Dambrova M, Schiöth HB, Greiner R, Gautam V. HMDB 5.0: the Human Metabolome Database for 2022. *Nucleic Acids Res* 2022; **50**: D622-D631 [PMID: 34986597 DOI: 10.1093/nar/gkab1062]

34 **Kanehisa M**, Furumichi M, Sato Y, Kawashima M, Ishiguro-Watanabe M. KEGG for taxonomy-based analysis of pathways and genomes. *Nucleic Acids Res* 2023; **51**: D587-D592 [PMID: 36300620 DOI: 10.1093/nar/gkac963]

35 **Huang Y**, Wu Q, Tam PKH. Immunomodulatory Mechanisms of Mesenchymal Stem Cells and Their Potential Clinical Applications. *Int J Mol Sci* 2022; **23** [PMID: 36077421 DOI: 10.3390/ijms231710023]

36 **Jerkic M**, Szaszi K, Laffey JG, Rotstein O, Zhang H. Key Role of Mesenchymal Stromal Cell Interaction with Macrophages in Promoting Repair of Lung Injury. *Int J Mol Sci* 2023; **24** [PMID: 36834784 DOI: 10.3390/ijms24043376]

37 **Wang Y**, Zhang Y, Lu B, Xi J, Ocansey DKW, Mao F, Hao D, Yan Y. hucMSC-Ex Alleviates IBD-Associated Intestinal Fibrosis by Inhibiting ERK Phosphorylation in Intestinal Fibroblasts. *Stem Cells Int* 2023; **2023**: 2828981 [PMID: 36845967 DOI: 10.1155/2023/2828981]

38 **Soe HJ**, Khan AM, Manikam R, Samudi Raju C, Vanhoutte P, Sekaran SD. High dengue virus load differentially modulates human microvascular endothelial barrier function during early infection. *J Gen Virol* 2017; **98**: 2993-3007 [PMID: 29182510 DOI: 10.1099/jgv.0.000981]

39 **Jiao Y**, Zhang T, Zhang C, Ji H, Tong X, Xia R, Wang W, Ma Z, Shi X. Exosomal miR-30d-5p of neutrophils induces M1 macrophage polarization and primes macrophage pyroptosis in sepsis-related acute lung injury. *Crit Care* 2021; **25**: 356 [PMID: 34641966 DOI: 10.1186/s13054-021-03775-3]

40 **Kao TI**, Chen PJ, Wang YH, Tseng HH, Chang SH, Wu TS, Yang SH, Lee YT, Hwang TL. Bletinib ameliorates neutrophilic inflammation and lung injury by inhibiting Src family kinase phosphorylation and activity. *Br J Pharmacol* 2021; **178**: 4069-4084 [PMID: 34131920 DOI: 10.1111/bph.15597]

41 **Chen DQ**, Shen MJ, Wang H, Li Y, Tang AL, Li S, Xiong MC, Guo Y, Zhang GQ. Sirt3 Maintains Microvascular Endothelial Adherens Junction Integrity to Alleviate Sepsis-Induced Lung Inflammation by Modulating the Interaction of VE-Cadherin and β-Catenin. *Oxid Med Cell Longev* 2021; **2021**: 8978795 [PMID: 34630854 DOI: 10.1155/2021/8978795]

42 **Botros L**, Pronk MCA, Juschten J, Liddle J, Morsing SKH, van Buul JD, Bates RH, Tuinman PR, van Bezu JSM, Huveneers S, Bogaard HJ, van Hinsbergh VWM, Hordijk PL, Aman J. Bosutinib prevents vascular leakage by reducing focal adhesion turnover and reinforcing junctional integrity. *J Cell Sci* 2020; **133** [PMID: 32198280 DOI: 10.1242/jcs.240077]

43 **Wang YW**, Wu YH, Zhang JZ, Tang JH, Fan RP, Li F, Yu BY, Kou JP, Zhang YY. Ruscogenin attenuates particulate matter-induced acute lung injury in mice *via* protecting pulmonary endothelial barrier and inhibiting TLR4 signaling pathway. *Acta Pharmacol Sin* 2021; **42**: 726-734 [PMID: 32855531 DOI: 10.1038/s41401-020-00502-6]

44 **Zhang L**, Li Q, Liu W, Liu Z, Shen H, Zhao M. Mesenchymal Stem Cells Alleviate Acute Lung Injury and Inflammatory Responses Induced by Paraquat Poisoning. *Med Sci Monit* 2019; **25**: 2623-2632 [PMID: 30967525 DOI: 10.12659/MSM.915804]

45 **Płóciennikowska A**, Hromada-Judycka A, Borzęcka K, Kwiatkowska K. Co-operation of TLR4 and raft proteins in LPS-induced pro-inflammatory signaling. *Cell Mol Life Sci* 2015; **72**: 557-581 [PMID: 25332099 DOI: 10.1007/s00018-014-1762-5]

46 **Chai L**, Wang Q, Si C, Gao W, Zhang L. Potential Association Between Changes in Microbiota Level and Lung Diseases: A Meta-Analysis. *Front Med (Lausanne)* 2021; **8**: 723635 [PMID: 35096850 DOI: 10.3389/fmed.2021.723635]

47 **Brooke JS**. Stenotrophomonas maltophilia: an emerging global opportunistic pathogen. *Clin Microbiol Rev* 2012; **25**: 2-41 [PMID: 22232370 DOI: 10.1128/CMR.00019-11]

48 **Ryan MP**, Sevjahova L, Gorman R, White S. The Emergence of the Genus Comamonas as Important Opportunistic Pathogens. *Pathogens* 2022; **11** [PMID: 36145464 DOI: 10.3390/pathogens11091032]

49 **Lin JN**, Lai CH, Yang CH, Huang YH. Elizabethkingia Infections in Humans: From Genomics to Clinics. *Microorganisms* 2019; **7** [PMID: 31466280 DOI: 10.3390/microorganisms7090295]

50 **Liu Z**, Xu W. Neutrophil and Macrophage Response in Acinetobacter Baumannii Infection and Their Relationship to Lung Injury. *Front Cell Infect Microbiol* 2022; **12**: 890511 [PMID: 35873147 DOI: 10.3389/fcimb.2022.890511]

51 **Chen YR**, Zheng HM, Zhang GX, Chen FL, Chen LD, Yang ZC. High Oscillospira abundance indicates constipation and low BMI in the Guangdong Gut Microbiome Project. *Sci Rep* 2020; **10**: 9364 [PMID: 32518316 DOI: 10.1038/s41598-020-66369-z]

52 **Keshavarzian A**, Green SJ, Engen PA, Voigt RM, Naqib A, Forsyth CB, Mutlu E, Shannon KM. Colonic bacterial composition in Parkinson's disease. *Mov Disord* 2015; **30**: 1351-1360 [PMID: 26179554 DOI: 10.1002/mds.26307]

53 **Herp S**, Durai Raj AC, Salvado Silva M, Woelfel S, Stecher B. The human symbiont Mucispirillum schaedleri: causality in health and disease. *Med Microbiol Immunol* 2021; **210**: 173-179 [PMID: 34021796 DOI: 10.1007/s00430-021-00702-9]

54 **Huang L**, Wang J, Kong L, Wang X, Li Q, Zhang L, Shi J, Duan J, Mu H. ROS-responsive hyaluronic acid hydrogel for targeted delivery of probiotics to relieve colitis. *Int J Biol Macromol* 2022; **222**: 1476-1486 [PMID: 36195227 DOI: 10.1016/j.ijbiomac.2022.09.247]

55 **Johnstone J**, Meade M, Lauzier F, Marshall J, Duan E, Dionne J, Arabi YM, Heels-Ansdell D, Thabane L, Lamarche D, Surette M, Zytaruk N, Mehta S, Dodek P, McIntyre L, English S, Rochwerg B, Karachi T, Henderson W, Wood G, Ovakim D, Herridge M, Granton J, Wilcox ME, Goffi A, Stelfox HT, Niven D, Muscedere J, Lamontagne F, D'Aragon F, St-Arnaud C, Ball I, Nagpal D, Girard M, Aslanian P, Charbonney E, Williamson D, Sligl W, Friedrich J, Adhikari NK, Marquis F, Archambault P, Khwaja K, Kristof A, Kutsogiannis J, Zarychanski R, Paunovic B, Reeve B, Lellouche F, Hosek P, Tsang J, Binnie A, Trop S, Loubani O, Hall R, Cirone R, Reynolds S, Lysecki P, Golan E, Cartin-Ceba R, Taylor R, Cook D; Prevention of Severe Pneumonia and Endotracheal Colonization Trial (PROSPECT) Investigators and the Canadian Critical Care Trials Group. Effect of Probiotics on Incident Ventilator-Associated Pneumonia in Critically Ill Patients: A Randomized Clinical Trial. *JAMA* 2021; **326**: 1024-1033 [PMID: 34546300 DOI: 10.1001/jama.2021.13355]

56 **Gadaleta RM**, van Mil SW, Oldenburg B, Siersema PD, Klomp LW, van Erpecum KJ. Bile acids and their nuclear receptor FXR: Relevance for hepatobiliary and gastrointestinal disease. *Biochim Biophys Acta* 2010; **1801**: 683-692 [PMID: 20399894 DOI: 10.1016/j.bbalip.2010.04.006]

57 **Ackland J**, Barber C, Heinson A, Azim A, Cleary DW, Christodoulides M, Kurukulaaratchy RJ, Howarth P, Wilkinson TMA, Staples KJ; WATCH study investigators. Nontypeable Haemophilus influenzae infection of pulmonary macrophages drives neutrophilic inflammation in severe asthma. *Allergy* 2022; **77**: 2961-2973 [PMID: 35570583 DOI: 10.1111/all.15375]

58 **Yue C**, Li J, Jin H, Hua K, Zhou W, Wang Y, Cheng G, Liu D, Xu L, Chen Y, Zeng Y. Autophagy Is a Defense Mechanism Inhibiting Invasion and Inflammation During High-Virulent Haemophilus parasuis Infection in PK-15 Cells. *Front Cell Infect Microbiol* 2019; **9**: 93 [PMID: 31106159 DOI: 10.3389/fcimb.2019.00093]

World Journal of Stem Cells

Submit a Manuscript: https://www.f6publishing.com

World J Stem Cells 2023 September 26; 15(9): 931-946

DOI: 10.4252/wjsc.v15.i9.931

ISSN 1948-0210 (online)

ORIGINAL ARTICLE

Basic Study

Integrin beta 3-overexpressing mesenchymal stromal cells display enhanced homing and can reduce atherosclerotic plaque

Hai-Juan Hu, Xue-Ru Xiao, Tong Li, De-Min Liu, Xue Geng, Mei Han, Wei Cui

Specialty type: Cell and tissue engineering

Provenance and peer review: Unsolicited article; Externally peer reviewed.

Peer-review model: Single blind

Peer-review report's scientific quality classification

Grade A (Excellent): A
Grade B (Very good): B, B, B
Grade C (Good): C
Grade D (Fair): D
Grade E (Poor): 0

P-Reviewer: Kotlyarov S, Russia; Liao Z, Singapore; Shalaby MN, Egypt; Ventura C, Italy; Ventura C, Italy

Received: May 31, 2023
Peer-review started: May 31, 2023
First decision: June 14, 2023
Revised: June 22, 2023
Accepted: August 23, 2023
Article in press: August 23, 2023
Published online: September 26, 2023

Hai-Juan Hu, Tong Li, De-Min Liu, Xue Geng, Wei Cui, First Division, Department of Cardiology, The Second Hospital of Hebei Medical University and Institute of Cardiocerebrovascular Disease of Hebei Province, Shijiazhuang 050000, Hebei Province, China

Xue-Ru Xiao, Department of Obstetrics, Shijiazhuang People's Hospital, Shijiazhuang 050030, Hebei Province, China

Mei Han, Key Laboratory of Medical Biotechnology of Hebei Province, Department of Biochemistry and Molecular Biology, College of Basic Medicine, Cardiovascular Medical Science Center, Hebei Medical University, Shijiazhuang 050017, Hebei Province, China

Corresponding author: Wei Cui, PhD, Professor, First Division, Department of Cardiology, The Second Hospital of Hebei Medical University and Institute of Cardiocerebrovascular Disease of Hebei Province, No. 215 Heping West Road, Shijiazhuang 050000, Hebei Province, China. cuiweihb2h@163.com

Abstract

BACKGROUND

Umbilical cord (UC) mesenchymal stem cell (MSC) transplantation is a potential therapeutic intervention for atherosclerotic vascular disease. Integrin beta 3 (ITGB3) promotes cell migration in several cell types. However, whether ITGB-modified MSCs can migrate to plaque sites *in vivo* and play an anti-atherosclerotic role remains unclear.

AIM

To investigate whether ITGB3-overexpressing MSCs ($MSCs^{ITGB3}$) would exhibit improved homing efficacy in atherosclerosis.

METHODS

UC MSCs were isolated and expanded. Lentiviral vectors encoding ITGB3 or green fluorescent protein (GFP) as control were transfected into MSCs. Sixty male apolipoprotein $E^{-/-}$ mice were acquired from Beijing Vital River Lab Animal Technology Co., Ltd and fed with a high-fat diet (HFD) for 12 wk to induce the formation of atherosclerotic lesions. These HFD-fed mice were randomly separated into three clusters. GFP-labeled MSCs ($MSCs^{GFP}$) or $MSCs^{ITGB3}$ were transplanted into the mice intravenously *via* the tail vein. Immunofluorescence staining, Oil red O staining, histological analyses, western blotting, enzyme-linked immunosorbent assay, and quantitative real-time polymerase chain

reaction were used for the analyses.

RESULTS

ITGB3 modified MSCs successfully differentiated into the "osteocyte" and "adipocyte" phenotypes and were characterized by positive expression (> 91.3%) of CD29, CD73, and CD105 and negative expression (< 1.35%) of CD34 and Human Leukocyte Antigen-DR. In a transwell assay, $MSCs^{ITGB3}$ showed significantly faster migration than $MSCs^{GFP}$. ITGB3 overexpression had no effects on MSC viability, differentiation, and secretion. Immunofluorescence staining revealed that ITGB3 overexpression substantially enhanced the homing of MSCs to plaque sites. Oil red O staining and histological analyses further confirmed the therapeutic effects of $MSCs^{ITGB3}$, significantly reducing the plaque area. Enzyme-linked immunosorbent assay and quantitative real-time polymerase chain reaction revealed that MSC^{ITGB3} transplantation considerably decreased the inflammatory response in pathological tissues by improving the dynamic equilibrium of pro- and anti-inflammatory cytokines.

CONCLUSION

These results showed that ITGB3 overexpression enhanced the MSC homing ability, providing a potential approach for MSC delivery to plaque sites, thereby optimizing their therapeutic effects.

Key Words: Atherosclerosis; Inflammation; Integrin beta 3; Mesenchymal stem cells; Arg-Gly-Asp structure; Umbilical cord

Core Tip: Mesenchymal stem cell (MSC) transplantation is considered a new treatment for atherosclerosis. However, research regarding homing of MSCs to atherosclerotic lesions is insufficient. Here, we transplanted integrin beta 3 (ITGB3)-overexpressing MSCs into a mouse model of atherosclerosis. ITGB3-overexpressing MSCs were more greatly accumulated in atherosclerotic plaques. These MSCs prevented plaque progression by shifting the local cytokine profile. The use of ITGB3-overexpressing MSCs may be a novel tool to treat atherosclerosis.

Citation: Hu HJ, Xiao XR, Li T, Liu DM, Geng X, Han M, Cui W. Integrin beta 3-overexpressing mesenchymal stromal cells display enhanced homing and can reduce atherosclerotic plaque. *World J Stem Cells* 2023; 15(9): 931-946
URL: https://www.wjgnet.com/1948-0210/full/v15/i9/931.htm
DOI: https://dx.doi.org/10.4252/wjsc.v15.i9.931

INTRODUCTION

Atherosclerosis is a serious public health problem and the most commonly diagnosed cardiovascular disease in the general population[1]. Implementing early detection of atherosclerosis[2] with systemic pharmacological treatments[3] and percutaneous coronary intervention[4] has contributed to substantial progress in the treatment of atherosclerosis-related diseases[5,6]. Despite medical improvements, the incidence of atherosclerosis-related diseases remains high[7]. Atherosclerotic plaques are still associated with high mortality rates in patients with high-risk or visible advanced plaque disease. Therefore, more studies are needed to discover and explore effective molecules and targets for treatments.

Mesenchymal stem cell (MSC) transplantation accomplished improvements in experimental studies of atherosclerosis [8-11]. MSCs have the ability to secrete many cytokines that mitigate vascular inflammation and regulate the local microenvironment owing to the effects of their secreted anti-inflammatory factors within the vascular plaque[12-14]. However, some limitations preclude the translation of stem cell therapy into clinical applications[15,16], such as stem cells accurately homing to plaques. To determine this, we need to understand the specific mechanisms that underlie the migration and adhesion of MSCs under physiological and pathological conditions. Some studies have attempted to genetically decorate MSCs with specific receptors required for efficient homing. For example, Shahror *et al*[17] found that overexpression of fibroblast growth factor 21 considerably increased MSC migration to and adhesion in the injured brain tissue. Moreover, overexpression of C-X-C chemokine receptor 5 (CXCR5) increased the migratory capability of MSCs toward CXCL13, which changed most substantially in animal models of contact allergy, accompanied by decreases in inflammatory cellular infiltration and reduced levels of pro-inflammatory cytokine production[18]. It is well established that damaged tissues release specific types of cytokines and chemokines. Therefore, elucidating the interrelationships between tissue-specific chemokines and matching receptors on MSCs could offer novel ways of promoting homing and treatment effects of these cells.

The integrin family of receptors, a major family of migration-promoting receptors, plays an important role in the crosstalk between cells and their surroundings[19,20]. Arg-Gly-Asp (RGD) site-containing proteins and corresponding integrin receptors constitute the primary recognition system for cell adhesion[21,22]. Many inflammatory cytokines, such as intercellular cell adhesion molecule-1 (ICAM-1), osteopontin (OPN), and vascular cell adhesion molecule-1 (VCAM-1), contain an RGD motif in their structure[23,24]. The primary sequence of integrin beta 3 (ITGB3), a well-preserved region in all integrin beta subunits, has been called the RGD crosslinking region[25]. Based on this information, we genetically

modified MSCs using *ex vivo* lentiviral transduction to overexpress ITGB3. In the current study, we first demonstrated that ITGB3-overexpressing MSCs ($MSCs^{ITGB3}$) showed enhanced chemotaxis toward plaque tissues *in vivo* and inflammatory cells *in vitro*. Compared with green fluorescent protein (GFP)-labeled MSCs ($MSCs^{GFP}$), $MSCs^{ITGB3}$ reduced the formation of atherosclerotic plaques in homozygous apolipoprotein-E $(ApoE)^{-/-}$ mice, suggesting that ITGB3 enhances homing of modified stem cells to plaque tissue, thereby promoting their therapeutic efficacy in the $ApoE^{-/-}$ mouse model of atherosclerosis.

MATERIALS AND METHODS

Isolation of human umbilical cord MSCs

Human umbilical cord (UC) samples were collected from three healthy donors. All the donors provided written informed consent. MSCs were isolated and cultured from the UCs as reported previously[26]. Briefly, the UC tissue was collected from healthy pregnant women undergoing labor. After removing the UC tissue's arteries and veins, the remaining Wharton's jelly was cut into small pieces for patch cultures. The tissue fragments were cultured at 37 °C and 5% CO_2 in mesenchymal stem cell medium (MSC medium; Sciencell, Carlsbad, CA, United States) containing 5% fetal bovine serum (FBS), stem cell growth supplements, penicillin, and streptomycin. After 10-15 d, fibroblast-like MSCs migrated out of the tissue patches. The studies involving pregnant participants were reviewed and approved by The Ethical Committee of The Second Hospital of Hebei Medical University (approval number: 2021-R496).

Raw264.7, vascular smooth muscle cell, and primary microvascular endothelial cell cultures

The murine macrophage cell line Raw264.7 was purchased from the Cell Resource Center of Shanghai Institutes for Biological Sciences, the Chinese Academy of Science (Shanghai, China). Vascular smooth muscle cells were isolated from mouse aortas and cultured in low-glucose Dulbecco's modified Eagle's medium containing 10% FBS. Lung primary microvascular endothelial cells were obtained from the lungs of 4-week-old C57 mice through two series of immunoselection with CD31- and CD102-conjugated magnetic beads using a previously described procedure[27] and subsequently cultured in endothelial cell medium containing 5% FBS and endothelial cell growth supplements.

Lentiviral vector construction and transduction

Lentiviral vector (LV) encoding ITGB3 and GFP as control were generated and packaged by Hanbio Biosciences (Shanghai, China). All LVs were used for MSC transfection with an infection multiplicity of 30-40. MSCs were plated at a density of 3-5 × 10^5 cells/cm^2 in each six-well plate, depending on the subsequent use. When MSCs reached 40%-50% confluence, the transfection was performed in the presence of polybrene (Cyagen Biosciences, Santa Clara, CA, United States). Following transfection for 72 h, the transfection effectiveness of the virus was checked through fluorescent staining.

AS model induction and MSC delivery

$ApoE^{-/-}$ mice (7–8-week-old) were acquired from Beijing Vital River Lab Animal Technology Co., Ltd (Beijing, China). Sixty male $ApoE^{-/-}$ mice were housed in Hebei Medical University and fed with standard chow and drinking water for 1 wk to adapt to the new surroundings. Then, all animals were fed a high-fat diet (HFD) for 12 wk to induce the formation of atherosclerotic lesions. These HFD-fed mice were randomly separated into three clusters and received the following treatment: (1) HFD mice (n = 20) were injected 200 μL of phosphate-buffered saline (PBS) into the caudal vein every week from week 9, four times in total; (2) MSC^{GFP} mice (n = 20) receiving 200 μL of PBS containing 1 × 10^6 $MSCs^{GFP}$ intravenously through the tail vein every week from week 9; and (3) MSC^{ITGB3} mice (n = 20) receiving 200 μL of PBS containing 1 × 10^6 $MSCs^{ITGB3}$ intravenously through the tail vein every week from week 9. The animals were euthanized after 12 wk of HFD, the aorta and aortic sinus were collected, and histological samples were processed for subsequent atherosclerosis assessment. At the same time, blood samples were collected to determine lipid levels. All animal procedures complied with the Guide for the Care and Use of Experimental Laboratory Animals and were approved by the Animal Care Committee of The Second Hospital of Hebei Medical University (No. 2021-R496).

Echocardiographic assessment

At the end of week 12, 10 mice were gas-anesthetized *via* a facemask and kept on a minimal dose of isoflurane (1.0%-2.0%). The mice were placed in a supine position and maintained spontaneous breathing with isoflurane insufflation throughout the echocardiographic assessment. Echocardiographic data were recorded by a VisualSonics Vevo2100 Imaging System (Fujifilm Visual Sonics Inc., Tokyo, Japan) with an EZ-SA800 Single Animal System (E-Z Systems Inc., Bethlehem, PA, United States). Ascending aorta functions were evaluated from the parasternal view of the long axis. The diameter of the systolic aorta was measured at the peak anterior movement point of the ascending aorta, and the diameter of the diastolic aorta was measured using a Q-wave (end-diastolic) echocardiogram. The average diameter measurements of five consecutive heart cycles were selected for data analysis. Meanwhile, left ventricle function and heart chamber dimensions were also evaluated, including the left ventricular ejection fraction (EF) and left ventricular fractional shortening (FS), using accompanying software. The data were recorded and analyzed.

Murine aortic tissue culture

Murine aortic rings were cultured as described previously[28]. Briefly, after 12 wk of HFD, external organs and tissues

were removed. Then, the whole aortic vessel was separated from the adipose and surrounding tissue. The aorta was divided into 2-4 mm rings and cultured in low-glucose Dulbecco's modified Eagle's medium supplemented with 5% FBS. Aortic rings were maintained at 37 °C in 5% CO_2 for 24 h for further experiments.

Hematoxylin and eosin staining, Masson's trichrome staining, and oil red O staining

The aortic arch and aortic valve were harvested after 12 wk of HFD. The animals were euthanized, and the left ventricles were cannulated and injected with PBS containing heparin. Thereafter, the aortic arch and aortic valve were separated, embedded in optimal cutting temperature compound, shortly frozen in liquid nitrogen, and sliced. Subsequently, hematoxylin and eosin (HE) staining was performed to assess plaque size. The cross-sectional areas of the plaque were measured with Image-Pro Plus (IPP) 6.0 software (Media Cybernetics Corp., Rockville, MD, United States). Collagen depositions were assessed using Masson's trichrome staining. Average values were determined from at least three sections in each sample.

For oil red O (ORO) staining, the fixed whole aorta was incubated with 0.3% ORO solution (Sigma-Aldrich, St Louis, MO, United States) for 20 min and, then, washed with 60% isopropanol. Frozen aortic arch and aortic valve sections were incubated with ORO for 5 min, washed with PBS, and counterstained with hematoxylin. The atherosclerotic lesions were photographed using a light microscope (Carl Zeiss, Jena, Germany) and quantified using IPP 6.0 software.

Cell viability assay

The effects of LV transfection on MSC viability were evaluated using cell counting kit 8 (CCK-8) assays as described previously[29]. Briefly, MSCs, $MSCs^{ITGB3}$, and $MSCs^{GFP}$ were seeded into 96-well plates at a density of 1×10^4 cells/well, respectively. After 24 h, CCK-8 was added to each well and incubated at 37 °C for 1 h. The absorbance was measured at 450 nm using a VersaMax (Ocean Springs, MI, United States) microplate scanner.

Chemotaxis assays

Chemotaxis assays were operated in 24-well transmembrane chambers with 8-μm pore filters. To test the ability of stem cells to migrate toward defined chemokines, Raw264.7, vascular smooth muscle cells, and primary microvascular endothelial cells were separately seeded into the lower chamber (1×10^5 cells/well). After achieving confluence, serum-free cells were stimulated with tumor necrosis factor-α (TNF-α, 20 ng/mL) for 24 h. Then MSCs, $MSCs^{GFP}$, and $MSCs^{ITGB3}$ were respectively plated into the upper chamber at 2×10^4 cells/well. After incubation for 24 h, the upper layer of cells was removed, and the lower layer was stained with crystal violet.

For the vascular atherosclerotic plaque, mice were sacrificed after week 12. Aortic rings were separately cultured for 24 h in Dulbecco's modified Eagle's medium with 5% FBS. Next, MSCs, $MSCs^{GFP}$, and $MSCs^{ITGB3}$ were respectively plated into the upper chamber at 2×10^4 cells/well. The medium for re-suspending MSCs matched the medium in the lower chamber. After incubation for 24 h, non-migrated cells were removed from the upper surface, and the cells that had migrated across the membrane to the lower surface were fixed with 4% paraformaldehyde and stained with crystal violet. For each membrane, five fields of view were imaged and analyzed. Each experiment was repeated at least three times, and the number of migrated cells was expressed as the mean ± standard error of the mean (SEM) of total cell counts per field.

RNA extraction and quantitative real-time polymerase chain reaction

Total RNA of cells or tissue samples was extracted using TRIzol reagent, according to the manufacturer's protocol. cDNA was synthesized using the M-MLV First Strand Kit. Quantitative real-time polymerase chain reaction (qRT-PCR) using SYBR Green qPCR SuperMix were performed using an ABI 7500. qRT-PCR analyses were repeated at least three times. The qRT-PCR data were standardized to β-actin expression, using the $2^{-\Delta\Delta Ct}$ method. The primers used are listed in Supplementary Table 1. The average threshold cycle for each gene was determined from at least three independent experiments.

Western blot analysis

Cell or tissue lysates were extracted with lysis buffer. Equal amounts of protein were separated by 10% sodium dodecyl-sulfate polyacrylamide gel electrophoresis and transferred to a polyvinylidene fluoride membrane. The membranes were blocked with 5% bovine serum albumin for 1 h at room temperature, incubated with specific antibodies against VCAM-1, ICAM-1, OPN, and GAPDH at 4 °C overnight, and, then, incubated with horseradish peroxidase-conjugated anti-mouse or anti-rabbit immunoglobulin G for 1 h at room temperature. Antigen-antibody complexes were assessed using the GE ImageQuant™ LAS 4000 detection system (GE Healthcare Inc., Chicago, IL, United States). The protein bands of interest were quantified with IPP 6.0 software.

Statistical analyses

Data analysis was performed with GraphPad Prism 8 software (GraphPad Software, Inc., San Diego, CA, United States). Data are displayed as mean ± SEMs, and each independent experiment was repeated three times. The statistical significance of differences between two groups was determined using the unpaired Student's t-test, and comparisons of more than two groups were performed using a one-way analysis of variance. For all statistical comparisons, significance was considered at $P < 0.05$.

RESULTS

Inflammatory factors containing the RGD motif are highly upregulated in atherosclerotic vessels

Atherosclerosis is a chronic inflammatory disease of the arteries with high expression of adherence molecules. We tested the expression of VCAM-1, ICAM-1, and OPN because studies have shown that they contain the RGD motif that can bind to the ITGB3 receptor[19,20,30]. Our results demonstrated that the protein expression levels of VCAM-1, ICAM-1, and OPN were six to eight times higher in atherosclerotic than in control blood vessels (Figure 1A). Similarly, qRT-PCR and immunofluorescence staining also confirmed that the three adhesion factors considerably increased at sites of inflammation (Figure 1B–D).

The ITGB3 receptor is scarcely expressed on human UC-derived MSCs, and ITGB3 overexpression by MSCs does not affect other MSC characteristics

Inflammatory factors that are highly expressed at plaque sites and matching receptors expressed on the surface of MSCs play an important role in guiding stem cells. Thus, we analyzed the expression of the ITGB3 receptor using western blot, qRT-PCR, and fluorescence staining methods. First, human MSCs at the third passage had very low expression of the ITGB3 receptor at the protein and mRNA levels (Figure 2A and B). Second, immunofluorescence staining confirmed that MSCs barely expressed the ITGB3 receptor (Figure 2C and D). To further determine whether overexpression of ITGB3 receptor in MSCs can promote their homing capability toward plaque tissues, MSCs were transfected with LVs encoding ITGB3 and GFP ($MSCs^{ITGB3}$ for short) or GFP ($MSCs^{GFP}$ for short). We found that both $MSCs^{ITGB3}$ and $MSCs^{GFP}$ highly expressed GFP, confirming the stable expression of the GFP reporter gene (Figure 2C). In contrast to $MSCs^{GFP}$ and MSCs, $MSCs^{ITGB3}$ showed substantially stronger expression of ITGB3 at the protein, mRNA, and fluorescence staining levels (Figure 2A–D). Moreover, ITGB3 overexpression did not affect stem cell viability according to CCK8 analyses (Figure 2E). To further verify whether transfection of ITGB3 affects the differentiation properties of MSCs, we observed several typical stem cell markers using flow cytometry and qRT-PCR analyses. The results showed that in $MSCs^{ITGB3}$, MSC-specific markers (CD73, CD105, and CD29), but not hemopoietic stem cell antigens (CD34 and human leukocyte antigen-DR), were highly expressed (Figure 2F and G). The differentiation of $MSCs^{ITGB3}$ into adipocytes and osteoblasts was separately evaluated using ORO and Alizarin red staining (Figure 2H and I). Moreover, marker genes in induced adipocytes and osteoblasts were verified through qRT-PCR (Figure 2J and K). These findings confirmed that transfected MSCs still have stem cell properties.

ITGB3 enhances MSC migration toward inflammatory sites in vitro and in vivo

ITGB3 is vital for cell migration, adhesion, and invasion[20-22,31]. Therefore, we next checked whether $MSCs^{ITGB3}$ could promote MSC migration *in vitro* and *in vivo*. The *in vitro* cell chemotaxis assay showed that in the presence of TNF-α, $MSCs^{ITGB3}$ displayed a significantly increased migration toward the bottom chamber, especially if it contained macrophages (Figure 3A and B). However, in the absence of TNF-α, all cells showed similar, very low, nonspecific migration toward the lower, cell-containing chamber (Figure 3A and B). We also performed transwell-based chemotaxis assays using atherosclerotic aorta samples *in vitro* (Figure 3C and D). $MSCs^{ITGB3}$ had the highest migratory activity, indicating that the atherosclerotic plaque secreted inflammatory factors which were chemoattractants for $MSCs^{ITGB3}$, but not for $MSCs^{GFP}$ (Figure 3C and D). Next, we observed whether MSCs migrate to plaque sites *in vivo* following intravenous infusion. $MSCs^{ITGB3}$ and $MSCs^{GFP}$ were injected into HFD mice through the tail vein every week from weeks 9 to 12. The aortas were collected from each group at the end of week 12 for in situ fluorescence staining. The results showed that $MSCs^{ITGB3}$ were highly aggregated at sites of inflammation, whereas $MSCs^{GFP}$ had less positive staining at such sites (Figure 3E and F). Meanwhile, the qRT-PCR results also revealed that there was a higher GFP expression in the MSC^{ITGB3} group when compared to the GFP expression in the $MSCs^{GFP}$ group (Figure 3G). However, there were negligible MSCs in the myocardium, and no difference between the two groups was observed (Supplementary Figure 1). These data suggested that ITGB3 overexpression promoted the targeted migration of MSCs to plaque sites *in vivo*, possibly by targeting inflammatory factors containing the RGD structure.

$MSCs^{ITGB3}$ reduce the progression of atherosclerotic plaques in $ApoE^{-/-}$ mice fed an HFD

To explore the effects of $MSCs^{ITGB3}$ on the progression of atherosclerosis, the whole aorta, aortic root, and aortic arch were stained with 0.5% ORO, and the stained areas were quantified to determine the atherosclerotic plaque area. The stained area in the aorta was substantially decreased in the MSC^{ITGB3} group when compared with that of the HFD and MSC^{GFP} groups (Figure 4A and B). The stained areas in the aortic root and aortic arch decreased in the MSC^{ITGB3} group compared with the corresponding in the HFD and MSC^{GFP} groups (Figure 4C). HE and Masson's trichrome staining analyses of sections taken from the aortic root and aortic arch demonstrated that $MSCs^{ITGB3}$ inhibited aortic plaque formation and collagen deposition more effectively than $MSCs^{GFP}$ (Figure 4D and E). Aortic stiffness is the earliest detectable evidence of changes in arterial wall function. Echocardiographic results showed that both systolic and diastolic diameters were considerably increased while the vessel wall thickness was decreased in the MSC^{ITGB3} group (Figure 4F). However, left ventricular EF and FS were not different among the three groups (Supplementary Figure 2). The number of macrophages in atherosclerotic plaques at the aortic arch was determined by F4/80 staining. The F4/80 staining-positive areas were notably reduced in the MSC^{ITGB3} group compared with the HFD group (Figure 4G).

$MSCs^{ITGB3}$ do not alter the biochemical parameters of $ApoE^{-/-}$ mice fed an HFD

To evaluate the effects of $MSCs^{ITGB3}$ on biochemical features *in vivo*, we recorded changes in mouse body weight and

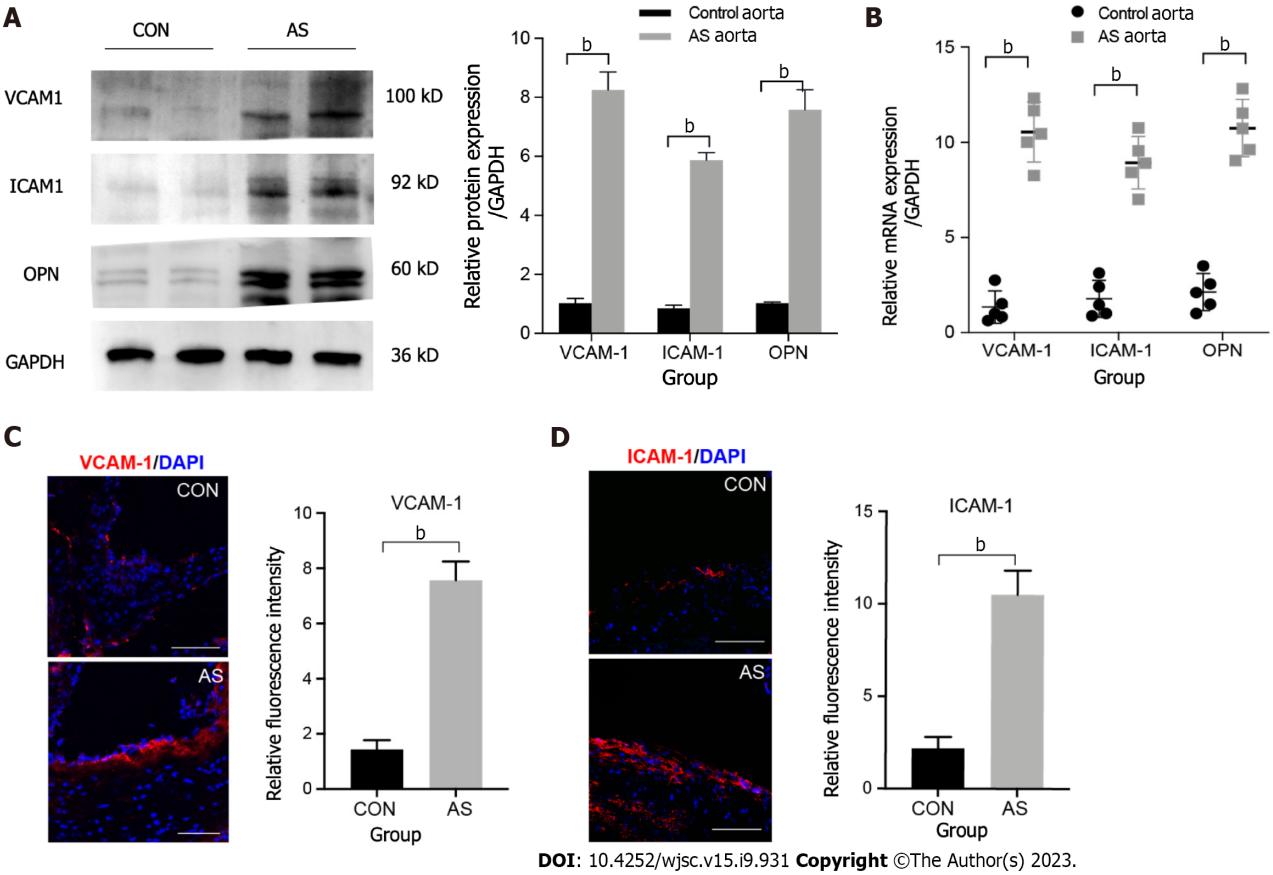

DOI: 10.4252/wjsc.v15.i9.931 **Copyright** ©The Author(s) 2023.

Figure 1 Expression of inflammatory factors in the vascular atherosclerotic plaque. A: Expression of mouse vascular cell adhesion molecule-1 (VCAM-1), intercellular cell adhesion molecule-1 (ICAM-1), and osteopontin (OPN) expression in total tissue lysates of normal and atherosclerotic (AS) aorta analyzed using western blot. GAPDH was used as the internal control. The experiment was repeated thrice with tissues isolated from independent mice; a representative blot is shown; B: Expression levels of various inflammatory factors involved in atherosclerosis analyzed using quantitative real-time polymerase chain reaction of mRNA samples extracted from normal and AS vessels of three independent mice. Data are presented as the mean ± SEM for each group. Fold change represents the expression of each inflammatory factor in AS vessel of a mice fed with high fat diet for 12 wk compared with that in normal blood vessel; C: Representative images of normal and AS vascular sections stained for VCAM1 (red) and ICAM1 (red). The experiment was repeated three times with tissues isolated from independent mice; a representative image is shown. Nuclei were visualized by DAPI staining (blue). Scale bars = 100 mm; D: Representative images of normal and AS vascular sections stained for ICAM1 (red). The experiment was repeated three times with tissues isolated from independent mice; a representative image is shown. Nuclei were visualized by DAPI staining (blue). Scale bars = 100 μm. $^{b}P < 0.001$. AS: Atherosclerotic; OPN: Osteopontin; qRT-PCR: Quantitative real-time polymerase chain reaction; SEM: Standard error of the mean; VCAM-1: Vascular cell adhesion molecule-1; ICAM-1: Intercellular cell adhesion molecule-1.

measured blood lipid concentrations. The results showed that the body weight did not vary among the three groups during the experiment (Supplementary Figure 3A). Plasma lipid analyses, including those measuring total cholesterol, high-density lipoprotein cholesterol, triglyceride, and low-density lipoprotein cholesterol levels, were performed on terminal blood samples obtained by cardiac puncture but showed no statistical differences among the HFD, MSC^{GFP}, and MSC^{ITGB3} groups (Supplementary Figure 3B). These results suggest that intravenous injection of stem cells did not interfere with lipid metabolism in mice receiving an HFD.

MSCs^{ITGB3} modulate cytokine expression in the AS mouse model

The levels of inflammatory factors are positively correlated with the degree of inflammation in atherosclerosis. Cytokines play a pivotal role in chronic inflammatory diseases[31]. They affect the expression of adherence molecules, permeability of endothelial cell, as well as proliferation and migration of inherent cells in blood vessels, all of which are associated with atherosclerosis. Interleukin (IL)-1β, an established driver of atherosclerotic disease[32], is involved in the entire process of atherosclerotic lesion progression[33]. Advanced atherosclerotic plaques can be alleviated and stabilized through IL-1β inhibition. After observing that MSC^{ITGB3} treatment can reduce the plaque area, we further investigated whether MSC^{ITGB3} infusion can decrease the levels of pro-inflammatory factors or increase the levels of anti-inflammatory factors in the serum and aorta tissue. Our results showed that pro-inflammatory factors, including TNF-α, IL-1β, and IL-6, showed a significant downward trend in mice who had received MSC^{ITGB3} or MSC^{GFP} treatment. However, the treatment effect of MSCs^{ITGB3} was more pronounced than that of MSCs^{GFP}. Likewise, mice receiving MSCs^{ITGB3} or MSCs^{GFP} showed significantly increased levels of anti-inflammatory factors, such as IL-4, IL-10, and tumor necrosis factor-stimulated gene-6 in the serum and aorta tissue (Figure 5). These results indicate that MSC^{ITGB3} treatment primarily reduces pathological inflammatory responses by improving the balance between secreted pro- and anti-inflammatory factors.

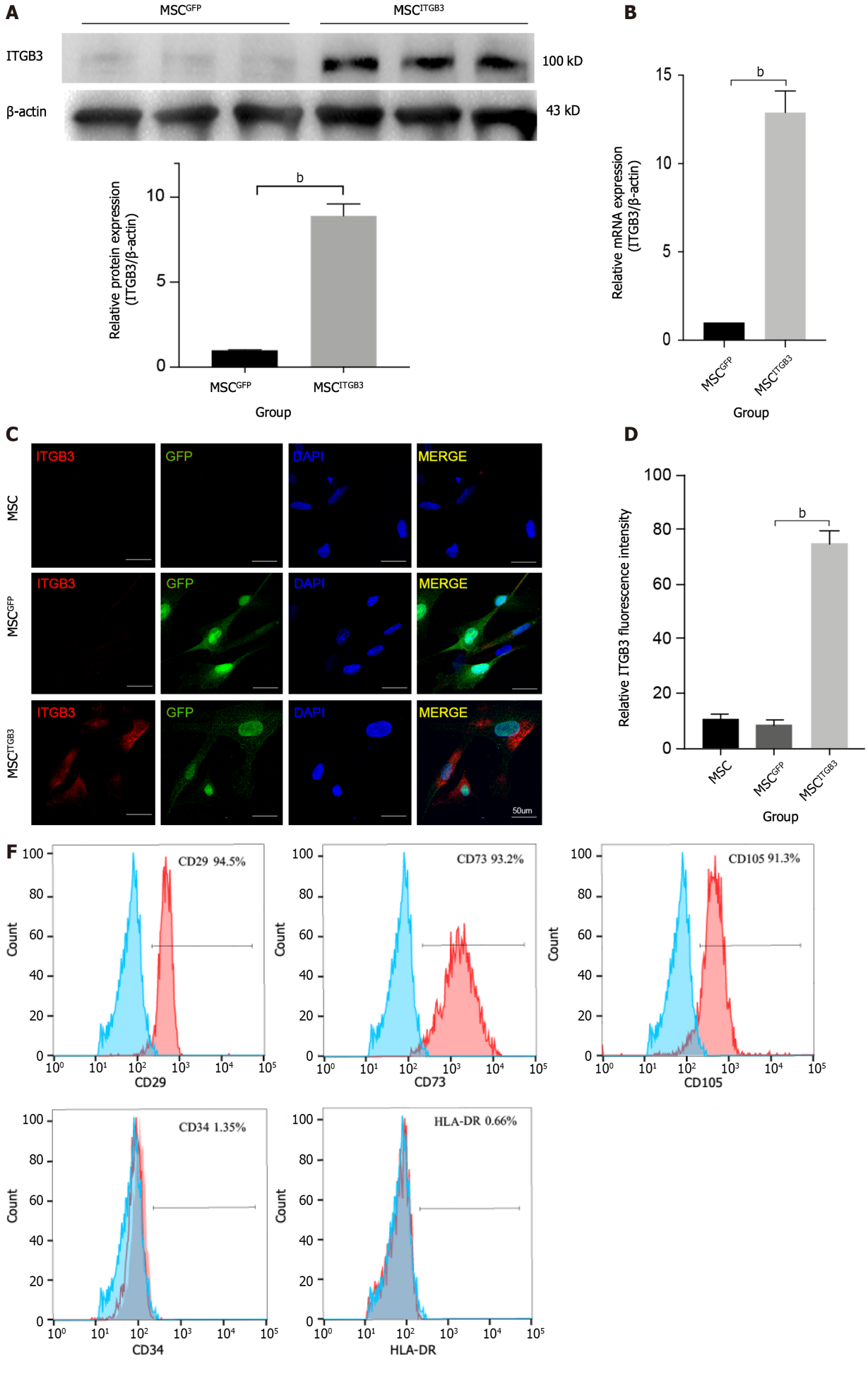
A
MSCGFP
MSCITGB3
ITGB3
β-actin
100 kD
43 kD
Relative protein expression (ITGB3/β-actin)
b
Group
B
Relative mRNA expression (ITGB3/β-actin)
C
MSC
MSCGFP
MSCITGB3
ITGB3
GFP
DAPI
MERGE
50um
D
Relative ITGB3 fluorescence intensity
F
CD29 94.5%
CD73 93.2%
CD105 91.3%
CD34 1.35%
HLA-DR 0.66%
Count
CD29
CD73
CD105
CD34
HLA-DR

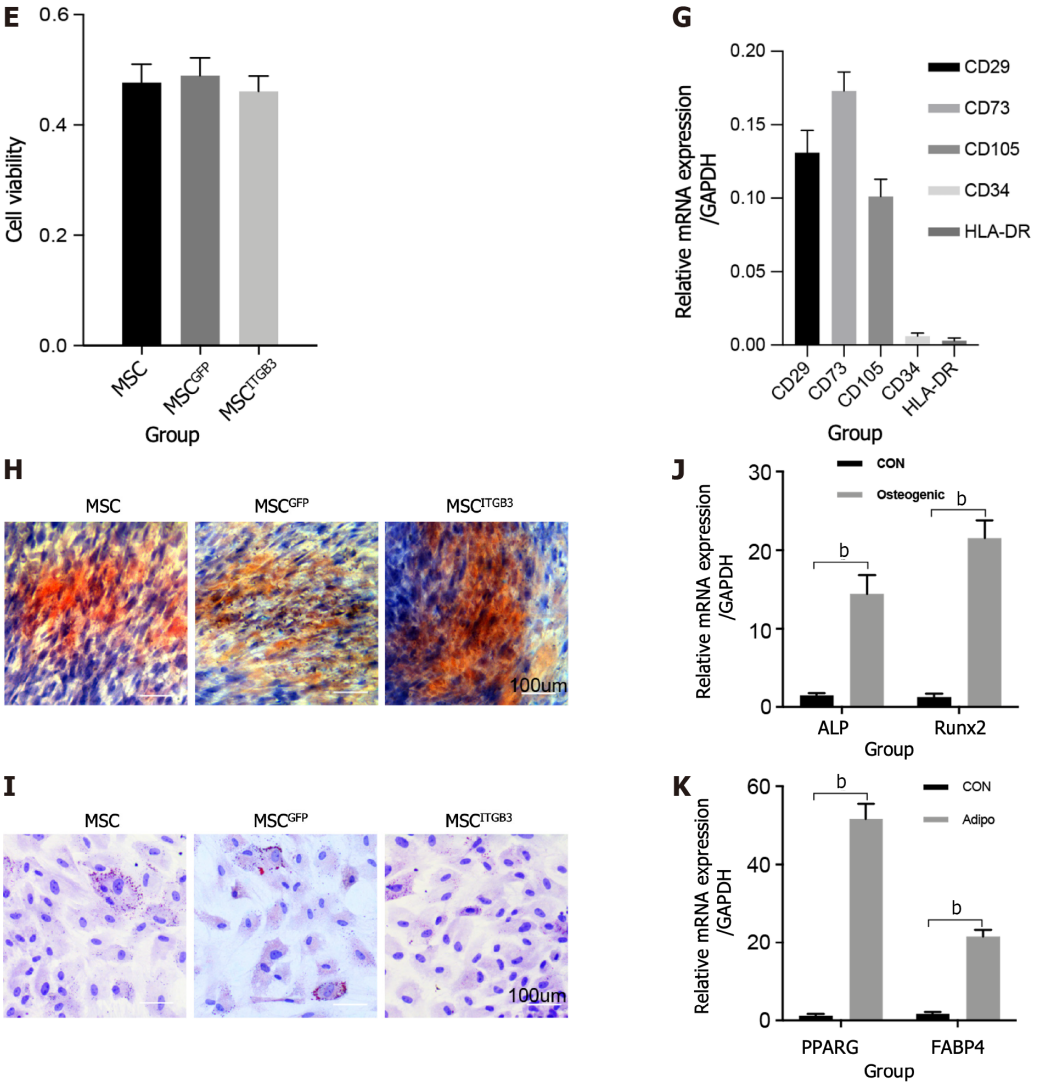

DOI: 10.4252/wjsc.v15.i9.931 **Copyright** ©The Author(s) 2023.

Figure 2 Expression of integrin subunit beta 3 on human umbilical cord-derived mesenchymal stem cells. A: Western blot; B: Quantitative real-time polymerase chain reaction (qRT-PCR) analysis of Integrin subunit beta 3 (ITGB3) expression; C: Representative immunofluorescence image; D: Quantification of ITGB3 and green fluorescence protein staining in untransfected and transfected mesenchymal stem cells (MSCs); E: Cell viability of untransfected and transfected MSCs determined by CCK8 assay. The experiment was repeated three times; F and G: Analysis of cell surface markers on MSC^{ITGB3} using flow cytometry to determine whether they have pluripotent characteristics; H: Osteogenic differentiation of MSC^{ITGB3} identified using Alizarin red staining; I: Oil Red O staining shows differentiation of MSC^{ITGB3} into adipocytes; J: qRT-PCR analysis of marker genes in induced osteoblasts; K: qRT-PCR analysis of marker genes in induced adipocyte. $^{b}P < 0.001$. GFP: Green fluorescence protein; ITGB3: Integrin subunit beta 3; MSC: Mesenchymal stem cell; ORO: Oil Red O; qRT-PCR: Quantitative real-time polymerase chain reaction.

DISCUSSION

In this study, adhesion molecules containing the RGD motif were highly expressed in an atherosclerosis model, and transfection of ITGB3 into MSCs improved their targeting capability. As expected, intravenous injection of MSCs^{ITGB3} substantially reduced atherosclerotic plaque in the ApoE$^{-/-}$ HFD mouse model.

Owing to their adaptive immunomodulatory properties and superior secretory potential, MSCs have attracted extensive attention in the treatment of atherosclerotic diseases[8,14]. The route of MSC administration is critical for their therapeutic efficiency, and systemic delivery *via* intravenous infusion is the primary approach for many cell therapies. However, several problems occur with this approach, and one of the major hurdles is insufficient cell engraftment into the damaged tissue[34]. It is well known that the therapeutic level of MSCs mainly depends on intercellular interactions and their regulation by the local microenvironment. Therefore, the therapeutic effect of intravenously injected MSCs may be closely related to their localization. It is predicted that the effectiveness of cell therapy can be improved by increasing local recruitment, further promoting tissue repair. However, methods to increase intercellular interactions that promote local engraftment of MSCs remain unclear.

Integrins, as transmembrane receptors, mediate cell connections by integrating Ig superfamily counterreceptors (ICAM-1 and VCAM-1) on adjacent cells[20]. Adhesion molecules and integrin receptors have been identified to facilitate cell migration toward target organs and adhesion in target tissues. Therefore, intravenous injection of MSCs^{ITGB3} may

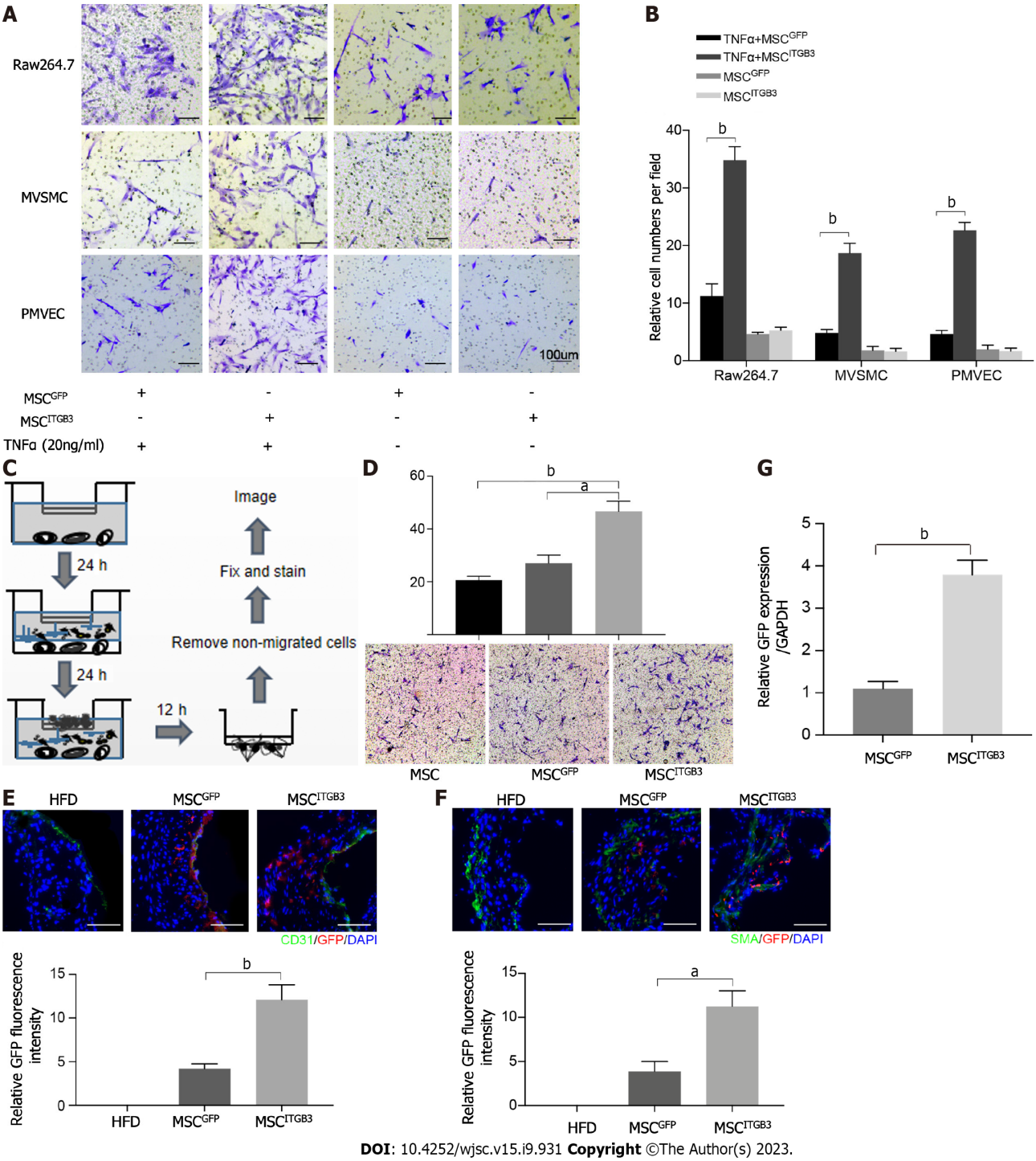

DOI: 10.4252/wjsc.v15.i9.931 **Copyright** ©The Author(s) 2023.

Figure 3 Integrin subunit beta 3 enhances mesenchymal stem cell migration *in vitro* and *in vivo*. A: *In vitro* migration of integrin subunit beta 3 (ITGB3)-overexpressing mesenchymal stem cell (MSC) (MSCs^{ITGB3}) toward lower Raw264.7, MVSMC and PMVEC stimulated by tumor necrosis factor α. Scale bars = 100 μm; B: Quantification of migrated cells. Data are presented as the mean ± SEM; C: Experimental scheme of chemotactic assays with mouse atherosclerotic vascular samples. The blood vessel was divided into three parts. For each of the experiments, each part was cultured for 24 h in medium. To perform the assay, a suspension of 2 × 10^5 MSCs, 2 × 10^5 MSCs^{GFP}, or 2 × 10^5 MSCs^{ITGB3} in medium were seeded in the upper chamber. Following incubation for 24 h, non-migrated cells were removed; D: Representative image and quantification of migrated cells stuck in the porous membrane or the lower layer of the transwell stained with 0.1% crystal violet; E: MSCs^{ITGB3} and MSCs^{GFP}, both expressing green fluorescence, were intravenously injected into mice. The expression of green fluorescent protein (GFP) and CD31 was examined by frozen staining. GFP-positive cells were quantified per microscopic field of vascular staining in triplicate mice; F: The expression of GFP and SMA were examined by frozen staining. GFP-positive cells were quantified per microscopic field of vascular staining in triplicate mice. Scale bars = 100 μm; G: Expression levels of GFP in atherosclerosis analyzed using quantitative real-time polymerase chain reaction of mRNA samples extracted from MSC^{GFP} and MSC^{ITGB3} vessels of three mice. Data are presented as the mean ± SEM for each group. The data are representative of three independent experiments. $^aP < 0.05$, $^bP < 0.001$. GFP: Green fluorescent protein; ITGB3: Integrin subunit beta 3; MSC: Mesenchymal stem cell; qRT-PCR: Quantitative real-time polymerase chain reaction; SEM: Standard error of the mea; TNF: Tumor necrosis factor.

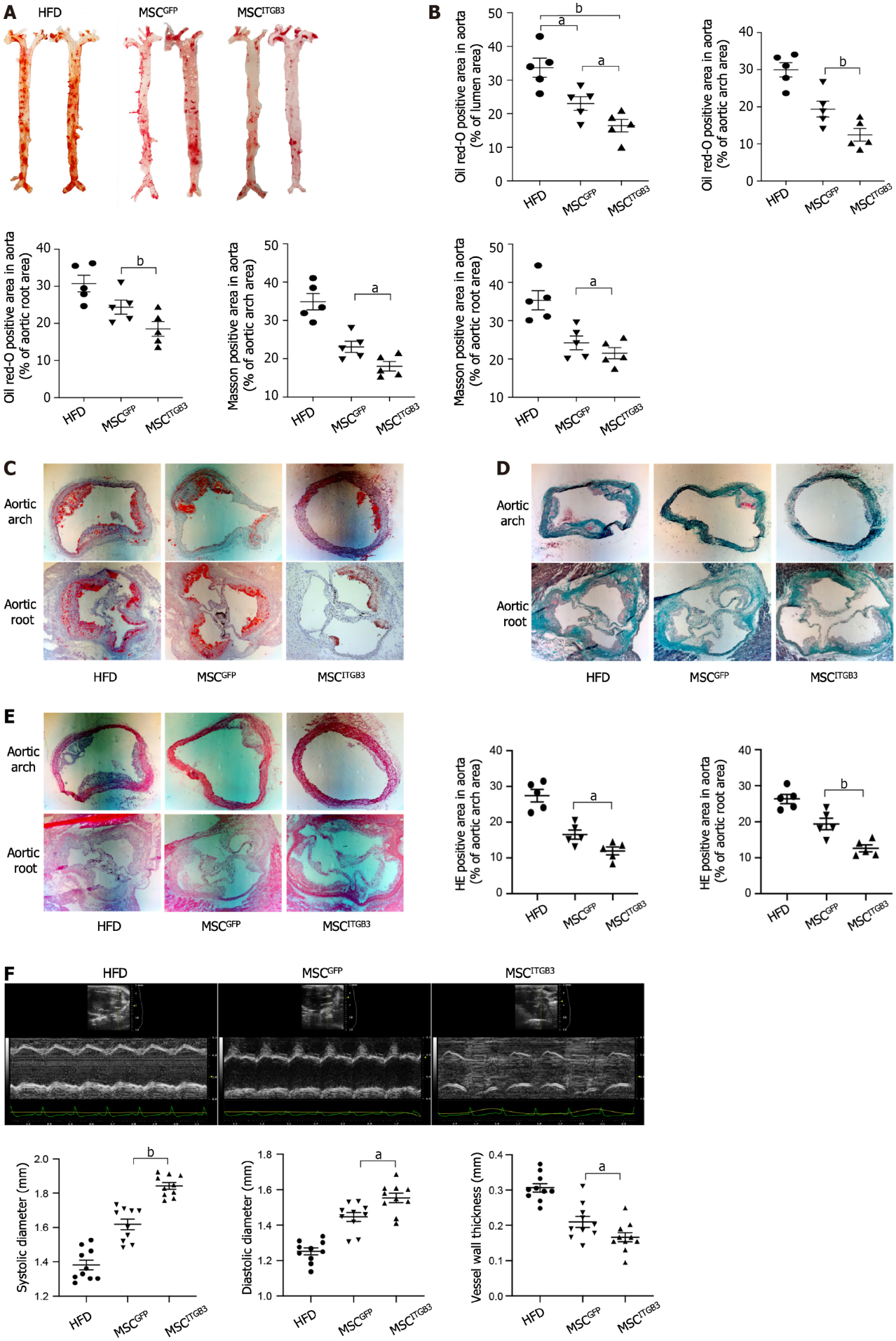
A
HFD
MSCGFP
MSCITGB3
B
Oil red-O positive area in aorta (% of lumen area)
Oil red-O positive area in aorta (% of aortic arch area)
Oil red-O positive area in aorta (% of aortic root area)
Masson positive area in aorta (% of aortic arch area)
Masson positive area in aorta (% of aortic root area)
C
Aortic arch
Aortic root
D
E
HE positive area in aorta (% of aortic arch area)
HE positive area in aorta (% of aortic root area)
F
Systolic diameter (mm)
Diastolic diameter (mm)
Vessel wall thickness (mm)

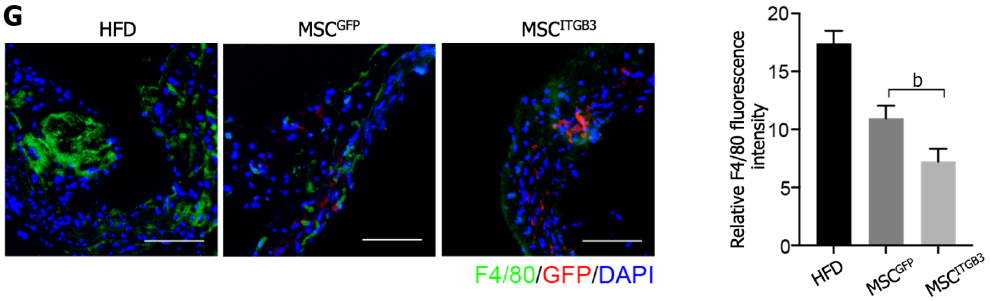

DOI: 10.4252/wjsc.v15.i9.931 **Copyright** ©The Author(s) 2023.

Figure 4 Injection of mesenchymal stem cell^{ITGB3} attenuates atherosclerotic *in vivo*. A: Representative *en face* images of mouse aortas stained with Oil Red O (ORO); B: Quantification of the atherosclerotic plaque area as a ratio of the stained area to the total area of the aorta; C: Representative section of mouse aortic arch and aortic root stained with ORO. The ORO-positive area in the aortic root is shown as the ratio of the stained area to the total area of the aortic sinus; D: Representative section of mouse aortic arch and aortic root stained with Masson staining. The Masson staining-positive area in the aortic arch and aortic root is shown as the ratio of the stained area to the total area of the aortic sinus; E: Representative section of mouse aortic arch and aortic root stained with hematoxylin eosin (HE) staining. The HE staining-positive area in the aortic arch and aortic root is shown as the ratio of the stained area to the total area of the aortic sinus; F: Ultrasonography of the aorta in each group, including representative images, systolic diameter, diastolic diameter, and vessel wall thickness; G: Representative images of aortic arch section stained with anti-F4/80 antibody. The F4/80-positive area in the atherosclerotic plaque is shown as the ratio of the stained area to the total area of the atherosclerotic plaque. Scale bar = 100 μm. $^{a}P < 0.05$, $^{b}P < 0.001$. AS: Atherosclerotic; HE: Hematoxylin eosin; MSC: Mesenchymal stem cell; ORO: Oil Red O.

provide a new approach to improve stem cell homing. Previous studies have also verified that MSCs with altered chemokine receptors, such as CXCR5[18], integrin α4[35], and CCR5 and CXCR6[36], significantly increased cell motion to lesion sites and enhanced the therapeutic effect of MSCs. MSC homing to a target organ requires the proper integration of interactions of chemokines secreted by injured tissue and adhesion molecules with matching receptors on MSCs. Therefore, determining disease-specific ligand expression profiles will provide the precise signal necessary for MSC homing. In our study, we elucidated that the ITGB3/RGD motif axis is a specific regulator for MSC homing in atherosclerosis. Adhesion molecules containing the RGD motif, such as VCAM-1, ICAM-1, and OPN, are highly expressed in atherosclerotic plaque and are involved in a variety of immune functions, including T cell activation, migration, and extravasation[37]. High VCAM-1 and ICAM-1 expression levels have also been reported in the inflamed tissue, including vascular plaque[38]. We found that the RGD structure acts as an important feature of the plaque tissue that chemoattracts the migration of MSCs^{ITGB3} to lesions *in vivo*. Moreover, our findings demonstrated that the ITGB3-RGD motif axis is the atherosclerosis-specific regulator for MSC homing. Factors containing RGD structures can be observed in various inflammatory tissues, including the site of atherosclerotic lesions[39]. However, the expression of ITGB3 was almost absent on the surface of MSCs. Thus, MSCs^{ITGB3} may serve as a disease-specific therapeutic tool to improve MSC homing when treating atherosclerosis. MSC transplantation and homing appear to improve atherosclerosis *via* different mechanisms. There is a substantial amount of evidence indicating that transplanted MSCs primarily promote local microenvironmental improvement through their paracrine secretory effects[40-42]. The anti-inflammatory cytokines secreted by MSCs can reduce inflammation and modulate immune response while enhancing normal cell survival and differentiation[9,11]. It has also been documented that the anti-inflammatory properties of MSCs are primarily mediated by extracellular vesicles (EVs)[8,43]. Various disease models, such as those involving endothelial cell senescence[44], autoimmune diseases[45], arterial stiffness and hypertension[46], and lung injury[47], have demonstrated that EVs derived from MSCs can mitigate cell death, prevent apoptosis, and enhance recovery. In this regard, as a result of the continuous release of EVs in the vicinity of the damage site, transplantation of MSCs overexpressing ITGB3 with improved migratory capability could play a more effective role in treating atherosclerotic disease.

A previous study found that ITGB3 stimulated the progression of human pancreatic ductal adenocarcinoma *via* activation of the STAT3 pathway[48]. Furthermore, ITGB3 promoted cell senescence and profibrotic changes through p53 signaling activation and secretion of transforming growth factor beta in cultured tubular cells[49]. However, these studies have not examined the specific effect of ITGB3 overexpression on MSC migration and homing *in vivo*. Further research is necessary to elucidate the underlying mechanisms of how overexpression of ITGB3 intensifies homing abilities of MSCs.

This study has certain limitations. First, the MSCs^{ITGB3} were generated by lentiviral infection. As lentiviral vectors can randomly integrate into the genome resulting in deleterious mutations, their therapeutic application in humans is limited by an inherent risk of tumorigenesis. Second, other suitable methods are needed to increase the expression of ITGB3. Third, the current experiment did not specifically investigate the survival time of MSCs^{ITGB3} *in vivo*. The next step will be to trace the target location and lifespan of MSCs^{ITGB3} through *in vivo* imaging technology.

CONCLUSION

Collectively, we genetically modified MSCs *in vitro* and found that ITGB3 overexpression substantially upregulated MSC migration, aggregation in plaque sites, and immunomodulatory properties of MSCs *in vivo*. Although the therapeutic potential of modified MSCs in atherosclerosis has not yet been translated into clinical practice, our work improves our

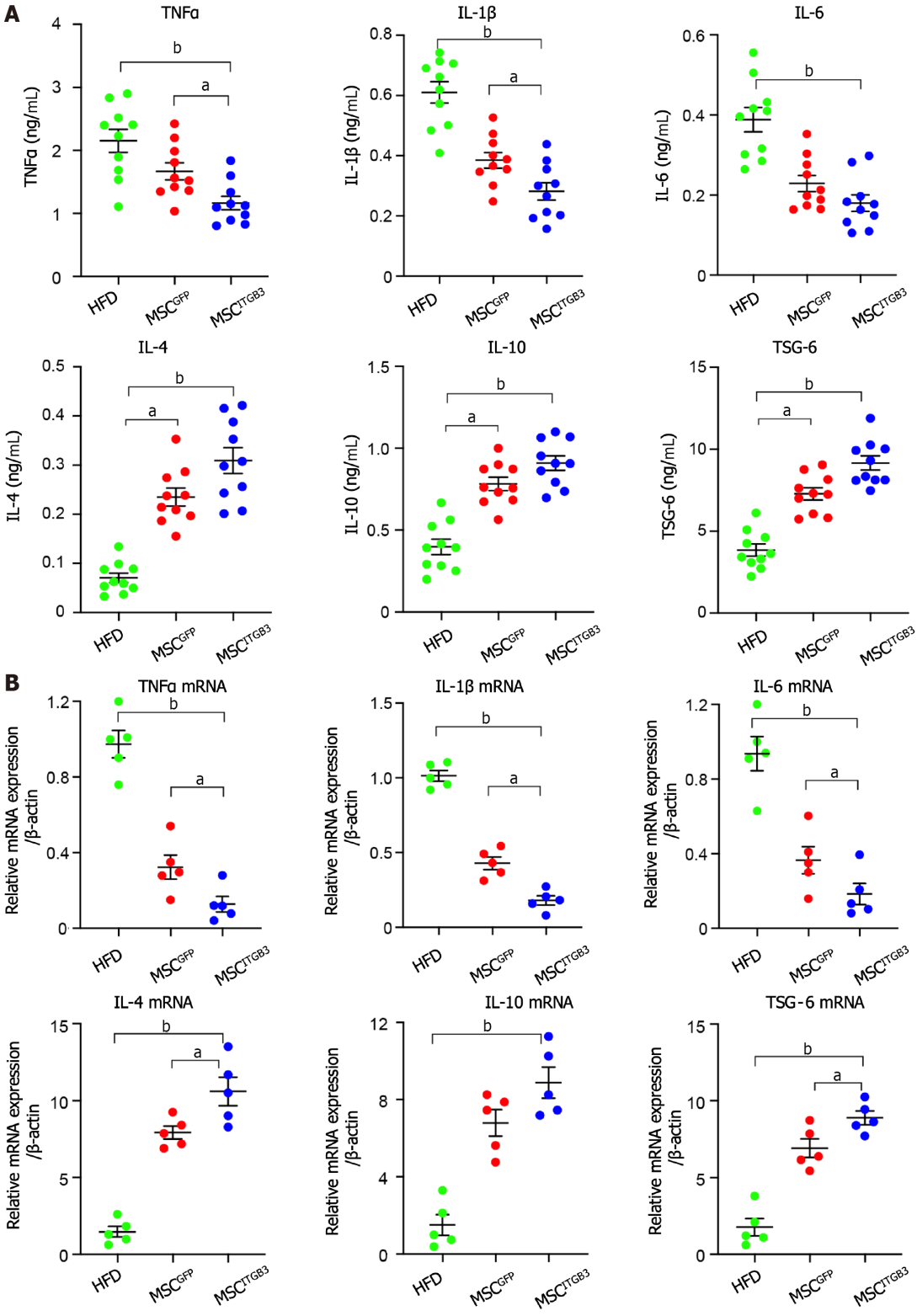

DOI: 10.4252/wjsc.v15.i9.931

Figure 5 Mesenchymal stem cell^{ITGB3} modulated cytokine expressions in an atherosclerotic mouse model. A: Serum pro-inflammatory factors tumor necrosis factor (TNF)α, interleukin (IL)-1β, and IL-6 and anti-inflammatory factors IL-4, IL-10, and tumor necrosis factor-stimulated gene-6 (TSG-6) levels measured using ELISA; B: mRNA expression of pro-inflammatory factors TNFα, IL-1β, and IL-6 and anti-inflammatory factors IL-4, IL-10, and TSG-6 in aortic tissue, quantified using quantitative real-time polymerase chain reaction. Expression is shown relative to the expression of housekeeping genes (β-actin). All values are expressed as mean ± SEM. $^{a}P < 0.05$, $^{b}P < 0.001$. ELISA: Enzyme-linked immunosorbent assay; IL: Interleukin; MSC: Mesenchymal stem cell; qRT-PCR: Quantitative real-time polymerase chain reaction; SEM: Standard error of the mean; TNF-α: Tumor necrosis factor-a; TSG-6: Tumor necrosis factor-stimulated gene-6.

understanding of the adhesion molecule–integrin receptor axis, as well as of stem cell features, and may provide novel insights into the rapid and targeted delivery of MSCs to disease sites, thereby optimizing their therapeutic effects.

ARTICLE HIGHLIGHTS

Research background

Umbilical cord mesenchymal stem cell (MSC) transplantation is a potential therapeutic intervention for atherosclerotic vascular disease. Integrin beta 3 (ITGB3) promotes cell migration in several cell types. However, whether ITGB3-modified MSCs can migrate to plaque sites *in vivo* and play an anti-atherosclerotic role remains unclear.

Research motivation

Atherosclerosis is a serious public health problem and more treatment options are needed to explore and identify effective molecules and targets.

Research objectives

The objective of our study was to evaluate the chemotaxis ability of ITGB3-overexpressing MSCs toward inflammatory cells *in vitro* and plaque tissues *in vivo,* promoting their therapeutic efficacy in the atherosclerosis mouse model.

Research methods

Umbilical cord MSCs were isolated and expanded. Lentiviral vectors encoding ITGB3 or green fluorescent protein (GFP) as control were transfected into MSCs. Male apolipoprotein $E^{-/-}$ mice were fed with a high-fat diet (HFD) for 12 wk to induce the formation of atherosclerotic lesions. The HFD-fed mice were randomly separated into three clusters. GFP-labeled MSCs ($MSCs^{GFP}$) or $MSCs^{ITGB3}$ were transplanted into the mice intravenously *via* the tail vein. Immunofluorescence staining, Oil red O staining, histological analyses, western blotting, enzyme-linked immunosorbent assay, and quantitative real-time polymerase chain reaction were used for the analyses. Statistical evaluation between two groups was determined using the unpaired Student's t-test, and comparisons of more than two groups were performed using a one-way analysis of variance.

Research results

$MSCs^{ITGB3}$ successfully differentiated into the "osteocyte" and "adipocyte" phenotypes and were characterized by positive expression (> 91.3%) of CD29, CD73, and CD105 and negative expression (< 1.35%) of CD34 and human leukocyte antigen-DR. $MSCs^{ITGB3}$ showed significantly faster migration than $MSCs^{GFP}$. ITGB3 overexpression had no effects on MSC viability, differentiation, and secretion. Immunofluorescence staining revealed that ITGB3 overexpression substantially enhanced the homing of MSCs to plaque sites. Oil red O staining and histological analyses further confirmed the therapeutic effects of $MSCs^{ITGB3}$, significantly reducing the plaque area. Enzyme-linked immunosorbent assay and quantitative real-time polymerase chain reaction revealed that MSC^{ITGB3} transplantation considerably decreased the inflammatory response in pathological tissues by improving the dynamic equilibrium of pro- and anti-inflammatory cytokines.

Research conclusions

The study demonstrated that ITGB3 overexpression enhanced the MSC homing ability, providing a potential approach for MSC delivery to plaque sites, thereby optimizing their therapeutic effects.

Research perspectives

The ITGB3-modified MSCs can migrate the plaque sites and play an anti-inflammation role, which may be an effective strategy to treat vascular atherosclerotic related diseases.

FOOTNOTES

Author contributions: Cui W and Han M designed and coordinated the study; Hu HJ, Xiao XR, Li T, Liu DM and Geng X performed the experiments and acquired and analyzed data; Cui W interpreted the data; Hu HJ and Liu DM wrote the manuscript; all authors revised the manuscript and approved the final version of the article.

Supported by National Natural Science Foundation of China, No. 82100301; and Key Science and Technology Research Program of Hebei Provincial Department of Health, No, 20221014.

Institutional review board statement: The study was reviewed and approved by the Ethical Committee of the Second Hospital of Hebei Medical University, No. 2021-R496.

Institutional animal care and use committee statement: Laboratory Animal Use and Management Committee has been carefully discussed and voted on May 27, 2021 for the subject animal-related content, 10 voters, 10 people suggested a formal experiment, and

made the following recommendations. The design is reasonable, in line with the animal requirements. The ethics committee agreed to carry out a formal experiment.

Informed consent statement: All study participants or their legal guardian provided informed written consent about personal and medical data collection prior to study enrolment.

Conflict-of-interest statement: All the authors report no relevant conflicts of interest for this article.

Data sharing statement: No additional data are available.

ARRIVE guidelines statement: The authors have read the ARRIVE guidelines, and the manuscript was prepared and revised according to the ARRIVE guidelines.

Country/Territory of origin: China

ORCID number: Hai-Juan Hu 0000-0002-7954-4638; Xue-Ru Xiao 0000-0002-0858-3939; Tong Li 0009-0004-9052-4437; De-Min Liu 0000-0002-8784-1026; Xue Geng 0000-0001-9601-2476; Mei Han 0000-0002-5338-4875; Wei Cui 0000-0002-1214-4146.

S-Editor: Fan JR
L-Editor: A
P-Editor: Zhang XD

REFERENCES

1 **Mäkinen PI**, Ylä-Herttuala S. Therapeutic gene targeting approaches for the treatment of dyslipidemias and atherosclerosis. *Curr Opin Lipidol* 2013; **24**: 116-122 [PMID: 23314926 DOI: 10.1097/MOL.0b013e32835da13c]
2 **Jenkins A**, Januszewski A, O'Neal D. The early detection of atherosclerosis in type 1 diabetes: why, how and what to do about it. *Cardiovasc Endocrinol Metab* 2019; **8**: 14-27 [PMID: 31646294 DOI: 10.1097/XCE.0000000000000169]
3 **Gragnano F**, Calabrò P. Role of dual lipid-lowering therapy in coronary atherosclerosis regression: Evidence from recent studies. *Atherosclerosis* 2018; **269**: 219-228 [PMID: 29407597 DOI: 10.1016/j.atherosclerosis.2018.01.012]
4 **Prpic R**, Teirstein PS, Reilly JP, Moses JW, Tripuraneni P, Lansky AJ, Giorgianni JA, Jani S, Wong SC, Fish RD, Ellis S, Holmes DR, Kereiakas D, Kuntz RE, Leon MB. Long-term outcome of patients treated with repeat percutaneous coronary intervention after failure of gamma-brachytherapy for the treatment of in-stent restenosis. *Circulation* 2002; **106**: 2340-2345 [PMID: 12403664 DOI: 10.1161/01.cir.0000036366.62288.74]
5 **He L**, Zhao R, Wang Y, Liu H, Wang X. Research Progress on Catalpol as Treatment for Atherosclerosis. *Front Pharmacol* 2021; **12**: 716125 [PMID: 34326774 DOI: 10.3389/fphar.2021.716125]
6 **Tang J**, Rakshit M, Chua HM, Darwitan A, Nguyen LTH, Muktabar A, Venkatraman S, Ng KW. Liposome interaction with macrophages and foam cells for atherosclerosis treatment: effects of size, surface charge and lipid composition. *Nanotechnology* 2021; **32** [PMID: 34536952 DOI: 10.1088/1361-6528/ac2810]
7 **Kobiyama K**, Ley K. Atherosclerosis. *Circ Res* 2018; **123**: 1118-1120 [PMID: 30359201 DOI: 10.1161/CIRCRESAHA.118.313816]
8 **Takafuji Y**, Hori M, Mizuno T, Harada-Shiba M. Humoral factors secreted from adipose tissue-derived mesenchymal stem cells ameliorate atherosclerosis in Ldlr-/- mice. *Cardiovasc Res* 2019; **115**: 1041-1051 [PMID: 30388208 DOI: 10.1093/cvr/cvy271]
9 **Zhang X**, Huang F, Li W, Dang JL, Yuan J, Wang J, Zeng DL, Sun CX, Liu YY, Ao Q, Tan H, Su W, Qian X, Olsen N, Zheng SG. Human Gingiva-Derived Mesenchymal Stem Cells Modulate Monocytes/Macrophages and Alleviate Atherosclerosis. *Front Immunol* 2018; **9**: 878 [PMID: 29760701 DOI: 10.3389/fimmu.2018.00878]
10 **Golpanian S**, Wolf A, Hatzistergos KE, Hare JM. Rebuilding the Damaged Heart: Mesenchymal Stem Cells, Cell-Based Therapy, and Engineered Heart Tissue. *Physiol Rev* 2016; **96**: 1127-1168 [PMID: 27335447 DOI: 10.1152/physrev.00019.2015]
11 **Li Q**, Sun W, Wang X, Zhang K, Xi W, Gao P. Skin-Derived Mesenchymal Stem Cells Alleviate Atherosclerosis *via* Modulating Macrophage Function. *Stem Cells Transl Med* 2015; **4**: 1294-1301 [PMID: 26400926 DOI: 10.5966/sctm.2015-0020]
12 **Colmegna I**, Stochaj U. MSC - targets for atherosclerosis therapy. *Aging (Albany NY)* 2018; **11**: 285-286 [PMID: 30591619 DOI: 10.18632/aging.101735]
13 **Yang W**, Yin R, Zhu X, Yang S, Wang J, Zhou Z, Pan X, Ma A. Mesenchymal stem-cell-derived exosomal miR-145 inhibits atherosclerosis by targeting JAM-A. *Mol Ther Nucleic Acids* 2021; **23**: 119-131 [PMID: 33335797 DOI: 10.1016/j.omtn.2020.10.037]
14 **Lin Y**, Zhu W, Chen X. The involving progress of MSCs based therapy in atherosclerosis. *Stem Cell Res Ther* 2020; **11**: 216 [PMID: 32503682 DOI: 10.1186/s13287-020-01728-1]
15 **Barbash IM**, Chouraqui P, Baron J, Feinberg MS, Etzion S, Tessone A, Miller L, Guetta E, Zipori D, Kedes LH, Kloner RA, Leor J. Systemic delivery of bone marrow-derived mesenchymal stem cells to the infarcted myocardium: feasibility, cell migration, and body distribution. *Circulation* 2003; **108**: 863-868 [PMID: 12900340 DOI: 10.1161/01.CIR.0000084828.50310.6A]
16 **Lin P**, Correa D, Kean TJ, Awadallah A, Dennis JE, Caplan AI. Serial transplantation and long-term engraftment of intra-arterially delivered clonally derived mesenchymal stem cells to injured bone marrow. *Mol Ther* 2014; **22**: 160-168 [PMID: 24067545 DOI: 10.1038/mt.2013.221]

17 **Shahror RA**, Ali AAA, Wu CC, Chiang YH, Chen KY. Enhanced Homing of Mesenchymal Stem Cells Overexpressing Fibroblast Growth Factor 21 to Injury Site in a Mouse Model of Traumatic Brain Injury. *Int J Mol Sci* 2019; **20** [PMID: 31142002 DOI: 10.3390/ijms20112624]

18 **Zhang X**, Huang W, Chen X, Lian Y, Wang J, Cai C, Huang L, Wang T, Ren J, Xiang AP. CXCR5-Overexpressing Mesenchymal Stromal Cells Exhibit Enhanced Homing and Can Decrease Contact Hypersensitivity. *Mol Ther* 2017; **25**: 1434-1447 [PMID: 28454789 DOI: 10.1016/j.ymthe.2017.04.004]

19 **Hynes RO**. Integrins: bidirectional, allosteric signaling machines. *Cell* 2002; **110**: 673-687 [PMID: 12297042 DOI: 10.1016/s0092-8674(02)00971-6]

20 **Ross TD**, Coon BG, Yun S, Baeyens N, Tanaka K, Ouyang M, Schwartz MA. Integrins in mechanotransduction. *Curr Opin Cell Biol* 2013; **25**: 613-618 [PMID: 23797029 DOI: 10.1016/j.ceb.2013.05.006]

21 **D'Souza SE**, Ginsberg MH, Burke TA, Lam SC, Plow EF. Localization of an Arg-Gly-Asp recognition site within an integrin adhesion receptor. *Science* 1988; **242**: 91-93 [PMID: 3262922 DOI: 10.1126/science.3262922]

22 **D'Souza SE**, Ginsberg MH, Matsueda GR, Plow EF. A discrete sequence in a platelet integrin is involved in ligand recognition. *Nature* 1991; **350**: 66-68 [PMID: 2002847 DOI: 10.1038/350066a0]

23 **Dashdulam D**, Kim ID, Lee H, Lee HK, Kim SW, Lee JK. Osteopontin heptamer peptide containing the RGD motif enhances the phagocytic function of microglia. *Biochem Biophys Res Commun* 2020; **524**: 371-377 [PMID: 32005517 DOI: 10.1016/j.bbrc.2020.01.100]

24 **Wang JH**, Stehle T, Pepinsky B, Liu JH, Karpusas M, Osborn L. Structure of a functional fragment of VCAM-1 refined at 1.9 a resolution. *Acta Crystallogr D Biol Crystallogr* 1996; **52**: 369-379 [PMID: 15299708 DOI: 10.1107/S0907444995012352]

25 **D'Souza SE**, Haas TA, Piotrowicz RS, Byers-Ward V, McGrath DE, Soule HR, Cierniewski C, Plow EF, Smith JW. Ligand and cation binding are dual functions of a discrete segment of the integrin beta 3 subunit: cation displacement is involved in ligand binding. *Cell* 1994; **79**: 659-667 [PMID: 7525080 DOI: 10.1016/0092-8674(94)90551-7]

26 **Han YF**, Tao R, Sun TJ, Chai JK, Xu G, Liu J. Optimization of human umbilical cord mesenchymal stem cell isolation and culture methods. *Cytotechnology* 2013; **65**: 819-827 [PMID: 23306781 DOI: 10.1007/s10616-012-9528-0]

27 **Nie L**, Guo X, Esmailzadeh L, Zhang J, Asadi A, Collinge M, Li X, Kim JD, Woolls M, Jin SW, Dubrac A, Eichmann A, Simons M, Bender JR, Sadeghi MM. Transmembrane protein ESDN promotes endothelial VEGF signaling and regulates angiogenesis. *J Clin Invest* 2013; **123**: 5082-5097 [PMID: 24177422 DOI: 10.1172/JCI67752]

28 **Sonou T**, Ohya M, Yashiro M, Masumoto A, Nakashima Y, Ito T, Mima T, Negi S, Kimura-Suda H, Shigematsu T. Mineral Composition of Phosphate-Induced Calcification in a Rat Aortic Tissue Culture Model. *J Atheroscler Thromb* 2015; **22**: 1197-1206 [PMID: 26119071 DOI: 10.5551/jat.28647]

29 **Wang D**, Tian L, Wang Y, Gao X, Tang H, Ge J. Circ_0001206 regulates miR-665/CRKL axis to alleviate hypoxia/reoxygenation-induced cardiomyocyte injury in myocardial infarction. *ESC Heart Fail* 2022; **9**: 998-1007 [PMID: 35023295 DOI: 10.1002/ehf2.13725]

30 **Barry ST**, Ludbrook SB, Murrison E, Horgan CM. Analysis of the alpha4beta1 integrin-osteopontin interaction. *Exp Cell Res* 2000; **258**: 342-351 [PMID: 10896785 DOI: 10.1006/excr.2000.4941]

31 **Warnatsch A**, Ioannou M, Wang Q, Papayannopoulos V. Inflammation. Neutrophil extracellular traps license macrophages for cytokine production in atherosclerosis. *Science* 2015; **349**: 316-320 [PMID: 26185250 DOI: 10.1126/science.aaa8064]

32 **Vromman A**, Ruvkun V, Shvartz E, Wojtkiewicz G, Santos Masson G, Tesmenitsky Y, Folco E, Gram H, Nahrendorf M, Swirski FK, Sukhova GK, Libby P. Stage-dependent differential effects of interleukin-1 isoforms on experimental atherosclerosis. *Eur Heart J* 2019; **40**: 2482-2491 [PMID: 30698710 DOI: 10.1093/eurheartj/ehz008]

33 **Libby P**. Interleukin-1 Beta as a Target for Atherosclerosis Therapy: Biological Basis of CANTOS and Beyond. *J Am Coll Cardiol* 2017; **70**: 2278-2289 [PMID: 29073957 DOI: 10.1016/j.jacc.2017.09.028]

34 **Nystedt J**, Anderson H, Tikkanen J, Pietilä M, Hirvonen T, Takalo R, Heiskanen A, Satomaa T, Natunen S, Lehtonen S, Hakkarainen T, Korhonen M, Laitinen S, Valmu L, Lehenkari P. Cell surface structures influence lung clearance rate of systemically infused mesenchymal stromal cells. *Stem Cells* 2013; **31**: 317-326 [PMID: 23132820 DOI: 10.1002/stem.1271]

35 **Kumar S**, Ponnazhagan S. Bone homing of mesenchymal stem cells by ectopic alpha 4 integrin expression. *FASEB J* 2007; **21**: 3917-3927 [PMID: 17622670 DOI: 10.1096/fj.07-8275com]

36 **Pesaresi M**, Bonilla-Pons SA, Sebastian-Perez R, Di Vicino U, Alcoverro-Bertran M, Michael R, Cosma MP. The Chemokine Receptors Ccr5 and Cxcr6 Enhance Migration of Mesenchymal Stem Cells into the Degenerating Retina. *Mol Ther* 2021; **29**: 804-821 [PMID: 33264643 DOI: 10.1016/j.ymthe.2020.10.026]

37 **Singh M**, Thakur M, Mishra M, Yadav M, Vibhuti R, Menon AM, Nagda G, Dwivedi VP, Dakal TC, Yadav V. Gene regulation of intracellular adhesion molecule-1 (ICAM-1): A molecule with multiple functions. *Immunol Lett* 2021; **240**: 123-136 [PMID: 34715236 DOI: 10.1016/j.imlet.2021.10.007]

38 **Zhong L**, Simard MJ, Huot J. Endothelial microRNAs regulating the NF-κB pathway and cell adhesion molecules during inflammation. *FASEB J* 2018; **32**: 4070-4084 [PMID: 29565737 DOI: 10.1096/fj.201701536R]

39 **Kitagawa T**, Kosuge H, Uchida M, Iida Y, Dalman RL, Douglas T, McConnell MV. RGD targeting of human ferritin iron oxide nanoparticles enhances in vivo MRI of vascular inflammation and angiogenesis in experimental carotid disease and abdominal aortic aneurysm. *J Magn Reson Imaging* 2017; **45**: 1144-1153 [PMID: 27689830 DOI: 10.1002/jmri.25459]

40 **Seo Y**, Kang MJ, Kim HS. Strategies to Potentiate Paracrine Therapeutic Efficacy of Mesenchymal Stem Cells in Inflammatory Diseases. *Int J Mol Sci* 2021; **22** [PMID: 33806241 DOI: 10.3390/ijms22073397]

41 **Ogay V**, Sekenova A, Li Y, Issabekova A, Saparov A. The Therapeutic Potential of Mesenchymal Stem Cells in the Treatment of Atherosclerosis. *Curr Stem Cell Res Ther* 2021; **16**: 897-913 [PMID: 33511957 DOI: 10.2174/1574888X16999210128193549]

42 **Liu X**, Wei Q, Lu L, Cui S, Ma K, Zhang W, Ma F, Li H, Fu X, Zhang C. Immunomodulatory potential of mesenchymal stem cell-derived extracellular vesicles: Targeting immune cells. *Front Immunol* 2023; **14**: 1094685 [PMID: 36860847 DOI: 10.3389/fimmu.2023.1094685]

43 **Guo Z**, Zhao Z, Yang C, Song C. Transfer of microRNA-221 from mesenchymal stem cell-derived extracellular vesicles inhibits atherosclerotic plaque formation. *Transl Res* 2020; **226**: 83-95 [PMID: 32659442 DOI: 10.1016/j.trsl.2020.07.003]

44 **Xiao X**, Xu M, Yu H, Wang L, Li X, Rak J, Wang S, Zhao RC. Mesenchymal stem cell-derived small extracellular vesicles mitigate oxidative stress-induced senescence in endothelial cells *via* regulation of miR-146a/Src. *Signal Transduct Target Ther* 2021; **6**: 354 [PMID: 34675187 DOI: 10.1038/s41392-021-00765-3]

45 **Xu F**, Fei Z, Dai H, Xu J, Fan Q, Shen S, Zhang Y, Ma Q, Chu J, Peng F, Zhou F, Liu Z, Wang C. Mesenchymal Stem Cell-Derived Extracellular Vesicles with High PD-L1 Expression for Autoimmune Diseases Treatment. *Adv Mater* 2022; **34**: e2106265 [PMID: 34613627 DOI: 10.1002/adma.202106265]

46 **Feng R**, Ullah M, Chen K, Ali Q, Lin Y, Sun Z. Stem cell-derived extracellular vesicles mitigate ageing-associated arterial stiffness and hypertension. *J Extracell Vesicles* 2020; **9**: 1783869 [PMID: 32939234 DOI: 10.1080/20013078.2020.1783869]

47 **Wang J**, Huang R, Xu Q, Zheng G, Qiu G, Ge M, Shu Q, Xu J. Mesenchymal Stem Cell-Derived Extracellular Vesicles Alleviate Acute Lung Injury Via Transfer of miR-27a-3p. *Crit Care Med* 2020; **48**: e599-e610 [PMID: 32317602 DOI: 10.1097/CCM.0000000000004315]

48 **Cheng C**, Liu D, Liu Z, Li M, Wang Y, Sun B, Kong R, Chen H, Wang G, Li L, Hu J, Li Y, Zhao Z, Zhang T, Zhu S, Pan S. Positive feedback regulation of lncRNA TPT1-AS1 and ITGB3 promotes cell growth and metastasis in pancreatic cancer. *Cancer Sci* 2022; **113**: 2986-3001 [PMID: 35534983 DOI: 10.1111/cas.15388]

49 **Li S**, Jiang S, Zhang Q, Jin B, Lv D, Li W, Zhao M, Jiang C, Dai C, Liu Z. Integrin β3 Induction Promotes Tubular Cell Senescence and Kidney Fibrosis. *Front Cell Dev Biol* 2021; **9**: 733831 [PMID: 34805144 DOI: 10.3389/fcell.2021.733831]

World Journal of Stem Cells

Submit a Manuscript: https://www.f6publishing.com

World J Stem Cells 2023 September 26; 15(9): 947-959

DOI: 10.4252/wjsc.v15.i9.947

ISSN 1948-0210 (online)

ORIGINAL ARTICLE

Basic Study

Enhanced wound healing and hemostasis with exosome-loaded gelatin sponges from human umbilical cord mesenchymal stem cells

Xin-Mei Hu, Can-Can Wang, Yu Xiao, Peng Jiang, Yu Liu, Zhong-Quan Qi

Specialty type: Cell and tissue engineering

Provenance and peer review: Unsolicited article; Externally peer reviewed.

Peer-review model: Single blind

Peer-review report's scientific quality classification

Grade A (Excellent): 0
Grade B (Very good): B, B, B
Grade C (Good): 0
Grade D (Fair): 0
Grade E (Poor): 0

P-Reviewer: Silva-Junior AJD, Brazil; Wang S, China; Li SC, United States

Received: August 14, 2023
Peer-review started: August 14, 2023
First decision: August 22, 2023
Revised: August 31, 2023
Accepted: September 14, 2023
Article in press: September 14, 2023
Published online: September 26, 2023

Xin-Mei Hu, Can-Can Wang, Yu Xiao, Peng Jiang, Yu Liu, Zhong-Quan Qi, Medical College, Guangxi University, Nanning 530004, Guangxi Zhuang Autonomous Region, China

Corresponding author: Zhong-Quan Qi, MD, PhD, Professor, Medical College, Guangxi University, No. 100 Daxuedong Road, Nanning 530004, Guangxi Zhuang Autonomous Region, China. yxyyz@gxu.edu.cn

Abstract

BACKGROUND

Rapid wound healing remains a pressing clinical challenge, necessitating studies to hasten this process. A promising approach involves the utilization of human umbilical cord mesenchymal stem cells (hUC-MSCs) derived exosomes. The hypothesis of this study was that these exosomes, when loaded onto a gelatin sponge, a common hemostatic material, would enhance hemostasis and accelerate wound healing.

AIM

To investigate the hemostatic and wound healing efficacy of gelatin sponges loaded with hUC-MSCs-derived exosomes.

METHODS

Ultracentrifugation was used to extract exosomes from hUC-MSCs. Nanoparticle tracking analysis (NTA), transmission electron microscopy (TEM), and western blot techniques were used to validate the exosomes. *In vitro* experiments were performed using L929 cells to evaluate the cytotoxicity of the exosomes and their impact on cell growth and survival. New Zealand rabbits were used for skin irritation experiments to assess whether they caused adverse skin reactions. Hemolysis test was conducted using a 2% rabbit red blood cell suspension to detect whether they caused hemolysis. Moreover, *in vivo* experiments were carried out by implanting a gelatin sponge loaded with exosomes subcutaneously in Sprague-Dawley (SD) rats to perform biocompatibility tests. In addition, coagulation index test was conducted to evaluate their impact on blood coagulation. Meanwhile, SD rat liver defect hemostasis model and full-thickness skin defect model were used to study whether the gelatin sponge loaded with exosomes effectively stopped bleeding and promoted wound healing.

RESULTS

The NTA, TEM, and western blot experimental results confirmed that exosomes

were successfully isolated from hUC-MSCs. The gelatin sponge loaded with exosomes did not exhibit significant cell toxicity, skin irritation, or hemolysis, and they demonstrated good compatibility in SD rats. Additionally, the effectiveness of the gelatin sponge loaded with exosomes in hemostasis and wound healing was validated. The results of the coagulation index experiment indicated that the gelatin sponge loaded with exosomes had significantly better coagulation effect compared to the regular gelatin sponge, and they showed excellent hemostatic performance in a liver defect hemostasis model. Finally, the full-thickness skin defect healing experiment results showed significant improvement in the healing process of wounds treated with the gelatin sponge loaded with exosomes compared to other groups.

CONCLUSION

Collectively, the gelatin sponge loaded with hUC-MSCs-derived exosomes is safe and efficacious for promoting hemostasis and accelerating wound healing, warranting further clinical application.

Key Words: Human umbilical cord mesenchymal stem cells; Exosomes; Gelatin sponge; Safety; Hemostasis; Wound healing

Core Tip: In this study, we loaded exosomes derived from human umbilical cord mesenchymal stem cells onto a gelatin sponge, a common hemostatic substance in clinics, to stop bleeding and promote wound healing. The fabricated material appears relatively safe, provides better hemostatic activity than gelatin sponge alone, and promotes good wound healing.

Citation: Hu XM, Wang CC, Xiao Y, Jiang P, Liu Y, Qi ZQ. Enhanced wound healing and hemostasis with exosome-loaded gelatin sponges from human umbilical cord mesenchymal stem cells. *World J Stem Cells* 2023; 15(9): 947-959
URL: https://www.wjgnet.com/1948-0210/full/v15/i9/947.htm
DOI: https://dx.doi.org/10.4252/wjsc.v15.i9.947

INTRODUCTION

In recent years, biomaterials have increasingly been used in clinical practice. Notably, gelatin sponges have been widely used in various surgical procedures owing to their excellent characteristics. Gelatin sponges are highly accessible, cheap, and easy to use, allowing use as a dry material or impregnated with saline or thrombin prior to use. Furthermore, gelatin sponges exhibit a robust absorption capacity and can absorb approximately 40 times their own weight of water or liquid and expand to 200% of their original volume, thus increasing the local platelet concentration[1]. Moreover, the expanded gelatin particles help limit blood flow and provide a packing effect in the limited space, thereby promoting the formation of blood clots during wound healing.

Gelatin sponges were first used in neurosurgery in the 1940s and have since been widely used in various surgical procedures. In recent years, many new applications have been developed for absorbable gelatin sponges. Wang *et al*[2] have fabricated an Au/Ag gelatin sponge by adding Au/Ag to the gelatin matrix, which improved its antibacterial performance. Yang *et al*[3] have used a cocktail of ropivacaine, dexamethasone, and vitamin B12 to impregnate a gelatin sponge for promoting leg pain relief and functional recovery after percutaneous endoscopic lumbar discectomy. Notably, Jogo *et al*[4] have loaded gelatin sponge particles with 5% ethanolamine oleate iopamidol and used the mixture to examine the effect of retrograde occlusion of veins in gastric varices. Incorporating colloidal Ag into gelatin sponges was beneficial in promoting bone healing in infected skull defects[5]. Accordingly, gelatin sponges can be used to promote wound healing and combined with various drugs or substances to improve their therapeutic effects.

Mesenchymal stem cells (MSCs) have been shown to markedly improve wound closure, angiogenesis, and wound healing. However, stem cell therapy is complex, expensive, and time-consuming. Recent studies have demonstrated the effectiveness of stem cell-derived exosomes in treating wounds. Exosomes are emerging as a new mode of intercellular communication. Additionally, exosomes play an important role in wound repair[6]. Exosomes are membrane-derived vesicles interacting with target receptor cells, enabling inter cellular communication[7]. Growing evidence suggests that exosomes are crucial in coagulation, intercellular signaling, and waste metabolism[8]. The biological characteristics of exosomes derived from MSCs are similar to those of umbilical cord (UC)-MSCs, making them valuable for tissue repair.

Recently, an increasing number of studies have explored the combined application of exosomes and biological materials. Wang *et al*[9] have fabricated an injectable, viscous, heat-sensitive, multifunctional polysaccharide-based wound dressing capable of sustained exosomes release to accelerate wound healing by stimulating the angiogenic process of the wound tissue. Tao *et al*[10] have combined exosomes released by synovial MSCs overexpressing miR-126-3p with chitosan, demonstrating that this strategy could be used to treat skin wounds. Xu *et al*[11] have assembled exosomes on chitosan/silk hydrogel sponges based on platelet-rich plasma to examine wound healing in a diabetic rat model, revealing their capacity to promote wound healing during diabetes. Furthermore, Nooshabadi *et al*[12] have employed an exosome-loaded chitosan hydrogel to study wound healing and dermal reconstruction in mice. The authors found that the exosome-loaded chitosan hydrogel exhibited a wound closure capacity of approximately 83.6% and a high degree of

re-epithelization[12]. Based on the above literature, novel dressings made by combining exosomes and a variety of biological materials afford better effects than conventional dressings.

In the present study, we loaded a common clinically used gelatin sponge with exosomes to synthesize a novel gelatin sponge with improved characteristics. The safety and effectiveness of the improved gelatin sponge in hemostasis and promotion of healing were studied both *in vivo* and *in vitro*. The findings will provide novel avenues for further research on the potential applications of human UC MSCs (hUC-MSCs)-derived exosomes in tissue repair. Furthermore, our study provided evidence for the feasibility of using a bioscaffold synthesized by combining exosomes and biological materials simply and non-invasively to stop bleeding and promote wound healing, thereby supporting the further use of exosomes for clinical applications.

MATERIALS AND METHODS

Statement of animal treatment

All animals were obtained from Changsha Tianqin Biotechnology Co., Ltd. (Changsha, China) and were housed under ordinary conditions. The animals were maintained under a 12-h light/12-h dark cycle at stable temperature (22-26 °C) and humidity (50%-70%). They were given free access to food and water throughout the study period.

Extraction and characterization of exosomes derived from hUC-MSCs

hUC-MSCs were purchased from Guangxi TaiMeiRenSheng Biotechnology Co. Ltd. Fourth-passage cells at logarithmic phase were inoculated in T175 air-permeable cell culture flasks with a dedicated medium (HUXUC-90011, Cyagen). The cells were cultured at 37 °C in an incubator containing 5% CO_2. When the adherent cells reached a confluence of 80%-90%, the used cell medium was discarded and replaced with a serum-free medium. After 48 h, cells were centrifuged and cell supernatants were collected. Exosomes in the cell supernatants were extracted by ultracentrifugation. Impurities in the cell supernatants were removed by centrifugation at 300 × *g* for 10 min, followed by the removal of dead cells by centrifugation at 2000 × *g* for 20 min; then, cell debris was removed by centrifugation at 10000 × *g* for 30 min. Subsequently, cell supernatants were filtered using a 0.22 μM membrane filter and centrifuged in an ultracentrifuge (Beckman, America) for 120 min at 120000 × *g*, and the supernatants were discarded. The precipitated exosomes were re-suspended in phosphate buffered saline (PBS) and centrifuged again for 120 min at 120000 × *g*, and the exosomes precipitate were finally re-suspended in filtered PBS. All centrifugations were performed at 4 °C.

Exosomes were identified using a nanoparticle tracking analyzer (ZetaView, Particle Metrix, Germany), which was used to measure their concentration and particle size. A transmission electron microscope (HT-7700, Hitachi High-tech Company) was used to observe the shape and size of exosomes. Western blot was used to detect the surface marker proteins, CD9, Tsg101, and Calnexin, in exosomes. The protein concentration of hUC-MSCs-derived exosomes was determined using a BCA protein quantitation kit (Zoman, Biotechnology, ZD301). After adding the required proportion of loading buffer, the sample was heated at 95 °C for protein denaturation. Protein from each sample was separated on a sodium dodecyl sulfate-polyacrylamide gel and then transferred to polyvinylidene fluoride membranes. After blocking with 5% skim milk for 2 h, the membranes were incubated overnight with anti-CD9 (20597-1-AP, Proteintech), anti-Tsg101 (28283-1-AP, Proteintech), and anti-Calnexin (10427-2-AP, Proteintech) antibodies. Subsequently, the secondary antibody (SA00001-2, Proteintech) was added, followed by incubation for 1.5 h. Band visualization was achieved using a chemiluminescence kit (P0018FM, Beyotime, China) and observed on a chemiluminescent imaging system (MiniChemi 610, Sagecreation, China).

Characterization of gelatin sponge loaded with hUC-MSCs derived-exosomes

An absorbable gelatin sponge was purchased from Jiangxi Xiangen Medical Technology Development Co., Ltd. It was sliced into appropriate sizes, and immersed in the exosome solution mixed with trehalose, to ensure that the gelatin sponge fully absorbed the exosomes. Subsequently, the loaded gelatin sponge was freeze-dried and characterized *via* scanning electron microscopy.

Cell viability assay

The effect of the hUC-MSCs-derived exosomes on mouse epithelioid fibroblasts (L929) was evaluated using the CCK-8 assay. Briefly, L929 cells were inoculated into 96-well plates and divided into control, sponge extract, and exosome groups. The cell density was adjusted to 10000 cells/well and then incubated at 37 °C in a 5% CO_2 incubator for 12 h. Subsequently, the medium in the exosome group was adjusted to ensure that each well contained 6 × 10^6 particles of exosomes and then incubated at 37 °C under 5% CO_2 for a further 6 h. After 6 h, 10 μL of CCK-8 reagent was added to all groups, followed by incubation in the dark for 1 h. Finally, the absorbance of each well was measured at 450 nm using a microplate reader.

Hemolysis assay

Briefly, 5 mL of fresh blood from New Zealand rabbits was stirred in one direction with a glass rod, followed by fibrin removal; then, 20 mL of normal saline was added. The mixture was mixed well and centrifuged at 2000 rpm for 10 min. The supernatant was discarded, normal saline was added, and the process was repeated 3-4 times until the supernatant was clear. Finally, the supernatant was discarded, and 1 mL of fresh blood was added to 49 mL of normal saline to obtain a 2% rabbit red blood cell suspension for subsequent use. The assay was divided into negative control, positive control,

sponge, and exosome-loaded sponge groups. Subsequently, 500 μL of the 2% rabbit red blood cell suspension was added to each group, and an equal volume of liquid was added (normal saline was added to the negative control group, and Triton X-100 with a mass fraction of 0.5% was added to the positive control group. Gelatin sponge extract at a concentration of 10 mg/mL was added to the sponge group, and gelatin sponge extract with 1×10^9 exosomes was added to the exosome-loaded sponge group). Then, the solutions were mixed evenly and incubated at 37 °C for 3 h. The samples were then centrifuged at 3000 rpm for 3 min. The optical density (OD) of the supernatant was measured at a wavelength of 545 nm, and the hemolysis rate was calculated by photography. The hemolysis rate was calculated as $(OD_{sam} - OD_{neg})/(OD_{pos} - OD_{neg}) \times 100\%$ (1)[13].

Skin irritation test

The skin irritation test was performed using three New Zealand rabbits. The hair on their backs was carefully removed. Four specific areas on their skin were identified and treated with different fluids. They were blank group without any articles, NaCl group with 0.9%NaCl solution, sponge group with 10 mg/mL sponge extract, and exosome group with 5×10^8 exosomes solution. The application was repeated every 24 h until absorption was complete. The rabbits were closely monitored to assess any changes in their skin condition, such as redness, swelling, inflammation, or other related symptoms. After 72 h, skin samples were harvested from treated sites for histopathological examination to observe any signs of inflammation in the skin tissue.

Histocompatibility assay

Eighteen male Sprague-Dawley (SD) rats were divided into blank control, sponge, and exosome-loaded sponge groups. After anesthesia with 10% chloral hydrate, the hair on their back was removed, the subcutaneous bags were excised, and 1 cm × 1 cm × 0.5 cm of either gelatin sponges or gelatin sponges loaded with exosomes were implanted into them, while the blank control group was not implanted with any gelatin sponge. The adjacent skin was collected for pathological analysis on day 7 and 14, respectively, to evaluate the *in vivo* biocompatibility of the gelatin sponges.

Whole blood coagulation index test

The gelatin sponges were cut into 1 cm × 1 cm × 0.5 cm sections, and preheated in an oven at 37 °C for 5 min. In the sponge and exosome groups, the gelatin sponges were infiltrated with 100 μL of normal saline and 100 μL of exosome solution containing 5×10^8 exosomes, respectively. Next, 100 μL of rat whole blood was added to each gelatin sponge in both groups for adequate absorption, followed by 10 μL of 0.2 M calcium chloride solution, and incubated at 37 °C for 15 min. Subsequently, 25 mL of deionized water was used to rinse blood from the gelatin sponge surface without coagulation. Finally, the absorbance (Abs1) of the washed liquid was measured at 540 nm by using a microplate reader. For the blank control (Abs0), 100 μL of whole blood was added to 25 mL of deionized water, and the blood coagulation index (BCI) was calculated using the formula: $BCI\ (\%) = Abs1/Abs0 \times 100\%$ (2).

Hemostatic assay using rat liver defect hemostasis model

The hemostatic capacity of the exosome-loaded gelatin sponge was evaluated using a rat liver defect hemostasis model [14]. Twelve SD rats were divided into sponge and exosome-loaded sponge groups (n = 6 rats/group), with an equal distribution of male and female rats. After anesthesia induction with 10% chloral hydrate, an abdominal incision was made to expose the liver, and the tissue fluid around the liver was carefully removed using a dry cotton ball to prevent inaccurate blood weight measurements. The liver was placed on a pre-weighed filter paper, and a 0.5 cm long and 0.2 cm deep wound was created on the liver using a scalpel. The gelatin sponge loaded with exosomes was immediately placed at the bleeding site and bleeding was observed. After the bleeding stopped completely, the bleeding time was recorded, and the blood-absorbed filter paper was weighed. The weight difference between the front and rear of the filter paper was considered as the weight of blood loss from the rat liver.

Effect of exosomes-loaded gelatin sponge on healing of skin full-thickness defect model

Eighteen male SD rats (220-280 g) were randomly divided into control, sponge, and exosome-loaded sponge groups. After anesthesia induction with 10% chloral hydrate, the hair on the back of rats was removed, and a full-thickness skin defect wound (approximately 1.5 cm × 1.5 cm) was created on their backs. Photographs were taken to record the original area, and the wound was covered with either a gelatin sponge or an exosome-loaded gelatin sponge, and wrapped with a transparent dressing; the control group received only a transparent dressing. On day 7 and 14 post the procedure, the gauze was opened to observe and record wound healing. All wounds were photographed, the area was analyzed using Image J software (National Institutes of Health, Bethesda, MD), and skin samples around the wounds were collected and fixed with 4% paraformaldehyde for pathological analysis.

Masson staining and immunohistochemistry

Masson's trichrome staining was used to determine collagen content and wound maturity. Image J software was used to analyze the areas of interest. The collagen content was quantified. Ki67 was used to evaluate local whole-cell proliferation and CD31 staining was used to evaluate angiogenesis. Sections were incubated with antibodies against Ki67 (1:600, #AF0198, Affinity) or CD31 (1:1000, Cat No.28083-1-AP, Proteintech). Subsequently, the secondary antibody was added (2118D1104, Beijing Zhongshan Jinqiao Biotechnology Co., Ltd.). Six randomly selected areas were imaged using an inverted microscope for each specimen, and the number of Ki67- and CD31- positive cells/positive blood vessels was detected using image J software.

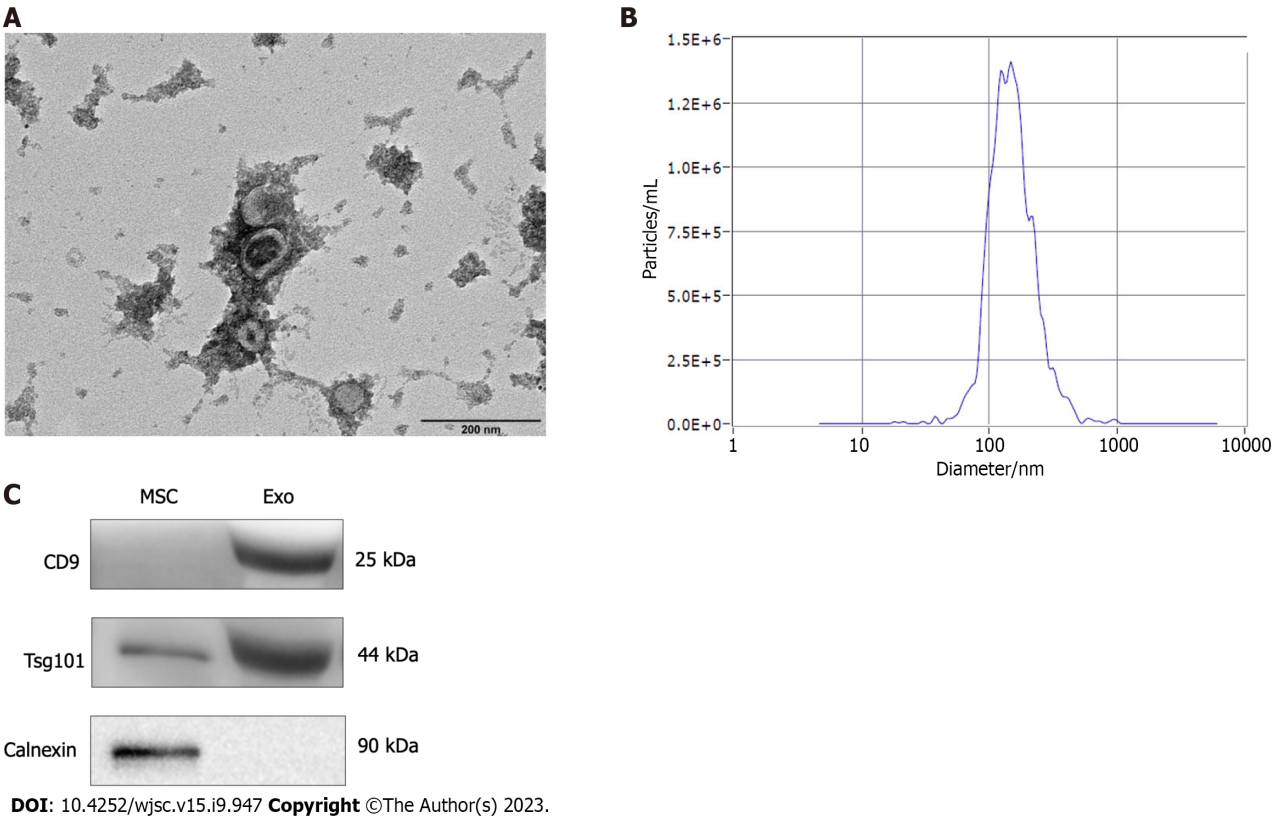

DOI: 10.4252/wjsc.v15.i9.947

Figure 1 Characterization of human umbilical cord mesenchymal stem cell-derived exosomes. A: Morphology of the exosomes assessed by transmission electron microscopy. Scale bar = 200 nm; B: Grain size of the exosomes; C: Surface protein markers of exosomes. MSC: Mesenchymal stem cell; Exo: Exosome.

Statistical analysis

SPSS 26.0 (IBM Corp., Armonk, NY, United States) and GraphPad Prism 8.0 (GraphPad Software Inc.; San Diego, CA, United States) were used for statistical analyses. Paired or unpaired *t*-tests were used for comparisons between two groups, and one-way analysis of variance (ANOVA) was used for comparisons among three or more groups. $P < 0.05$ was considered statistically significant.

RESULTS

Identification of exosomes

We successfully isolated exosomes from hUC-MSCs by ultracentrifugation. After successful separation, the morphology of the exosomes was observed by using TEM, and a typical cup-shaped structure was observed (Figure 1A). The exosome concentration and particle size were measured using a nano-particle size analyzer. The average exosome particle size was 144.7 nm, consistent with the particle size of exosomes (30-150 nm) (Figure 1B). Western blot results showed that the extracted exosomes successfully expressed the surface marker proteins CD9 and Tsg101, but not Calnexin (Figure 1C).

Characterization of gelatin sponge loaded with exosomes

The exosomes on the gelatin sponge were detected *via* scanning electron microscopy. The gelatin sponge with exosomes was coarser than the sponge without exosomes, and exosome particles could be observed (Figures 2A and B).

Cytotoxicity and biocompatibility of gelatin sponge loaded with exosomes

The gelatin sponge loaded with exosomes did not induce significant toxicity toward L929 cells as the cells remained viable following exposure to them (Figure 3A). Moreover, the hemolytic assay showed that no hemolysis was observed with the naked eye using the gelatin sponge loaded with exosomes (Figure 3C). Measuring the OD value of the solution and calculating the hemolysis rate, we found that the hemolysis rates of the gelatin sponge and exosome-loaded gelatin sponge in whole blood were -0.01% and 0.18%, respectively, which were within the permissible range for biological materials (less than 5%), indicating that the exosome-loaded gelatin sponge was safe for use (Figure 3B). All experimental rabbits had an intact epidermis, with normal sebaceous glands, hair follicles, and hair structures; there were no notable pathological changes, such as inflammatory cell infiltration, tissue congestion, and edema (Figure 3D).

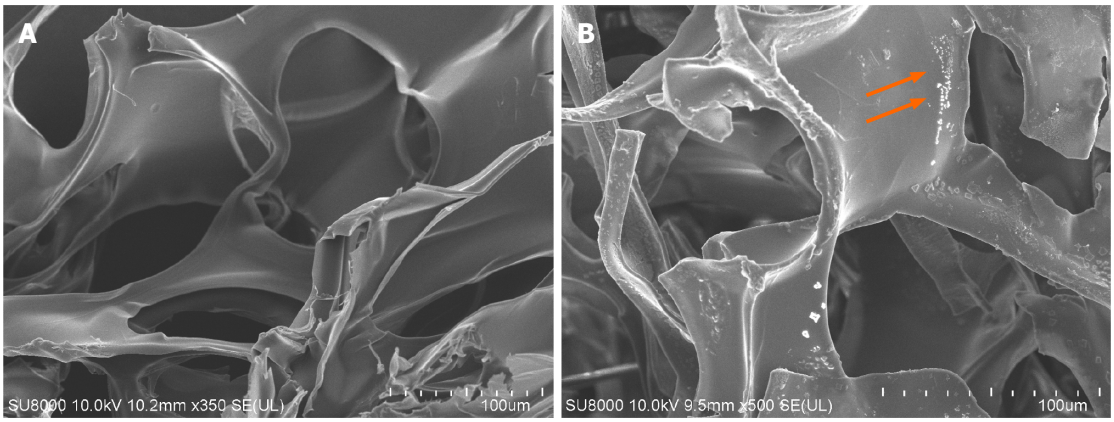

DOI: 10.4252/wjsc.v15.i9.947 **Copyright** ©The Author(s) 2023.

Figure 2 Characterization of gelatin sponge loaded with exosomes. A: SEM image of the gelatin sponge; B: SEM images of the gelatin sponge loaded with exosomes. The orange arrows show the exosomes.

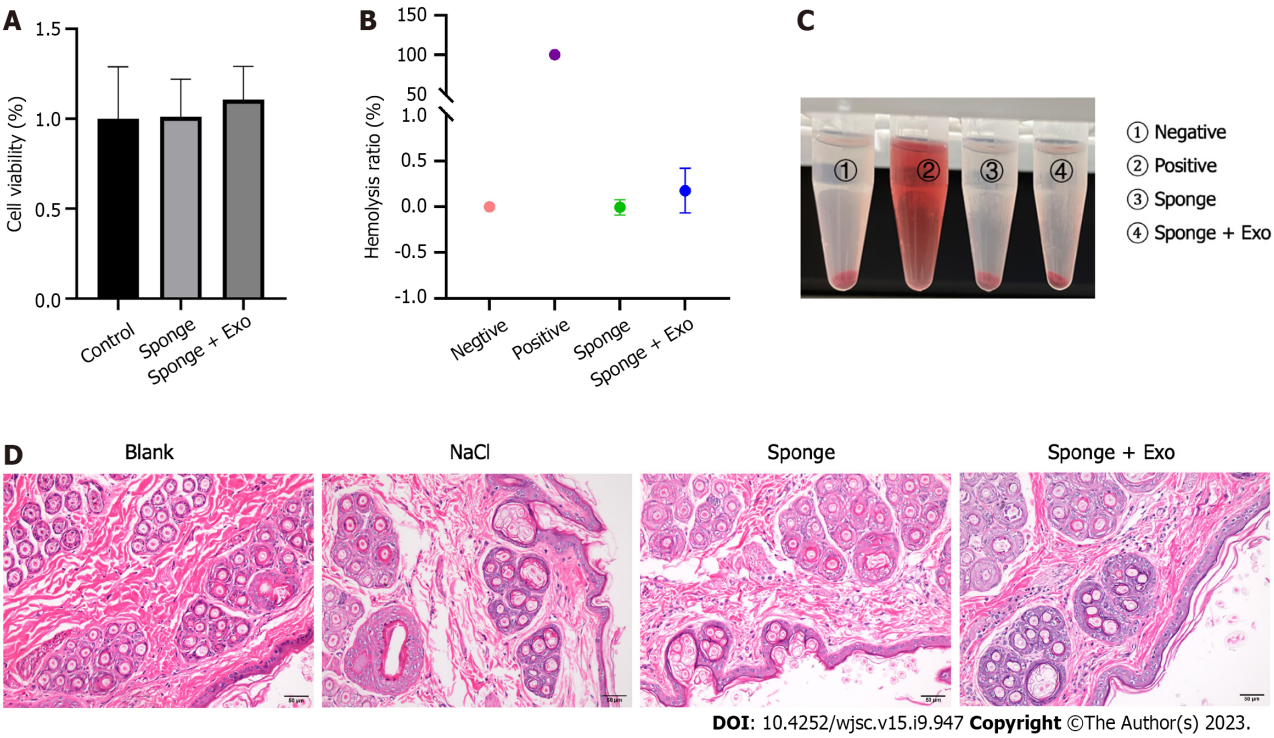

DOI: 10.4252/wjsc.v15.i9.947 **Copyright** ©The Author(s) 2023.

Figure 3 Biosafety of gelatin sponge loaded with exosomes. A: Cell viability of gelatin sponge loaded with exosomes; B and C: Hemolysis ratio of gelatin sponge loaded with exosomes; D: Representative diagram of pathological condition of rabbit skin after stimulation with exosome and sponge extract. Scale bar = 50 μm. Exo: Exosome.

To investigate the *in vivo* biocompatibility of gelatin sponge loaded with exosomes, we implanted the gelatin sponge into the dorsal subcutaneous space of SD rats, and observed the condition of the implant on day 7 and day 14 (Figures 4A and B). A portion of the gelatin sponge was retained in the body on day 7 and day 14; however, the gelatin sponge on day 14 was obviously smaller than that on day 7, indicating that the gelatin sponge could be degraded in the body. Adjacent skin tissue samples were collected for pathological analysis. After 7 and 14 d of implantation, there was no obvious inflammatory response around the tissue, and no obvious tissue fibrosis or necrosis was observed (Figure 4C), indicating that the gelatin sponge loaded with exosomes showed good biocompatibility.

Hemostatic effect of gelatin sponge loaded with exosomes

We evaluated the clotting ability of gelatin sponge and gelatin sponge loaded with exosomes. Our findings showed that the BCI values of the gelatin sponge and exosome-loaded gelatin sponge groups were 45.63% and 31.47%, respectively, indicating that both groups had significant clotting ability, and the clotting ability of the exosome-loaded gelatin sponge was significantly higher than that of the gelatin sponge group (Figure 5A).

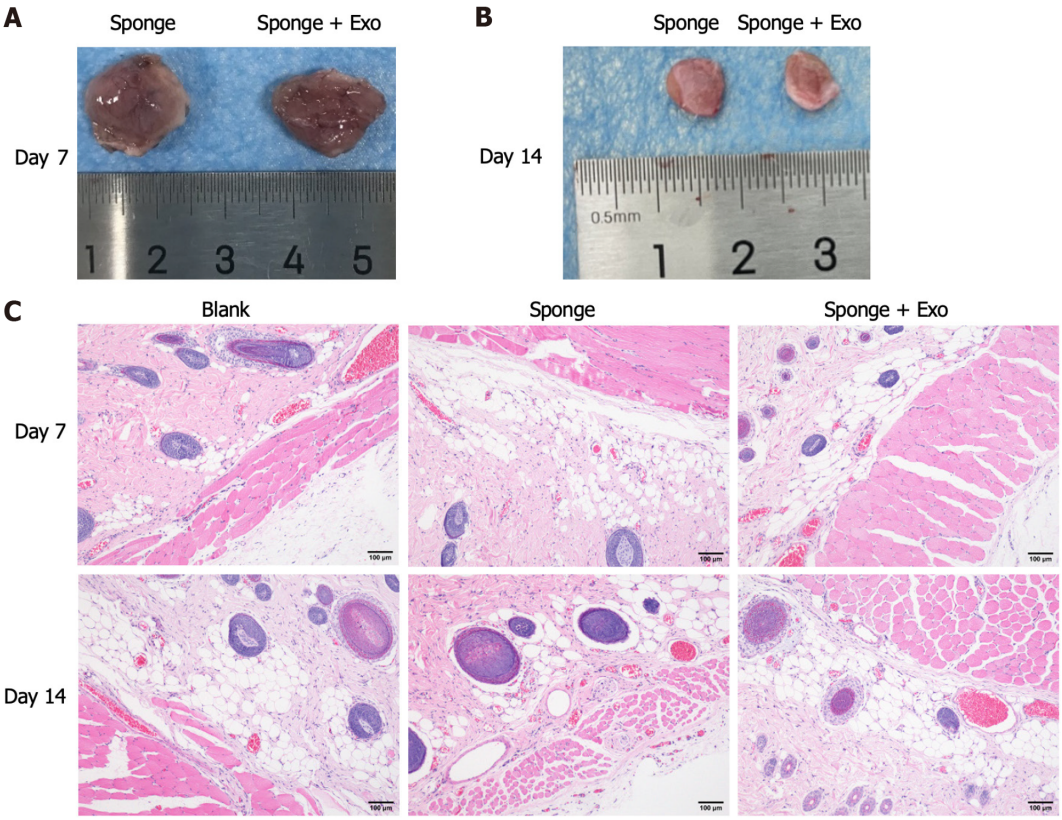

DOI: 10.4252/wjsc.v15.i9.947 **Copyright** ©The Author(s) 2023.

Figure 4 Biocompatibility of gelatin sponge loaded with exosomes. A and B: The size of the gelatin sponge remaining on day 7 and day 14; C: Hematoxylin and eosin staining of the adjacent skin tissues in the dorsal subcutaneous space of SD rats after 7 and 14 d of implantation. Scale bar = 100 μm. Exo: Exosome.

After establishing a liver defect model, we covered the wound with a gelatin sponge and recorded blood loss and hemostasis time. The blood loss and hemostasis time of the gelatin sponge group loaded with exosomes were significantly lower than those of the gelatin sponge group, indicating that the gelatin sponge loaded with exosomes had a better hemostatic effect than the conventional gelatin sponge (Figures 5B-D).

Effect of gelatin sponge loaded with exosomes in promoting wound healing

After establishing a rat full-thickness skin defect model, the wound was covered with a gelatin sponge, and the gauze was opened on day 7 and day 14 post the procedure to observe and record the wound healing status. The wound size of all groups decreased with time. Moreover, the wound size of the gelatin sponge group loaded with exosomes was smaller than that of the other two groups, indicating that the gelatin sponge loaded with exosomes promoted wound healing better than the conventional gelatin sponge (Figures 6A and B). Histopathological results showed that on day 14, the gelatin sponge loaded with exosomes group demonstrated better regeneration of hair follicles and sebaceous glands than the other two groups (Figure 6C).

Masson's trichrome staining was performed on the skin adjacent to the wound to evaluate the formation and distribution of collagen, which is important for promoting wound healing. Microscopic observations showed that collagen fibers in the skin of all three groups were relatively few on day 7. However, on day 14, the collagen fibers in the skin of the three groups gradually increased along with gradual healing of the wound (Figure 7A). Statistical analysis showed that the collagen fibers in the exosome-loaded gelatin sponge group were significantly higher than those in the other two groups on day 14; on day 7, the collagen fibers in the gelatin sponge and exosome-loaded gelatin sponge groups were significantly higher than those in the control group (Figure 7B). These findings suggested that the exosome-loaded gelatin sponge promoted wound healing by promoting collagen fiber synthesis.

To explore the possible mechanism of action of gelatin sponges loaded with exosomes, we employed immunohistochemical techniques to evaluate angiogenesis and cell proliferation in the granulation tissue. To evaluate angiogenesis, we stained the skin near the wound for CD31. On day 7 and day 14, the number of CD31-positive blood vessels in the exosome-loaded gelatin sponge group was significantly higher than that in the control group; on day 14, this number was significantly higher than that in the gelatin sponge group (Figures 7C and D). Subsequently, we detected the proliferation of whole cells of granulation tissue in the skin near the wound and found that the proportion of Ki67-positive cells in the exosome-loaded gelatin sponge group was significantly higher than that in the control and gelatin sponge groups on day 7 and day 14. However, there was no statistically significant difference in the proportion of Ki67-positive cells between the gelatin sponge and control groups (Figures 7E and F). These results indicated that the gelatin sponge loaded with exosomes could promote cell proliferation and angiogenesis, thereby accelerating wound healing.

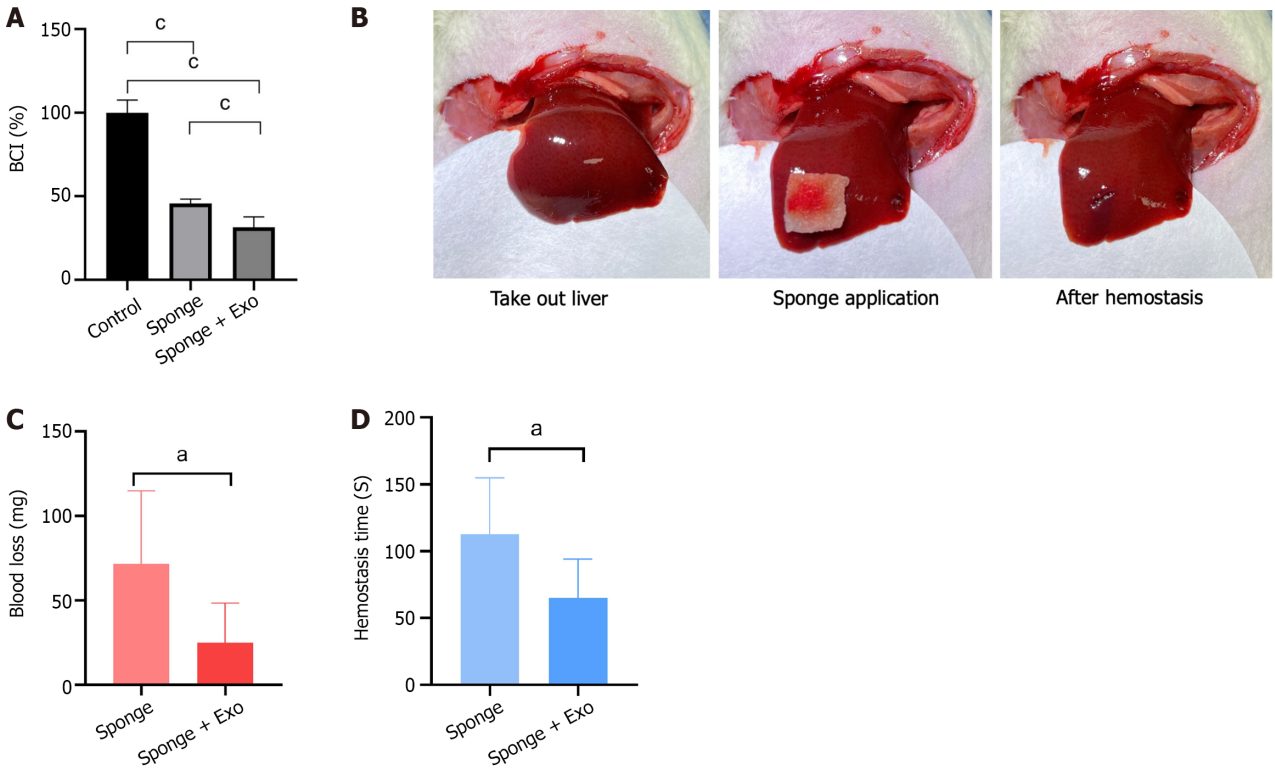

DOI: 10.4252/wjsc.v15.i9.947 **Copyright** ©The Author(s) 2023.

Figure 5 Hemostatic effect of gelatin sponge loaded with exosomes. A: Clotting ability of exosome-loaded gelatin sponge; B: Experimental process of hemostasis in liver injury model; C: Hepatic blood loss in rats; D: Time required for hemostasis. $^{a}P < 0.05$, $^{c}P < 0.001$. $n = 6$. Exo: Exosome.

DISCUSSION

Wound healing presents an important challenge for both clinicians and patients. Poor wound healing can negatively impact the patient's quality of life and exacerbate pain, stress, and depression[15,16]. Therefore, methods that effectively promote wound healing are particularly important. Several studies have demonstrated that MSCs accelerate wound closure by promoting skin cell migration, angiogenesis, epithelization, and granulation tissue formation. However, the clinical application of MSCs faces ethical issues, and there is a lack of long-term follow-up evidence regarding their safety. Therefore, alternative cell-free therapies are required. With the emergence of the paracrine hypothesis, the therapeutic applications of exosomes have become more extensive. Exosomes exhibit functions similar to MSCs[17]. Given their immunogenicity, compared with that of MSCs, exosomes can be considered a good alternative[18]. Recently, an increasing number of studies have shown that stem cell-derived exosomes contain mRNA, microRNAs, growth factors, and various other proteins, and potentially participate in processes such as hemostasis, angiogenesis, and wound healing[19,20]. For example, exosomes derived from hUC-MSCs containing miR-21, miR-23a, miR-125b, and miR-145 inhibit fibroblast proliferation and reduce scar formation during wound healing[21].

In the current study, we proposed a new method for loading exosomes into gelatin sponges to achieve wound healing. Our analyses showed that exosome-loaded gelatin sponge was safe and reliable for use. *In vivo* and *in vitro* experiments showed that exosome-loaded gelatin sponge exhibited a good hemostatic effect and promoted the formation of wound granulation tissue, collagen deposition, and angiogenesis, thereby promoting wound healing. Although several studies have shown that exosomes are well-tolerated in animal models, their clinical safety needs to be verified. Considering the goal of exosome-loaded gelatin sponges for clinical application, the safety of exosome-loaded gelatin sponges was verified in this study. We confirmed that the exosome-loaded gelatin sponge was safe for use, as determined by hemolysis, skin irritation, and histocompatibility experiments, consistent with the results of Sun *et al*[22]. These findings provide further evidence for the clinical application of exosomes.

Healing of skin injuries is a complex process that mainly includes four stages: Hemostasis, inflammation, proliferation, and remodeling[23]. The first stage involves hemostasis and clot formation to prevent blood loss. The second stage is the inflammatory stage, which includes coagulation, phagocytosis, removal of foreign bodies, and recruitment of growth factors and anti-inflammatory cells to injury site. The third stage involves proliferation, including fibrous proliferation, angiogenesis, and cell migration. Finally, fibroblasts continue to secrete collagen during the remodeling phase[24,25]. Type I collagen replaces type III collagen at the wound site. Subsequently, scar formation occurs *via* apoptosis.

In this study, we conducted *in vitro* and *in vivo* experiments to verify the potential role of a gelatin sponge loaded with exosomes in coagulation and hemostasis. We found that the coagulation index of the gelatin sponge loaded with exosomes was significantly lower than that of the control group and the gelatin sponge group, thereby suggesting that the gelatin sponge loaded with exosomes had significant coagulation ability; this finding was also confirmed in the liver

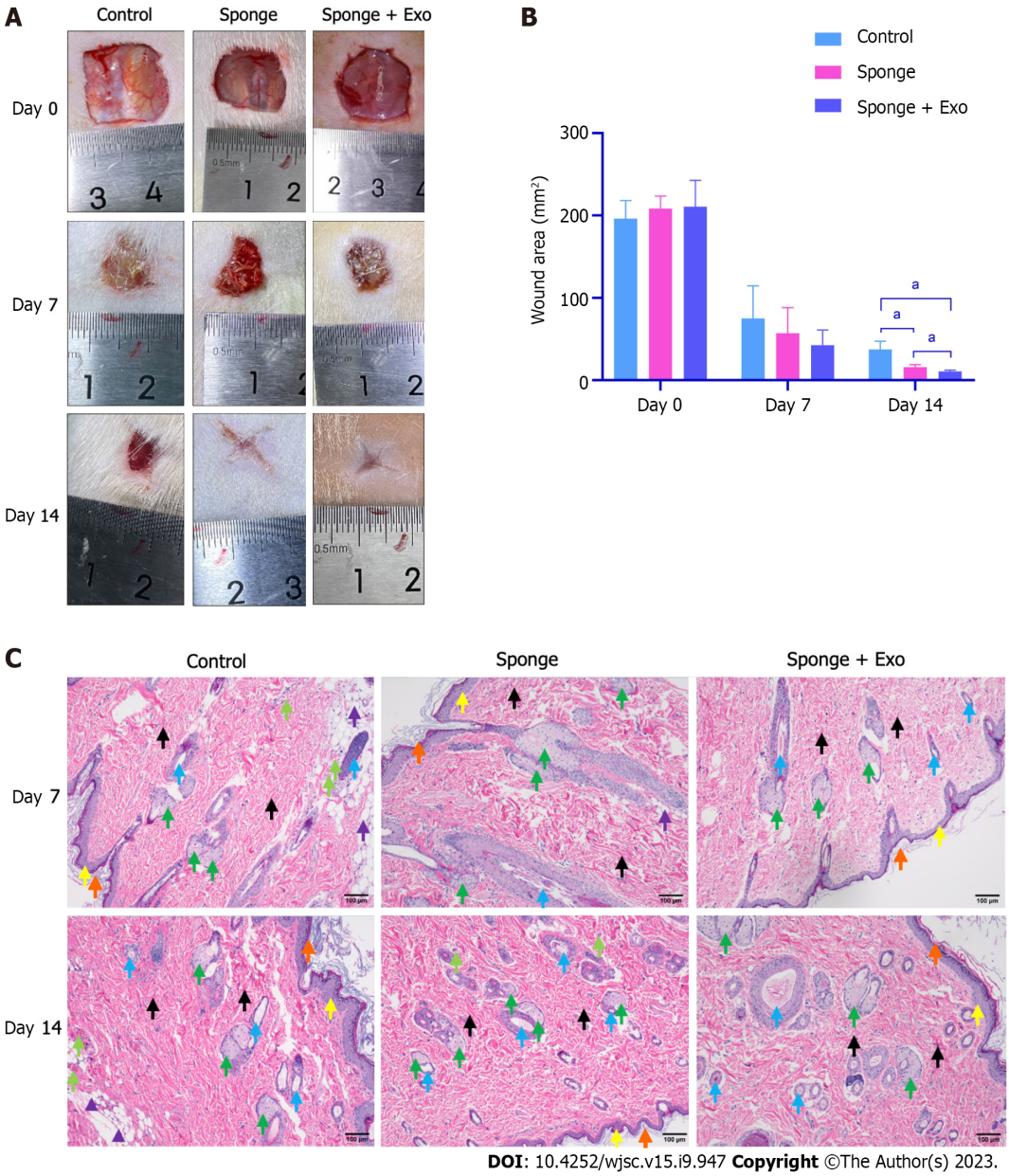

DOI: 10.4252/wjsc.v15.i9.947

Figure 6 Wound healing effect of gelatin sponge loaded with exosomes. A: Representative images of rat wounds; B: Statistical analysis of the wound area; C: Hematoxylin and eosin-stained wound tissue sections as observed under a light microscope. The orange arrows indicate the stratum corneum, the yellow arrows indicate the granular layer, the green arrows indicate the sebaceous gland, the blue arrows indicate the hair follicle, the black arrows indicate the collagen fibers, the light green arrows indicate the blood vessels, and the purple arrows indicate the subcutaneous fat. Scale bar = 100 μm. $^{a}P < 0.05$. $n = 3$. Exo: Exosome.

injury hemostasis experiment, where the gelatin sponge group loaded with exosomes reduced bleeding in rats and shortened the bleeding time. These data proved that the gelatin sponge loaded with exosomes afforded a better hemostatic effect than the conventional gelatin sponge, and had a significant effect in promoting wound healing during this stage of hemostasis.

Angiogenesis is essential for wound repair. Blood vessels provide progenitor cells, oxygen, and nutrients to maintain proliferation and remodeling of the wound site[26]. CD31 is an endothelial cell marker demonstrating the degree of tissue vascularization. In the current study, we evaluated angiogenesis by immunohistochemical staining for CD31 in the skin adjacent to the wound. The results showed that the number of CD31-positive blood vessels in the exosome-loaded gelatin sponge group was significantly higher than that in the control and gelatin sponge groups, indicating that the exosome-loaded gelatin sponge had a better angiogenic effect than the conventional gelatin sponge. This may be related to the provascular effects of exosomes. Many studies have shown that exosomes participate in angiogenesis signaling pathways and affect the occurrence, development, and maturation of blood vessels[27]. Zhang *et al*[28] have extracted exosomes from induced pluripotent stem cells and studied their effects on the proliferation, migration, and angiogenesis of hUC blood venous endothelial cells. They found that in a rat model of full-thickness skin defects, exosomes could promote not only angiogenesis at the wound site but also the maturation of blood vessels[28]. Fat-derived exosomes can also be ingested by the vascular endothelium to promote blood vessel formation *in vivo* and *in vitro*[29].

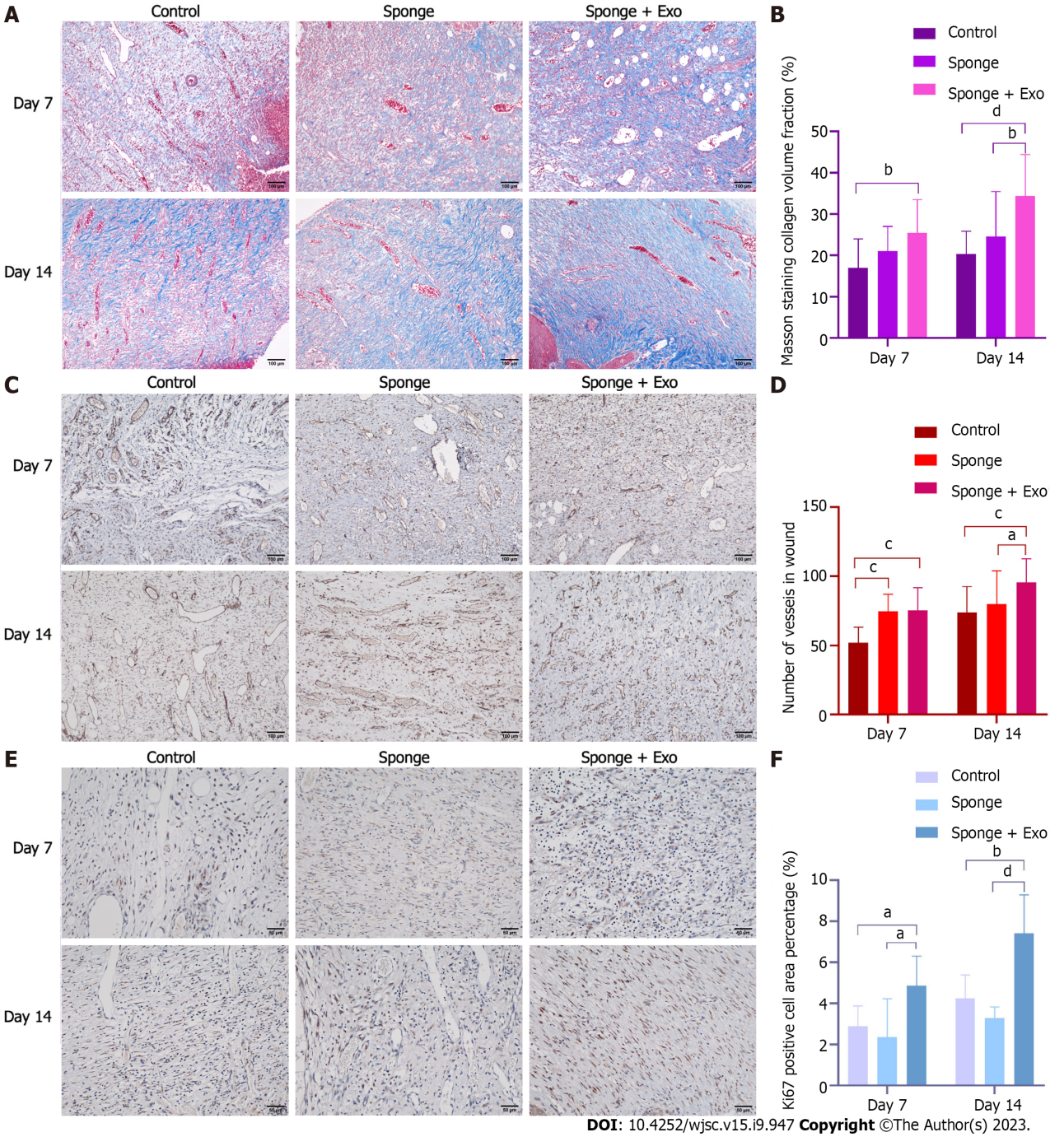

DOI: 10.4252/wjsc.v15.i9.947

Figure 7 Gelatin sponge loaded with exosomes promotes collagen formation, cell proliferation, and angiogenesis during the wound healing process. A: Masson-stained wound tissue sections as observed. Scale bar = 100 μm; B: Statistical analysis of the percentage of collagen volume with respect to tissue volume; C: CD31-positive vessels in wound tissue sections. Scale bar = 100 μm; D: Statistical analysis of CD31-positive vessels; E: Ki67-positive cells in wound tissue sections. Scale bar = 50 μm; F: Statistical analysis of Ki67 positive cell area percentage. $^{a}P < 0.05$, $^{b}P < 0.01$, $^{c}P < 0.001$, $^{d}P < 0.0001$. Exo: Exosome.

Masson's trichrome staining is a classical technique used to distinguish collagen and muscle fibers. In the current study, we performed Masson's trichrome staining on the skin near the wounds of rats. We found that the collagen fibers produced in the exosome-loaded gelatin sponge group were significantly higher than those in the gelatin sponge and control groups at the end of the observation period. This indicates that the exosome-loaded gelatin sponge could promote the formation of collagen fibers. This finding is consistent with that of Kim *et al*[30], who employed exosomes to directly treat human skin tissue and found that exosomes can facilitate the migration of fibroblasts and nearby collagen synthesis, as well as promote the synthesis of collagen and elastin in human skin tissue. Ki67 is a marker of cell proliferation, and, in general, angiogenesis begins with endothelial cell proliferation, followed by their isolation, migration, adhesion, and differentiation from adjacent tissues[31]. Cell proliferation and migration are the two key steps in angiogenesis. In this study, we detected the proliferation of integral cells of granulation tissue in the skin near the wound and found that the proportion of Ki67-positive cells in the exosome-loaded gelatin sponge group was significantly higher than that in the

control and gelatin sponge groups. This finding was consistent with the results reported by Wang *et al*[9], who found that in diabetic rats, the expression of the Ki67 in the FEP@exo group was significantly higher than that in the FEP and control groups. These observations may be related to the promotion of cell proliferation. Moreover, the application of exosomes derived from hUC-MSCs has been explored in a rat skin burn model, revealing that exosomes could dose-dependently promote fibroblast proliferation[6,32].

In summary, using an exosome-loaded gelatin sponge for wound healing could be safe and reliable and promote wound healing by promoting cell proliferation, collagen fiber formation, and blood vessel formation.

CONCLUSION

In conclusion, our study has proposed a novel method that uses hUC-MSC-derived exosomes loaded onto gelatin sponges for wound healing, which afforded good hemostatic and wound healing-promoting effects. The exosome-loaded gelatin sponge is safe and could provide new avenues for the clinical application of exosomes. Gelatin sponges are a common hemostatic material used in clinical practice. Moreover, they are inexpensive and readily available. Therefore, combining exosomes and gelatin sponges has strong clinical adaptability and is conducive to the clinical transformation and application of exosomes.

ARTICLE HIGHLIGHTS

Research background

Hemostasis and wound healing are one of the common problems in clinics which need to be paid attention to. Gelatin sponge is often used as a hemostatic material in clinics. Exosomes have been proved to play an important role in wound repair. Therefore, it is worth studying whether the combination of exosomes derived from human umbilical cord mesenchymal stem cells (hUC-MSCs) and a gelatin sponge could promote hemostasis and wound healing more efficiently.

Research motivation

Poor wound healing would contribute a negative impact on patients' quality of life and aggravate pain, stress and depression, so it is of great significance to find ways to effectively promote wound healing.

Research objectives

The present study aimed to investigate the hemostatic and wound healing efficacy of a gelatin sponge loaded with hUC-MSCs-derived exosomes.

Research methods

After the exosomes were extracted and characterized by ultracentrifugation, we loaded the exosomes on a gelatin sponge. Then, *in vitro* and *in vivo* experiments, including cell viability assay, hemolysis assay, skin irritation test, and histocompatibility assay were performed to verify the safety of the exosome-loaded gelatin sponge. Subsequently, whole blood coagulation index test, hemostatic assay using a rat liver defect hemostasis model, and full-thickness skin defect healing promoting test were performed to verify the effects of the exosome-loaded gelatin sponge in hemostasis and wound healing.

Research results

We successfully extracted exosomes from hUC-MSCs. The safety experiments showed that the gelatin sponge loaded with exosomes would not cause abnormal proliferation of L929 cells, hemolysis, or irritation to skin and tissues. In addition, the exosome-loaded gelatin sponge had a better hemostatic effect than the traditional gelatin sponge, which can promote the formation of collagen fibers and blood vessels around the wound and increase the proportion of Ki67-positive cells, thus promoting the wound healing.

Research conclusions

In a word, gelatin sponge loaded with hUC-MSCs-derived exosomes is safe. It is better than traditional gelatin sponge in stopping bleeding and promoting wound healing.

Research perspectives

The gelatin sponge loaded with exosomes derived from hUC-MSCs may be a potential material to stop bleeding and promote wound healing.

FOOTNOTES

Author contributions: Qi ZQ and Hu XM contributed to the study conception and design; Hu XM, Wang CC, and Xiao Y contributed to data collection, analysis, and interpretation; Hu XM contributed to manuscript writing; Hu XM, Wang CC, Xiao Y, Jiang P, and Liu Y performed the animal experiments; Qi ZQ, Hu XM, and Xiao Y contributed to the conception, design, financial support, and final approval of the manuscript; and all the authors have read and approved the final manuscript.

Supported by the National Key R&D Program of China, No. 2018YFA0108304; the National Natural Science Foundation of China, No. 81771721 and 81971505; and the Innovation Project of Guangxi Graduate Education, No. YCBZ2022004 and YCBZ2022045.

Institutional animal care and use committee statement: All of the experimental procedures involving animals were reviewed and approved by the Ethics Committee of Guangxi University, Nanning, China (No. GXU-2021-1000).

Conflict-of-interest statement: All the authors report no relevant conflicts of interest for this article.

Data sharing statement: No additional data are available.

ARRIVE guidelines statement: The authors have read the ARRIVE guidelines, and the manuscript was prepared and revised according to the ARRIVE guidelines.

Country/Territory of origin: China

ORCID number: Xin-Mei Hu 0000-0001-9054-9731; Zhong-Quan Qi 0000-0002-7210-4955.

S-Editor: Wang JJ
L-Editor: Wang TQ
P-Editor: Zhang XD

REFERENCES

1 **Sae-Jung S**, Apiwatanakul P. Chitosan Pad, Cellulose Membrane, or Gelatin Sponge for Peridural Bleeding: An Efficacy Study on a Lumbar Laminectomized Rat Model. *Asian Spine J* 2018; **12**: 195-201 [PMID: 29713399 DOI: 10.4184/asj.2018.12.2.195]
2 **Wang X**, Guo J, Zhang Q, Zhu S, Liu L, Jiang X, Wei DH, Liu RS, Li L. Gelatin sponge functionalized with gold/silver clusters for antibacterial application. *Nanotechnology* 2020; **31**: 134004 [PMID: 31751976 DOI: 10.1088/1361-6528/ab59eb]
3 **Yang JS**, Liu KX, Chu L, Chan YK, Fan H, Li XM, Liu P, Liu TJ, Hao DJ. Cocktail Treatment with a Gelatin Sponge Impregnated with Ropivacaine, Dexamethasone, and Vitamin B12 Promotes Early Postoperative Recovery after Percutaneous Endoscopic Lumbar Discectomy: A Retrospective, Case-Controlled Study. *Pain Physician* 2020; **23**: E211-E218 [PMID: 32214306]
4 **Jogo A**, Yamamoto A, Kaminoh T, Nakano M, Kageyama K, Sohgawa E, Hamamoto S, Sakai Y, Hamuro M, Nishida N, Miki Y. Utility of low-dose gelatin sponge particles and 5% ethanolamine oleate iopamidol mixture in retrograde transvenous obliteration (GERTO) for gastric varices. *Br J Radiol* 2020; **93**: 20190751 [PMID: 32017608 DOI: 10.1259/bjr.20190751]
5 **Dong Y**, Liu W, Lei Y, Wu T, Zhang S, Guo Y, Liu Y, Chen D, Yuan Q, Wang Y. Effect of gelatin sponge with colloid silver on bone healing in infected cranial defects. *Mater Sci Eng C Mater Biol Appl* 2017; **70**: 371-377 [PMID: 27770905 DOI: 10.1016/j.msec.2016.09.015]
6 **Zhang B**, Wang M, Gong A, Zhang X, Wu X, Zhu Y, Shi H, Wu L, Zhu W, Qian H, Xu W. HucMSC-Exosome Mediated-Wnt4 Signaling Is Required for Cutaneous Wound Healing. *Stem Cells* 2015; **33**: 2158-2168 [PMID: 24964196 DOI: 10.1002/stem.1771]
7 **Vlassov AV**, Magdaleno S, Setterquist R, Conrad R. Exosomes: current knowledge of their composition, biological functions, and diagnostic and therapeutic potentials. *Biochim Biophys Acta* 2012; **1820**: 940-948 [PMID: 22503788 DOI: 10.1016/j.bbagen.2012.03.017]
8 **van der Pol E**, Böing AN, Harrison P, Sturk A, Nieuwland R. Classification, functions, and clinical relevance of extracellular vesicles. *Pharmacol Rev* 2012; **64**: 676-705 [PMID: 22722893 DOI: 10.1124/pr.112.005983]
9 **Wang M**, Wang C, Chen M, Xi Y, Cheng W, Mao C, Xu T, Zhang X, Lin C, Gao W, Guo Y, Lei B. Efficient Angiogenesis-Based Diabetic Wound Healing/Skin Reconstruction through Bioactive Antibacterial Adhesive Ultraviolet Shielding Nanodressing with Exosome Release. *ACS Nano* 2019; **13**: 10279-10293 [PMID: 31483606 DOI: 10.1021/acsnano.9b03656]
10 **Tao SC**, Guo SC, Li M, Ke QF, Guo YP, Zhang CQ. Chitosan Wound Dressings Incorporating Exosomes Derived from MicroRNA-126-Overexpressing Synovium Mesenchymal Stem Cells Provide Sustained Release of Exosomes and Heal Full-Thickness Skin Defects in a Diabetic Rat Model. *Stem Cells Transl Med* 2017; **6**: 736-747 [PMID: 28297576 DOI: 10.5966/sctm.2016-0275]
11 **Xu N**, Wang L, Guan J, Tang C, He N, Zhang W, Fu S. Wound healing effects of a Curcuma zedoaria polysaccharide with platelet-rich plasma exosomes assembled on chitosan/silk hydrogel sponge in a diabetic rat model. *Int J Biol Macromol* 2018; **117**: 102-107 [PMID: 29772339 DOI: 10.1016/j.ijbiomac.2018.05.066]
12 **Nooshabadi VT**, Khanmohamadi M, Valipour E, Mahdipour S, Salati A, Malekshahi ZV, Shafei S, Amini E, Farzamfar S, Ai J. Impact of exosome-loaded chitosan hydrogel in wound repair and layered dermal reconstitution in mice animal model. *J Biomed Mater Res A* 2020; **108**: 2138-2149 [PMID: 32319166 DOI: 10.1002/jbm.a.36959]
13 **Yu Y**, Fan P, Li J, Wang S. Preparation of Biocompatible Manganese Selenium-Based Nanoparticles with Antioxidant and Catalytic Functions.

Molecules 2023; **28** [PMID: 37298973 DOI: 10.3390/molecules28114498]

14 **Tang J**, Yi W, Yan J, Chen Z, Fan H, Zaldivar-Silva D, Agüero L, Wang S. Highly absorbent bio-sponge based on carboxymethyl chitosan/poly-γ-glutamic acid/platelet-rich plasma for hemostasis and wound healing. *Int J Biol Macromol* 2023; **247**: 125754 [PMID: 37429345 DOI: 10.1016/j.ijbiomac.2023.125754]

15 **Eaglstein WH**, Falanga V. Chronic wounds. *Surg Clin North Am* 1997; **77**: 689-700 [PMID: 9194887 DOI: 10.1016/s0039-6109(05)70575-2]

16 **Frykberg RG**, Banks J. Challenges in the Treatment of Chronic Wounds. *Adv Wound Care (New Rochelle)* 2015; **4**: 560-582 [PMID: 26339534 DOI: 10.1089/wound.2015.0635]

17 **Yu B**, Zhang X, Li X. Exosomes derived from mesenchymal stem cells. *Int J Mol Sci* 2014; **15**: 4142-4157 [PMID: 24608926 DOI: 10.3390/ijms15034142]

18 **Moghadasi S**, Elveny M, Rahman HS, Suksatan W, Jalil AT, Abdelbasset WK, Yumashev AV, Shariatzadeh S, Motavalli R, Behzad F, Marofi F, Hassanzadeh A, Pathak Y, Jarahian M. A paradigm shift in cell-free approach: the emerging role of MSCs-derived exosomes in regenerative medicine. *J Transl Med* 2021; **19**: 302 [PMID: 34253242 DOI: 10.1186/s12967-021-02980-6]

19 **Rackov G**, Garcia-Romero N, Esteban-Rubio S, Carrión-Navarro J, Belda-Iniesta C, Ayuso-Sacido A. Vesicle-Mediated Control of Cell Function: The Role of Extracellular Matrix and Microenvironment. *Front Physiol* 2018; **9**: 651 [PMID: 29922170 DOI: 10.3389/fphys.2018.00651]

20 **Wu P**, Zhang B, Shi H, Qian H, Xu W. MSC-exosome: A novel cell-free therapy for cutaneous regeneration. *Cytotherapy* 2018; **20**: 291-301 [PMID: 29434006 DOI: 10.1016/j.jcyt.2017.11.002]

21 **Fang S**, Xu C, Zhang Y, Xue C, Yang C, Bi H, Qian X, Wu M, Ji K, Zhao Y, Wang Y, Liu H, Xing X. Umbilical Cord-Derived Mesenchymal Stem Cell-Derived Exosomal MicroRNAs Suppress Myofibroblast Differentiation by Inhibiting the Transforming Growth Factor-β/SMAD2 Pathway During Wound Healing. *Stem Cells Transl Med* 2016; **5**: 1425-1439 [PMID: 27388239 DOI: 10.5966/sctm.2015-0367]

22 **Sun L**, Xu R, Sun X, Duan Y, Han Y, Zhao Y, Qian H, Zhu W, Xu W. Safety evaluation of exosomes derived from human umbilical cord mesenchymal stromal cell. *Cytotherapy* 2016; **18**: 413-422 [PMID: 26857231 DOI: 10.1016/j.jcyt.2015.11.018]

23 **Monaco JL**, Lawrence WT. Acute wound healing an overview. *Clin Plast Surg* 2003; **30**: 1-12 [PMID: 12636211 DOI: 10.1016/s0094-1298(02)00070-6]

24 **Diegelmann RF**. Analysis of collagen synthesis. *Methods Mol Med* 2003; **78**: 349-358 [PMID: 12825284 DOI: 10.1385/1-59259-332-1:349]

25 **Madden JW**, Smith HC. The rate of collagen synthesis and deposition in dehisced and resutured wounds. *Surg Gynecol Obstet* 1970; **130**: 487-493 [PMID: 5413430]

26 **Okonkwo UA**, DiPietro LA. Diabetes and Wound Angiogenesis. *Int J Mol Sci* 2017; **18** [PMID: 28671607 DOI: 10.3390/ijms18071419]

27 **Todorova D**, Simoncini S, Lacroix R, Sabatier F, Dignat-George F. Extracellular Vesicles in Angiogenesis. *Circ Res* 2017; **120**: 1658-1673 [PMID: 28495996 DOI: 10.1161/CIRCRESAHA.117.309681]

28 **Zhang J**, Guan J, Niu X, Hu G, Guo S, Li Q, Xie Z, Zhang C, Wang Y. Exosomes released from human induced pluripotent stem cells-derived MSCs facilitate cutaneous wound healing by promoting collagen synthesis and angiogenesis. *J Transl Med* 2015; **13**: 49 [PMID: 25638205 DOI: 10.1186/s12967-015-0417-0]

29 **Liang X**, Zhang L, Wang S, Han Q, Zhao RC. Exosomes secreted by mesenchymal stem cells promote endothelial cell angiogenesis by transferring miR-125a. *J Cell Sci* 2016; **129**: 2182-2189 [PMID: 27252357 DOI: 10.1242/jcs.170373]

30 **Kim YJ**, Yoo SM, Park HH, Lim HJ, Kim YL, Lee S, Seo KW, Kang KS. Exosomes derived from human umbilical cord blood mesenchymal stem cells stimulates rejuvenation of human skin. *Biochem Biophys Res Commun* 2017; **493**: 1102-1108 [PMID: 28919421 DOI: 10.1016/j.bbrc.2017.09.056]

31 **Lamalice L**, Le Boeuf F, Huot J. Endothelial cell migration during angiogenesis. *Circ Res* 2007; **100**: 782-794 [PMID: 17395884 DOI: 10.1161/01.RES.0000259593.07661.1e]

32 **Zhang B**, Wu X, Zhang X, Sun Y, Yan Y, Shi H, Zhu Y, Wu L, Pan Z, Zhu W, Qian H, Xu W. Human umbilical cord mesenchymal stem cell exosomes enhance angiogenesis through the Wnt4/β-catenin pathway. *Stem Cells Transl Med* 2015; **4**: 513-522 [PMID: 25824139 DOI: 10.5966/sctm.2014-0267]

Published by **Baishideng Publishing Group Inc**
7041 Koll Center Parkway, Suite 160, Pleasanton, CA 94566, USA
Telephone: +1-925-3991568
E-mail: bpgoffice@wjgnet.com
Help Desk: https://www.f6publishing.com/helpdesk
https://www.wjgnet.com